2014

Nature of Catalytic Active Sites in Supported MOx/ZSM-5 Catalysts: Anchoring Sites, Electronic Structures, Molecular Structures and Reactivity

Yadan Tang
Lehigh University

Nature of Catalytic Active Sites in Supported MOx/ZSM-5 Catalysts: Anchoring Sites, Electronic Structures, Molecular Structures and Reactivity

by

Yadan Tang

A Dissertation

Presented to the Graduate and Research Committee

of Lehigh University

in Candidacy for the Degree of

Doctor of Philosophy

in

Chemistry Department

Lehigh University

January 2015

Certificate of Approval

Approved and recommended for acceptance as a dissertation in partial fulfillment of the requirements for the degree of Doctor of Philosophy

Yadan Tang

Nature of Catalytic Active Sites in Supported MO_x/ZSM-5 Catalysts: Anchoring Sites, Electronic Structures, Molecular Structures and Reactivity

_____
Defense Date

_____
Dissertation Director

Dr. Israel E. Wachs, Ph.D.

_____
Approved Date

Committee Members:

_____
Dr. James E. Roberts, Ph.D.

_____
Dr. Dave Moore, Ph.D.

_____
Dr. David Vicic, Ph.D

_____
Dr. Mark A. Synder, Ph.D.

ACKNOWLEDGMENTS

This moment is filled with joy, sweat and gratitude that I have been dreaming about for a very long time. I cannot climb up to this height without the encouragement and enlightment from faculty, colleagues, and group members. In these years far apart from my home, my family and friends have provided me great moral support which I cannot imagine to live without in this journey. My heart is filled with gratitude and I am eager to express to all of you.

I cannot have this opportunity to the success as a graduate student without the acceptance to Chemistry department at Lehigh University. I would like to express my gratitude to whoever reached the decision. This is a gate open for me to the profound knowledge about science which has helped me through my graduate research overwhelmingly thanks to great graduate chemistry courses available to us.

I cannot have the opportunity to the world of surface science and catalysis without Professor Israel E. Wachs. Dr. Wachs is my mentor, my friend and my respectful family at the same time. I got the opportunity to join his group after auditing his catalysis course, and it has become the most important decision to my education and my life. His honest advice, critical thought and encouragement have helped me shape myself during my research and my interpretation of catalysis science. His precise knowledge of the field makes him the first one whenever I needed direction and suggestions. The most impressive thing about him is that he is extremely careful about his own research and still remains open-minded to any doubt coming from others and seeks critical feedback from every conference which he believes is one of the most efficient ways for improvement in research. He never hesitates to expose us to a great

extent to professional conferences and training. I have had the great opportunity to get training at Brookhaven national laboratory for synchrotron experiments with the generous help of Dr. Anatoly Frenkel from Yeshiva University. Dr. Wachs is also a very knowledgeable friend and always willing to give great advice or tips for travelling. I learned the best Italian dessert shop in New York from him. I had the chance to tour around New York by cruise and felt like touching deeply into the flesh of the city while listening to all the old stories of her from Dr. Wachs.

There are four significant people, my committee members, whom I must thank for doing so much more than just signing the paper. I am honored to have all of them as my committee. Dr. James Roberts has been a knowledgeable mentor for NMR spectroscopy and scientific interpretation of data with great accuracy. I can count on his advice so that I know that I am on the right track of processing and interpreting data. Dr. Dave Moore has provided so many important suggestions to my research thanks to his critical thinking. I remembered a word from him at one of the TA meetings:" it is amazed that we always learned\\ new things every time we go back to the general chemistry book." Learning is always looking back to what you have learned and digging further. Dr. Mark Synder has been extremely helpful while I was consulting him about how to measure heat capacity using calorimetry. Without his professional insights, I might have wasted much of my time on the wrong measurement. He has also generously helped our group for many BET measurements. Dr. David Vicic has joined my committee members recently, and his profound knowledge about organometallic and catalysis throughout his active experience in academia is a great addition to my committee.

I am lucky to have a great and professional team to work with in Dr. Wachs'group. Dr. Michael Ford, a research scientist, never refused to provide help for experimental set-ups. His experience and meticulous thought always brings me confidence to the final set-up. He also does not hesitate to help me with proof-reading of manuscript and thesis. I am impressed with one of his words: If you know that you can help someone and you choose not to, that is wrong. Dr. Chip Roberts, a recent graduate, provided training for me and also worked with me for the formic acid project. His delightful personality has also been a positive influence during my first year in the group. Dr. Julie Molinari, a recent graduate and a great friend, is a successful and talented female scientist and always an inspiration for me. Chris Keturakis, a graduate student, worked on the maintenance and operation of instruments in the lab with great intelligence and patience. He has been the catalyst of the lab which ensures the progress of our work on good-quality instruments. He always provides useful suggestions to us before we can hear from technicians from company. Soe Lwin, a graduate student, joined the group the same year as me. He is a very diligent and productive student, and has helped me with the X-ray absorption spectroscopy on supported WOx/ZSM-5 and ReOx/ZSM-5 catalysts. I am also very glad to work with current graduate students including Minghui Zhu, Anisha Chakrabarti and Dongchang Qin.

I would like to thank to one of my dearest sisters, Lili Liu, a recent graduate student of the Chemistry department. We lived in the same apartment our first year at Lehigh but at a different time, we were in the same group but at a different time, but I am glad that we are friends at all times. Her positive, happy and devoted personality greatly influenced me. Without her invitation to numerous activities, I could not have enjoyed

living independently and thinking positively. I cherish all the memories shared with her through all these years like a family.

I also would like to give thanks to all my friends at Lehigh University whom I have shared precious memories with. Dr. Peng Chen, Dr. Minghui Wang and his wife Nisha Zhu, Yaqing Ning, Cong Liu, Berenika Kokoszka, Yiqun Liu, Long Xu, Chang Wang, Cen Lin, Le Zhao, Beibei Zeng, etc.

I have saved my most important words for my beloved family. I am truly blessed to have such a wonderful family that has never stopped loving me and supporting me even though I cannot be with them over the most important times for the past six years. I am extremely lucky to be raised by Guirong He and Shengshui Tang, my Mom and Dad. I am also very lucky to have the support and love from Jinlian Wang and Yan Guo, my Mom-in-law and Father-in-law. I wish that I could have more time with them over the past six years. Finally, I would like to Thank Hongliang Guo, my husband, my friend and my spiritual support through all these years. Without him, I cannot be where I am today.

Words are not enough to express my gratitude to everyone, but I have to stop here. Graduate school in Lehigh University has been a unique and fruitful experience for me. It provided education for being a good researcher, an independent woman and a positive and open person. This knowledge will help me moving on with my new life ahead of me.

TABLE OF CONTENTS

List of Figures

Chapter 1

Chapter 2

Chapter 3

Chapter 4

Chapter 5

Chapter 6

List of Tables

Chapter 2

Chapter 3

Chapter 4

Chapter 5

ABSTRACT

The non-oxidative dehydroaromatization (DHA) of methane to aromatics by ZMS-5 supported group V-VII transition metal oxide (VOx, CrOx, MoOx, WOx and ReOx) catalysts has received much attention in recent years. Despite the intensive catalysis studies, many fundamental issues still remain unclear such as the anchoring sites and molecular structures of the initial supported MOx phases on the ZSM-5 support (Si/Al= 15, 25, 40 and 140), and the nature of the M catalytic active sites during the CH_4 DHA reaction. A systematic *in situ* molecular spectroscopic study under fully dehydrated conditions and *operando* spectroscopic study during methane DHA were investigated over a series of supported MOx/ZSM-5 catalysts in order to resolve the molecular level details.

The *in situ* Raman spectra identified that the initially supported MOx phases are completely dispersed as surface monoxo (M=O) and dioxo (O=M=O) MOx species on the ZSM-5 supports. The corresponding *in situ* UV-vis spectra of supported MOx/ZSM-5 catalysts have high edge energy (Eg) values for the Ligand-to-Metal-Charge Transfer (LMCT) transitions and the absence of d-d transitions are consistent with that the supported MOx species are isolated and fully oxidized (V^{+5}, Cr^{+6}, Mo^{+6}, W^{+6} and Re^{+7}) on the ZSM-5 support, respectively.

The reactivity of the supported MOx/ZSM-5 catalysts was studied with temperature-programmed *operando* Raman-MS spectroscopy. The supported VOx/ZSM-5 and CrOx/ZSM-5 catalysts were not selective to benzene and formed only carbon monoxide and hydrogen. Only supported ReOx/ZSM-5, MoOx/ZSM-5 and WOx/ZSM-5 were

found to be active catalysts for methane DHA and the temperature for initial benzene formation decreased in the order of WOx/ZSM-5 (~800 ^{o}C) < MoO_x/ZSM-5 (~700 ^{o}C) <ReOx/ZSM-5 (~650 ^{o}C). The poor reactivity of VOx/ZSM-5 and CrOx/ZSM-5 catalysts might be due to the failure to form metal carbide or metallic species, which have been identified as the active sites of supported MoOx/ZSM-5, WOx/ZSM-5 and ReOx/ZSM-5 catalysts for methane DHA. Despite the high reactivity of the supported ReOx/ZSM-5 catalyst, the volatility of the ReOx phase and its high cost does not make for a practical catalyst. The supported WOx/ZSM-5 catalyst is selective towards benzene at high temperatures, but the excessive temperatures lead to severe coke deposition that deactivates this catalyst. The supported MoOx/ZSM-5 catalyst appears to be the best catalyst for methane DHA because of its high selectivity towards benzene (80-90%) and near equilibrium conversion, but it also undergoes catalyst deactivation because of coking. *Operando* Raman-MS and XANES/EXAFS spectroscopic studies is consistent with the initial isolated surface MoOx sites undergoing dynamic structural changes and do not correlate to the reactivity. The presence of a high concentration of Brønsted acid sites (low Si/Al ratio of ZSM-5) leads to better catalytic reactivity of the supported MOx/ZSM-5 catalysts (M=Mo, W and Re). The active sites of MoOx/ZSM-5 catalysts for methane DHA are identified as poorly ordered $Mo_4O_yC_z$ nanoparticles anchoring on Al sites of ZSM-5 *via in situ* EXAFS/XANES.

The present study provides a better understanding about the isolated surface MO_x molecular structures present for the supported MOx sites on ZSM-5 and their transformation to active phases during the methane dehydroaromatization reaction at elevated temperatures.

Chapter 1.

Literature Review of methane dehydroaromatization to Liquid Aromatic by supported transition metal oxide MOx/ZSM-5 (M=V, Cr, Mo, W and Re) catalysts

Abstract

The non-oxidative conversion of methane to aromatics by supported MOx/ZSM-5(M=V, Cr, Mo, W and Re) catalysts has generated much interested in recent years because of the enormous potential impact of such a catalytic technology to the world's energy portfolio. In spite of the extensive number of studies on this catalytic reaction, a general consensus has not been reached on many of the fundamental details such as the anchoring sites, molecular structures of the surface MOx species on ZSM-5 supports and the catalytic active sites present during methane dehydroaromatization (DHA) reaction. This chapter will provide a critical review on the reported molecular findings of supported transition metal oxides of group V-VII on ZSM-5 and the proposed catalytic active sites of these catalysts for methane DHA. The unresolved fundamental molecular understandings of these significant catalytic systems poses a great hindrance in the progress of these important catalytic systems, and further effort is required to resolve these issues if this technology is to proceed forwards.

Introduction

The molecular and electronic structures of highly dispersed group V-VII transition metal oxide supported on zeolites have received significant attention in recent years due to their industrial potential as catalysts for numerous chemical reactions[1-18]. For example, supported V_2O_5/ZSM-5 catalysts have been studied for selective catalytic reduction (SCR) of NO_x with ammonia[1], and oxidative dehydrogenation (ODH) of ethane to ethylene with CO_2[2]. Supported MoO_3/ZSM-5 catalysts have been investigated for non-oxidative dehydroaromatization (DHA) of methane[3], and partial oxidation of methane to formaldehyde[4]. Supported CrO_3/ZSM-5 catalysts have been examined for SCR of NO_x with hydrocarbons[5], propane dehydrogenation to propylene[6], ODH of ethane to ethylene with CO_2[7], photocatalytic partial oxidation of propane to acetone[8], toluene disproportionation[9], non-oxidative DHA of methane[10] and neutralization of volatile organic compounds (VOC) and chlorinated VOCs[11,12,13,14]. Supported WO_3/ZSM-5 catalysts have been studied for methane oxidation[15] and non-oxidative DHA of methane[16], and supported Re_2O_5/ZSM-5 catalysts have been found to be effective for conversion of ethane to benzene[17] and non-oxidative DHA of methane.[18]

The recent significant discovery of shale gas has renewed the interest in the supported MOx/ZSM-5 catalysts for the effective natural gas to liquid fuel technology (GTL).[19] The state-of-the-art GTL technology based on the production of syngas (carbon monoxide and hydrogen) has been explored for industrial implementation.[19] Production of syngas is a capital and energy intensive multistep process. Consequently, there is a great motivation for the development of a direct route based on methane coupling either in the presence of

oxygen or *via* a non-oxidative process. Wang and co-workers' initial report of the direct conversion of methane into benzene on supported MoO_3/ZSM-5 catalysts in 1993 evoked much interest[3]. This pioneering work inspired multiple investigations of similar catalyst systems involving group V-VII transition metal oxides supported on zeolites[10]. By far the most effective catalyst for this reaction was found to be supported MoO_3/ZSM-5 due to its high selectivity towards benzene and near equilibrium conversion. Mamonov. *et al.*[19] and Ismagilov *et al.*[20] provided a thorough review of methane DHA over supported molybdenum oxide on zeolites with regards to catalyst synthesis and reaction conditions, different zeolite supports, the active sites and reaction mechanism. Spivey *et al.*[21] presented an overview of catalytic aromatization of methane by emphasizing the thermodynamics, kinetics and reactor design of methane DHA by supported molybdenum oxide on zeolite catalysts.

The supported metal oxide phases on ZSM-5 are usually molecularly dispersed below monolayer surface coverage or the maximum dispersion limit. The supported surface metal oxide components provide redox/acid/basic sites while the ZSM-5 support contributes strong Brønsted acid sites and shape-selectivity not available for non-zeolitic supported metal oxide catalyst systems. Above monolayer coverage or maximum dispersion limit, crystalline metal oxides nanoparticles (NPs) also form on the zeolite external surface and are generally undesirable because of their lower catalytic activity and tendency to block the micropores of ZSM-5.[22]

In spite of extensive characterization studies about supported MOx/ZSM-5 catalysts, the details about the anchoring sites, molecular and electronic structures of surface MOx species on ZSM-5 supports are still not resolved. Although there is some agreement that

the anchoring sites for the MOx species on the ZSM-5 supports are the surface Brønsted acid sites and Si-OH sites, there is no consensus about the nature of the MOx species. The lack of consensus is strongly related to the application of different characterization techniques under different conditions (ambient, *ex situ* and *in situ*). Many of the characterization measurements were taken under ambient and *ex situ* conditions, with only a few *in situ* spectroscopic studies reported. The dynamic nature of catalysts under different environmental conditions is well established and the characterization under ambient conditions, at which condition the catalysts are hydrated, is not representative of the actual states of catalysts under relevant environmental conditions (dehydrated and reaction conditions).[23,24] The objectives of the current research are to 1) identify the anchoring sites of the surface MOx species on the ZSM-5 support, 2) determine the molecular structures of the initial surface MOx species, 3) establish the catalytic active sites responsible methane DHA by supported MOx/ZSM-5 catalysts under reaction conditions; 4) correlation of the structure-activity/selectivity relationships for methane DHA, and 5) determining the rate-determining-step for methane DHA by supported MOx/ZSM-5 catalysts.

1.1. Anchoring sites of surface MOx species in supported MOx/ZSM-5 catalysts

A large number of studies have addressed the location of surface MOx species in the zeolite matrix. The successful introduction of surface metal oxide species within the

zeolite channel is greatly influenced by catalyst synthesis methods. Supported MOx/ZSM-5 catalysts can be prepared by two synthesis methods: (1) a solid-state reaction of the physical mixture of bulk metal precursors (oxides/chloride salts) with zeolite at elevated temperatures(500-700 ^{o}C), and (2) an incipient wetness impregnation method from which the active metal precursors (ammonium metal salts) are dissolved into an aqueous or organic solution before mixing with the zeolite support; the volume of solution is controlled to reach the wet point of the zeolite so that capillary action draws the metal-containing solution to the zeolite matrix. Lunsfords *et al.*[25] and Iglesia *et al.*[16] investigated supported MOx/ZSM-5 catalysts prepared by impregnation and solid-state reaction, respectively. They both suggested that catalysts obtained from the solid-state reaction lead to a majority of surface metal oxide species at ion exchange sites inside the zeolite channels, whereas catalysts obtained from impregnation lead to a large amount of metal oxide species at the external surface of zeolite and a small fraction of metal oxide species inside the zeolite channels. However, Iglesia *et al.* claimed the anchoring sites of surface MO_x species (such as WO_x[16], MoO_x[26,27,28] and ReO_x[29]) without direct experimental evidence but only on the basis of titration of residual protons of zeolites assuming the supported MO_x/ZSM-5 as single-site catalysts. Lunsfords *et al.*[25] and many other groups have investigated the anchoring sites of supported MOx/ZSM-5 by FT-IR techniques. Earlier FT-IR studies were based on ambient or *ex situ* FT-IR, and only a few recent studies are *in situ* FTIR. The IR studies based on a hydrated catalyst under ambient conditions are not representative of the actual catalysts under dehydrated conditions. In this section, literature findings on the anchoring sites of surface metal oxides species in supported MOx/ZSM-5 catalysts is discussed.

1.1.1. Supported V_2O_5/ZSM-5

The anchoring sites of surface VOx species are greatly affected by the preparation methods. Weckhuysen *et al.*[25] investigated the location of surface VOx species *via in situ* FT-IR and observed that the surface VOx species mainly leads to the consumption of external silanol groups of zeolites for samples prepared by impregnation, while surface VOx species mainly leads to the consumption of framework Brønsted acid sites for samples prepared by solid state reaction of $VOCl_3$ and HZSM-5. It is consistent with the conclusions on the supported V_2O_5/ZSM-5 by solid state reaction reported by other groups.[30,31] Wichterlova *et al.*[30] claimed that surface VOx species anchor at Brønsted acid sites and external silanol sites *via* ambient FTIR. As mentioned previously, the FTIR study based on a hydrated sample at ambient condition is not representative of the actual catalyst under dehydrated conditions. Later in an *in situ* FTIR study, Lacheen *et al.*[31] observed a monotonic decrease in the surface Brønsted acid hydroxyls with increasing $V/Al_{framework}$ ratio as well as consumption of a small number of external silanols on supported VOx/ZSM-5 prepared from the solid-state reaction as shown in **Figure 1- 1**. The introduction of each V-atom replaced ~1 proton of the Brønsted acid site. This study claimed that surface VOx species anchor at Brønsted acid sites only.

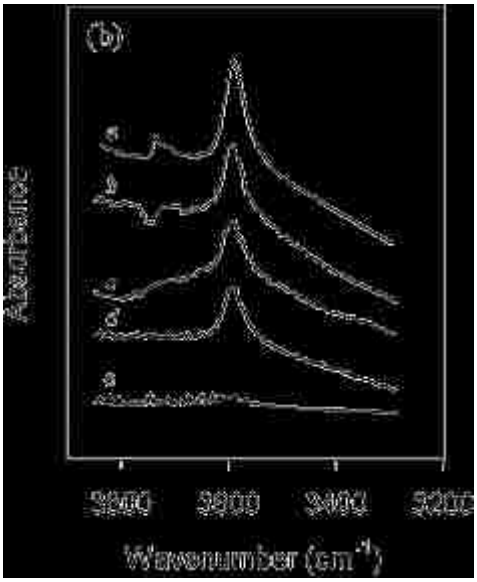

Figure 1- 1 Fourier transformed infrared spectra in the hydroxyl stretching region (a) H-ZSM5, (b) $V/Al_{f,i}$= 0.2, (c) $V/Al_{f,i}$= 0.4, (d) $V/Al_{f,i}$= 0.65, (e) $V/Al_{f,i}$= 1. Spectral intensities were normalized with the Si−O−Si overtone bands between 1730 and 2100 cm^{-1}.[31]

1.1.2. Supported CrO_3/ZSM-5

The anchoring sites of surface CrOx species on ZSM-5 are under debate due to the lack of *in situ* characterizations. Greene *et al.*[13] and Slinki *et al.*[24] reported that surface CrOx species anchor at surface Brønsted acid sites in supported CrO_3/ZSM-5 obtained by impregnation based on ambient FTIR and *in situ* ESR, respectively. An FTIR study based on a hydrated catalyst under ambient conditions is not representative of the actual catalysts under dehydrated conditions. In contrast to these conclusions, Lunsford *et al.*[10] observed *via in situ* FTIR that a substantial amount of Brønsted acid protons and silanol hydroxyls present on the supported 2% CrO_3/ZSM-5(Si/Al=15) prepared by the impregnation method, but further conclusion about the anchoring site is not possible from this study due to the absence of the FTIR spectra of parent HZSM-5 as a reference. Ghorbel *et al.*[32] investigated the anchoring sites of supported CrO_3/ZSM-5 obtained by

solid-state exchange synthesis from solid mixture of various chromium salt and HZSM-5 *via in situ* diffuse reflectance Infrared Fourier transform spectroscopy (DRIFTs). The study suggested that surface CrOx species anchor mainly at Brønsted acid sites with a small amount of CrOx species at external silanol sites of ZSM-5, as shown in **Figure 1- 2**. A closer examination of the DRIFT spectra of the parent ZSM-5 and CrO_3/ZSM-5 leads to the concern if the baseline correction was correctly applied. It seems like that the intense band at 3593 cm^{-1} of HZSM-5 is due to a high baseline of the spectra rather than the presence of substantial amount of Brønsted acidity as concluded. Therefore, quantitative DRIFT analysis based on these spectra is subject to question.

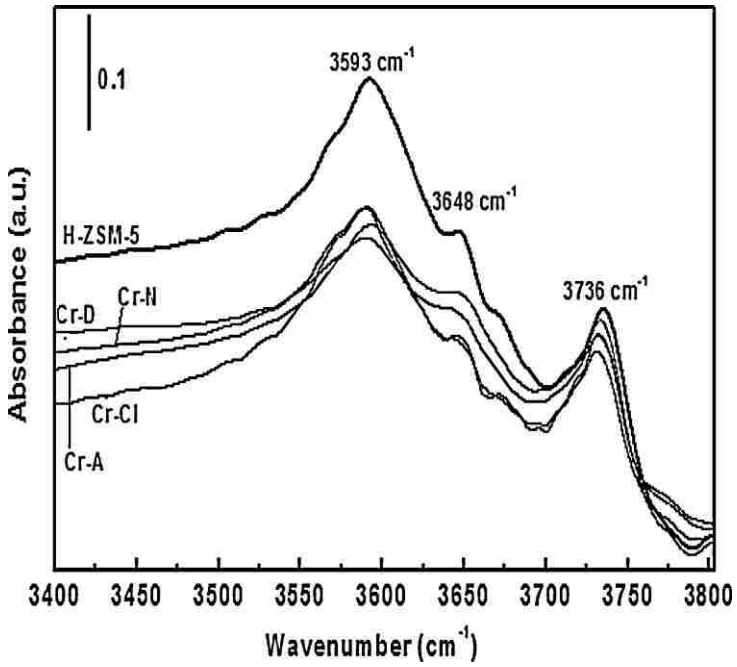

Figure 1- 2 DRIFT spectra of H–ZSM-5 and chromium containing catalysts. Cr-D, Cr-N, Cr-Cl and Cr-A represent supported CrO_3/ZSM-5(Si/Al=15) prepared from solid-state reaction with HZSM-5 and chromium salts such as ammonium dichromate, chromium nitrate, chromium chloride and chromium acetate, respectively[32]

1.1.3. Supported MoO_3/ZSM-5

There is general consensus from multiple reported *in situ* IR studies[33,34] that both surface Al-$(OH)^+$-Si Brønsted acid and external Si-OH sites are the anchoring sites for surface MoOx species on H-ZSM-5. Xu *et al.*[34] reported that MoOx species preferably anchor at surface Brønsted acid sites over silanol hydroxyls for 6% MoOx/ZSM-5 (Si/Al=25) with *in situ* IR where dehydration was performed in vacuum. Lunsford and co-workers[33] observed with *in situ* IR spectroscopy that MoOx species migrated from external surface Si-OH sites and extra-framework Al-OH hydroxyls to framework Al-$(OH)^+$-Si sites at elevated calcination temperatures for 2% MoOx/ZSM-5 (Si/Al=25) obtained by impregnation of aqueous ammonium heptamolybdate. In contrast to the above synthesis method, Borry *et al.*[27] and Li *et al.*[26] prepared the catalysts by solid-state reaction of crystalline MoO_3 onto the ZSM-5 support at 500-700 ^oC. From titration of the residual protons it was assumed that surface Mo_2O_5 dimers are formed and anchor at two adjacent Al-$(OH)^+$-Al Brønsted acid sites, but no direct supporting information about the anchoring sites or dimeric structures were provided. It is important to note that the probability of finding a high concentration of two adjacent Al framework Brønsted acid sites is low according to Lowenstein's rule and not enough of such paired sites are present for anchoring high loadings of MoOx on ZSM-5.[35]

1.1.4. Supported WO_3/ZSM-5

Direct experimental FTIR results have not been provided in the literature to elucidate the anchoring sites of surface WOx species in supported WO_3/ZSM-5.[36] The Brønsted acidity of ZSM-5(Si/Al=38) after the introduction of 3% W ions prepared by incipient

impregnation was chemically probed by NH_3-temperature programmed desorption (NH_3-TPD) and not found to be perturbed by addition of WOx by Xiong *et al.*[36] The NH_3-TPD method, however, cannot differentiate between Brønsted acidity of the parent HZSM-5 and new Brønsted acidity of surface WOx species, which has been shown for similar catalyst systems (WO_3/SiO_2, WO_3/Al_2O_3 and WO_3/ZrO_2).[37,38,] Therefore, it is still uncertain whether surface WO_3 species will anchor at Brønsted acid sites of ZSM-5. Ding *et al.*[16] suggested that the surface WOx species require two neighboring Brønsted acid sites of ZSM-5 solely based on titration of the residual protons of ZSM-5, but as already indicated the probability of finding a high concentration of two adjacent Brønsted acid sites is low at higher coverage according to Lowenstein's rule.[35]

1.1.5. Supported Re_2O_7/ZSM-5

The anchoring sites of ReOx species in supported Re_2O_7/ZSM-5 has received limited attention due to the highly volatile nature of Re-oxo species. *In situ* IR studies[18,29] reported that surface ReOx species prefer to anchor at Brønsted acid sites with a small amount of ReOx species at external silanol sites. The proposed monomeric ReOx species requires one Brønsted acid sites and the dimeric Re_2Ox requires two neighboring Brønsted acid sites, but the probability of finding a high concentration of two adjacent Brønsted acid sites is low as already indicated according to the Lowenstein's rule. [35]

1.2. Molecular structures of surface MOx species on supported MOx/ZSM-5 catalysts

1.2.1. Supported V_2O_5/ZSM-5

The proposed molecular structures for surface VOx species are shown in **Figure 1- 3**.

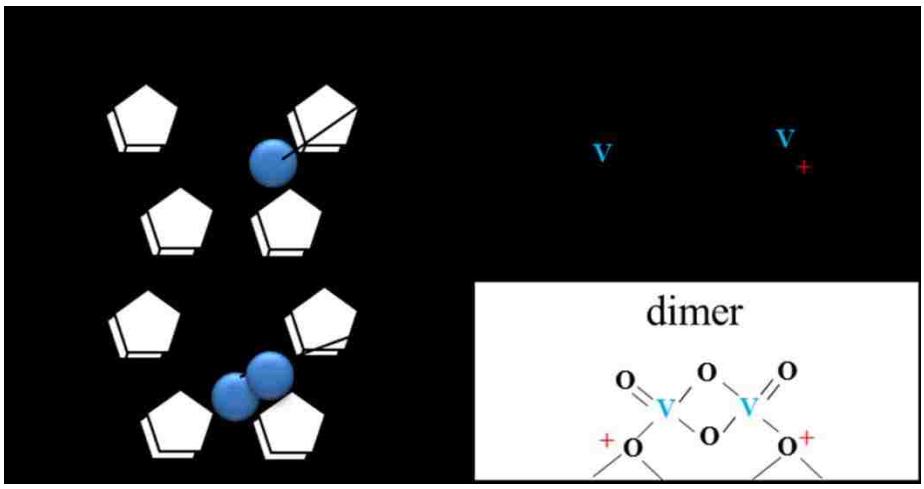

Figure 1- 3 Schematic of proposed molecular structures of monomeric VO_x and dimeric $V_2O_4^{2+}$ species in ZSM-5

For the supported V_2O_5/ZSM-5 catalysts, it was initially proposed that dehydrated surface $V^{(IV)}O^{2+}$ species anchor at cationic sites of the zeolites through solid-state reaction of V_2O_5 with high silica-containing zeolites from *in situ* ESR measurements by Slinkin *et al.*[39,40] and Wicherlova *et al.*[30] Slinkin *et al.*[39,40] observed VO^{2+} on cationic sites of zeolites while Wichterlova *et al.*[30] proposed the presence of VO^{2+} species on both the Brønsted acid sites and extra-framework Si-OH sites based on dehydrated ESR under vacuum and hydrated IR spectroscopy at room temperature. Investigation employing ESR techniques cannot characterize the ESR-inactive V^{5+} ions. Anpo *et al.*[41] investigated the supported V_2O_5/ZSM-5 catalysts prepared by solid state sublimation preparation *via*

ex situ UV-vis DRS spectroscopy and *ex situ* vanadium K-edge extended X-ray absorption fine structure (EXAFS). It was revealed that V_2O_5 is transformed to dispersed mono-oxo vanadyl group ($O_3V^{(V)}$=O) based on the strong pre-edge feature of the supported V_2O_5/ZSM-5, however, the presence of multiple UV-vis absorption bands at 235, 275 and 340 nm were not addressed. Furthermore, the XAS is a bulk technique and provides the average information of all structures present on the catalysts. In a subsequent work, Anpo *et al.*[41] assigned the multiple UV-vis bands and concluded the presence of both $V^{(V)}$ and $V^{(VI)}$ are present on the ZSM-5 support: (1) $V^{(v)}O_4$ based on UV-vis band at 235 and 340 nm, and (2) $V^{(VI)}O^{2+}$ of square pyramidal coordination based on UV-vis band at 275 nm. However, the multiple UV-vis absorption bands (235, 275 and 340 nm) and V-O-V coordination from the *ex situ* EXAFS for the supported V_2O_5/ZSM-5 indicate the presence of oligomeric VOx species on ZSM-5, which implies that the sample is partially hydrated under their characterization conditions. It has been reported that the nature of surface transition metal oxides species is polymeric under ambient conditions and isolated under dehydrated conditions below monolayer coverage on various metal oxide supports (Al_2O_3, SiO_2, ZrO_2 and TiO_2)[42,43]. Therefore, it is important to properly characterize the catalyst under dehydrated conditions with the help of *in situ* spectroscopy. More recently, Lacheen and Iglesia[31] have proposed the presence of monomeric dioxo VO_2^+ and dimeric $V_2O_4^{2+}$ species located on cationic sites of zeolites for supported VOx/ZSM-5 (Si/Al~13.4) *via in situ* FTIR, *in situ* Raman and *in situ* EXAFS fit. The Raman vibrations at 1065-1076 cm^{-1} were assigned to the V=O vibration using theoretical stretching frequencies from DFT and *in situ* EXAFS analysis. The vibration of 1065-1076 cm^{-1} is too high for terminal V=O bonds for since mono-oxo V=O structures

vibrate in the 1015-1040 cm^{-1} range[44,45] and dioxo O=V=O bonds would give rise to ν_s and ν_{as} vibrations at even lower wavenumbers.[46] Raman bands at ~1070 cm^{-1} have been shown to originate from Si-O vibrations and are not associated with surface vanadia species.[47,48,49] The proposed dimeric surface $V_2O_4^{2+}$ species on ZSM-5 cannot be a significant species as indicated by the absence of a V-O-V correlation in the second coordination sphere of the *in situ* FT-EXAFS.

1.2.2. Supported CrO_3/ZSM-5

The proposed surface CrOx structure on ZSM-5 are summarized and shown in **Figure 1-4**. Isolated dioxo $(O=)_2CrO_2$, isolated trioxo $(O=)_3CrO$ and nanocrystalline Cr_2O_3 were proposed as the surface CrOx structures present on ZSM-5 support.

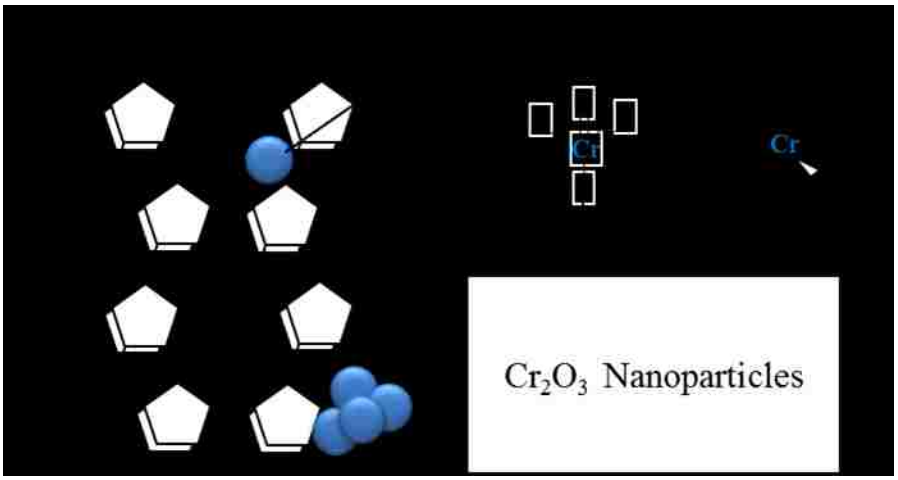

Figure 1- 4 Schematic of proposed molecular structure of monomeric CrO_4 and Cr_2O_3 nanoparticles present in ZSM-5

Early characterization studies employing IR, ESR (Cr^{+5} and Cr^{+3}) and Mossbauer spectroscopy (Cr^{+5} and Cr^{+6} cations) under vacuum only identified the oxidation state of CrO_x species under oxidative environments up to 500 ^oC, and no further structural details were mentioned.[24,50,51]

The presence of surface dioxo $(O=)_2CrO_2$ species on ZSM-5 (Si/Al=29-1900) have recently also been proposed.[24,52,53,54] The isolated CrO_4 and $CrO_{5/6}$ Cr^{6+}/Cr^{5+} structures were proposed from *in situ* ESR measurements[24]. The *in situ* XANES pre-edge peak was present at 5.993 keV that is characteristic of $Cr^{6+}O_4$ structures containing terminal Cr=O bonds[53]. The *in situ* EXAFS indicates the major presence of Cr=O bond in the first coordination shell and the presence of small amount of Cr_2O_3 NPs due to the presence of weak Cr-O-Cr bond at 0.25-0.42 nm at the second and third coordination shells. This analysis also neglects the possible presence of multiple surface CrO_x species on the ZSM-5 support, which are known to be present on other oxide support materials such as SiO_2, Al_2O_3 and Al_2O_3/SiO_2.[44,53 ,55] Corresponding IR spectra exhibited a weak band at ~925 cm^{-1} that was assigned to the Cr=O double bond of the surface CrO_4 species,[8] but IR bands in this region have been shown to arise from vibrations of bridging Cr-O-support bonds and not vibrations of Cr=O bonds.[56] Isolated surface CrOx species with Raman band at 1007-1015 cm^{-1} was reported by Ghorbel *et al.*[32] *via in situ* Raman; however, the incorporation of surface CrO_x species into the zeolite channel did not appear to be successful in this study as indicated by the weak and broad Raman bands.

Isolated trioxo surface (Al-)$OCr(=O)_3$(-Si) species on ZSM-5 (Si/Al=15 and 40) have also been proposed in which the surface CrOx contains one bridging Cr—O—support bond and three terminal Cr=O bonds, but no supporting experiment evidence was provided.[13] An isolated trioxo $Cr(=O)_3$ structure would be expected to give rise to four Raman vibrations located at ~908 (ν_s), 933 (ν_{as}), 947 (ν_{as}), and 955 (ν_{as}) cm^{-1}, which have been reported for the trioxo $CsBrCr(=O)_3$ reference compound.[57] Without direct

confirmation with *in situ* Raman spectroscopy, the surface trioxo $(O=)_3CrO$ structure on ZSM-5 cannot be validated and a trioxo chromate structure is highly unlikely.[56]

Ghorbel *et al.* [32] reported *via in situ* Raman the presence of polychromates (sharp Raman band at ~375 cm^{-1}) on supported CrO_3/ZSM-5 catalysts prepared by the solid-state reaction (Si/Al=15, Cr/Al=0.5, 1 and 1.5). Polychromate surface CrO_x species; however, would be expected to also exhibit Raman vibrations at 980-930 $cm^{-1}(\nu_{as})$, ~900 $cm^{-1}(\nu_s)$, 818-840 $cm^{-1}(\nu_{as}(CrOCr))$ and 563-512 cm^{-1} $(\nu_s(CrOCr))$.[53] The absence of these characteristic Raman bands is due to the absence of polychromate species on ZSM-5 or only present in a negligible amount which is below the detection limit of Raman spectroscopy (subnanosize). The observed sharp Raman band at 375 cm^{-1} accompanied by shoulder bands at ~298cm^{-1} and 440-450cm^{-1} are actually from the stretching vibrations of five-, six- and four-membered silica rings of the ZSM-5 support[47,48,49]

The presence of Cr_2O_3 nanoparticles on supported CrO_3/ZSM-5 catalysts was also proposed. Ghorbel *et al.* [32] reported the presence of Cr_2O_3 nanoparticles as evident from the sharp characteristic Raman band at 541-550 cm^{-1}. Mimura and Yamashita *et al.*[54] observed the presence of Cr_2O_3 NPs on a dehydrated supported CrO_3/ZSM-5 with high Si/Al ratio *via in situ* XAS measurements.

1.2.3. Supported MoO_3/ZSM-5

Different surface MoO_x structures have been proposed in the literature by many groups[4,26,27,58] as shown in **Figure 1- 5**.

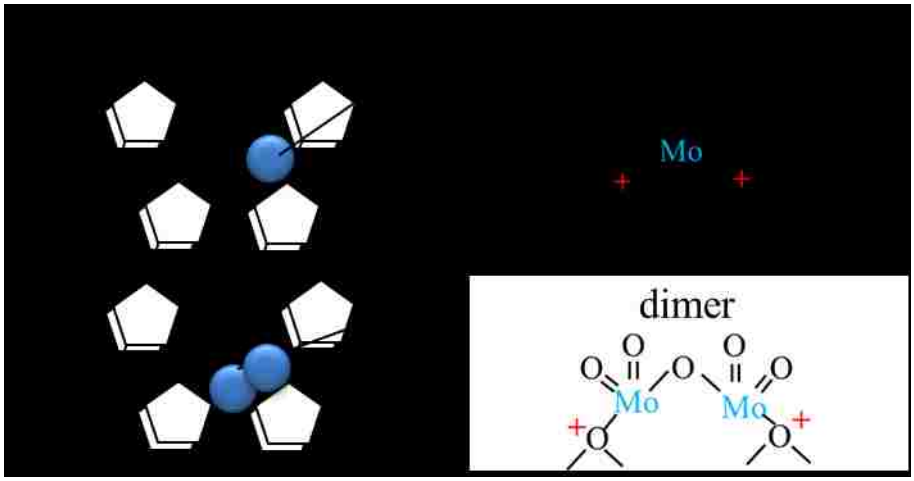

Figure 1- 5 Schematic of proposed molecular structures of monomeric MoO_4 on two neighboring Brønsted acid sites and dimeric Mo_2O_7 on two neighboring Brønsted acid sites in ZSM-5

Isolated MoO_4/MoO_6 was proposed as the dominate species below monolayer Mo content and polyoxomolybdenum Mo_5O_x species at higher Mo contents based on ambient UV-Vis studies.[4] The presence of polymeric Mo_5O_x species are not feasible since hydrated supported molybdate oxide species are known to be present as hydrated $(MoO_4)^{2-}$, $(Mo_7O_{24})^{6-}$ and $(Mo_8O_{26})^{4-}$ clusters.[59] The *in situ* EXAFS/XANES studies[26] claimed dimeric $(Mo_2O_5)^{2+}$ structure for the solid-state-exchanged MoO_x/ZSM-5 (Si/Al=19) catalyst, but the absence of Mo-O-Mo distances in the EXAFS do not support the dimeric structure. There has also been inconsistency in the assignment of the *in situ* Raman bands for supported MoO_3/ZSM-5 catalysts. With visible Raman spectroscopy, vibrations were detected at 970 and 1045 cm^{-1} that were assigned to dimeric and isolated surface molybdena species, respectively.[27] With UV Raman spectroscopy, vibrations at 868 and 962 cm^{-1} were assigned to the dimeric Mo-O-Mo stretch and isolated mono-oxo $O=MoO_4$ species, respectively.[58] Theoretical vibration frequencies of isolated dioxo MoOx species appears at 975 $cm^{-1}(\nu_s)$ and 956 $cm^{-1}(\nu_{as})$ reported by Bao *et al.*[60]; however,

the dioxo $(O=)_2MoO_2$ model requires two adjacent Brønsted acid sites which is against Lowenstein's rule. In a subsequent study, Bao *et al.*[61] proposed a dimeric $(O\equiv)_2$Mo-O-Mo$(\equiv O)_2$ structure which can overcome the long distance between two close but non-neighboring Brønsted acid sites (e.g: -Al-O-Si-O-Al-) in the zeolite support with high Si/Al ratio. However, the presence of terminal Mo≡O bond is not supported by any experimental result. The most recent combined Raman and DFT studies of supported MoO_3/ZSM-5 catalysts indicate that the vibration at 962-970 cm^{-1} is actually from isolated surface dioxo $(O=)_2$Mo(OH)O species anchored at a single Brønsted acid site, the band at 1045 cm^{-1} corresponds to $Al_2(MoO_4)_3$ NPs[59] and the band at 868 cm^{-1} is characteristic of Mo-O-Al/Si bonds.[59,62]

1.2.4. Supported WO_3/ZSM-5

There is almost unanimous agreement among all researchers that the dehydrated surface WOx species on ZSM-5 are present as isolated species shown in **Figure 1- 6**.

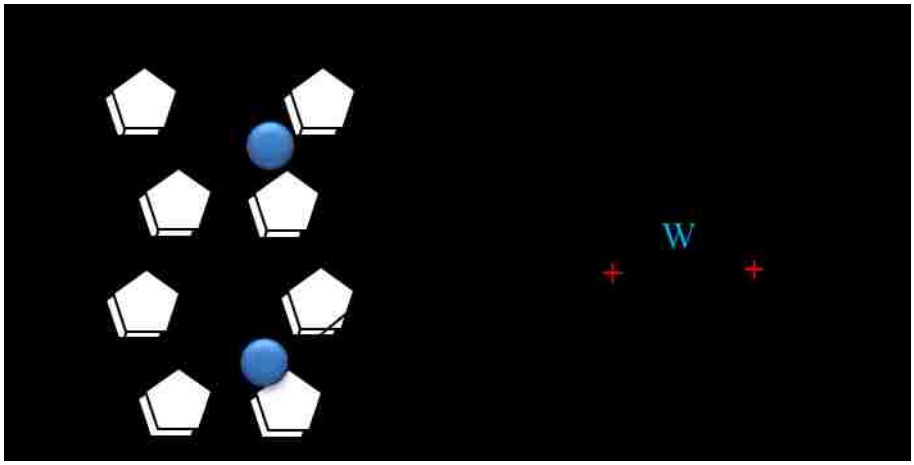

Figure 1- 6 Schematic of proposed molecular structure of monomeric dioxo WO_4 on two neighboring Brønsted acid sites in ZSM-5

min *et al.*[15] concluded that surface WOx species present on ZSM-5 are isolated from the high Eg values of their *in situ* UV-vis spectra (LMCT ~215 nm). *In situ* EXAFS measurements[16] showed the absence of bridging W-O-W bonds in the second coordination shell which precludes the presence of dimeric or oligomeric WOx species. Although the dehydrated WOx species on ZSM-5 were proposed to possess a dioxo $(O=)_2WO_2$ structure, neither the XANES pre-edge feature nor the number of terminal W=O bonds were reported. The local structure and oxidation state of the dehydrated WOx centers were probed with W L_{III} XANES and fitted to the EXAFS spectra. The XANES/EXAFS method averages the structural information and cannot establish if several distinct isolated WOx species are present on ZSM-5, which require molecular characterization with techniques such as *in situ* Raman spectroscopy.

1.2.5. Supported Re_2O_7/ZSM-5

The proposed surface ReOx structures on ZSM-5 are summarized in **Figure 1- 7**.

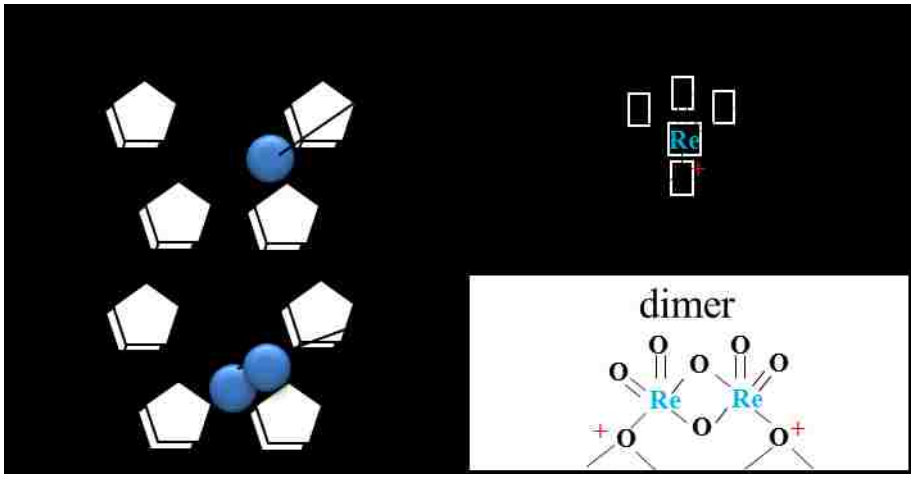

Figure 1- 7 Schematic of proposed molecular structure of ReO_4 on a Brønsted acid site and dimeric $Re_2O_6^{2+}$ on two neighboring Brønsted acid sites in ZSM-5

For the supported Re_2O_7/ZSM-5 catalyst system, several research groups proposed that the surface rhenia species present on ZSM-5 are isolated trioxo $(O=)_3ReO$ species anchored to two oxygen sites associated with framework alumina (e.g. Si-O*-Al-O*-Si) from *ex situ* XAS measurements[63], *in situ* Raman[18] and *in situ* XAS measurements[18]. Lacheen *et al.*[18,29] proposed that surface ReOx species on ZSM-5 are present as monomeric ReO_4 on a single Brønsted acid site and dimeric $Re_2O_6^{2+}$ species on two adjacent Al Brønsted acid sites, but direct supporting molecular structural information of the dimeric species was not provided. The absence of bridging Re-O-Re Raman vibrations of dimeric $Re_2O_6^{2+}$ species at 456 (ν_s) and 185 (δ) cm^{-1} and the absence of Re-O-Re coordination in their *in situ* EXAFS do not support the presence of the surface dimer Re_2O_7 structure. Furthermore, all rhenia oligomers are also volatile[18], thus, the Re_2O_7 dimer is not stable on the ZSM-5 support. Finally, it was previously indicated that the probability of finding a high concentration of two adjacent Al Brønsted acid sites is low according to Lowenstein's rule.[35] All studies containing direct molecular structural data clearly indicate that the surface ReOx species are isolated on the ZSM-5 support and possess trioxo $(O=)_3ReO$ structure.

1.3. Catalytic active sites for methane dehydroaromatization (DHA)

The catalytic activities of the supported MOx/ZSM-5 for methane dehydroaromatization (DHA) were investigated by Lunsford *et al.* [10] and Iglesia *et al.*[16,27,31,29] The catalytic activities decrease in an order of Mo > W > V > Cr.[10] Iglesia *et al.*[18] reported that the

supported Re_2O_7/ZSM-5 catalysts are also active for selective conversion of methane to benzene. The benzene formation rate decreases in an order of Re > Mo > W>>V.[10,18] The volatility of ReOx species, however, precludes practical Re-containing catalysts. The most promising catalyst for methane DHA is supported MoO_3/ZSM-5 due to its near equilibrium conversion and high selectivity towards benzene. Consequently, there are more studies exploring the catalytic active sites for methane DHA by supported MoO_3/ZSM-5, less on supported WO_3/ZSM-5 and Re_2O_7/ZSM-5, and fewer on supported V_2O_5/ZSM-5 and CrO_3/ZSM-5.

The nature of the catalytic active sites of the transition metal ion sites is still under debates despite extensive studies. It is generally accepted that the supported MoO_3/ZSM-5 are bifunctional catalysts[33,64]. The presence of both transition metal ion sites and the Brønsted acid sites of the ZSM-5 are required[33]. The transition metal ion sites are responsible for the activation of methane and formation of C_2+ species. The Brønsted acid sites of the ZSM-5 are responsible for the dimerization or oligomerization of C_2+ species to aromatics by its unique shape selectivity which are not available for non-zeolitic supported metal oxide catalysts[33].

1.3.1. Supported V_2O_5/ZSM-5 and CrO_3/ZSM-5

There are very limited studies on the active components of supported V_2O_5/ZSM-5 and CrO_3/ZSM-5 for methane DHA possibly due to their low catalytic activity. *Ex situ* XPS studies[10] investigated the oxidation states of V_2O_5/ZSM-5 and CrO_3/ZSM-5 catalysts before and after reaction with methane on stream at 750 ^oC for 3-4 hours. The presence of reduced metal phase Cr^{3+} and V^{3+} on the spent CrO_3/ZSM-5 and V_2O_5/ZSM-5 catalysts at

benzene initiation suggested that reduced Cr^{3+} and V^{3+} species are the active components for methane DHA. The local geometry and coordination number of these proposed active components, however, are still unclear. Lacheen *et al.*[31] assumed the same metal carbide species VC_x as the active component for methane DHA analogous to the MoCx and WCx species on supported MoO_3/ZSM-5 and WO_3/ZSM-5, respectively. This conclusion, however, is based on postulation and requires further direct experimental support.

1.3.2. Supported MoO_3/ZSM-5

Many *ex situ* XPS[10] and *ex situ*[65,66] XANES/EXAFS studies were employed to investigate the molecular structure of a spent MoO_3/ZSM-5 after methane DHA. Crystalline and amorphous molybdenum carbide and molybdenum oxycarbide species were reported as the catalytic active sites for methane DHA. However, amorphous molybdenum carbide species are not stable upon exposure to air which is highly likely to happen in *ex situ* characterizations. Therefore, ex situ studies cannot well represent the catalytic active sites of a working catalyst.

Limited *in situ*[26,67,68] XANES/EXAFS studies have focused on elucidating the active components of the supported MoO_3/ZSM-5 for CH_4 DHA. Poorly ordered MoC_y and possible MoO_xC_y species with approximate pore size of ZSM-5 host (~0.6 nm) were identified as the active phases of supported MoO_3/ZSM-5 for methane DHA.

Theoretical DFT calculations have also been applied to investigate the active components for methane activation, but the reported DFT models are not based on realistic molecular structures (e.g.: mononuclear MoO_2^{2+},[60] dinuclear $Mo_2O_5^{2+}$,[61] polynuclear Mo_3O_9,[69] dimeric molybdenum oxycarbide Mo_2OxCy,[70] and mononuclear

and dinuclear molybdenum carbene models.[71] Only recently, supported Mo_2C species with different domain sizes on ZSM-5 models were reported[72]. From this DFT study, the dimeric Mo_2C_x and Mo_4C_x carbide species is more stable on double Al-Al site and external Si-site[72].

1.3.3. Supported WO_3/ZSM-5

The active components of supported WO_3/ZSM-5 for methane DHA remain controversial despite both *ex situ* XPS[10, 25] and *in situ* XANES/EXAFS[16] studies. *Ex situ* XPS[10] observed a majority of W^{6+} species and a small amount of W^{4+} species on a spent WO_3/ZSM-5 prepared *via* impregnation after reaction with methane for 2-24 hours at 750 ^oC. This study ascribed the low reactivity of the catalyst to the small amount of reduced W^{4+} species. In contrast to this conclusion, *in situ* XANES/EXAFS studies[16] have observed that isolated WOx species on ZSM-5 prepared by solid-state reaction were reduced to poorly ordered WC_y (~0.6 nm) clusters with methane on stream for 3 hours at 700 ^oC. It is crucial to conduct *in situ* XAS in order to elucidate the molecular details of the active component of supported WO_3/ZSM-5 catalysts during methane DHA.

1.3.4. Supported Re_2O_7/ZSM-5

The active component of supported Re_2O_7/ZSM-5 for methane DHA has attracted little attention in the literature. *In situ* EXAFS studies[29] observed that surface ReO_x species was converted to metallic Re clusters in a size of ~0.6 nm at the initial stage of benzene formation. Therefore, the metallic Re cluster is proposed as the active component for methane DHA.

1.4. Rate-determining-step for methane DHA

The high-dissociation energy of the C-H bonds (435 kJ/mol) of CH_4 makes the activation of methane highly endothermic and requires high temperatures to initiate C-H bond activation for non-oxidative conversion of methane. Therefore, the C-H bond breaking has generally been considered the rate-determining-step for the conversion of methane to higher hydrocarbons. Chaudhary *et al.*[73] provided a review on non-oxidative activation of methane. In this review, isotopic kinetic experiments to determine the rate determining step for non-oxidative methane activation based on surface science studies on single crystals under ultra-high vacuum were discussed. Ceyer and coworkers[74,75] observed a large kinetic isotopic effect for methane activation with molecular beams for the interaction of CH_4/CD_4 with Ni(111). Beebe and co-workers[76] observed a large kinetic isotope effect for activation of CH_4 vs. CD_4 on Ni(100), whereas no such effect was observed for the Ni(110) surface.

Several research groups[77,78] have claimed that the removal of surface hydrogen formed in dehydrogenation steps is the rate-determining-step. The removal of surface hydrogen will shift the thermodynamic equilibrium towards benzene formation according to the methane dehydroaromatization equilibrium as follows:

$$6CH_4 \leftrightarrow C_6H_6 + 9H_2$$

The absence of kinetic isotopic measurements for CH_4 activation by supported MOx/ZSM-5 catalysts has prevented the determination of the rate-determining-step for the conversion of methane to liquid aromatics.

Summary of methane DHA by supported MOx/ZSM-5 catalysts

There is a lack of general consensus on the anchoring sites, molecular structure and active components for methane dehydroaromatization (DHA) by supported MOx/ZSM-5 catalysts (M=Cr, V, Mo, W and Re). Based on the critical review above, the proposed molecular structures of MOx/ZSM-5 catalysts are summarized in **Figure 1- 8**.

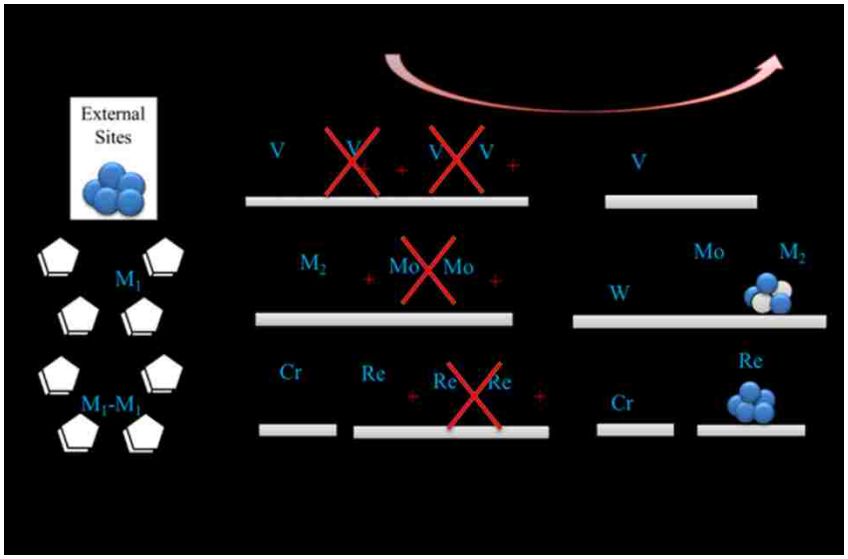

Figure 1- 8 Summary of the proposed anchoring sites, molecular structures of the surface metal oxides, and the catalytic active sites during methane DHA reaction in literatures

Systematic *in situ* and *operando* molecular spectroscopic studies of supported MOx/ZSM-5 catalysts during methane DHA should provide significant fundamental insights about the anchoring sites, molecular structures and catalytic active sites for methane DHA. The objectives of the paper are to provide a critical review of the reported studies on the anchoring sites, the molecular structure and the catalytic active phase of supported MOx/ZSM-5 (M=V, Cr, Mo, W and Re) for methane DHA reactions.

References

1. Wark, M.; Brückner, A.; Liese, T.; Grünert, W., *Journal of Catalysis* **1998,** *175* (1), 48-61.
2. Chang, Y. F.; Somorjai, G. A.; Heinemann, H., *Journal of Catalysis* **1995,** *154* (1), 24-32.
3. Wang, L.; Tao, L.; Xie, M.; Xu, G.; Huang, J.; Xu, Y., *Catalysis Letters* **1993,** *21* (1-2), 35-41.
4. de Lucas, A.; Valverde, J. L.; Rodriguez, L.; Sanchez, P.; Garcia, M. T., *Applied Catalysis A: General* **2000,** *203* (1), 81-90.
5. Traa, Y.; Burger, B.; Weitkamp, J., *Microporous and Mesoporous Materials* **1999,** *30* (1), 3-41.
6. Katranas, T. K.; Triantafyllidis, K. S.; Vlessidis, A. G.; Evmiridis, N. P., Dehydrogenation of propane over Ga and Cr modified, "fresh" and steamed, MFI-type zeolites. In *Studies in Surface Science and Catalysis*, Aldo Gamba, C. C. a. S. C., Ed. Elsevier: 2005; Vol. Volume 155, pp 347-354.
7. Mimura, N.; Takahara, I.; Inaba, M.; Okamoto, M.; Murata, K., *Catalysis Communications* **2002,** *3* (6), 257-262.
8. Yamashita, H.; Ohshiro, S.; Kida, K.; Yoshizawa, K.; Anpo, M., *Research on Chemical Intermediates* **2003,** *29* (7-9), 881-890.
9. Chaudhari, P. K.; Saini, P. K.; Chand, S. J. **Comparative performance of ion-exchanged ZSM-5 and Y-zeolite catalysts for toluene disproportionation reaction** *Journal of Science and Industrial Research* [Online], 2002, p. 810-816.
10. Weckhuysen, B. M.; Wang, D.; Rosynek, M. P.; Lunsford, J. H., *Journal of Catalysis* **1998,** *175* (2), 338-346.
11. Abdullah, A. Z.; Abu Bakar, M. Z.; Bhatia, S., *Industrial & Engineering Chemistry Research* **2003,** *42* (24), 6059-6067.
12. Abdullah, A. Z.; Bakar, M. Z. A.; Bhatia, S., *Catalysis Communications* **2003,** *4* (11), 555-560.
13. Rachapudi, R.; Chintawar, P. S.; Greene, H. L., *Journal of Catalysis* **1999,** *185* (1), 58-72.
14. Swanson, M. E.; Greene, H. L.; Qutubuddin, S., *Applied Catalysis B: Environmental* **2004,** *52* (2), 91-108.
15. Amin, N. A. S.; Pheng, S. E., *Catalysis Communications* **2006,** *7* (6), 403-407.
16. Ding, W.; Meitzner, G. D.; Marler, D. O.; Iglesia, E., *The Journal of Physical Chemistry B* **2001,** *105* (18), 3928-3936.
17. Solymosi, F.; Tolmacsov, P., *Catalysis Letters* **2004,** *93* (1-2), 7-11.
18. Lacheen, H. S.; Cordeiro, P. J.; Iglesia, E., *Chemistry – A European Journal* **2007,** *13* (11), 3048-3057.
19. Mamonov, N. A.; Fadeeva, E. V.; Grigoriev, D. A.; Mikhailov, M. N.; Kustov, L. M.; Alkhimov, S. A., *Russian Chemical Reviews* **2013,** *82* (6), 567.
20. Ismagilov, Z. R.; Matus, E. V.; Tsikoza, L. T., *Energy & Environmental Science* **2008,** *1* (5), 526-541.
21. Spivey, J. J.; Hutchings, G., *Chemical Society Reviews* **2014,** *43* (3), 792-803.
22. Wachs, I. E.; Kim, T., *Metal Oxide Catalysis*. Wiley: New York, 2009.
23. Wachs, I. E.; Roberts, C. A., *Chemical Society Reviews* **2010,** *39* (12), 5002-5017.
24. Slinkin, A. A.; Kucherov, A. V.; Gorjachenko, S. S.; Aleshin, E. G.; Slovetskaja, K. I., *Zeolites* **1990,** *10* (2), 111-116.
25. Weckhuysen, B. M.; Wang, D.; Rosynek, M. P.; Lunsford, J. H., *Journal of Catalysis* **1998,** *175* (2), 347-351.
26. Li, W.; Meitzner, G. D.; Borry Iii, R. W.; Iglesia, E., *Journal of Catalysis* **2000,** *191* (2), 373-383.
27. Borry, R. W.; Kim, Y. H.; Huffsmith, A.; Reimer, J. A.; Iglesia, E., *The Journal of Physical Chemistry B* **1999,** *103* (28), 5787-5796.
28. Ding, W.; Li, S.; D Meitzner, G.; Iglesia, E., *The Journal of Physical Chemistry B* **2000,** *105* (2), 506-513.
29. Lacheen, H. S.; Cordeiro, P. J.; Iglesia, E., *Journal of the American Chemical Society* **2006,** *128* (47), 15082-15083.
30. Petras, M.; Wichterlova, B., *The Journal of Physical Chemistry* **1992,** *96* (4), 1805-1809.
31. Lacheen, H. S.; Iglesia, E., *The Journal of Physical Chemistry B* **2006,** *110* (11), 5462-5472.

32. Ayari, F.; Mhamdi, M.; Debecker, D. P.; Gaigneaux, E. M.; Alvarez-Rodriguez, J.; Guerrero-Ruiz, A.; Delahay, G.; Ghorbel, A., *Journal of Molecular Catalysis A: Chemical* **2011,** *339* (1–2), 8-16.
33. Wang, D.; Lunsford, J. H.; Rosynek, M. P., *Journal of Catalysis* **1997,** *169* (1), 347-358.
34. Liu, W.; Xu, Y., *Journal of Catalysis* **1999,** *185* (2), 386-392.
35. Bell, R. G.; Jackson, R. A.; Catlow, C. R. A., *Zeolites* **1992,** *12* (7), 870-871.
36. Xiong, Z.-T.; Zhang, H.-B.; Lin, G.-D.; Zeng, J.-L., *Catalysis Letters* **2001,** *74* (3-4), 233-239.
37. Ross-Medgaarden, E. I.; Wachs, I. E., *The Journal of Physical Chemistry C* **2007,** *111* (41), 15089-15099.
38. Vuurman, M. A.; Wachs, I. E., *Journal of Physical Chemistry* **1992,** *96* (12), 5008-5016.
39. Kucherov, A. V.; Slinkin, A. A., *Zeolites* **1987,** *7* (1), 38-42.
40. Kucherov, A. V.; Slinkin, A. A., *Journal of Molecular Catalysis* **1994,** *90* (3), 323-354.
41. Zhang, S. G.; Higashimoto, S.; Yamashita, H.; Anpo, M., *The Journal of Physical Chemistry B* **1998,** *102* (29), 5590-5594.
42. Wachs, I. E., *Applied Catalysis A: General* **2011,** *391* (1–2), 36-42.
43. Wachs, I. E., *Dalton Transactions* **2013,** *42* (33), 11762-11769.
44. Lee, E. L.; Wachs, I. E., *Journal of Physical Chemistry C* **2007,** *111* (39), 14410-14425.
45. Gao, X. T.; Bare, S. R.; Weckhuysen, B. M.; Wachs, I. E., *Journal of Physical Chemistry B* **1998,** *102* (52), 10842-10852.
46. Nakamoto, K., *Infrared and Raman Spectra of Inorganic and Coordination Compounds*. Wiley: New York, 1986.
47. Yu, Y.; Xiong, G.; Li, C.; Xiao, F.-S., *Microporous and Mesoporous Materials* **2001,** *46* (1), 23-34.
48. Dutta, P. K.; Puri, M., *The Journal of Physical Chemistry* **1987,** *91* (16), 4329-4333.
49. Dutta, P. K.; Rao, K. M.; Park, J. Y., *The Journal of Physical Chemistry* **1991,** *95* (17), 6654-6656.
50. Aparicio, L. M.; Ulla, M. A.; Millman, W. S.; Dumesic, J. A., *Journal of Catalysis* **1988,** *110* (2), 330-347.
51. Wichterlova, B.; Tvaruzkova, Z.; Novakova, J., *Journal of the Chemical Society, Faraday Transactions 1: Physical Chemistry in Condensed Phases* **1983,** *79* (7), 1573-1583.
52. Flanigen, E. M., *Molecular Sieves*. AMERICAN CHEMICAL SOCIETY: 1973; Vol. 121.
53. Vuurman, M. A.; Wachs, I. E., *Journal of Molecular Catalysis* **1992,** *77* (1), 29-39.
54. Mimura, N.; Okamoto, M.; Yamashita, H.; Oyama, S. T.; Murata, K., *The Journal of Physical Chemistry B* **2006,** *110* (43), 21764-21770.
55. Lee, E. L.; Wachs, I. E., *Journal of Physical Chemistry C* **2008,** *112* (51), 20418-20428.
56. Wells, A. F., *Structural inorganic chemistry*. 5th ed. ed.; Clarendon Press: New York, 1984.
57. Müller, A.; Schmidt, K. H.; Ahlborn, E.; Lock, C. J. L., *Spectrochimica Acta Part A: Molecular Spectroscopy* **1973,** *29* (10), 1773-1788.
58. Rzhevskii, A. M.; Choi, P.; Ribeiro, F. H.; Gulotty, R. J.; Olken, M. M., *Catalysis Letters* **2001,** *73* (2-4), 187-191.
59. Tian, H.; Roberts, C. A.; Wachs, I. E., *The Journal of Physical Chemistry C* **2010,** *114* (33), 14110-14120.
60. Zhou, D.; Ma, D.; Liu, X.; Bao, X., *The Journal of Chemical Physics* **2001,** *114* (20), 9125-9129.
61. Zhou, D.; Zhang, Y.; Zhu, H.; Ma, D.; Bao, X., *The Journal of Physical Chemistry C* **2007,** *111* (5), 2081-2091.
62. Tian, H.; Wachs, I. E.; Briand, L. E., *The Journal of Physical Chemistry B* **2005,** *109* (49), 23491-23499.
63. Tada, M.; Bal, R.; Sasaki, T.; Uemura, Y.; Inada, Y.; Tanaka, S.; Nomura, M.; Iwasawa, Y., *The Journal of Physical Chemistry C* **2007,** *111* (27), 10095-10104.
64. Ma, D.; Zhu, Q.; Wu, Z.; Zhou, D.; Shu, Y.; Xin, Q.; Xu, Y.; Bao, X., *Physical Chemistry Chemical Physics* **2005,** *7* (16), 3102-3109.
65. Aritani, H.; Tanaka, T.; Funabiki, T.; Yoshida, S.; Eda, K.; Sotani, N.; Kudo, M.; Hasegawa, S., *The Journal of Physical Chemistry* **1996,** *100* (50), 19495-19501.
66. Aritani, H.; Shinohara, S.; Koyama, S.-i.; Otsuki, K.; Kubo, T.; Nakahira, A., *Chemistry Letters* **2006,** *35* (4), 416-417.
67. Lacheen, H. S.; Iglesia, E., *Journal of Catalysis* **2005,** *230* (1), 173-185.

68. Kim, Y.-H.; Borry Iii, R. W.; Iglesia, E., *Microporous and Mesoporous Materials* **2000,** *35–36* (0), 495-509.
69. Fu, G.; Xu, X.; Lu, X.; Wan, H., *Journal of the American Chemical Society* **2005,** *127* (11), 3989-3996.
70. Rutkowska-Zbik, D.; Grybos, R.; Tokarz-Sobieraj, R., *Structural Chemistry* **2012,** *23* (5), 1417-1424.
71. Xing, S.; Zhou, D.; Cao, L.; Li, X., *Chinese Journal of Catalysis* **2010,** *31* (4), 415-422.
72. Gao, J.; Zheng, Y.; Fitzgerald, G. B.; de Joannis, J.; Tang, Y.; Wachs, I. E.; Podkolzin, S. G., *The Journal of Physical Chemistry C* **2014**.
73. Choudhary, T. V.; Aksoylu, E.; Wayne Goodman, D., *Catalysis Reviews* **2003,** *45* (1), 151-203.
74. Johnson, A. D.; Daley, S. P.; Utz, A. L.; Ceyer, S. T., *Science* **1992,** *257* (5067), 223-225.
75. Lee, M. B.; Yang, Q. Y.; Ceyer, S. T., *Journal of Chemical Physics* **1987,** *87* (5), 2724-2741.
76. Beebe, T. P.; Goodman, D. W.; Kay, B. D.; Yates, J. T., *Journal of Chemical Physics* **1987,** *87* (4), 2305-2315.
77. Iglesia, E.; Baumgartner, J., *Catalysis Letters* **1993,** *21* (1-2), 55-70.
78. Choudhary, V. R.; Kinage, A. K.; Choudhary, T. V., *Science* **1997,** *275* (5304), 1286-1288.

Chapter 2.

Catalyst Synthesis and Experimental Techniques

Abstract

In this Chapter, the synthesis procedures of all ZSM-5 based supported transition metal oxides catalysts and characterization techniques are described in detail. The supported MOx/ZSM-5 catalysts are prepared *via* an incipient wetness impregnation method. The anchoring sites, molecular and electronic structures of dehydrated and fully oxidized MOx/ZSM-5 catalysts were characterized *via* several molecular spectroscopic techniques such as *in situ* FT-IR spectroscopy, *in situ* UV-vis diffuse reflectance spectroscopy (DRS), *in situ* Raman spectroscopy, temperature-programmed reduction spectroscopy (TPR) and *in situ* X-ray absorption spectroscopy (XAS). The theoretical calculations construct catalyst models of dispersed transition metal oxide species anchoring on the internal and external surface of ZSM-5 supports. The validity of the catalyst models was verified by comparing the calculated vibrational frequencies with the experimental values from spectroscopic results. The reactivity of the supported MOx/ZSM-5 catalysts for methane dehydroaromatization (DHA) has been investigated *via operando* Raman-MS which allows simultaneous analysis of the surface of the catalyst and the reaction product coupling with an online mass spectrometer. The nature of catalytic active phase of supported MoO_3/ZSM-5 during methane DHA has been investigated by *in situ* XAS during methane DHA reaction. The rate determining step of methane DHA has been examined by isotopic CD_4/CH_4 temperature-programmed surface reaction spectroscopy (CD_4/CH_4-TPSR).Thanks to the collaboration with Dr. Jie Gao and Professor Simon Podkolzin at Stevens Institute of Technology for Density Functional Theory (DFT), with Professor Anatoly Frenkel at Yeshiva University & Brookhaven National Laboratory for

in situ XAS for dehydrated MOx/ZSM-5 catalysts, and with Dr. Jeffrey Miller and Dr. James Gallagher at Argonne National Laboratory for *in situ* XAS during methane DHA reaction for supported MoO_3/ZSM-5 catalysts.

2.1. Catalyst synthesis

The zeolite-supported transition metal oxides in group V-VII (V, Cr, Mo, W and Re) consisting of highly dispersed metal oxides on ZSM-5 were prepared by the incipient-wetness impregnation method[1,2,3]. The ZSM-5 supports (Si/Al=15-140, Zeolyst International), were dried and calcined at 500 ^{o}C for 2 hours prior to the impregnation. The ZSM-5 zeolites varied from high-silica content (Si/Al=140), which contains less than one aluminum per unit cell, to high-alumina content (Si/Al=15), which consists of approximately six aluminum atoms per unit cell[4]. The details about the ZSM-5 supports are provided in **Table 2- 1**.

Table 2- 1 Details about the parent ZSM-5

Nomenclature for Zeolite Support	Zeolyst Product Name	Si/Al mole ratio	SiO_2:Al_2O_3 mole ratio	Surface Area (m^2/g) [a]
ZSM-5 (Si/Al=140)	CBV28014	140	280	400
ZSM-5 (Si/Al=40)	CBV8014	40	80	425
ZSM-5 (Si/Al=25)	CBV5524G	25	50	425
ZSM-5 (Si/Al=15)	CBV3024E	15	30	400

[a] **Surface area provided by manufacturer.**

The zeolite supports were impregnated with a non-aqueous (toluene) solution of vanadium triisopropoxide ($VO(CHO(CH_3)_2)_3$, Alfa Aesar, 97%) precursor and aqueous solutions of corresponding precursors of chromium (III) nitrate ($Cr(NO_3)_3 \bullet 9H_2O$, Alfa Aesar, 98.5%), ammonium heptamolybdate ($(NH_4)_6Mo_7O_{24} \bullet 4H_2O$, Aldrich, 99.98%), ammonium metatungstate ($(NH_4)_6H_2W_{12}O_{40} \bullet xH_2O$, Pfaltz and Bauer, 99.5%), and perrhenic acid ($HReO_4$, Alfa Aesar, 75-80%). The zeolite supports were initially dried for 2 hours at 115 ^{o}C for the non-aqueous preparations prior to surface modification inside a glove box (Vacuum Atmospheres, Omni-Lab VAC 101965) under nitrogen

environments. After the impregnation, the vanadium samples were allowed to dry overnight under the nitrogen atmosphere. The vanadium samples were then calcined at 110 ^{o}C and held for 1 hour under flowing N_2 (Airgas, Ultra High Purity) in a programmable furnace (Thermolyne, Model 48000), and subsequently followed by 1 ^{o}C/min ramp under flowing air (Airgas, Zero grade) to 450 ^{o}C and held for 2 hours. The aqueous prepared catalysts were calcined under flowing air (Airgas, Zero grade) at 1 ^{o}C/min for 2 hours to 400 ^{o}C for the Re_2O_7/ZSM-5 catalysts, 450 ^{o}C for the MoO_3/ZSM-5 catalysts, and 500 ^{o}C for the CrO_3/ZSM-5 and WO_3/ZSM-5 catalyst systems. Thermal treatments were always performed below 550^{o}C to avoid ZSM-5 dealumination that is known to initiate at 600^{o}C[5]. All the catalysts were synthesized with between 1 to 5 % metal oxides on the zeolites, henceforth, identified as MOx/ZSM-5 (Si/Al=X), in which X represents the Si/Al molar ratio of zeolite supports.

2.2. *In situ* FT-IR spectroscopy

The surface hydroxyl groups of dehydrated MO_x/ZSM-5 catalysts were discriminated by *in situ* FT-IR spectroscopy. Transition metal oxides anchor at ZSM-5 *via* either ion exchange with Brønsted acid sites of ZSM-5 or via dehydration with Si-OH and Al-OH hydroxyls at external surfaces of ZSM-5[6,5]. The parent HZSM-5 (Si/Al=15) has four characteristic surface hydroxyl IR absorptions:(1) Brønsted acid Al-(OH)$^{+}$-Si site in which alumina is coordinated as an AlO_4 unit (3610 cm^{-1}) ; (2) terminal Si-OH (3741 cm^{-1}); (3) extra-framework Al-OH with AlO_6 coordination (3660 cm^{-1}; Al-OH-I) and (4) extra-framework Al-OH-II of Al_2O_3 nanoclusters (3783 cm^{-1}; Al-OH II)[7,8]. The integrated IR bands of the four surface hydroxyls are compared against the MOx loading

in order to determine the interaction of the MOx species with the different surface hydroxyl anchoring sites on the ZSM-5 support.

The *In situ* FTIR can also provide structural information of supported transition metal oxides catalysts which possess terminal M=O bonds with characteristic stretch mode at 800-1000 cm^{-1}. Unfortunately, the parent ZSM-5 has strong IR absorbance in the same IR range and the stretch mode of terminal M=O bonds are generally weak; therefore, *in situ* FTIR fails to provide structural information of the supported transition metal oxides on ZSM-5.

The *in situ* IR measurements were performed with a Thermo Scientific Nicolet 8700 Research FTIR spectrometer equipped with a liquid nitrogen cooled mercury-cadmium-telluride (MCT detector), a Harrick Praying Mantis accessory (model DRA-2), and a Harrick reaction chamber HT-100. The supported MOx/ZSM-5 catalysts (~20-35 mg) were initially dehydrated in the Harrick cell under 30 sccm 10 mol% O_2/Ar (Airgas, Inc., 10.00% Certified Mixture) at 500 ^oC for 120 mins and then cooled to 110 ^oC in 30 sccm10 % O_2/Ar (Airgas, Inc., 10.00% Certified Mixture) for collection of the *in situ* IR spectra of the dehydrated catalysts. The IR spectra were recorded with a resolution of 4 cm^{-1} using 72 signal averaged scans. The intensities of the IR spectra were normalized related to the Si-O-Si overtone bands between 1730 and 2100 cm^{-1}.

2.3. *In situ* UV-vis Diffuse Reflectance Spectroscopy (DRS)

In situ UV-vis DRS examines the electronic structures of surface metal oxide species. It can discriminate surface metal oxide species with different domain sizes (isolated monomers, dimers, polymeric chains, and three-dimensional crystalline structures)[9]. It

measures the ligand-to-metal charge transfer (LMCT) absorption bands of surface metal oxide species, which reflect the energy gap between HOMO and LUMO known as the band gap or edge energy (Eg)[9,10]. The Kubelka-Monk function, *F(R∞)*, was extracted from the UV-vis DRS absorbance, and the edge energy (E_g) for allowed transitions was determined by finding the intercept of the straight line from the low-energy rise of the $(F(R\infty)hv)^{1/n}$, in which n=0.5 for the direct allowed transition ion, *versus hv*, the incident photon energy.[11]

The *in situ* UV-vis measurements were obtained with a Varian Cary 5E UV-Vis-NIR spectrophotometer employing the integration sphere diffuse reflectance attachment (Harrick Praying Mantis Attachment, DRA-2). The catalyst samples were loaded as loose powder (~20 mg) into an *in situ* cell (Harrick, HVC-DR2) and the UV-vis spectra were collected from 200-800 nm. The reflectance of the SiO_2 support was used as the baseline standard. The catalyst temperature was accurately controlled by a temperature program controller (Harrick Scientific, Watlow Series 965 controller) and a thermocouple placed in the catalyst powder. The catalyst samples were calcined and dehydrated at 400 ^oC for 1 hour under 30 sccm 10% O_2/He (Airgas, certified, 9.735% O_2/He balance). The *in situ* UV-vis spectra were then collected at 400 ^oC and also at room temperature after dehydration.

2.4. *In situ* Raman spectroscopy

The molecular characterization of the supported metal oxide catalysts were established by combined in situ Raman spectroscopies, providing structural information. Raman spectroscopy is used to determine the number of terminal M=O bonds present in surface

metal oxide structures[12]. Raman spectroscopy features molecular vibrations of supported metal oxide species on ZSM-5 because the parent ZSM-5 does not have any Raman vibration in the vibration range of terminal M=O bonds of transition metal oxides[4,13,14]. The terminal transition metal oxide species present as mono-oxo (O=M), dioxo [$(O=)_2M$] and trioxo [$(O=)_3M$] functionalities[12]. These terminal M=O functionalities have Raman stretch modes in Raman spectra at 940-1040 cm^{-1}.[12,15] Mono-oxo gives rise to symmetric (ν_s) stretch mode and both dioxo and trioxo functionalities exhibit symmetric (ν_s) and asymmetric (ν_{as}) stretch modes[15].

The Raman spectroscopy is also useful for determining the dispersive nature of the metal oxide species on the ZSM-5 support[12]. The characteristic Raman signals of well-dispersed supported metal oxides are different from the Raman signals of crystalline phase from the formation of nanoparticles or bulk metal oxide structure.

The *in situ/operando* Raman spectra of the zeolite-supported metal oxide catalysts were obtained with a high resolution, dispersive Raman spectrometer system (Horiba-Jobin Yvon LabRam HR) equipped with three laser excitations (532, 442 and 325 nm). The sample power of the visible lasers used in the present study at 532 nm (green) and 442 nm (violet) were 10 and 28 mW, respectively, and the sample of the UV laser at 325 nm (not visible) was ~7 mW. The lasers were focused on the samples with a confocal microscope equipped with a 50X long working distance objective (Olympus BX-30-LWD) for the visible lasers and 15X objective (OFR LMU-15X-NUV) for the UV laser. The LabRam HR spectrometer was optimized for the best spectral resolution by employing a 900 groves/mm grating (Horiba-JobinYvon 51093140HR) for the visible lasers and a 2400 grooves/mm grating (Horiba-JobinYvon 53011140HR) for the UV

laser. The spectral resolution for both gratings is ~2 cm^{-1}. The calibration of each laser line was independently measured by an Hg lamp for the zero position and linearity of the gratings. The wavenumber calibration of the Raman spectrograph was checked using the silicon line at 520.7 cm^{-1}. The Rayleigh scattered light was rejected with holographic notch filters (Kaiser Super Notch) containing window cutoffs of ~100 cm^{-1} for the visible lasers and ~300 cm^{-1} for the UV laser. The Raman system was equipped with a UV-sensitive liquid-N_2 cooled CCD detector (Horiba-JobinYvon CCD-3000V). The catalyst samples, typically consisting between 5-10 mg of loose powder, were placed in a high temperature flow cell reactor (Linkam CCR1000) which contained a quartz window and o-ring seals that were cooled by flowing water. The sample temperature was controlled by a temperature controller (Linkam LinkPad). Typical reactor cell conditions were 400-500 ^{o}C, 10 ^{o}C/min heating and cooling rates, atmospheric pressure, and ~30 sccm gas flow rates metered by mass flow controllers (Brooks, Model 5850E series).

2.4.1. *In situ* Raman spectra of dehydrated supported MOx/ZSM-5 catalysts (M=V, Cr, Mo, Re and W) under oxidizing environment

The protocol for obtaining *in situ* Raman spectra under the oxidizing environment is as follows: the samples were initially dehydrated in the *in situ* cell at 400-500 ^{o}C and held for 30 minutes under flowing 10% O_2/Ar (Airgas, certified, 10.00% O_2/Ar balance). Samples exhibiting fluorescence were first pretreated in a separate programmable furnace (Thermolyne, Model 48000) at 500 ^{o}C for 2 hours under dry air. The Raman spectra were collected at a scanning rate of 20 seconds per scan and a total amount of 20 scans with a

200 micron size hole at which only laser angles parallel to the incident beam were acquired from the light scattered by the catalyst sample.

Each dehydrated supported MOx/ZSM-5 catalyst was examined with *in situ* Raman spectroscopy with visible and/or UV laser excitation to obtain the best resolution. Use of multiple laser excitations avoided sample fluorescence that sometimes plagued earlier Raman spectroscopic measurements and also provides the potential for resonance enhancement of weak Raman bands that may have been undetected in earlier studies.[16,17,18]

2.4.2. *Operando* Raman-MS spectra of dehydrated supported MOx/ZSM-5 catalysts (M=V, Cr, Mo, Re and W) during CH_4 DHA

Operando Raman-MS spectroscopy provides Raman measurements under reaction conditions with simultaneous analysis of gaseous reactants and products *via* an online mass spectrometer (Varian, 1200L quadrupole). All supported MOx/ZSM-5 catalysts were subjected to oxidation treatment prior to CH_4 reaction. A typical temperature-programmed *operando* Raman-MS experimental procedure involves the following steps: the sample (20-35 mg) was pretreated in an *in situ* Linkam cell reactor (9754 CCR-B) with 10% O_2/Ar (Airgas, certified, 10.00% O_2/Ar balance) at a flow rate of 30 sccm at 500 ^oC for 60-90 mins, and then the cell was flushed with UHP Ar (Airgas, Inc., ultrahigh purity) at the same temperature for 30 mins. After Ar flushing, a 1.5% CH_4/He gas mixture (Airgas, Inc., high purity) was introduced into the reaction cell at 30 sccm. The temperature was increased at a ramp rate of 1 ^oC/min up to 800 ^oC for VOx-, CrOx-, MoOx- and ReOx-ZSM5 catalysts and to 900 ^oC for WO_3/ZSM5 catalyst. Raman spectra

were acquired at a scanning rate of 30 sec/scan with a total amount of 10 scans with a 200 micron size hole. The gaseous products from the reactor cell were analyzed with the online mass spectrometer every 0.5 seconds. The mass/charge ratios of m/z=16 (CH_4), m/z=18 (H_2O), m/z=27 ($C_2H_3^+$), m/z=28 (CO), m/z=44 (CO_2) and m/z=78 (C_6H_6) were used to monitor the major gaseous components. This MS did not have the ability to detect H_2 and the line connecting the reactor cell and the MS was not heated resulting in H_2O not being detected due to its condensation on the line wall. Mass channels with m/z values from 10--200 were also collected to double check the fragmentation patterns of these primary molecules.

2.5. *In situ* X-ray Absorption spectroscopy

X-ray absorption spectroscopy (XAS) is the measurement of transitions from core electronic states of the metal to the excited electronic states (LUMO) and the continuum[1]. The former is known as the X-ray absorption near-edge structure (XANES) and the latter as extended X-ray absorption fine structure (EXAFS). The EXAFS is caused by the modulation of the x-ray intensity due to backscattering by a small fraction of the backscattered photoelectron wave[1,19]. This interference effect caused by single-scattering electrons with short mean-free paths provides information about the short-range atomic order (coordination number and bond distances) [1,19]. A typical XAS spectrum (shown in **Figure 2- 1**) is used for illustration: the XANES is the region of a XAS spectrum within ~50 eV of the absorption edge, and EXAFS is the region of a XAS spectrum from 50 to 1500 eV above the absorption edge[1,19]. The XANES spectra provide information such as the electronic structure and local symmetry of the metal site, and the EXAFS spectra

provide interatomic distances to ligands and neighboring atoms from the absorbing element. The experiment requires synchrotron radiation sources, which provide intense and tunable X-ray beams. Samples can be in the gas-phase, solution or condensed mater. *In situ* XAS is the measurement of the sample under reaction conditions with the aid of *in situ* reactors.

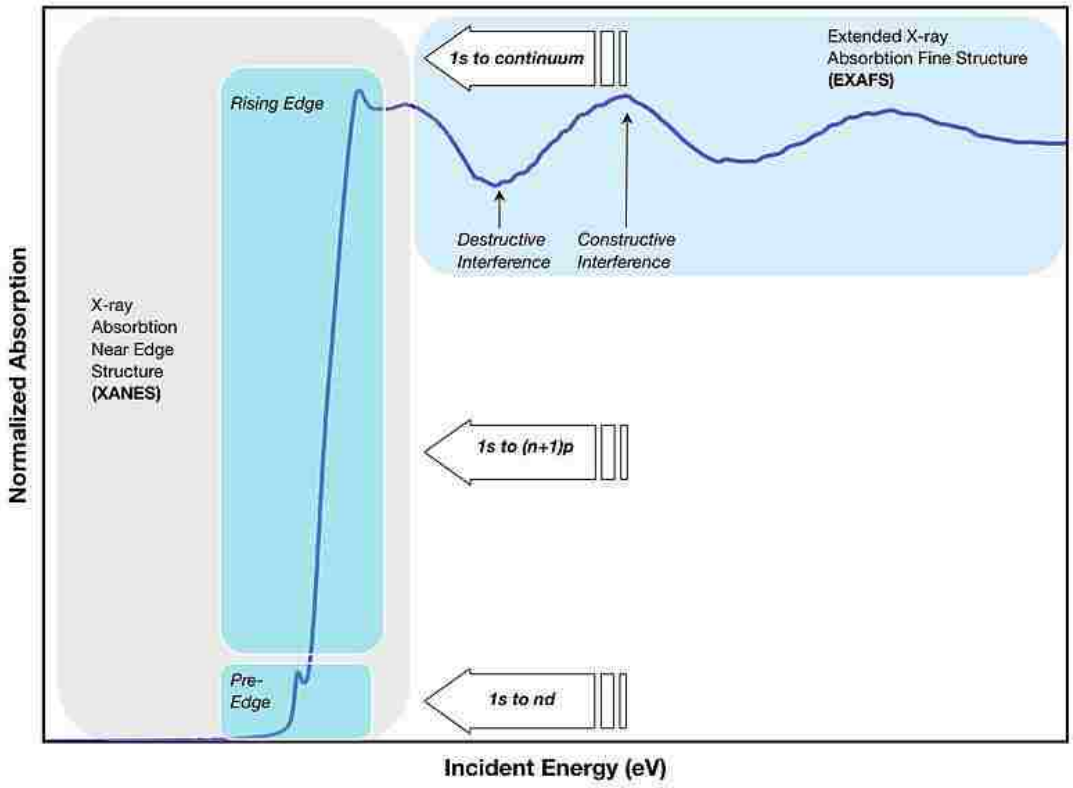

Figure 2- 1 Scheme of data regions for a XAS spectrum[19]

2.5.1. *In situ* XAS of dehydrated supported MOx/ZSM-5 catalysts (M=V, Cr, Mo, Re and W) in O_2 environment

The X-ray absorption spectroscopy (XAS) of V K-edge, Cr K-edge, Mo K-edge, Re L_1-edge and W L_1-edge of dehydrated supported MOx/ZSM-5 catalysts was performed in both transmission and fluorescence mode at the beam line X18A at the National Synchrotron Light Source (NSLS) at the Brookhaven National Laboratory, using

ionization chamber detectors for measuring incident and transmitted beam intensities, using a Passivated Implanted Planar Silicon (PIPS) detector (Canberra Industries) to measure fluorescent beam intensity. In addition, a fourth ionization chamber was used to detect the beam through a reference metal foil (V, Cr, Mo, Re and W foil was used respectively), for energy calibration and alignment purposes. A Nasner-Alder reactor with Inconel (stainless steel) sample holder was used for *in situ* measurements. Typically, the powder catalysts (~100 mg) were pressed into pellets with a diameter of 10 mm. The sample was subjected to dehydration and oxidation under 25 sccm of 20% O_2/He (Airgas, Inc., certified, 20.00% O_2/He balance) at 500 ^oC for 30 mins and cooled to 110 ^oC in UHP He (Airgas, Inc., ultra high purity) for the full XAS scan. $H_3PMo_{12}O_{40}.xH_2O$/$H_3PW_{12}O_{40}.xH_2O$ powder was mixed with boron nitride (BN) in order to dilute the Mo/W concentration to ca. 5 wt % Mo/W in BN. Roughly 100 mg of the mixture was pressed into a pellet with a diameter of 10 mm. The pellet was dehydrated at 150 ^oC for 30 mins in 20% O_2/He (25 sccm, Airgas, Inc., certified, 20.00% O_2/He balance) and then cooled to 110 ^oC in UHP He (Airgas, Inc., ultra high purity) for the full XAS scan in fluorescence mode. Reference compounds with well-defined crystalline structures such as Na_3VO_4, $Mg_2V_2O_7$, $(NH_4)_2CrO_4$, $(NH_4)_2Cr_2O_7$, MoO_3, WO_3, $Al_2(WO_4)_3$ Re_2O_7 and $(C_6H_5)_3SiReO_3$ require no dehydration and were measured at ambient conditions. Reference compounds were ground into fine powder and brushed onto scotch tape for sample preparation. These reference compounds were measured in transmission mode using ionization chamber detectors for measuring incident and transmitted beam intensities. Data processing and analysis were performed using Athena software. [20]

2.5.2. *In situ* XAS spectra of supported MoO_3/ZSM-5 catalysts during CH_4 DHA

In situ X-ray absorption spectroscopy measurements during CH_4 DHA reaction which requires a high temperature reactor (up to 700 ^oC) were acquired on the bending magnet beam line of the Materials Research Collaborative Access Team (MRCAT) at the Advanced Photon Source, Argonne National Laboratory. The data were collected in the transmission step scan mode. Photon energies were selected using a water-cooled, double-crystal Si(111) monochromator, which was detuned by approximately 50% to reduce harmonic reflections. The ionization chambers were optimized for the maximum current with linear response (~10^{10} photons detected/sec) with 10% absorption in the incident ion chamber and 70% absorption in the transmission X-ray detector. A Mo foil spectrum was acquired simultaneously with each sample measurement for energy calibration. Samples containing about 1.0-1.5 mg Mo ions were sufficient to achieve a significant signal in the XAS experiments. The following reference materials were used: (1) bulk Mo_2C synthesized in the X-ray absorption chamber from MoO_2 (99%m Sigma-Alrich) powder under flowing 20% CH_4/H_2 gas mixture at 650 ^oC for 2hrs following the procedure in reference [21], and (2) supported 5% MoO_3/SiO_2 catalyst which primarily consists of isolated surface dioxo $(O=)_2Mo(O\text{-}Si)_2$ sites (see preparation and characterization in reference 12).

2.6. Density Functional Theory (DFT) calculations

Gradient-corrected periodic density functional theory (DFT) calculations were performed with the DMol^3 code in Materials Studio 4.0 program by Accelrys Software, Inc by Dr.

Gao and Professor Podkolzin at Steven Institute of Technology. The calculations used the DNP basis set and the GGA RPBE functional. Tightly bound core electrons were represented with semicore pseudopotentials. Reciprocal-space integration over the Brillouin zone was approximated through Γ-point sampling (1×1×1 Monkhorst-Pack grid). The density mixing fraction of 0.2 with Direct Inversion in the Iterative Subspace (DIIS) and orbital occupancy with smearing of 0.005 Ha were used. The orbital cut-off distance was set at 0.44 nm for all atoms.

The ZSM-5 structure was modeled with a 64 tetrahedral (T) cluster (64 Si and 128 O atoms). The cluster was generated from the full MFI unit cell (96 Si and 192 O atoms) with the experimental lattice constants of a=2.0022, b=1.9899, and c=1.3383 nm. The dangling bonds of the boundary O atoms in the cluster were saturated by H atoms. In order to minimize cluster boundary effects and better simulate the overall zeolite structure, the coordinates of these terminal OH groups were constrained. The terminal O atoms were constrained at their original positions in the MFI unit cell. The terminal H atoms were constrained at the positions obtained with the following two-step procedure. First, the bonding Si atoms from the part of the zeolite framework that was cut out from the cluster were changed into H atoms. Second, the distance between the bonding O atoms in the cluster and the terminal H atoms was adjusted to 0.095 nm. Except for the terminal OH groups, all other cluster atoms were optimized with Mo oxide species. Frequency calculations were performed with a partial Hessian for MoO_x species. Calculated frequencies were adjusted with a factor of 1.01.

2.7. Temperature Programmed Techniques

Temperature-programmed techniques are consisted of a range of techniques for studying surface reactions and molecular adsorption on surfaces which utilize temperature-programming to discriminate between processes with different activation parameters. Of there, three useful techniques are used in this study: the temperature-programmed reduction (TPR) which monitors the consumption of hydrogen by a Thermal Conductivity Detector (TCD) due to the reduction of surface metal oxide species of fully oxidized MOx/ZSM-5 catalysts, the temperature-programmed oxidation (TPO) which monitors the evolution of carbon dioxide and water from the combustion of coke species deposited on CH_4-reacted MOx/ZSM-5 catalysts by a qaudrupole mass spectrometer (QMS), and the temperature programmed surface reaction (TPSR) which monitors the evolution of gas products from methane DHA on MOx/ZSM-5 catalysts. All three techniques involve heating of the sample in a controlled manner (preferably so as to give a linear temperature ramp) and monitoring the evolution of gaseous species from the surface of the sample by a quadrupole mass spectrometer (QMS) or Thermal Conductivity Detector (TCD), and the whole process is carried out with the aid of computer program which allows simultaneous analyses of 16 different mass channels. The data obtained from such an experiment consists of the intensity variation of each recorded mass fragment as a function of time or temperature. The TPR/TPO/TPSR profiles provide important information[22]: (1) the area under a peak is proportional to the amount of gas generated from surface reaction, (2) the kinetics of the surface reaction gives information of the state of evolved species, (3) the position of the peak (the peak

temperature) is related to the enthalpy of formation of the products, i.e. the activation energy of the reaction.

2.7.1. TPR experiments

The TPR experiments were performed on an Altamira temperature programmed system (AMI-200) monitored by an online thermal conductivity detector (TCD). Supported MoOx/ZSM-5 catalysts (30-35 mg) were loaded into a U-shaped quartz tube finished with quartz wool as bedding. The catalysts were oxidized and dehydrated at 500 ^{o}C in 10% O_2/Ar(30 sccm, Airgas, Inc. balanced with Ar), and then were flushed with UHP Ar at 110 ^{o}C for 30 mins the dehydrated catalysts were subjected to H_2-TPR using 5% H_2/Ar(30 sccm, Airgas, Inc. balanced with Ar) from 110 ^{o}C to 800 °C with a heating rate of 10 °C/min.

2.7.2. TPSR experiments

The CD_4/CH_4-TPSR experiments were conducted on the Altamira AMI-200 equipped with an online Dycor DM100 mass spectrometer. Typically, 30-35 mg of the supported MoOx/ZSM-5 catalyst was loaded in a U-type quartz tube using quartz wool as bedding. The catalyst was initially oxidized in 30 sccm 10% O_2/Ar (Airgas, Inc., 10.00% Certified Mixture) at 500 ^{o}C and held for 120 mins to obtain a fully dehydrated and oxidized supported MoOx/ZSM-5 catalyst. Subsequently, the fully oxidized catalyst was purged by Ar (Airgas, Inc., ultrahigh purity) at 500 ^{o}C for 30 mins to remove all gaseous molecular O_2. Finally, the sample was exposed to 30 sccm 5% CD_4 (Matheson, methane-d_4, >99%) or CH_4 (Airgas, Inc., 99.999%) balanced with Ar (Airgas, Inc., ultrahigh purity)

at 500 ^{o}C and the temperature was ramped to 800 ^{o}C with a heating rate of 1 ^{o}C/min. For CH_4-TPSR, the following mass/charge ratios were monitored: m/z=2 (H_2), m/z=15 (CH_3^+), m/z=16 (CH_4), m/z=18 (H_2O), m/z=27 ($C_2H_3^+$), m/z=28 (CO), m/z=29 ($C_2H_5^+$), m/z=30 (C_2H_6), m/z=44 (CO_2), m/z=77 ($C_6H_5^+$) and m/z=78 (C_6H_6). For CD_4-TPSR, the following mass/charge ratios were monitored: m/z=4 (D_2), m/z=18 (CD_3^+), m/z=20 (CD_4), m/z=28 (CO), m/z=32 (C_2D_4), m/z=34 ($C_2D_5^+$), m/z=36 (C_2D_6), m/z=44 (CO_2), m/z=82 ($C_6D_5^+$) and m/z=84 (C_6H_6). The analysis of fragmentations is to avoid overlapping signals with gas species of the same m/z value.

2.7.3. TPO experiments

The TPO experiments were conducted on Altamira AMI-200 equipped with a Dycor DM100 Mass spectrometer. Typically, 30-35 mg of supported MoO_3/ZSM-5 catalysts was loaded in a U-type quartz tube using quartz wool as bedding. Firstly, the sample was oxidized in 30 sccm 10% O_2/Ar (Airgas, Inc., 10.00% Certified Mixture) at 500 ^{o}C and was hold for 120 mins to obtain a fully dehydrated and oxidized MoO_3/ZSM-5 catalyst, and was purged by Ar (Airgas, Inc., ultrahigh purity) at 500 ^{o}C for 30 mins to remove any gaseous oxygen. Secondly, the sample was allowed to expose to 30 sccm 1.5 mol% CH_4/He(Airgas, Inc., He balanced) at 500 ^{o}C and the temperature of the quartz reactor was allowed to ramp up to 800^{o}Cwith a heat rate of 10^{o}C/min and cool down to 110 ^{o}C in UHP Ar. Finally, the methane-reacted catalyst was allowed to exposed to 10% O_2/Ar(Airgas, Inc., 10.00% Certified Mixture) and the temperature was increased from 110^{o}C to 800 ^{o}C at a heating rate of 10^{o}C/min. Mass/charge ratios of m/z=18 (H_2O),

m/z=28 (CO) and m/z=44(CO_2) corresponding to the gas products evolved from oxidation of the coke species were monitored, but CO was not evolved.

References

1. Gao, X. T.; Bare, S. R.; Weckhuysen, B. M.; Wachs, I. E., *Journal of Physical Chemistry B* **1998,** *102* (52), 10842-10852.
2. Jehng, J. M.; Hu, H. C.; Gao, X. T.; Wachs, I. E., *Catalysis Today* **1996,** *28* (4), 335-350.
3. Jehng, J. M.; Wachs, I. E., *Catalysis Letters* **1992,** *13* (1-2), 9-19.
4. Yu, Y.; Xiong, G.; Li, C.; Xiao, F.-S., *Microporous and Mesoporous Materials* **2001,** *46* (1), 23-34.
5. Weckhuysen, B. M.; Wang, D.; Rosynek, M. P.; Lunsford, J. H., *Journal of Catalysis* **1998,** *175* (2), 338-346.
6. Lacheen, H. S.; Cordeiro, P. J.; Iglesia, E., *Journal of the American Chemical Society* **2006,** *128* (47), 15082-15083.
7. Kiricsi, I.; Flego, C.; Pazzuconi, G.; Parker, W. O., Jr.; Millini, R.; Perego, C.; Bellussi, G., *The Journal of Physical Chemistry* **1994,** *98* (17), 4627-4634.
8. Glazneva, T. S.; Kotsarenko, N. S.; Paushtis, E. A., *kinetics and catalysis* **2008,** *49* (6), 859-867.
9. Wachs, I. E.; Kim, T., *Metal Oxide Catalysis*. Wiley: New York, 2009.
10. Rao, T. V. M.; Deo, G.; Jehng, J. M.; Wachs, I. E., *Langmuir* **2004,** *20* (17), 7159-7165.
11. Weber, R. S., *Journal of Catalysis* **1995,** *151* (2), 470-474.
12. Lee, E. L.; Wachs, I. E., *Journal of Physical Chemistry C* **2007,** *111* (39), 14410-14425.
13. Dutta, P. K.; Rao, K. M.; Park, J. Y., *The Journal of Physical Chemistry* **1991,** *95* (17), 6654-6656.
14. Dutta, P. K.; Puri, M., *The Journal of Physical Chemistry* **1987,** *91* (16), 4329-4333.
15. Tian, H.; Roberts, C. A.; Wachs, I. E., *The Journal of Physical Chemistry C* **2010,** *114* (33), 14110-14120.
16. Mimura, N.; Okamoto, M.; Yamashita, H.; Oyama, S. T.; Murata, K., *The Journal of Physical Chemistry B* **2006,** *110* (43), 21764-21770.
17. Tian, H.; Wachs, I. E.; Briand, L. E., *The Journal of Physical Chemistry B* **2005,** *109* (49), 23491-23499.
18. Mestl, G.; Srinivasan, T. K. K.; Knoezinger, H., *Langmuir* **1995,** *11* (10), 3795-3804.
19. Bare, S. R., *Langmuir* **1998,** *14* (6), 1500-1504.
20. Ravel, B.; Newville, M., *Journal of Synchrotron Radiation* **2005,** *12* (4), 537-541.
21. Lee, J. S.; Oyama, S. T.; Boudart, M., *Journal of Catalysis* **1987,** *106* (1), 125-133.
22. H. Sakakini, B.; S. Verbrugge, A., *Journal of the Chemical Society, Faraday Transactions* **1997,** *93* (8), 1637-1640.

Chapter 3.

Surface MoOx molecular structures and anchoring sites for supported MoO_3/ZSM-5 catalysts

Abstract

The anchoring sites, electronic and molecular structures of surface MoOx species for supported MoO_3/ZSM-5 catalysts are systematically investigated *via in situ* FTIR, *in situ* UV-Vis Diffuse Reflectance Spectroscopy (DRS), *in situ* Raman DRS and *in situ* X-ray absorption spectroscopy (XAS) which include X-ray absorption near edge spectroscopy (XANES) and extended X-ray absorption fine structure (EXAFS). The *in situ* FTIR results suggested that surface MoOx species prefer to anchor at Brønsted acid sites (Al-$(OH)^+$-Si) but also at external Si-OH and extra framework Al-OH sites at high Mo loading or low framework Al content of ZSM-5. Combined *in situ* UV-Vis DRS, *in situ* Raman and *in situ* XAS results, the surface MoOx species are essentially isolated and fully oxidized species. The absence of any d-d transition in the *in situ* UV-Vis spectra, the absence of crystalline MoO_3 or Mo-O-Mo vibration in the *in situ* Raman spectra, and the sharp pre-edge characteristic of tetrahedral coordination and the absence of Mo-Mo absorption in the *in situ* EXAFS spectra confirmed that surface MoOx species are predominate isolated dioxo $(O=)_2MoO_2$ species with tetrahedral coordination. Only a small amount of polymeric (MoOx)n species are present on catalysts with high Si content (Si/Al=140) as evident by the presence of weak Mo-Mo absorption in the *in situ* EXAFS spectra.

Introduction

The molecular and electronic structures of highly dispersed MoO_3/ZSM-5 have received significant attention in recent years since supported MoO_3/ZSM-5 is the most promising catalyst for non-oxidative conversion of methane to aromatics due to its near equilibrium conversion (*ca.* 12% at 700 ^oC)[1, 2]. Despite extensive studies of this catalyst system in the past decades, the anchoring sites, the electronic and molecular structure of surface MoO_x species in the supported Mo/ZSM-5 catalyst has been under debate in the literature. The literature findings about the anchoring sites and molecular structures for supported MoO_3/ZSM-5 catalysts are summarized in **Table 3- 1**.

Table 3- 1 Literature review on supported MoO_3/ZSM-5 for methane dehydroaromatization

Nature of MoO_x	Active Phase	Characterization Technique	Mo Location	Group
Dispersed MoO_4/MoO_6	Mo_2C	**ambient** UV-vis, IR and XPS	zeolite channels	Chen[2,22](**1995,1996)**
	Mo_2C, Mo^{4+} and Mo^{5+}	***ex situ*** XPS, ***in situ*** IR	Predominantly external surface	Lunsford[3, 23] (**1997, 1998**)
Dispersed MoO_x	Mo_2C $Mo(^{4+})O_xC_y$	**ambien**t XPS	not discussed	Solymosi [24](**1997**)
		ex situ XAS	not discussed	Ichikawa[25] (**1999**) Aritani[26,27] (**1996**, **2006**)
$(MoO_x)_n$ cluster isolated MoO_x	Mo_2C and Mo^{5+}	***ex situ*** IR, ***in situ*** EPR	(MoOx)n extr. Surface isolated MoO_x inside channel **Mo_2C extr. surface**	Xu[4, 28] (**1999**, **2000**)
Isolated Mo=O **Dimeric Mo_2O_5**	MoC_y	***in situ*** Raman/XAS	isolated ext. surface **Dimer in channels**	Iglesia[5] (**2000**)
Isolated Mo=O Dimeric Mo_2O_5	---	***in situ*** UV Raman	not discussed	Ribeiro[7] (**2001**)
$(MoOx)_n$ Cluster	β-Mo_2C	***ex situ*** HR-TEM	$(MoOx)_n$ cluster inside Mo_2C extr. surface	Ismagilov[9] (**2006**)

The ambient and *ex situ* characterizations are not representative of the actual dehydrated catalyst; therefore, only *in situ* characterizations are discussed in details below.

There is a general consensus from several *in situ* FTIR studies that surface MoO_x species anchor on both framework Al-$(OH)^+$-Si and external Si-OH of the ZSM-5 support. Lunsford *et al.*[3] investigated 2 wt% Mo/ZSM-5 catalyst by *in situ* FTIR technique and observed a greater consumption of terminal Si-OH hydroxyls than Brøntsed acid

hydroxyl groups associated with framework Al sites with the introduction of Mo species to ZSM-5, but calcination at elevated temperature leads to MoOx species migrated from the external surface Si-OH sites and extra-framework Al-OH hydroxyls to framework Al-$(OH)^+$-Si sites for 2% MoO_3/ZSM-5. Xu *et al.*[4] reported that MoOx species preferably anchor at Brønsted acid sites over external silanol hydroxyls for 6% MoOx/ZSM-5 with *in situ* IR in which study the dehydration was performed in vacuum. Iglesia *et al.*[5] assumed that surface Mo_2O_5 dimers anchor at two adjacent Al-$(OH)^+$-Al Brønsted acid sites, but no direct supporting information was provided. The probability of finding a high concentration of two adjacent Al framework Brønsted acid sites, however, is low according to Lowenstein's rule[6] and not enough of such paired sites are present for anchoring high loadings of MoOx on ZSM-5

The surface molybdenum oxides on ZSM-5 were proposed as well-dispersed MoO_4/ MoO_6[2] and dimeric Mo_2O_x[5,7] *via in situ* UV Raman and *in situ* XAS. Two independent *in situ* Raman studies[5,7] claimed the presence of dimeric Mo_2Ox species on supported MoO_3/ZSM-5 catalysts. Upon close examination, however, the reported Raman band positions of proposed dimeric Mo_2Ox structures do not match. Ribeiro *et al.*[7] assigned the 962 cm^{-1} as Mo=O stretch of monomeric O=MoO_4 and the 868 cm^{-1} as an Mo-O-Mo stretch mode for a dimer while Iglesia *et al.*[5] assigned 970 and 1045 cm^{-1} as the Mo=O stretch of dimeric Mo_2O_5 species. The 962 or 970 cm^{-1} is Mo=O stretch of isolated dioxo MoO_x species, and the 868 cm^{-1} is likely the stretch mode of Mo-O-Si/Al[8]. The 1045 cm^{-1} is close to the characteristic band of crystalline $Al_2(MoO_4)_3$ NPs[8], which reflects the high calcination temperature employed in those studies. In reality, however, there are different MoO_x structures present on the catalyst, and the molar ratio of atoms of the catalyst

should not be fit to one structure. Recently, Ismagilov *et al.*[9] observed the presence of $(MoO_x)_n$ clusters of 1-5 nm in size in 2wt % Mo/ZSM-5 catalyst prepared by wet-impregnation with *ex situ* HR-TEM.

Theoretical studies on the molecular structure of Mo species have been pursued by a few researchers recently. Bao *et al.*[10] investigated the structure of Mo/ZSM-5 catalyst *via* Density Functional Theory (DFT) calculations and suggested monomeric $O_2Mo(=O)_2$ interacted with two neighboring Brønsted acid protons which is against Lowenstein's rule[6]. Therefore, Bao *et al.*[11] later adopted the dimeric Mo structure which can overcome the long distance between two neighboring Brønsted acid sites in the zeolite support with high Si/Al ratio. However, in the later work, the proposed dimeric Mo_2O_5 species possess two terminal triple bonds (Mo≡O) which has not been reported elsewhere. And the calculated Raman vibrational frequencies of the dimer structure are not consistent with the Raman features from experimental measurements. A recently reported DFT study[12] combined with *in situ* Raman experimental results suggested that isolated MoO_4 species with two terminal Mo=O bonds are stable on both single framework Al sites and double framework Al sites with (-Al-O-Si-O-Al-) unit which is not against Lowenstein's rule. The calculated frequencies of the isolated MoO_4 species match with experimental *in situ* Raman results.

This study is aimed to resolve the debate over the fundamentals of the MoO_3/ZSM-5 catalyst for the conversion of methane to aromatics. The supported MoO_3/ZSM-5 catalysts with different Mo loadings and ZSM-5 with different Si/Al molar ratios are systematically investigated. The anchoring sites, electronic and molecular structures of the supported MoO_3/ZSM-5 were investigated *via in situ* spectroscopy and theoretical

calculation. *In situ* FT-IR spectroscopy reveals the anchoring sites of the zeolite host for surface MoOx species. *In situ* UV-vis Diffuse Reflectance Spectroscopy (DRS) provides information about the electronic structures of surface MoOx species (e.g.: monomer, dimer, polymer, chain, cluster or 3D crystalline structure). Combined *in situ* Raman DRS and *in situ* extended X-ray fine structure/ X-ray near edge energy spectroscopy (EXAFS/XANES) resolve the molecular structures such as the molecular vibrations, the local geometry of dominate species and interatomic distances. Based on the molecular information from spectroscopies, Density Functional Theory (DFT) is applied to construct the molecular structures of MoOx species on zeolite. The calculated vibrational frequencies are then compared with experimental values obtained from *in situ* spectroscopy.

3.1. Experimental methods

3.1.1. *In situ* FTIR spectroscopy

The *in situ* FTIR measurements were performed with a Thermo Scientific Nicolet 8700 spectrometer. More details about equipment can be found in Chapter 2, section 2.2.

3.1.2. *In situ* UV-vis spectroscopy

The *in situ* UV-vis Diffuse Reflection Spectroscopy (DRS) measurements were obtained with a Varian Cary 5E UV-Vis-NIR spectrophotometer, and more details are in Chapter 2, section 2.3.

3.1.3. *In situ* X-ray absorption spectroscopy (XAS)

The X-ray absorption spectroscopy (XAS) of Mo K-edge of dehydrated supported MoO_3/ZSM-5 catalysts was performed in both transmission and fluorescence mode at the beam line X18A at the National Synchrotron Light Source (NSLS) at the Brookhaven National Laboratory. Experimental details are described in Chapter 2, section 2.5.2.

3.1.4. *In situ* Raman spectroscopy

The *in situ* Raman spectra of the zeolite-supported metal oxide catalysts were obtained with a high resolution, dispersive Raman spectrometer (Horiba-Jobin Yvon LabRam HR) equipped with three laser excitations (532, 442 and 325 nm), and more details are provided in Chapter 2, section 2.4.1.

3.1.5. Density functional theory (DFT)

Gradient-corrected periodic density functional theory (DFT) calculations were performed with the $DMol^3$ code in Materials Studio 4.0 program by Accelrys Software, Inc. More details can be found in Chapter 2, section 2.6

3.1.6. Temperature programmed reduction (TPR)

The H_2-TPR was performed on an Altamira temperature programmed system (AMI-200) monitored by an online thermal conductivity detector (TCD). Experimental details are described in Chapter 2, section 2.7.1.

3.2. Results

3.2.1. *In situ* FTIR spectroscopy

The integrated *in situ* IR bands of the dehydrated MoOx/ZSM-5 (Si/Al=15) catalysts are presented as a function of molybdena loading in **Figure 3- 1**. The corresponding IR spectra are provided in **Figure 3- 2**. The ZSM-5(Si/Al=15) support possesses four surface hydroxyl groups, as shown in **Figure 3- 2**, that have been assigned to (1) Brønsted acid Al-$(OH)^+$-Si site in which alumina is coordinated as a AlO_4 unit (3610 cm^{-1}) ; (2) terminal Si-OH (3741 cm^{-1}); (3) extra-framework Al-OH with AlO_6 coordination (3660 cm^{-1}; Al-OH-I) and (4) extra-framework Al-OH-II of Al_2O_3 nanoclusters (3783 cm^{-1}; Al-OH II)[13].

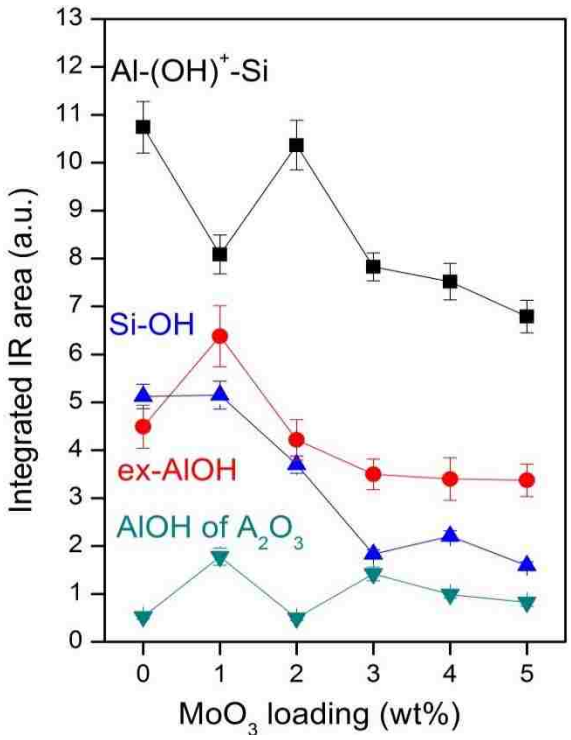

Figure 3- 1 Integrated IR bands of surface hydroxyls of dehydrated supported 0-5% MoO_3/ZSM-5 (Si/Al=15) catalysts

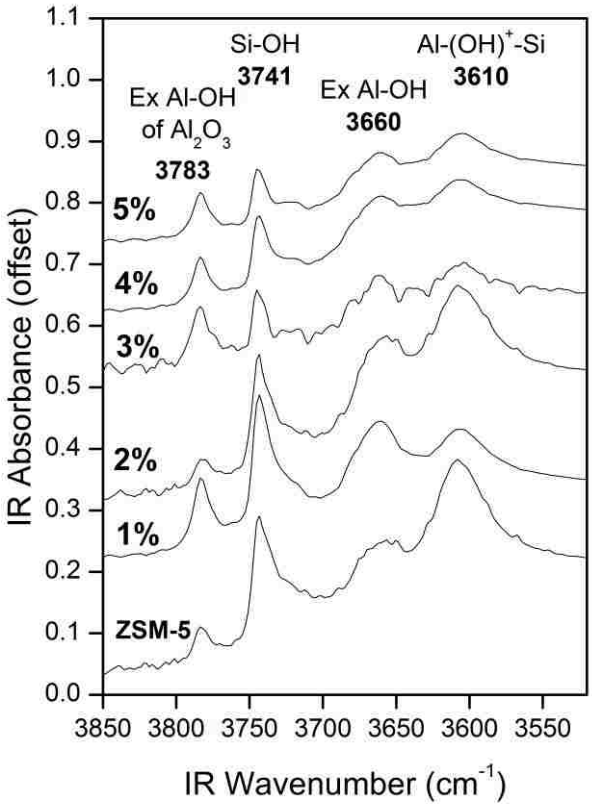

Figure 3- 2 *In situ* FT-IR spectra of dehydrated supported 0-5% MoO_3/ZSM-5(Si/Al=15) catalysts collected at 110 ^oC after calcined in 10% O_2/Ar at 500 ^oC for 120 mins

Introduction of just 1% MoO_3 has a significant effect upon the ZSM-5 surface hydroxyls, with the IR intensity of the surface Brønsted acid hydroxyls (3610 cm^{-1}) markedly decreased, the surface Al-OH-I and -II hydroxyls (3660 and 3783 cm^{-1}) increased and the external silanol Si-OH at 3741 cm^{-1} remain unchanged as shown in **Figure 3- 1**. These surface hydroxyl changes are consistent with that the initial surface MoOx species anchor at surface Brønsted acid hydroxyls and also cause a small degree of dealumination. Increasing the molybdena loading to 2% MoO_3/ZSM-5, restores the initial IR intensity for the Brønsted acid hydroxyls and decreases the intensity of all other surface hydroxyls. This trend suggests that surface MoOx is either migrating from the surface Brønsted acid

hydroxyls to the other surface hydroxyls or it is creating new surface Brønsted acid hydroxyls. Further increasing the molybdena loading decreases the intensity of the IR bands for all surface hydroxyls except the extra-framework Al-OH-II associated with Al_2O_3 NPs that slightly increases. These surface hydroxyl trends with increasing molybdena loading indicate that at low molybdena loadings the surface MoOx species initially anchor at surface Brønsted acid hydroxyls inside the channels and at high molybdena loadings also anchor at external surface Si-OH and extra-framework Al-OH hydroxyls. Introduction of molybdena to ZSM-5 also causes dealumination and may be creating some new surface hydroxyls at ~3600 cm^{-1}.

3.2.2. *In situ* UV-vis spectroscopy

The *in situ* UV-Vis DRS spectra of the supported MoO_3/ZSM-5 catalysts under dehydrated oxidizing conditions are summarized in **Figure 3- 3** and the UV-vis DRS spectra are given in **Figure 3- 4**.

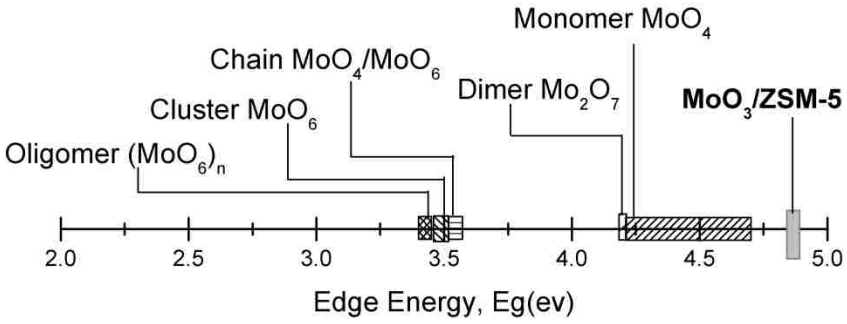

Figure 3- 3 The UV-vis edge energy (Eg) of molybdenum oxide reference compounds with known structures and supported MoOx on ZSM-5

Figure 3- 4 *In situ* UV-vis DRS spectra of dehydrated supported 2% MoO_3/ZSM-5: (A) 2% MoO_3/ZSM-5 (Si/Al=140), (B) 2% MoO_3/ZSM-5 (Si/Al=40), (C) 2% MoO_3/ZSM-5 (Si/Al=25), and (D) 2% MoO_3/ZSM-5 (Si/Al=15) under oxidizing conditions at 400 ^oC.

Only a single ligand-to-metal charge transfer (LMCT) transition of the O(2p) to Mo (3d) orbital is observed at 242-245 nm and becomes more pronounced at higher molybdena loading. Absence of a LMCT transition at ~400 nm, characteristic to crystalline MoO_3 nanoparticles, indicates that crystalline MoO_3 nanoparticles are not present in the catalyst. The corresponding UV-vis edge energy (Eg) values for the supported molybdena species on ZSM-5 are 4.6-4.9 eV, which unambiguously falls into the range of isolated MoO_x structures as shown by comparison with model reference compounds in **Figure 3- 3** [14, 15]. Furthermore, the single LMCT transition at 242-245 nm and high Eg value of 4.6-4.9 eV correspond to surface dioxo $O_2Mo(=O)_2$ species coordinated to alumina sites present for supported $MoO_3/Al_2O_3/SiO_2$, in which the alumina phase is highly dispersed (LMCT at

217 nm and Eg=4.9 eV), and not to supported MoO_3/SiO_2 with two LMCT transitions at 237 and 274 with a corresponding Eg value of 4.1 eV.[14, 15] Therefore, the predominant surface molybdena species present in the initial oxidized supported MoO_3/ZSM-5 catalysts consist of isolated surface MoO_x species interacting with alumina sites.

3.2.3. *In situ* XANES/EXAFS spectroscopy

The X-ray absorption spectra (XAS) of fully oxidized and dehydrated supported 2% MoO_3/ZSM-5 (Si/Al=25) (red) and supported 5% Mo/SiO_2 (blue) catalysts are compared in **Figure 3- 5**.

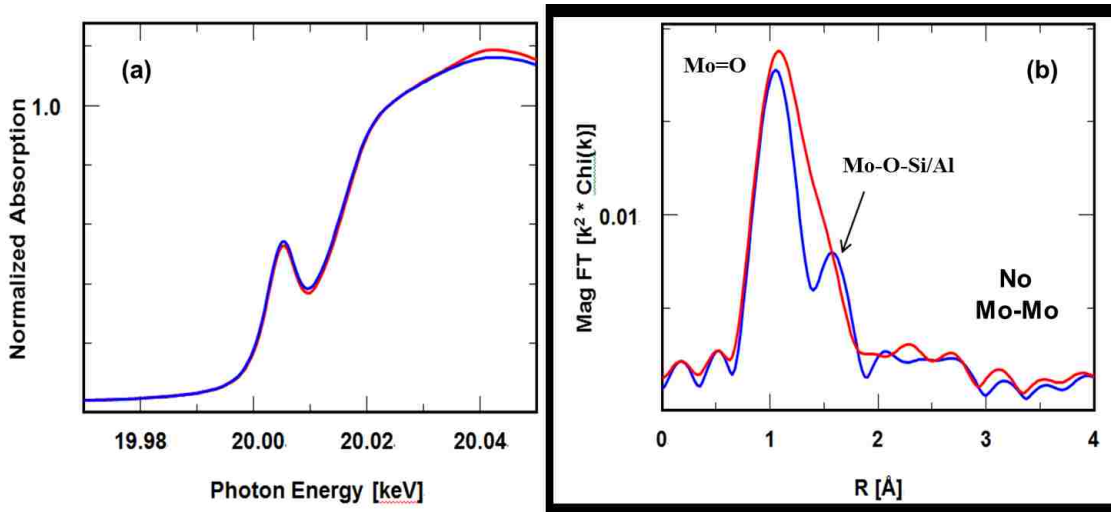

Figure 3- 5 *In situ* Mo k-edge XANES (a) and EXAFS (b) spectra of dehydrated 2% MoO_3/ZSM-5(Si/Al=25)(red) and 5 % MoO_3/SiO_2(blue) at 500 ^oC in 10% O_2/Ar for 2 hrs.

The supported 5 % Mo/SiO_2 catalyst, which is dominated by the surface dioxo O_2=MoO_2 structure, serves as a reference structure for the surface MoOx site (corresponding to the 998 cm^{-1} Raman band) on ZSM-5[15, 16]. The X-ray absorption near edge spectra (XANES) of the Mo K edge in **Figure 3- 5a** are identical for both catalysts, thus similar coordination geometry (MoO_4) are presented on both SiO_2 and ZSM-5 support since the

XANES feature is forbidden for centrosymmetric MoO_6 coordination. The edge energy of ~20.00 keV indicates that the supported molybdena phase is present as Mo^{+6} sites on the ZSM-5 support. The extended X-ray absorption fine structure (EXAFS) k-space spectra for the two catalysts are compared in **Figure 3- 5b**. The supported 5% MoO_3/SiO_2 catalyst exhibits two shells in the first coordination sphere at ~1.0 Å and ~1.5Å corresponding to the terminal Mo=O and bridging Mo-O-Si bonds, respectively, of the surface dioxo species. In addition, there is no Mo-Mo shell at ~3.5 Å in the second coordination sphere indicating that the surface dioxo MoO_4 sites are isolated. The extend X-ray absorption fine structure (EXAFS) k-space plot for the supported 2% MoO_3/ZSM-5 catalyst is very similar to that of the reference supported 5 % MoO_3/SiO_2 catalyst, but the shoulder at ~1.5 Å is not as pronounced. The broadening of the bridging Mo-O- band may be reflecting the presence of multiple bridging Mo-O- bonds, Mo-O-Si and Mo-O-Al, or multiple MoOx sites that may be present for the supported 2% MoO_3/ZSM-5 (Si/Al=25) catalyst.

The *in situ* XANES pre-edge intensity for dehydrated supported MoO_3/ZSM-5 is intermediate between that of the MoO_4 coordinated reference compounds $Al_2(MoO_4)_3$ (isolated MoO_4 sites) and MoO_3 (oligomeric MoO_6 sites)) (see **Figure 3- 6**).

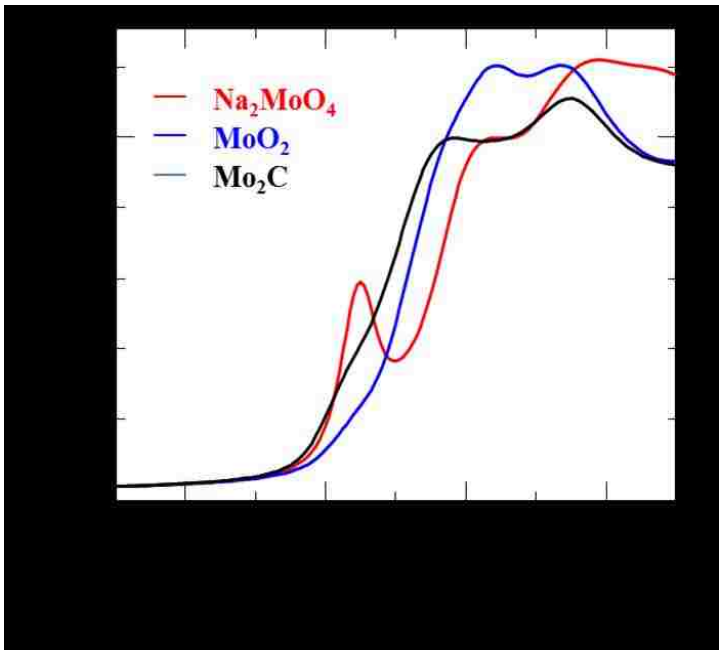

Figure 3- 6 XANES spectra of bulk Na_2MoO_4 which is consisted of isolated tetrahedral $Mo^{6+}O_4$ unit(red curve), bulk MoO_2 which is consisted of Mo^{4+} species with distorted octahedral symmetry(blue curve), and bulk Mo_2C which is consisted of Mo^{2+} with hexagonal bcc lattice unit(black curve).

The XAS spectra of supported MoO3/ZSM-5 with (Si/Al=25, 40 and 140) are given in **Figure 3- 7**. The intensity of the XANES pre-edge for supported MoOx/ZSM-5 also varies slightly with Si/Al ratio and is lowest for the highest Si/Al ratio. With the exception of the supported MoOx/ZSM-5 (Si/Al=140), the XANES pre-edge intensity for the other catalysts are stronger than for the mono-oxo MoO_6 containing cluster. The intermediate pre-edge intensity and its dependence on the Si/Al ratio indicates that the surface MoOx sites on ZSM-5 consist of a mixture of both MoO_4 and MoO_5/MoO_6 coordinated sites, which is consistent with the observation of multiple surface MoOx sites on ZSM-5 detected with *in situ* Raman spectroscopy.

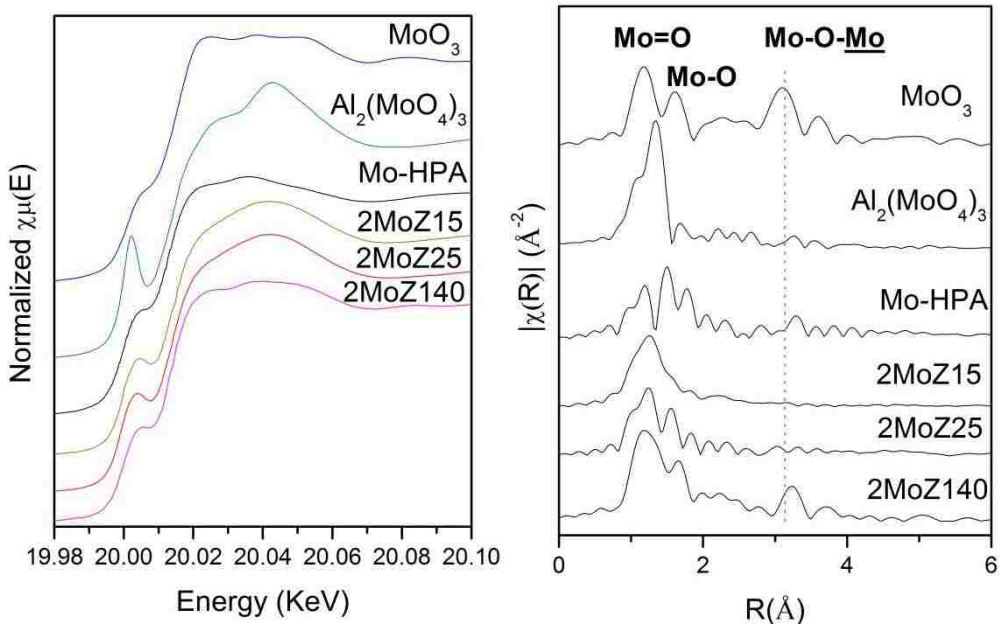

Figure 3- 7 Molybdenum k-edge *in situ* XANES (left) and EXAFS (right) of supported 2% MoO_3/ZSM-5 (Si/Al=15, 25, 140) (labeled as 2MoZ15, 2MoZ25 and 2MoZ140, respectively) under dehydrated condition (500 ^oC for 30 mins, and full XAS collection at 110 ^oC in flowing 10% O_2/He) and reference compounds phosphomolybdate acid (Mo-HPA, mono-oxo MoO_6 containing cluster), and $Al_2(MoO_4)_3$ (isolated tetrahedral MoO_4 unit) and MoO_3(oligomeric MoO_6 structure)

3.2.4. *In situ* Raman spectroscopy

In situ Raman spectra of the supported MoO_3/ZSM-5 catalysts with different Mo loadings (0-5 %) and different Si/Al ratios (Si/Al=15, 25, 40 and 140) are presented in **Figure 3- 8** and **Figure 3- 9**, respectively.

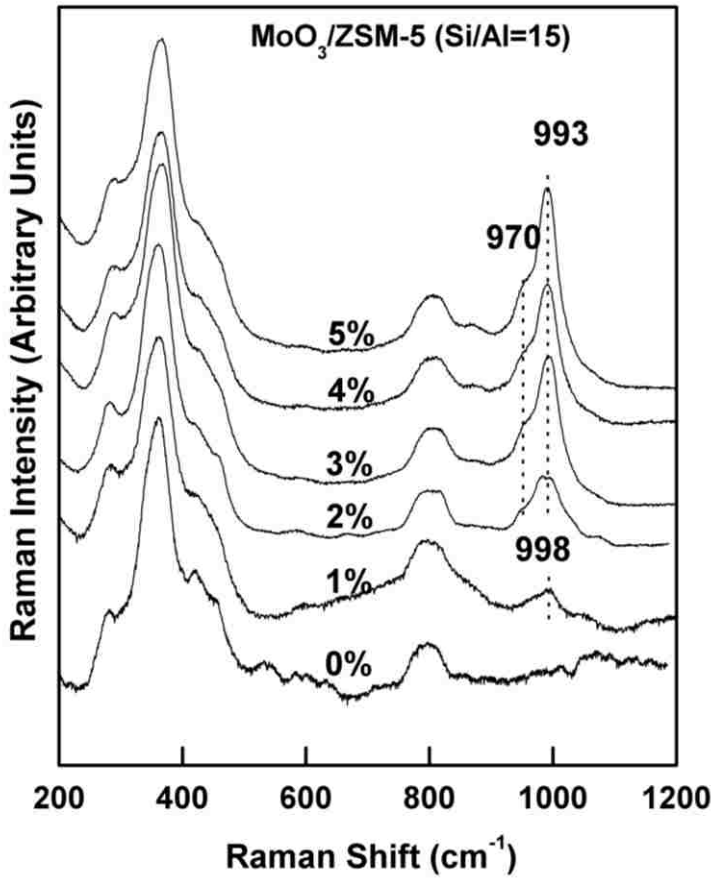

Figure 3- 8 *In situ* Raman spectra (442 nm) of dehydrated supported MoO_3/ZSM-5 catalysts as a function of MoO_3 loading (0-5 wt%) collected at 110 ^oC after calcination in 10% O_2/Ar at 500 ^oC for 120 mins.

As shown in **Figure 3- 8**, the *in situ* Raman spectra of H-ZSM-5 support exhibits the bending mode of six-membered rings at 293 cm^{-1}, the bending mode of five-membered rings at 378 cm^{-1}, the bending mode of four-membered rings 440-500 cm^{-1}, symmetric stretching vibrations of T-O bonds in ZSM-5 at ~810-820 cm^{-1} and asymmetric stretching

vibrations of T-O bonds in ZSM-5 at 1080-1250 cm^{-1}.[17] The absence of any Raman bands in the range of 900-1050 cm^{-1} from the ZSM-5 support indicates that Raman bands in this region when molybdena is present must arise from the supported molybdena phase. The absence of the characteristic sharp Raman band of crystalline MoO_3 at ~820 cm^{-1} for all the supported MoO_3/ZSM-5 catalysts indicates that the supported molybdena phase is 100% dispersed as surface MoO_x species on the ZSM-5 support.[15] The supported MoO_3/ZSM-5 (Si/Al=15) catalyst, containing a high Al content, exhibits a strong Raman band at 998 cm^{-1} with a shoulder at 970 cm^{-1} and the Raman intensity of these two bands increases with increasing molybdena loading. New Raman bands are observed when the Si/Al ratio of ZSM-5 is varied for constant molybdena loading, 2% MoO_3, as shown in **Figure 3- 9**.

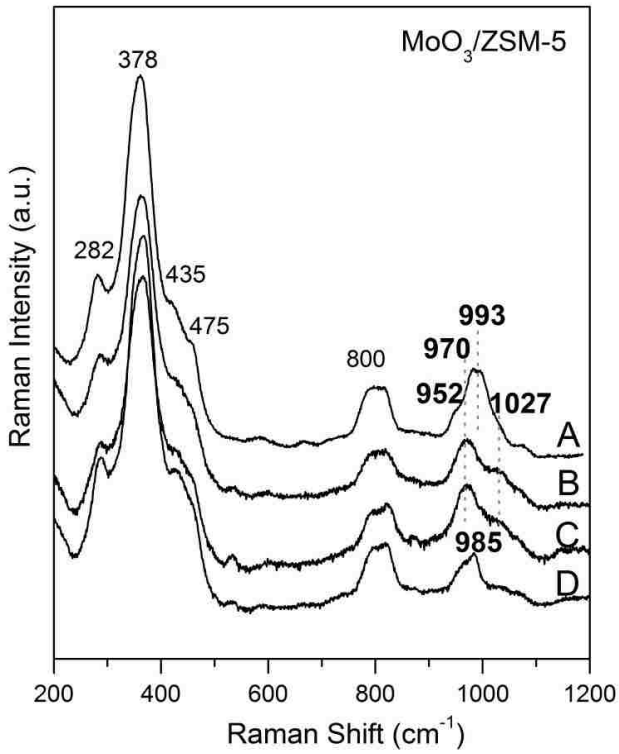

Figure 3- 9 *In situ* Raman spectra (442 nm) of dehydrated 2wt% MoO_3/ZSM-5 catalysts as a function of Si/Al ratio (A) 15, (B) 25, (C) 40 and (D) 140 collected at 110 ^oC after calcination in 10% O_2/Ar at 500 ^oC for 120 mins.

Lowering the Al content of ZSM-5 from Si/Al of 15 to 25/40, significantly diminishes the band at 993 cm^{-1} and enhances the 970 cm^{-1} band. The independent behavior of these two bands with the Si/Al ratio indicates that they originate from two distinct surface MoOx sites. In addition, a new weak Raman band at 1026 cm^{-1} appears as the Al content is lowered (higher Si/Al ratio). For the ZSM-5 support with the lowest Al content (Si/Al=140), the spectrum is dominated by a new band at 985 cm^{-1} and the weaker bands at 970 and 1026 cm^{-1} are also present. The new band at 985 cm^{-1} is likely due to an isolated Mo oxide species associated with Si sites since they are the dominate anchoring sites of ZSM-5 support at high-silica content. The absence of Mo-O-Mo bending vibrations in the 200-300 cm^{-1} region supports the presence of isolated surface MoOx sites on ZSM-5.

The Raman bands for the surface MoO_x species on the ZSM-5 support can be assigned from comparison to prior Raman studies with supported MoO_3/SiO_2 and $MoO_3/Al_2O_3/SiO_2$ catalysts.[14, 15] Supported MoO_3/SiO_2 catalysts exhibit Raman bands at 985 cm^{-1} of dioxo $(O=)_2MoO_2$ species and at 1021 cm^{-1} for mono-oxo $O=MoO_4$ species. This suggests that the 985 and 1026 cm^{-1} bands for supported MoO_3/ZSM-5 (Si/Al=140) originate from dioxo MoO_4 sites on silica and mono-oxo MoO_5 sites, respectively. The vibration of mono-oxo $O=MoO_4$ sites are somewhat comparable when present on SiO_2 (1021 cm^{-1}) and Al_2O_3 (1010-1018 cm^{-1}),[20] which complicates assigning their anchoring sites. Supported $MoO_3/Al_2O_3/SiO_2$ catalysts give rise to Raman bands at 1002 (strong) and 973 cm^{-1} (weak) corresponding to distorted dioxo $(O=)_2MoO_2$ sites that preferentially anchor at surface AlO_x sites on SiO_2. This suggests that the 998 cm^{-1} band observed for supported MoO_3/ZSM-5 (Si/Al=15) is related to dioxo surface MoO_4 sites anchored at

alumina sites. The origin of the 970 cm^{-1} Raman band for the supported MoO_3/ZSM-5 catalysts is not clear and DFT calculations are required to better assign the molecular structures and anchoring sites of the surface MoOx sites on ZSM-5.[18]

3.2.5. Density Functional Theory (DFT) calculations

Density Functional Theory (DFT) calculations were employed to assist in the molecular structural assignment and anchoring sites corresponding to the multiple Raman bands observed for the surface MoOx sites on the ZSM-5 support. The DFT calculations examined the surface MoOx molecular structures, dioxo MoO_4 and mono-oxo MoO_5, for all T sites of the ZSM-5 framework (T4, T5, T8, T10 and T11 sites)[12].

The surface MoOx site on high alumina ZSM-5 (Si/Al=15) gives rise to the Raman band at 998 cm^{-1} was assigned to isolated dioxo $(O=)_2MoO_2$ sites anchored to two adjacent Al atoms within the framework. According to Lowenstein's rule[6], the probability of having two adjacent Al atoms in one ring is very low for a Si-rich zeolite and, therefore, the two Al atoms must be from neighbouring 10 membered rings in the zeolite. The calculated surface MoOx molecular structure and anchoring sites on ZSM-5 are shown in **Figure 3- 10**. The calculated vibrational frequencies of the symmetric vibration of dioxo $(O=)_2MoO_2$ on different T sites is 992-999 cm^{-1} and is in good agreement with the experimentally observed Raman vibration at 998 cm^{-1}.

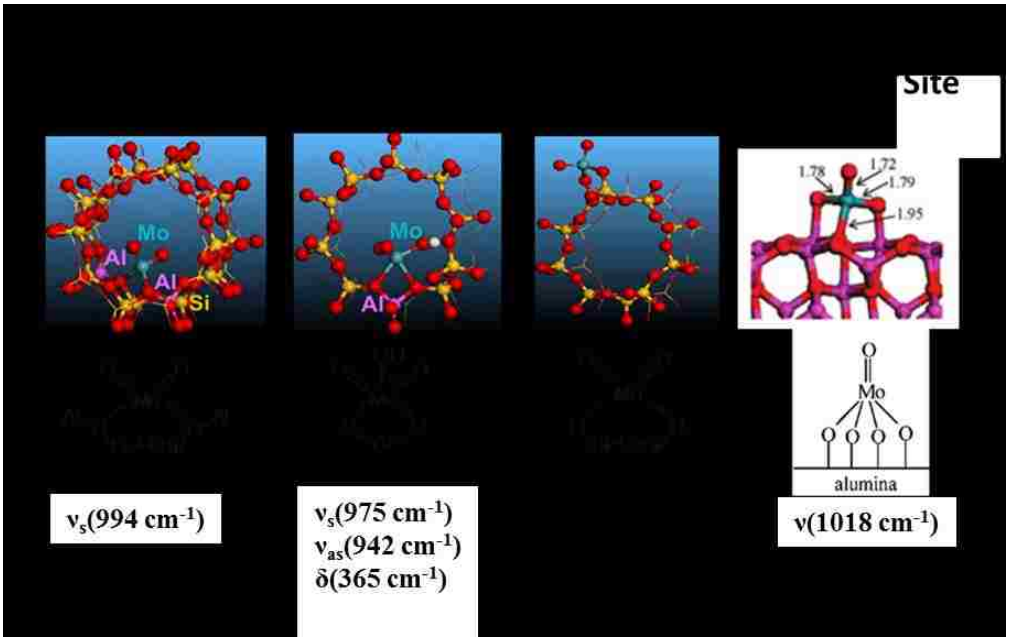

Figure 3- 10 DFT models of surface MoO_x species on ZSM-5 and corresponding calculated vibrational frequencies

The surface MoOx structure on intermediate alumina ZSM-5 (Si/Al=25 and 40) gives rise to the Raman band at 970 cm^{-1} which was assigned to isolated dioxo $(O=)_2(OH)MoO_2$ sites anchored at only one Al atom within the framework. The Mo-OH functionality was introduced to assure charge neutrality of the surface $(O=)_2(OH)MoO_2$ site on ZSM-5. The calculated vibrational mode for the symmetric stretch of the dioxo $(O=)_2(OH)MoO_2$ is at 975 cm^{-1}, which is 5 cm^{-1} higher than the experimentally determined Raman vibration at 970 cm^{-1}.

The DFT calculations revealed that framework Si sites do not anchor surface MoOx species, but that Si-OH sites on the external surface of the zeolite are able to coordinate with surface MoOx species. The surface MoOx sites on low alumina ZSM-5 (Si/Al=140) give rise to the Raman band at 983 cm^{-1}assigned to isolated dioxo $(O=)_2MoO_2$ sites anchored to two adjacent Si-OH sites on the external surface of ZSM-5, which coincides with the experimentally determined value.

The surface MoOx sites on the low alumina ZSM-5 (Si/Al=140) has the Raman band at 1026 cm^{-1} which was assigned to isolated dioxo $(O=)_2MoO_2$ sites anchored to two adjacent Al atoms on external Al_2O_3 NPs. The experimental Raman bands for mono-oxo $O=MoO_4$ species on bulk Al_2O_3 vibrate at 1010-1018 cm^{-1}, which is in agreement with the structure of surface MoOx species on Al_2O_3 supports.[18]

3.2.6. Temperature programmed reduction (TPR)

The H_2-temperature programmed reduction (TPR) technique is utilized to differentiate different surface $Mo^{6+}Ox$ species of MoO_3/ZSM-5 catalysts. It has been extensively applied to the study of supported metal oxide catalysts. Temperature Programmed Reduction (TPR) experiments measure the peak reduction temperature of surface $Mo^{6+}Ox$ species present on ZSM-5. The reduction of different surface $Mo^{6+}Ox$ species would yield different peak reduction temperatures. This measurement served as a basis for the conclusion of different surface $Mo^{6+}Ox$ species on ZSM-5 support drawn from vibrational and X-ray absorption spectroscopic studies.

In **Figure 3- 11**, the TPR profiles of bulk MoO_3 and MoO_2 showed that the reduction of $Mo^{6+} \rightarrow Mo^{4+}$ occurred at 300-600 ^oC, $Mo^{4+} \rightarrow (Mo^{2+}$ or $Mo^0)$ occurred at above 600 ^oC.[19,20,21].

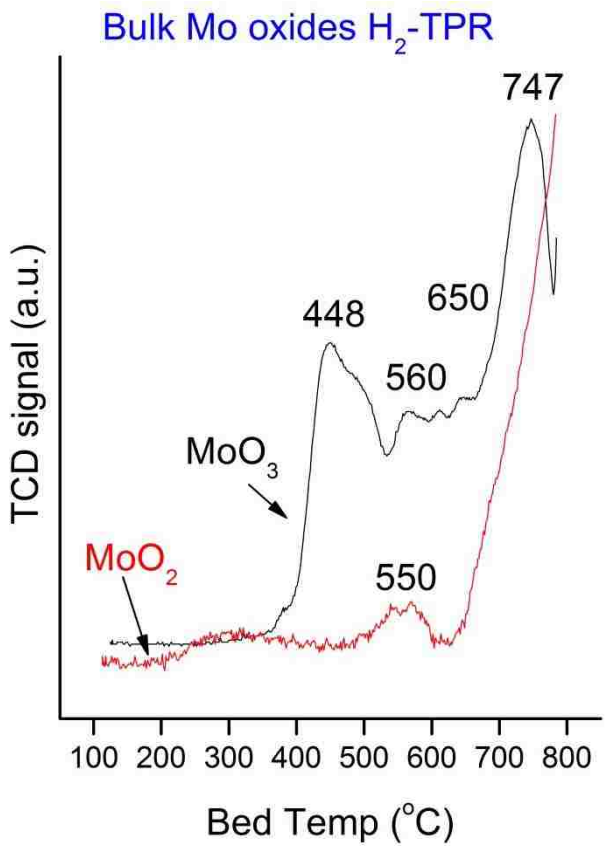

Figure 3- 11 TPR profiles of bulk MoO_3 (10 mg) and bulk MoO_2(10mg) in 5 vol% H_2/Ar

The supported 3% MoO_3/SiO_2 catalyst is a model catalyst which consists of dioxo $(O=)_2MoO_2$ species anchoring on Si sites[14]. The H_2-TPR profile revealed that the reduction of dioxo on Si sites corresponds to the reduction peak at 395 ^oC, and the reduction of dioxo on Al-Al sites corresponds to reduction peak at 345 ^oC in **Figure 3- 12**.

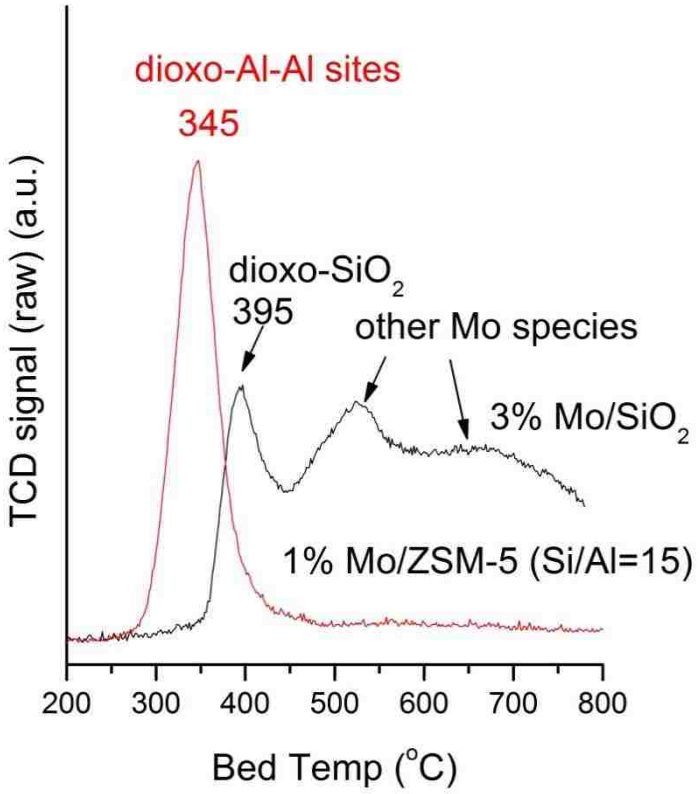

Figure 3- 12 TPR profiles of 1% MoO_3/ZSM-5 Si/Al=15 and 3% MoO_3/SiO_2 catalysts in 5 vol% H_2/Ar

The TPR profiles of supported MoO_3/ZSM-5 catalysts with varied Mo loading and Si/Al ratios are provided in **Figure 3- 13** and **Figure 3- 14**, respectively. The TPR spectra of 1% MoO_3/ZSM-5, as shown in **Figure 3- 13**, have a single peak reduction temperature at 344 ^oC. The perfectly symmetric reduction peak at 344 ^oC implies a single Mo oxide species present on ZSM-5. Combined with the *in situ* FTIR and *in situ* Raman results, the reduction peak at 344 ^oC is assigned as reduction of dioxo MoO_4 on double Al-Al sites to Mo^{4+} species. Similar reduction peaks with center temperatures varied within 10-30 ^oC can be found on TPR profiles of 2-5% MoO_3/ZSM-5 with constant Si/Al of 15 (see **Figure 3- 13**) and 2% MoO_3/ZSM-5 with Si/Al ratios of 15 to 140 (see **Figure 3- 14**). The reduction peak can be assigned as dioxo MoO_4 species on Al sites and the broad

shoulder centered at 395 ^{o}C is assigned as dioxo MoO_4 species on Si sites as shown in **Figure 3- 14**. Additional reduction peaks above 500 ^{o}C were also observed on the TPR profiles, which are assigned as further reduction of $Mo^{4+} \rightarrow Mo^{2+} \rightarrow Mo^{0}$.[19,20,21]

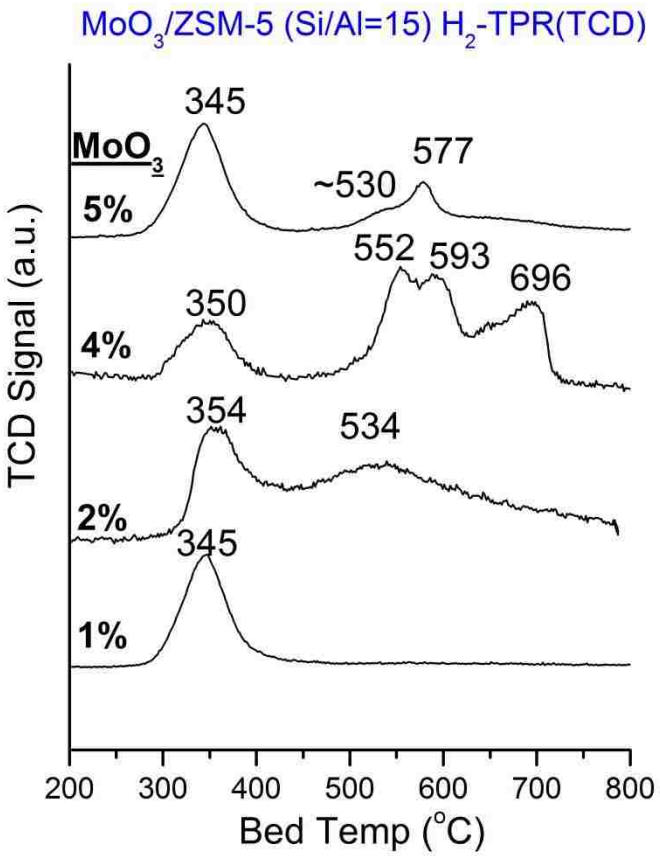

Figure 3- 13 TPR profiles of supported 1-5% MoO_3/ZSM-5 Si/Al=15 in 5 vol% H_2/Ar

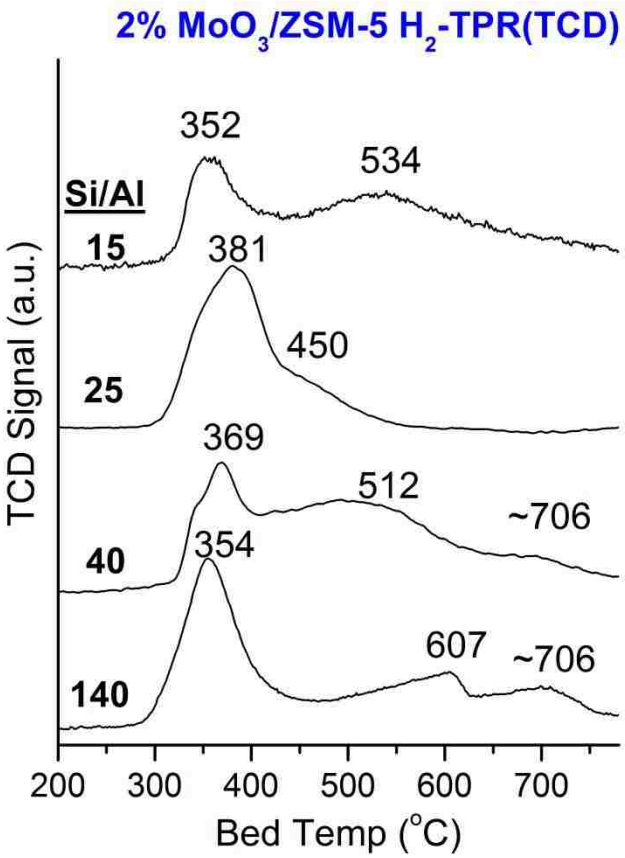

Figure 3- 14 TPR profiles of supported 2% MoO_3/ZSM-5 Si/Al=15-140 in 5 vol% H_2/Ar

The TPR results are consistent with the conclusions of surface MoOx species present on 1-5% MoO_3/ZSM-5 from *in situ* FTIR and Raman results. From *in situ* FTIR and Raman results of 1% MoO_3/ZSM-5 catalyst, only a dioxo O_2=MoO_2 species anchoring at double framework Brønsted acid sites with Raman vibration at 998 cm^{-1} is present on ZSM-5 (See **Figure 3- 2**, **Figure 3- 8** and **Figure 3- 12**). The reduction peak at 344 ^oC corresponds to the reduction of the dioxo species on double Al sites. From *in situ* FTIR and Raman results of supported MoO_3/ZSM-5 catalysts, surface MoOx species are identified as: (1) a dioxo species on double Brønsted Al sites with Raman vibration at 993 cm^{-1} which gives rise to a reduction peak at 344 ^oC; and (2) a dioxo species on a single Brønsted Al site with Raman vibration at 970 cm^{-1} which gives rise to the

reduction peak at 350-354 ^{o}C; (3) the dioxo species on external Si sites give rise to the reduction broad shoulder at 395-400 ^{o}C.

3.3. Discussion

3.3.1. Anchoring sites

The ZSM-5 support has four distinct surface hydroxyls which are able to accommodate surface MoOx species *via* either ion-exchange or dehydration reaction. The four surface hydroxyls are Brønsted acid Al-$(OH)^{+}$-Si, external Si-OH and extra-framework Al-OH surface hydroxyls. The supported MoOx species preferably anchor at surface Brønsted acid sites at low molybdena loadings and at external surface Si-OH and extra-framework Al-OH sites at high molybdena loadings (see **Figure 3- 1**). The current *in situ* IR study observed that the affinity of surface MoOx species to anchor at surface hydroxyls follows the trend Brønsted acid Al-$(OH)^{+}$-Si > external Si-OH > extra-framework Al-OH surface hydroxyls. There is a general consensus from multiple IR studies of supported MoO_3/ZSM-5 catalysts that both surface Al-$(OH)^{+}$-Si Brønsted acid sites and external Si-OH sites of HZSM-5 are anchoring sites for surface MoOx species.[4] There is one study, however, that has claimed that the surface MoOx species only anchor at surface Al-$(OH)^{+}$-Si Brønsted acid sites,[7,8] but supporting evidence was not provided.

3.3.2. Molecular and electronic structures of surface MoOx species on ZSM-5

The dehydrated supported molybdena phase is completely dispersed as surface MoOx species on the ZSM-5 supports for the catalyst compositions reported in this study. The surface MoOx sites on ZSM-5 in the calcined catalysts are fully oxidized as Mo^{+6} species (energy of the XANES pre-edge and absence of UV-vis d-d transitions). The surface MoOx sites are present as isolated species on the ZSM-5 supports (high UV-vis Eg values (**Figure 3- 3)**, absence of Raman bands for bridging Mo-O-Mo species (see **Figure 3- 8** and **Figure 3- 9**), and absence of Mo-Mo distances in the second coordination sphere from EXAFS spectra (**Figure 3- 5b**)[14]. Raman spectra revealed the presence of four distinct surface MoOx sites as a function of the ZSM-5 Si/Al ratio, which correspond to the four different surface hydroxyls present on the ZSM-5 support. The molecular structures of the four distinct surface MoOx sites were determined from combined Raman spectra and DFT calculations. The Raman band at 998 cm^{-1} was assigned to isolated surface dioxo $O_2Mo(=O)_2$ species associated with double Al-Al sites, 970 cm^{-1} was assigned to isolated surface dioxo $(O=)_2(OH)MoO_2$ sites associated with a single Al site, 985 cm^{-1} was assigned to isolated surface dioxo $(O=)_2MoO_2$ sites associated with double Si-Si sites on the external surface, and 1026 cm^{-1} was assigned to surface mono-oxo $O=MoO_4$ species on extra-framework double Al-Al sites.

Several researchers have proposed the presence of dimeric M_2Ox[5,7]. These structures are not supported by the present findings of the exclusive presence of isolated surface MoOx species that is reflected in the very high UV-vis DRS Eg value of 4.6-4.9 eV that are only present for isolated MoOx sites. The absence of Mo-Mo distances in the second

coordination shell in the previous EXAFS studies of supported MoO_3/ZSM-5 catalysts also suggests an isolated MoOx structure. Furthermore, a close examination of the reported Raman band positions of the proposed dimeric structures in different studies did not match. Ribeiro *et al.*[7] assigned the 962 cm^{-1} as Mo=O stretch of monomeric $O=MoO_4$ and the 868 cm^{-1} as Mo-O-Mo stretch mode for a dimer while Iglesia *et al.*[5] assigned 970 and 1045 cm^{-1} as the Mo=O stretch of dimeric Mo_2O_5 species. The 962 or 970 cm^{-1} is Mo=O stretch of isolated dioxo MoOx species, and the 868 cm^{-1} is likely the stretch mode of Mo-O-Si/Al. The band at 1045 cm^{-1} is close to the characteristic of crystalline $Al_2(MoO_4)_3$ NPs, which reflects the high calcination temperature employed in those studies.

3.4. Conclusions

The surface MoOx species were found to anchor at both Brønsted acid sites inside the zeolite channel, external silica sites and trace of them also at extra-framework alumina site. At low Mo loading, surface MoOx species generally prefer to anchor at Brønsted acid sites.

The dehydrated supported MoOx phase is highly dispersed on the ZSM-5 supports with the exception of the presence of crystalline MoO_3 NPs on the silica-rich ZSM-5 (Si/Al=140). The *in situ* UV-vis results indicate that the dispersed surface MoOx species are isolated (Eg=4.6-4.9 eV)[14, 15] and fully oxidized as $Mo^{+6}Ox$ species (absence of d-d transitions) under oxidizing conditions. Combined *in situ* Raman spectroscopy and DFT calculations revealed the presence of four distinct surface MoO_x structures on the MoO_3/ZSM-5 catalysts: 1) isolated dioxo $(O=)_2MoO_2$ species over two Brønsted acid sites at low Mo loading and high Al content; 2) isolated dioxo $(O=)_2MoO_2$ species over one Brønsted acid site at increasing Mo loading or low Al content; 3) isolated dioxo $(O=)_2MoO_2$ species over two Si-OH groups at low Al content; 4) isolated mono-oxo $O=MoO_4$ species over external Al sites.

References

1. Wang, D.; Lunsford, J.; Rosynek, M., *Topics in Catalysis* **1996,** *3* (3-4), 289-297.
2. Chen, L. Y.; Lin, L. W.; Xu, Z. S.; Li, X. S.; Zhang, T., *Journal of Catalysis* **1995,** *157* (1), 190-200.
3. Wang, D.; Lunsford, J. H.; Rosynek, M. P., *Journal of Catalysis* **1997,** *169* (1), 347-358.
4. Liu, W.; Xu, Y., *Journal of Catalysis* **1999,** *185* (2), 386-392.
5. Li, W.; Meitzner, G. D.; Borry Iii, R. W.; Iglesia, E., *Journal of Catalysis* **2000,** *191* (2), 373-383.
6. Bell, R. G.; Jackson, R. A.; Catlow, C. R. A., *Zeolites* **1992,** *12* (7), 870-871.
7. Rzhevskii, A. M.; Choi, P.; Ribeiro, F. H.; Gulotty, R. J.; Olken, M. M., *Catalysis Letters* **2001,** *73* (2-4), 187-191.
8. Tian, H.; Roberts, C. A.; Wachs, I. E., *The Journal of Physical Chemistry C* **2010,** *114* (33), 14110-14120.
9. Matus, E. V.; Ismagilov, I. Z.; Sukhova, O. B.; Zaikovskii, V. I.; Tsikoza, L. T.; Ismagilov, Z. R.; Moulijn, J. A., *Industrial & Engineering Chemistry Research* **2006,** *46* (12), 4063-4074.
10. Zhou, D.; Ma, D.; Liu, X.; Bao, X., *The Journal of Chemical Physics* **2001,** *114* (20), 9125-9129.
11. Zhou, D.; Zhang, Y.; Zhu, H.; Ma, D.; Bao, X., *The Journal of Physical Chemistry C* **2007,** *111* (5), 2081-2091.
12. Gao, J.; Zheng, Y.; Fitzgerald, G. B.; de Joannis, J.; Tang, Y.; Wachs, I. E.; Podkolzin, S. G., *The Journal of Physical Chemistry C* **2014**.
13. Kiricsi, I.; Flego, C.; Pazzuconi, G.; Parker, W. O., Jr.; Millini, R.; Perego, C.; Bellussi, G., *The Journal of Physical Chemistry* **1994,** *98* (17), 4627-4634; Glazneva, T. S.; Kotsarenko, N. S.; Paushtis, E. A., *kinetics and catalysis* **2008,** *49* (6), 859-867.
14. Lee, E. L.; Wachs, I. E., *Journal of Physical Chemistry C* **2008,** *112* (51), 20418-20428.
15. Lee, E. L.; Wachs, I. E., *Journal of Physical Chemistry C* **2007,** *111* (39), 14410-14425.
16. Lee, E. L.; Wachs, I. E., *Journal of Physical Chemistry C* **2008,** *112* (16), 6487-6498.
17. Yu, Y.; Xiong, G.; Li, C.; Xiao, F.-S., *Microporous and Mesoporous Materials* **2001,** *46* (1), 23-34.
18. Handzlik, J.; Sautet, P., *The Journal of Physical Chemistry C* **2008,** *112* (37), 14456-14463.
19. Regalbuto, J.; Ha, J.-W., *Catalysis Letters* **1994,** *29* (1-2), 189-207.
20. Ismail, H. M.; Zaki, M. I.; Bond, G. C.; Shukri, R., *Applied Catalysis* **1991,** *72* (1), L1-L12.
21. Rajagopal, S.; Marini, H. J.; Marzari, J. A.; Miranda, R., *Journal of Catalysis* **1994,** *147* (2), 417-428.
22. Chen, L.; Lin, L.; Xu, Z.; Zhang, T.; Li, X., *Catalysis Letters* **1996,** *39* (3-4), 169-172.
23. Weckhuysen, B. M.; Wang, D.; Rosynek, M. P.; Lunsford, J. H., *Journal of Catalysis* **1998,** *175* (2), 338-346; Weckhuysen, B. M.; Wang, D.; Rosynek, M. P.; Lunsford, J. H., *Journal of Catalysis* **1998,** *175* (2), 347-351.
24. Solymosi, F.; Cserényi, J.; Szöke, A.; Bánsági, T.; Oszkó, A., *Journal of Catalysis* **1997,** *165* (2), 150-161.
25. Liu, S.; Wang, L.; Ohnishi, R.; Ichikawa, M., *Journal of Catalysis* **1999,** *181* (2), 175-188.
26. Aritani, H.; Shinohara, S.; Koyama, S.-i.; Otsuki, K.; Kubo, T.; Nakahira, A., *Chemistry Letters* **2006,** *35* (4), 416-417.
27. Aritani, H.; Tanaka, T.; Funabiki, T.; Yoshida, S.; Eda, K.; Sotani, N.; Kudo, M.; Hasegawa, S., *The Journal of Physical Chemistry* **1996,** *100* (50), 19495-19501.
28. Jiang, H.; Wang, L.; Cui, W.; Xu, Y., *Catalysis Letters* **1999,** *57* (3), 95-102; Ma, D.; Shu, Y.; Bao, X.; Xu, Y., *Journal of Catalysis* **2000,** *189* (2), 314-325.

Chapter 4.

The catalytic active sites of supported MoO_3/ZSM-5 catalysts during methane Dehydroaromatization (DHA)

Abstract

Four distinct surface Mo oxide species have been identified in Chapter 3, and their catalytic roles for methane DHA are investigated in this chapter. This chapter discusses *operando* Raman-MS and *in situ* extended X-ray absorption fine structure (EXAFS) and X-ray absorption near edge spectroscopy (XANES) studies on the active components of supported MoO_3/ZSM-5 catalysts during methane DHA. *Operando* Raman-MS investigated the relative reactivity of four distinct MoOx species on supported MoO_3/ZSM-5 catalysts during methane DHA reaction. The reducibility of the four distinct surface MoOx species decreases in the order of dioxo $(O=)_2MoO_2$ on double Al-Al sites >dioxo $(O=)_2MoO_2$ on single Al sites >>dioxo $(O=)_2MoO_2$ on double Si-Si sites~ mono-oxo $O=MoO_4$ species on extra-framework Al sites. The *operando* Raman-MS observed that the initial reactivity of methane DHA does not correlate to different MoOx structures but increases with decreasing Si/Al ratio of the ZSM-5 support. The absence of correlation between reactivity and surface MoOx structure might be due to the dynamic structural change of surface MoOx species during methane DHA reaction. The correlation between reactivity and Si/Al ratio suggests that presence of Brønsted acidity is necessary for the catalytic oligomerization of intermediate C_2H_x species to benzene which is the reason for zeolites being applied to oil cracking. The reduction of surface MoOx species does not immediately initiate the formation of benzene, thus the initial fully oxidized MoOx species is not the catalytic active site for methane DHA reaction. The *in situ* EXAFS/XANES during methane DHA reaction condition provides the molecular information of catalytic active phase of the supported MoO_3/ZSM-5 catalysts.

In situ EXAFS/XANES demonstrated that the active site is the poorly ordered molybdenum oxycarbide (MoOxCy) nanoparticles with a predominate Mo^{2+} oxidation state.

Isotopic kinetic experiments using CH_4/CD_4 as feed gas have provided important information on the rate determining step of methane DHA on supported MoO_3/ZSM-5 catalysts. The results demonstrated that the rate determining step (rds) is the cleavage of C-H bond rather than the hydrogen removal based on two observations: 1) a significant isotopic kinetic effect for methane DHA over supported MoO_3/ZSM-5 catalysts, and 2) the immediate evolution of dihydrogen at the same time when methane activation and benzene formation occur, thus the hydrogen removal is not the rds.

Introduction

A large number of studies have been focused on addressing the state of molybdenum in the zeolite. Under reaction conditions, fully oxidized Mo species are converted to molybdenum carbide species, at which time no benzene is formed and is defined as the induction period[1]. Studies of the induction period of the methane dehydroaromatization reaction have proposed a reaction mechanism for the induction period in two steps[1]:

$$4MoO_3 + CH_4 \rightarrow 4MoO_2 + CO_2 + 2H_2O$$

$$4MoO_2 + CH_4 \rightarrow 4Mo_2C + CO_2 + 5H_2O + CO + 3H_2$$

The state and location of the molybdenum carbide species is more complicated than the proposed two steps. Small cluster or isolated Mo species were expected to be the active sites since bulk Mo_2C and MoO_3 are found not active but supported MoO_3 and Mo_2C catalysts (on support materials such as SiO_2, Al_2O_3 and ZSM-5) are active for nonoxidative conversion of methane to benzene and only carbon dioxide and water are formed.[2,3] Solymosi *et al.*[4] and Xu *et al.*[5] reported that supported MoO_3/SiO_2 and MoO_3/Al_2O_3 catalysts have very low activities and low conversions of methane (<1% at 700 ^oC), but the selectivity towards benzene is about 65-86%. Supported MoO_3/ZSM-5 catalysts have the highest activity and selectivity towards benzene (ca. 85%)[3]. Based on these observations, it was suggested that a dispersed Mo_2C species is responsible for the methane to benzene conversion.

Direct characterization of the catalytic active sites of the supported MoO_3/ZSM-5 catalysts was also reported as reviewed in Chapter 1. Early *ex situ* XPS studies[6] claimed Mo_2C as the catalytic active sites for methane DHA, and a small amount of Mo^{6+} remains

on the catalyst. *Ex situ* EXANES/XANES studies[7,8] claimed that molybdenum oxycarbide as the catalytic active sites for methane DHA. As mentioned previously, the *ex situ* characterization cannot represent the actual catalyst under reaction conditions, especially when the claimed Mo_2C species are not stable upon exposure to air.[9]

In situ EXAFS/XANES studies[10,11,12] under methane DHA reaction conditions were reported to elucidate the catalytic active sites of supported MoO_3/ZSM-5 catalyst. Under reaction conditions, the initial fully oxidized Mo^{6+} species were reduced to molybdenum oxycarbide (MoO_xC_y) clusters (containing ~10 Mo atoms) located inside the zeolite which are proposed as the catalytic active sites.

Theoretical calculations have also been applied to investigate the methane dissociation on molybdenum carbide on HZSM-5[13]. Mononuclear, dinuclear and polymeric clusters of molybdenum carbide structures on Brønsted acid sites of 5T and 12T zeolites were constructed. The activation energy for heterolytic dissociation of the C-H bond of methane on binuclear molybdenum carbide is lower than that on mononuclear molybdenum carbide. The theoretical calculation adopted the proposed molybdenum oxycabide structures and investigated the formation and energetics of dinuclear molybdenum oxycarbide structure from dinuclear octahedral molybdenum oxides by substituting the O atoms with C and CH_2 units[14]. They concluded that the formation of C_2H_2 species and C-O bond during the reduction of molybdenum oxides is energetically favorable (zero energy barrier), but C_2H_2 units have a tendency to aggregate and form carbonaceous species. This study supports the importance of Mo sites for the activation of methane which is consistent with experimental studies[2,3]. However, the model is based on unsupported molybdenum oxycarbide and the synergetic effect with the zeolite host is

ignored in this study. This calls for relevant DFT studies based on models which are close to the actual catalytic active sites of supported MoO_3/ZSM-5 during methane DHA.

The focus of this chapter is to investigate the reactivity of the initial surface MoOx species present for supported MoO_3/ZSM-5 catalysts during methane activation at high temperatures by *operando* Raman-MS spectroscopy (coupling of *in situ* Raman with an online mass spectrometer). The objectives of this chapter are to 1) investigate the reactivity of each distinct surface MoOx species, 2) establish the catalytic active sites of supported MoOx/ZSM-5 catalysts responsible for methane DHA, 3) correlate the structure-activity/selectivity relationships for methane DHA with steady-state kinetic studies and DFT calculations, and 4) determine the rate-determining-step for methane DHA by supported MoO_3/ZSM-5 catalysts by isotopic CH_4/CD_4-temperature programmed surface reaction (TPSR) experiments.

4.1. Experimental methods

4.1.1. *In situ* Raman spectroscopy

The *in situ* Raman spectra of the zeolite-supported metal oxide catalysts were obtained with a high resolution, dispersive Raman spectrometer (Horiba-Jobin Yvon LabRam HR) equipped with three laser excitations (532, 442 and 325 nm). More details are discussed in Chapter 2, section 2.4.

4.1.2. *Operando* Raman-MS spectroscopy during methane DHA

The *operando* Raman-MS spectroscopy provides Raman measurements under reaction conditions with simultaneous analysis of gaseous reactants and products *via* online mass spectrometer (Varian, 1200L quadrupole), and more details are provided in Chapter 2, section 2.4.2.

4.1.3. *In situ* X-ray absorption spectroscopy (XAS) during CH_4 DHA

In situ X-ray absorption spectroscopy measurements were obtained at Brookhaven National Laboratory, and the experimental details are provided in Chapter 2, section 2.5.2.

4.1.4. Isotopic CH_4/CD_4Temperature Programmed Surface Reaction (TPSR) spectroscopy

The isotopic CH_4/CD_4 temperature programmed surface reaction spectroscopy measurements were conducted on the Altamira (AMI-200) equipped with an online Dycor DM100 mass spectrometer. Please see more experimental details in Chapter 2, section 2.7.2.

4.1.5. Temperature Programmed Oxidation (TPO) of coke deposits on supported MoO_3/ZSM-5 catalysts from CH_4 DHA

The TPO experiments were conducted on the Altamira AMI-200 equipped with a Dycor DM100 Mass spectrometer. Please see more details about TPO in Chapter 2, section 2.7.3.

4.2. Results

4.2.1. Surface MoOx Species on ZSM-5

Four distinct surface MoO_x structures were identified for the MoO_3/ZSM-5 catalysts as indicated in Chapter 2: 1) isolated dioxo $(O=)_2MoO_2$ species over two Brønsted acid sites at low Mo loading and high Al content; 2) isolated dioxo $(O=)_2MoO_2$ species over one Brønsted acid site at increasing Mo loading or low Al content; 3) isolated dioxo $(O=)_2MoO_2$ species over two Si-OH groups at low Al content; and 4) isolated mono-oxo $O=MoO_4$ species at external Al sites.

4.2.2. Temperature-programmed *operando* Raman-MS spectroscopy during methane DHA

The *operando* Raman-MS spectra for all the supported MoO3/ZSM-5 catalysts are presented in figures from **Figure 4- 2** to **Figure 4- 9**, and the supported 2% MoO_3/ZSM-5(Si/Al=25) catalyst are shown in **Figure 4- 1** as a representative example. In **Figure 4- 1**, The MS spectra for methane and the CH_4 DHA reaction products indicate several reaction regimes: no reaction (550-665^oC), modest formation of CO and CO_2 (670-740^oC), H_2O is not detected because the line from the reactor cell to the MS is not heated), fast conversion of CH_4, sharp production of CO and initiation of benzene formation (740-760^oC), and continuous production of benzene (>750^oC). Although C_2H_4 formation is not observed in **Figure 4- 1** its formation was observed for some catalysts and appeared at the same temperature as the sharp CO peak (see **Figure 4- 6**).

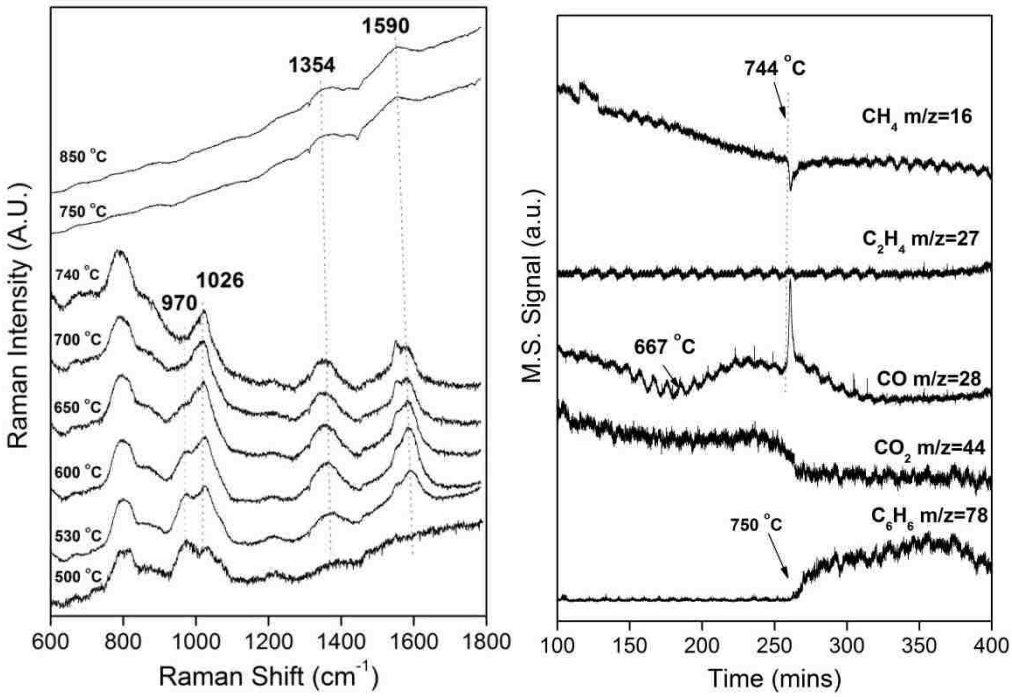

Figure 4- 1 *Operando* Raman-MS spectra of 2% MoO_3/ZSM-5 Si/Al=25 during CH_4 DHA reaction

The simultaneous changes taking place on the catalyst are provided by the Raman spectra shown in **Figure 4- 1**. Prior to CH_4 DHA, the Raman spectrum at 500 ^oC corresponds to the fully oxidized and dehydrated catalyst in flowing 10% O_2/He and exhibits Raman bands at 970 and 1026 cm^{-1} from the dioxo $(O=)_2MoO_2$ on framework single Al sites and mono-oxo $O=MoO_4$ on extra-framework Al_2O_3 nanoparticles. In the presence of flowing CH_4, the intensity of the initial dioxo surface MoO_4 species (970 cm^{-1}) continuously decreases between 530-730^oC and is complete reduced at 730-740 ^oC, resulting in CO/CO_2 formation. The intensity of mono-oxo surface $O=MoO_4$ species (1026 cm^{-1}) are almost unperturbed from 550-740 ^oC. Although not readily apparent in **Figure 4- 1**, the *operando* Raman-MS spectra indicate that the concentration of surface mono-oxo surface $O=MoO_4$ species (1026 cm^{-1}) increases during reaction, which may reflect the

dealumination taking place under the elevated reaction conditions (see figures from **Figure 4- 2** to **Figure 4- 9**).

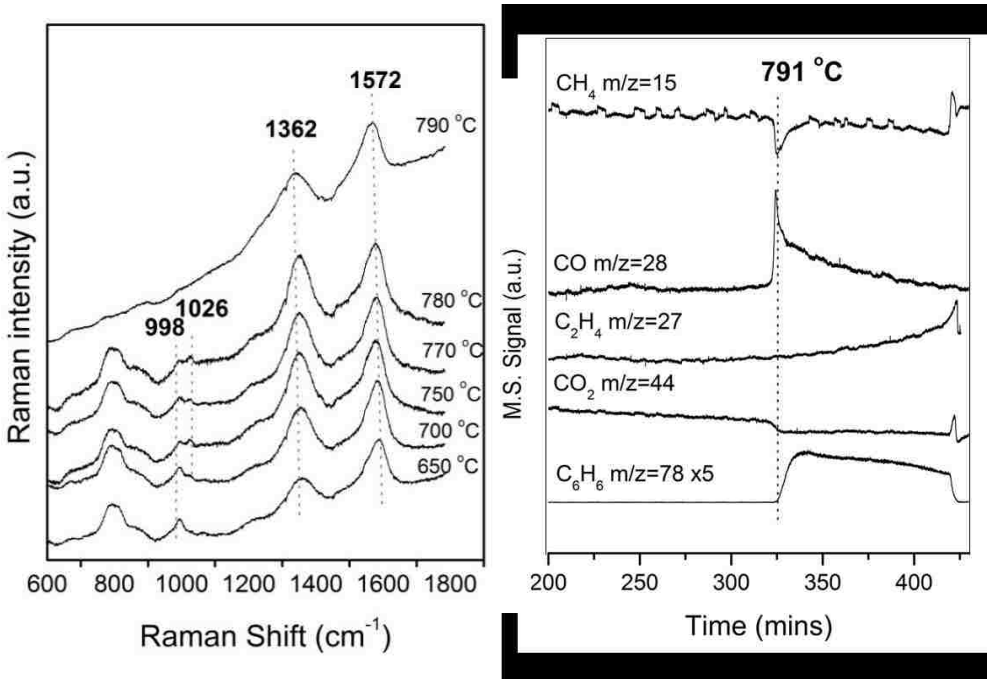

Figure 4- 2 Temperature-programmed *operando* Raman-MS (442 nm) spectra of 1 % MoO_3/ZSM-5 (Si/Al=15) in 1.5% CH_4/He flow

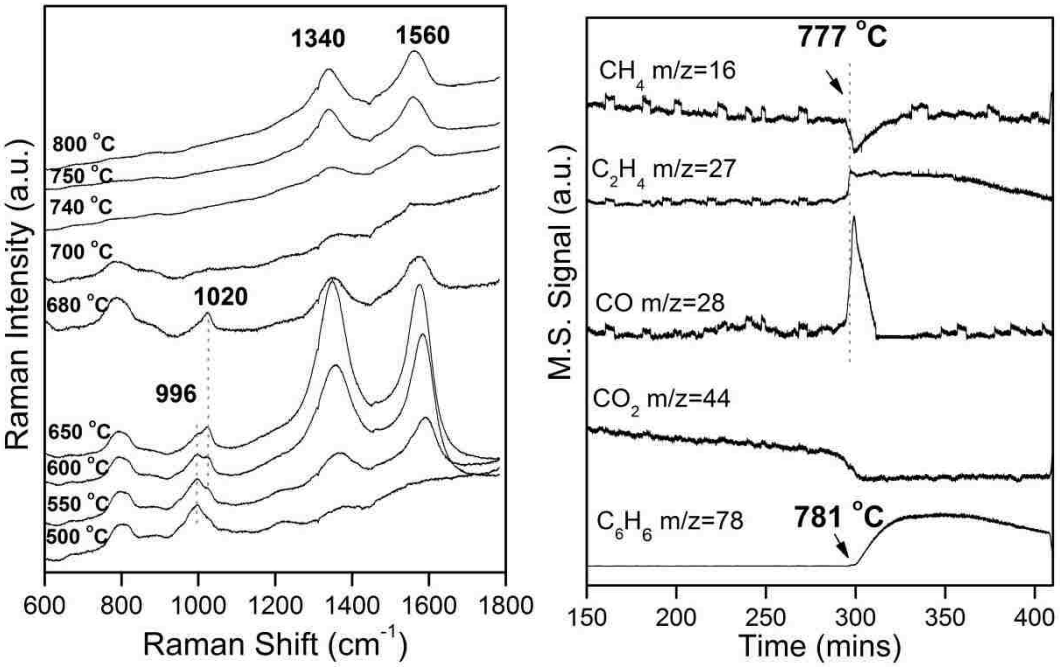

Figure 4- 3 Temperature-programmed *operando* Raman-MS (442 nm) spectra of 2 % MoO_3/ZSM-5 (Si/Al=15) in 1.5% CH_4/He flow

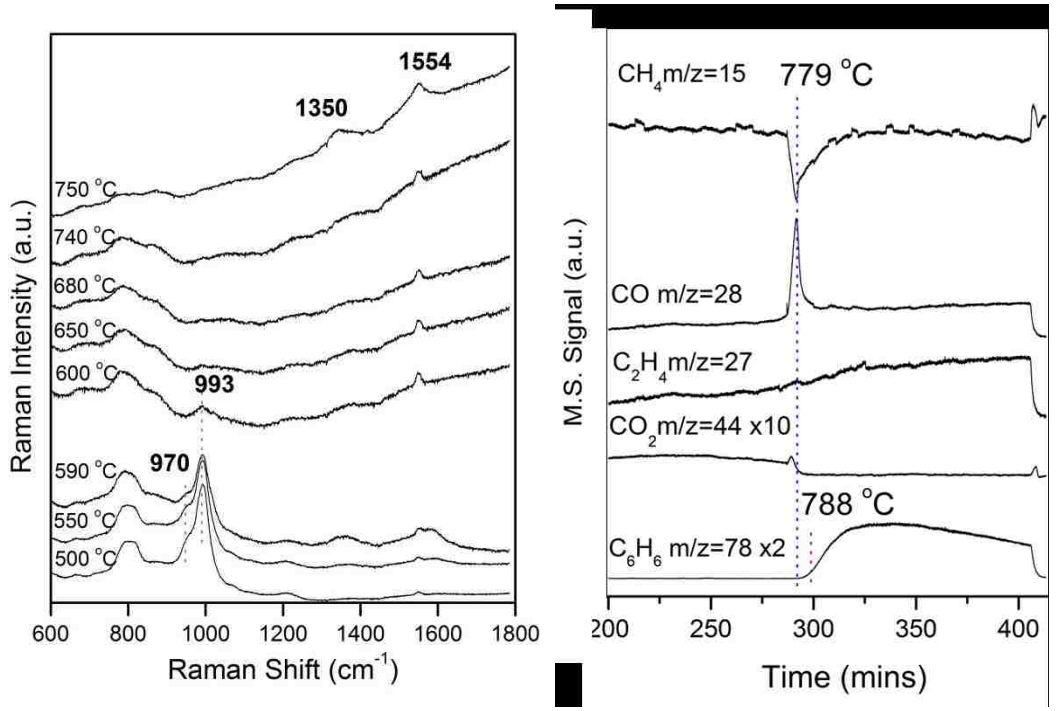

Figure 4- 4 Temperature-programmed operando Raman-MS (442 nm) spectra of 3 % MoO_3/ZSM-5 (Si/Al=15) in 1.5% CH_4/He flow

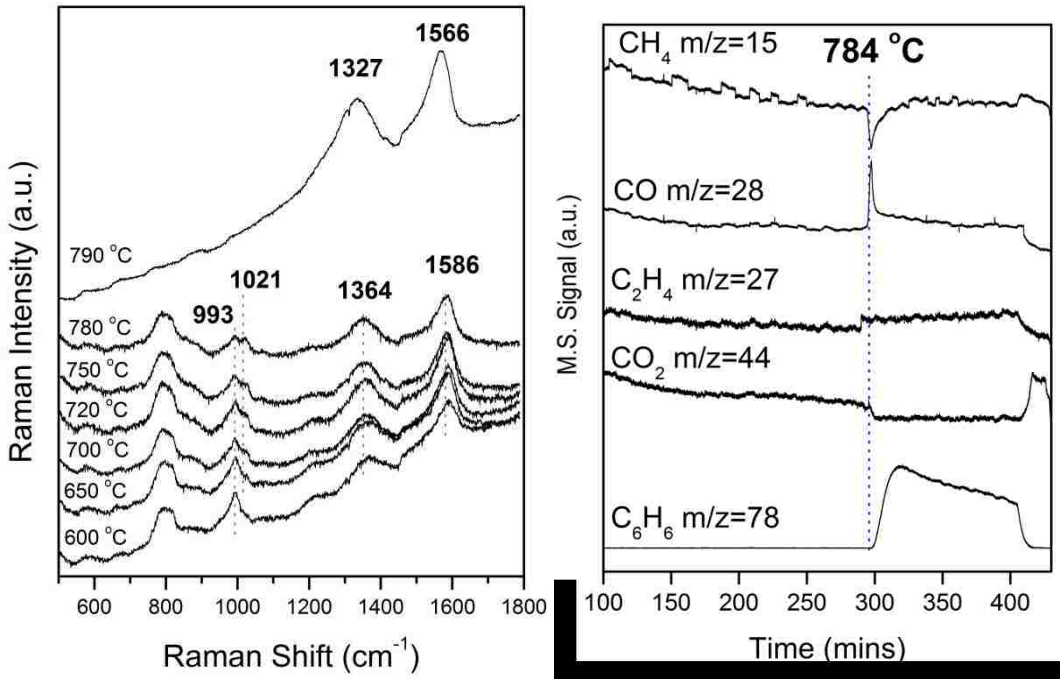

Figure 4- 5 Temperature-programmed *operando* Raman-MS (442 nm) spectra of 4 % MoO_3/ZSM-5 (Si/Al=15) in 1.5% CH_4/He flow

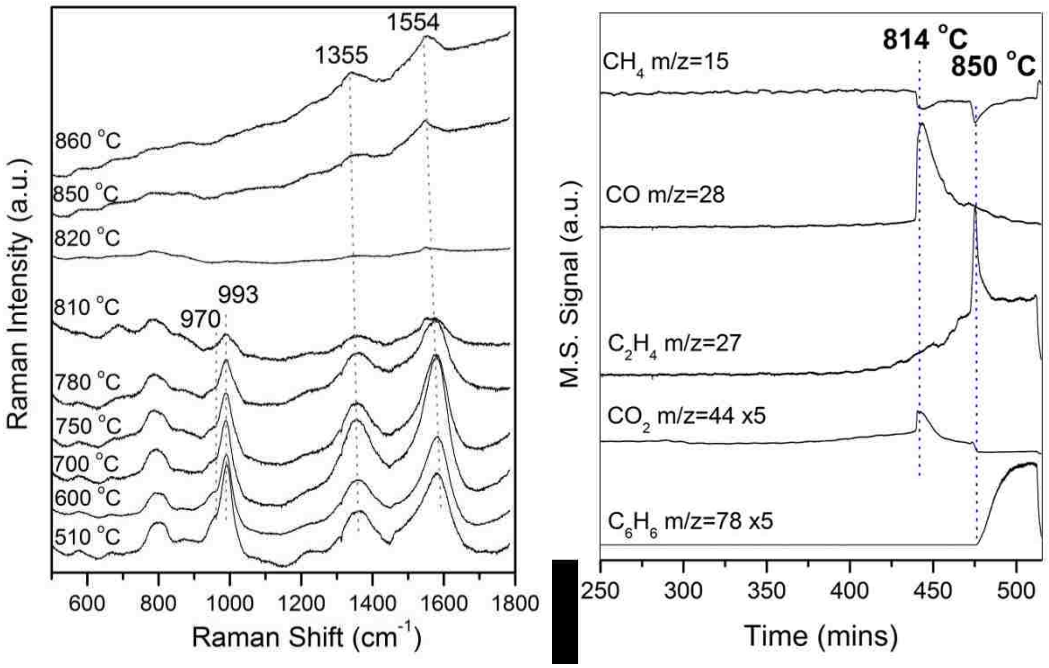

Figure 4- 6 Temperature-programmed operando Raman-MS (442 nm) spectra of 5% MoO_3/ZSM-5 (Si/Al=15) in 1.5% CH_4/He flow

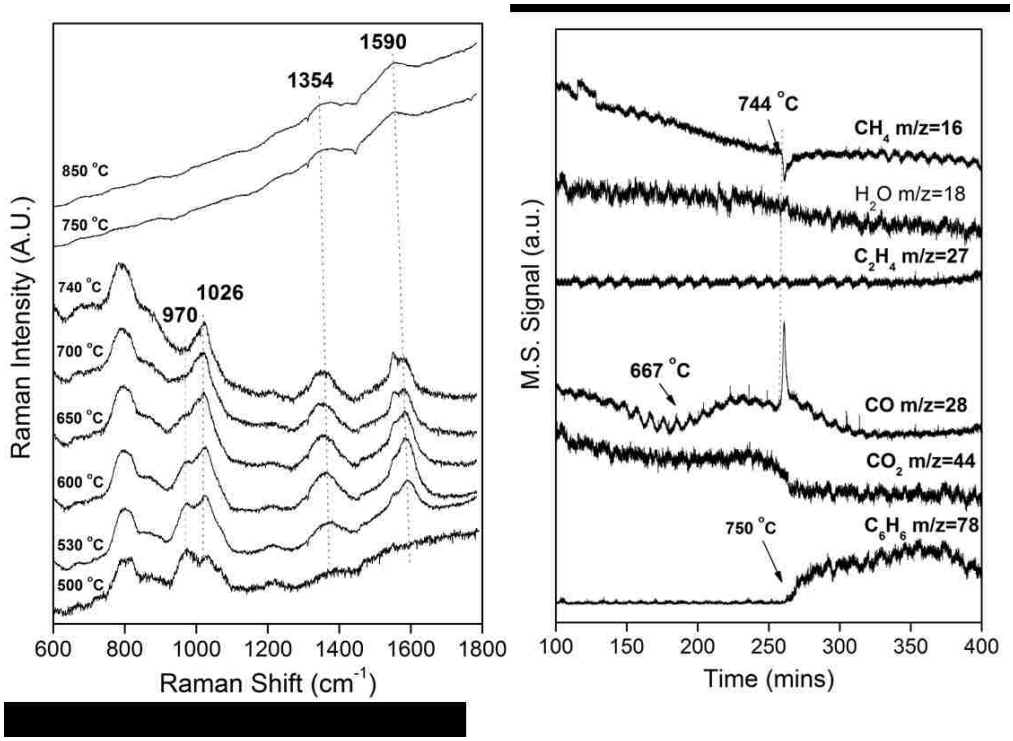

Figure 4- 7 Temperature-programmed *operando* Raman-MS (442 nm) spectra of 2 % MoO_3/ZSM-5 (Si/Al=25) in 1.5% CH_4/He flow

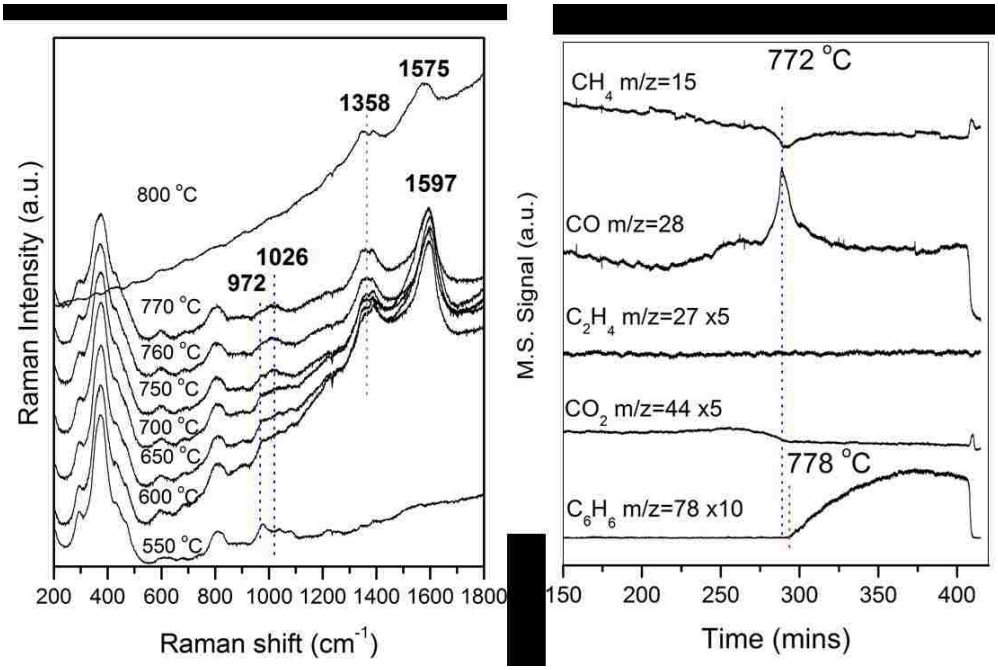

Figure 4- 8 Temperature-programmed *operando* Raman-MS (442 nm) spectra of 2 % MoO_3/ZSM-5 (Si/Al=40) in 1.5% CH_4/He flow

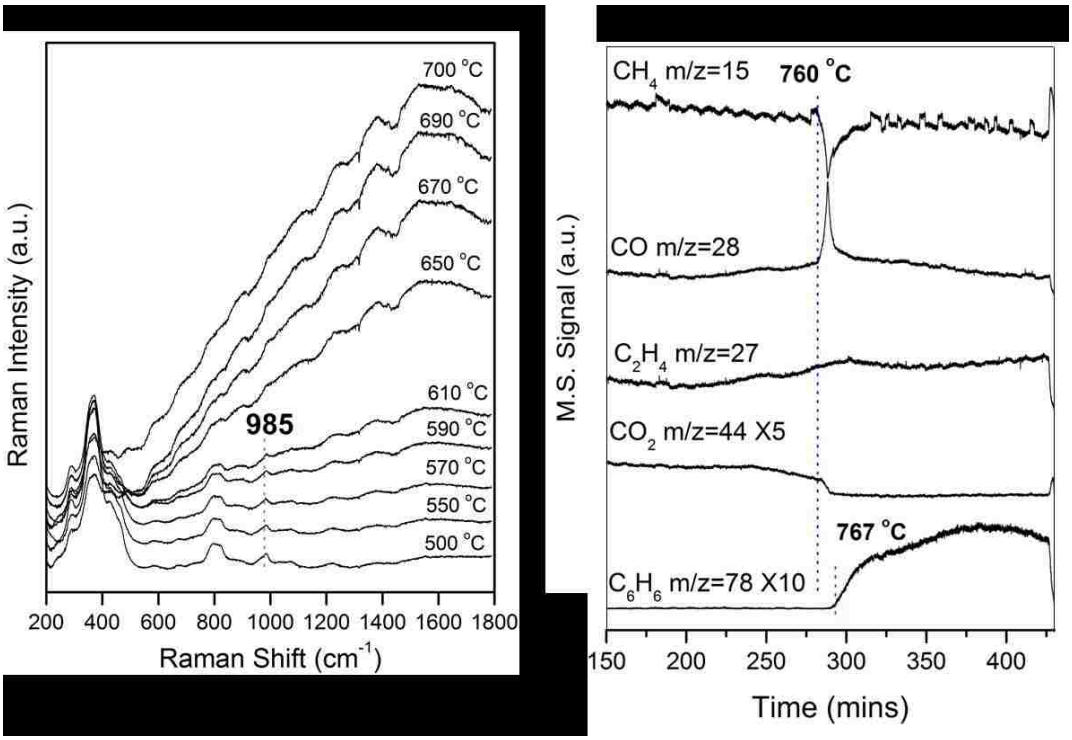

Figure 4- 9 Temperature-programmed *operando* Raman-MS (442 nm) spectra of 2 % MoO_3/ZSM-5 (Si/Al=140) in 1.5% CH_4/He flow

In addition, new Raman bands appear at 1354 and 1590 cm^{-1} above 530 ^{o}C that are the characteristic D and G bands of graphite-type species, respectively.[15] The somewhat broad Raman bands indicates that the surface coke species might be a mixture of olefins, conjugated olefins, aromatics, polycyclic aromatics and graphite.[15] Unlike the wide temperature range for reduction of the surface dioxo MoO_4 species (530-740^{o}C), the surface mono-oxo MoO_5 species are rapidly reduced in a very narrow temperature range (740-750^{o}C). Only after the surface mono-oxo MoO_5 species are reduced does the CH_4 DHA reaction initiate to from benzene. The formation of benzene at 750^{o}C may be related to either (1) reduction of the surface mono-oxo MoO_5 species or (2) just overcoming the activation barrier for methane activation at 750^{o}C. Above 740^{o}C, the characteristic Raman bands of the surface MoO_x species, which may have been completely reduced, and the ZSM-5 support are obscured by sample fluorescence and only the broad and weak Raman bands of surface coke at 1354 and 1590 cm^{-1} remain.

The reduction temperatures for the surface dioxo MoO_4 species and the temperatures for initiation of benzene formation for all the supported MoO_3/ZSM-5 catalysts are summarized in **Table 4- 1**. In general, reduction of the surface dioxo MoO_4 species precedes formation of benzene. The initiation of benzene formation or reduction of surface Mo oxide species is not affected by either Mo loading (see **Figure 4- 10** and **Figure 4- 11**). But the initial reactivity is slightly favored by catalysts with low Si/Al ratio of ZSM-5, which implies the presence of surface Brønsted acidity is necessary for the oligomerization towards benzene.

Table 4- 1 Reduction temperature of MoO_x species and evolution temperature of C_6H_6 over supported MoO_3/ZSM-5 catalysts derived from *operando* Raman-MS spectroscopy

	Mo loading (wt%)	Si/Al ratio	Al/Mo ratio	MoOx reduction temp (^oC)	C_6H_6 evolution temp (^oC)
1Mo-Z-15	1	15	14.0	790	791
2Mo-Z-15	2	15	7.0	777	781
3Mo-Z-15	3	15	4.7	779	788
4Mo-Z-15	4	15	3.5	780	784
5Mo-Z-15	5	15	2.8	820	850
2Mo-Z-25	2	25	4.3	740	750
2Mo-Z-40	2	40	2.8	760	778
2Mo-Z-140	2	140	0.8	788	791

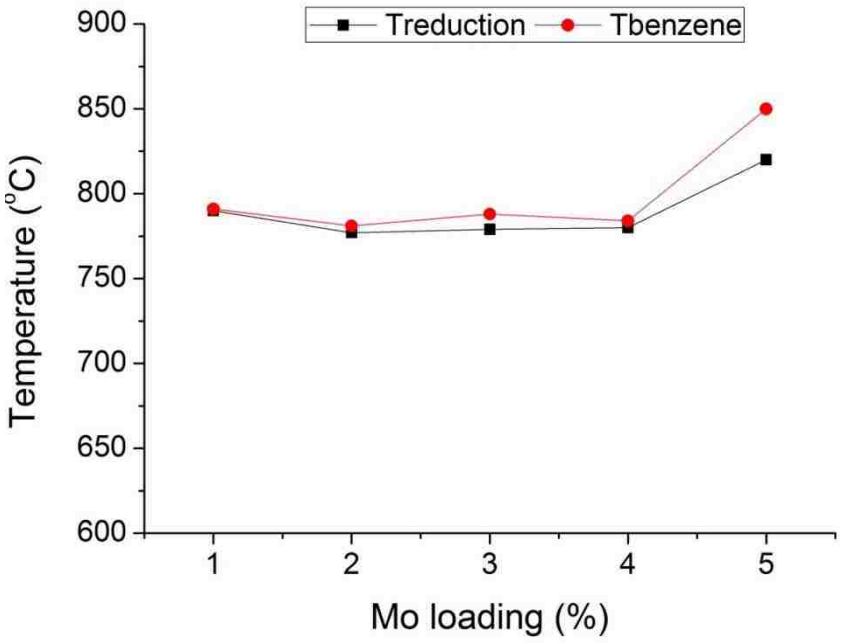

Figure 4- 10 The reduction temperature of surface dioxo MoOx structure and evolution temperature of benzene on supported MoO_3/ZSM-5 (Si/Al=15) against Mo content (1-5 wt%)

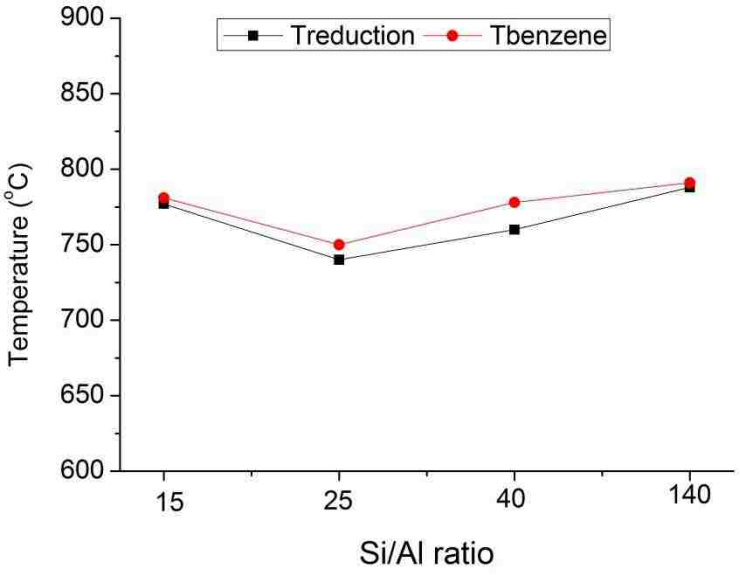

Figure 4- 11 The reduction temperature of surface dioxo MoOx structure and evolution temperature of benzene on supported 2wt% MoO_3/ZSM-5 against Si/Al ratio (15-140)

4.2.3. *In situ* XANES/EXAFS spectroscopy

Additional structural insights about the nature of the supported Mo species on ZSM-5 during methane DHA were accessed with *in situ* X-ray absorption measurements (XANES and EXAFS). The *in situ* XANES from the Mo K-edge of the supported MoO_3/ZSM-5 catalysts before and during methane DHA at 700 ^oC, after 90 minutes of reaction, are depicted in **Figure 4- 12**. The *in situ* EXAFS of the supported MoO_3/ZSM-5 during methane DHA at at 700 ^oC, after 90 minutes of reaction, are depicted in **Figure 4-13**. The *in situ* X-ray absorption spectra of bulk Mo reference compounds (MoO_2 and Mo_2C) with known structures are provided in **Figure 4- 14**. The energy position of the XANES pre-edge reflects the Mo oxidation state and the EXAFS provides information about the radial distribution of atoms around the Mo atom.

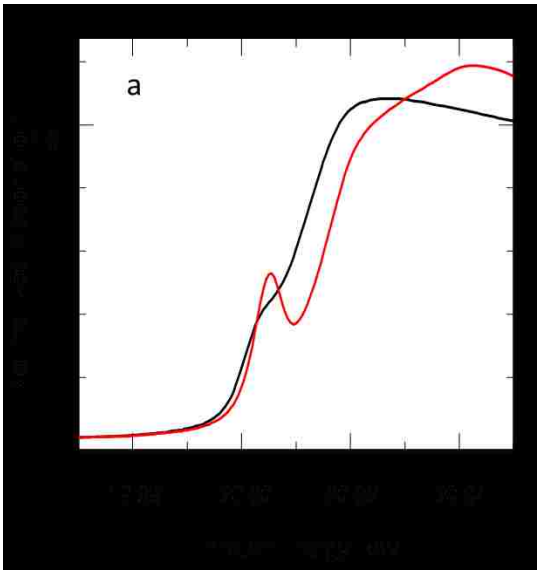

Figure 4- 12 *In situ* XANES spectra of 2 % MoO_3/ZSM-5 (Si/Al=25) before (red) and after (black) reaction with CH_4

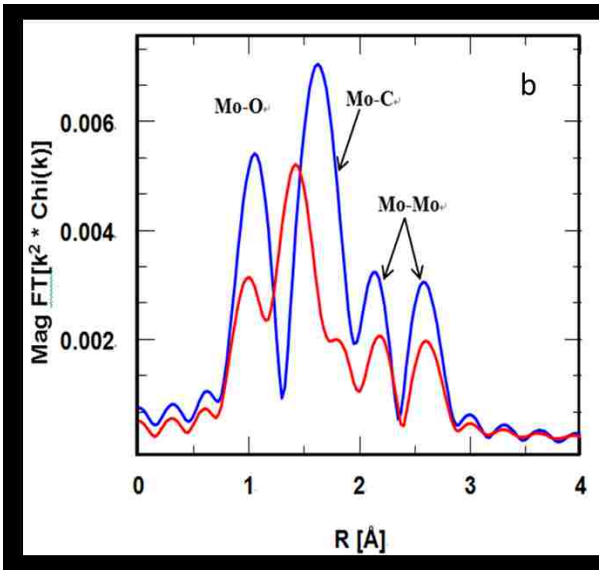

Figure 4- 13 *In situ* EXAFS spectra during CH_4 DHA of 4 % MoO_3/ZSM-5 (Si/Al=15) (blue) and 2% MoO_3/ZSM-5 (Si/Al=15) (red) reaction with CH4 for 30

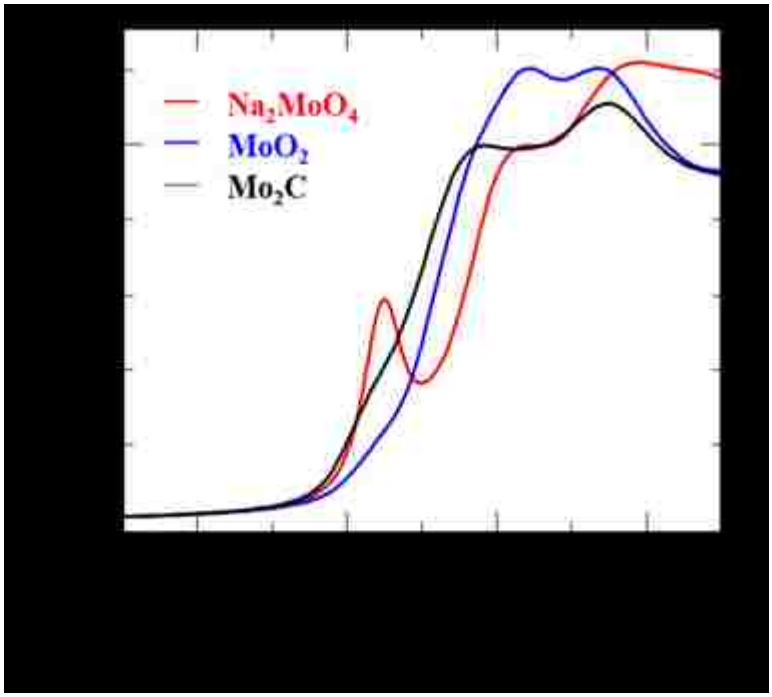

Figure 4- 14 XANES spectra of bulkNa_2MoO_4 which is consisted of isolated tetrahedral $Mo^{6+}O_4$ unit(red curve), bulk MoO_2 which is consisted of Mo^{4+} species with distorted octahedral symmetry(blue curve) and bulk Mo_2C which is consisted of Mo^{2+} with hexagonal bcc lattice unit(black curve).

The XANES pre-edge position of the fully oxidized, dehydrated supported 2% MoO_3/ZSM-5 (Si/Al=25) catalyst occurs at ~20.0167 keV, which is consistent with the

Mo^{+6} oxidation state.[12] The pronounced XANES pre-edge reflects the absence of center of symmetry, which implies MoO_4 or MoO_5 coordination.[12] The corresponding k-space EXAFS spectrum contains a strong signal at ~1.0Å from the terminal oxygen atoms, Mo=O bonds, and a weaker feature as a shoulder at ~1.5Å from the bridging Mo-O-Si/Al bonds.[16] There is no feature at ~3-4 Å characteristic of Mo-O-Mo bond distances in the second coordination sphere, thus surface MoOx sites are uniquely presented as monomer. After 90 minutes of methane DHA at 700^{o}C, The absence of the pronounced XANES pre-edge peak and the shift of the XANES edge (**Figure 4- 15**) to 20.0016 keV similar to bulk Mo_2C reference compound demonstrates that surface MoOx sites have been reduced to predominantly Mo^{2+}, but the edge is not identical to the crystalline Mo_2C reference, thus the nature of the active catalyst is somewhere different from the crystalline Mo_2C structure.

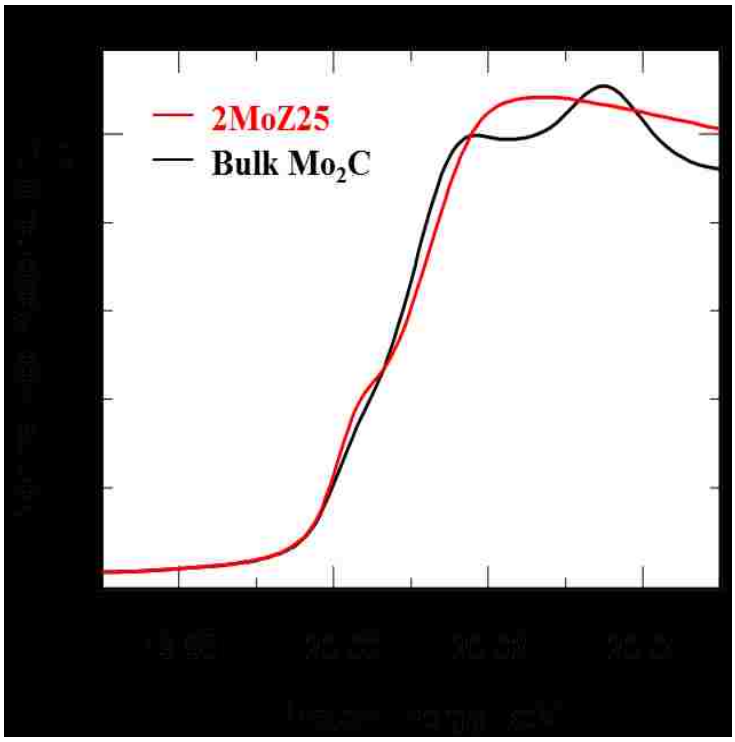

Figure 4- 15 *In situ* XANES of 2% MoO_3/ZSM-5 (Si/Al=25) during methane DHA at 700 ^oC for 90 mins (red curve) and bulk Mo_2C reference compound (prepared *in situ* from bulk MoO_3 with CH_4/H_2 gaseous mixture)

The EXAES also changes dramatically during methane DHA, the peak associated with terminal Mo=O bonds at ~1.0Å is significantly diminished and new bands at ~1.8Å and ~2.2/2.6Å appear from Mo-C and Mo-Mo distances of Mo_2C, respectively, are present (compare with the bulk Mo_2C reference compound in **Figure 4- 16**).

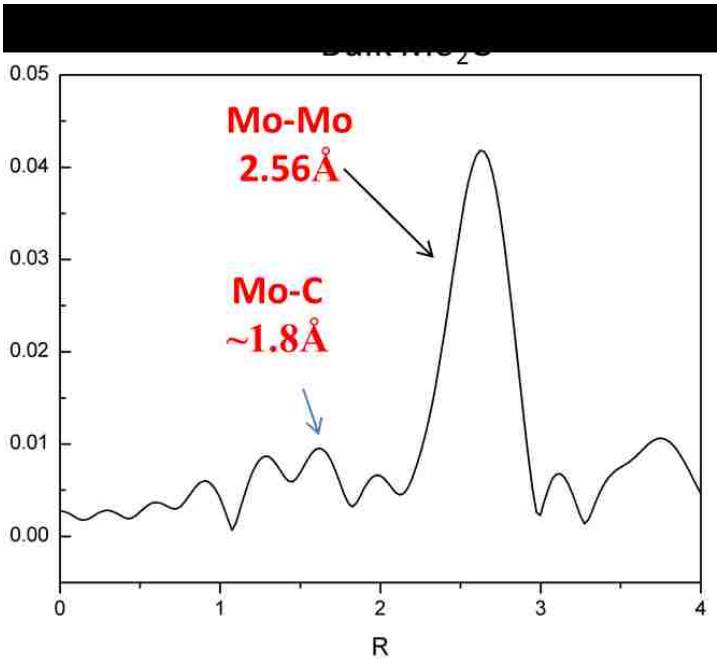

Figure 4- 16 *In situ* EXAFS spectra of bulk Mo_2C

Furthermore, the overall magnitude of the Mo EXAFS absorption (**Figure 4- 12b**) for the supported Mo/ZSM-5 catalyst is several hundred orders of magnitude lower than that of bulk crystalline Mo_2C, which corresponds to the conclusion that the former has a poorly ordered molyoxycarbide structure. The relative intensity of the Mo-C and Mo-Mo coordination peaks also do not resemble those of the bulk Mo_2C reference. Last, the relative intensity of Mo-C/Mo-Mo peaks in the EXAFS for the activated catalyst is drastically different from bulk Mo_2C reference. The activated catalyst has predominate Mo-C coordination and weak Mo-Mo absorption, whereas the bulk Mo_2C has a strong absorption from Mo-Mo coordination at 2.5Å and hundred times weaker absorption from Mo-C coordination at 1.8 Å.[12] The EXASF absorption intensity allows an estimation of the domain size of the activated catalyst. The weak Mo-Mo absorption corresponds to a small domain size, and the fitting results estimated that only three Mo atoms are in the second coordination sphere of the MoOxCy species. In summary, the XANES/EXAFS

findings suggest that a poorly ordered molybdenum oxycarbide (MoO_xC_y) nanoparticles rather than crystalline molybdenum carbide (Mo_2C) nanoparticles are present as the catalytic active sites for methane DHA by supported Mo/ZSM-5 catalysts. A recent DFT study[17] investigated the energetics of supported MoxCy clusters on ZSM-5 support with different anchoring sites, and the result suggested that Mo_4C clusters are stable anchoring at framework Al sites.

4.2.4. Isotopic CH_4/CD_4-Temperature Programmed Surface Reaction (TPSR) spectroscopy

The CH_4- and CD_4-TPSR spectra for the supported 2% MoO_3/ZSM-5 (Si/Al=15) catalyst are shown in **Figure 4- 17** and **Figure 4- 18**, respectively. The other products evolved from the reaction are given in **Figure 4- 19** and **Figure 4- 20**.

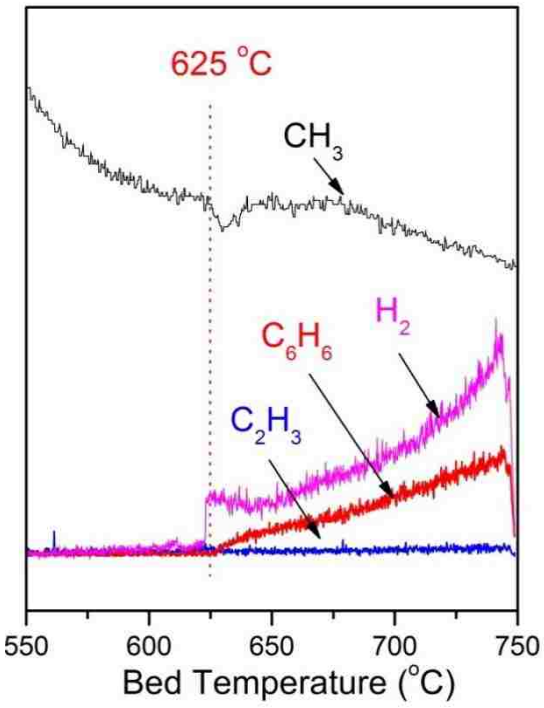

Figure 4- 17 CH_4 -TPSR spectra over 2 % MoO_3/ZSM-5 (Si/Al=15)

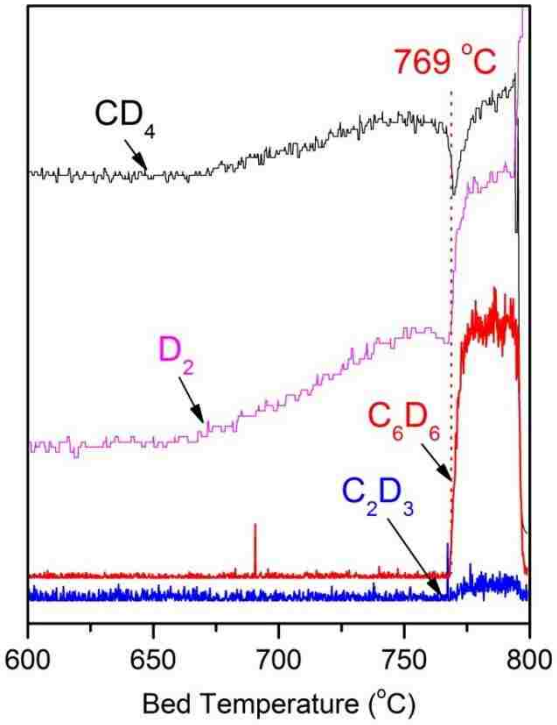

Figure 4- 18 CD_4-TPSR spectra over 2 % MoO_3/ZSM-5 (Si/Al=15)

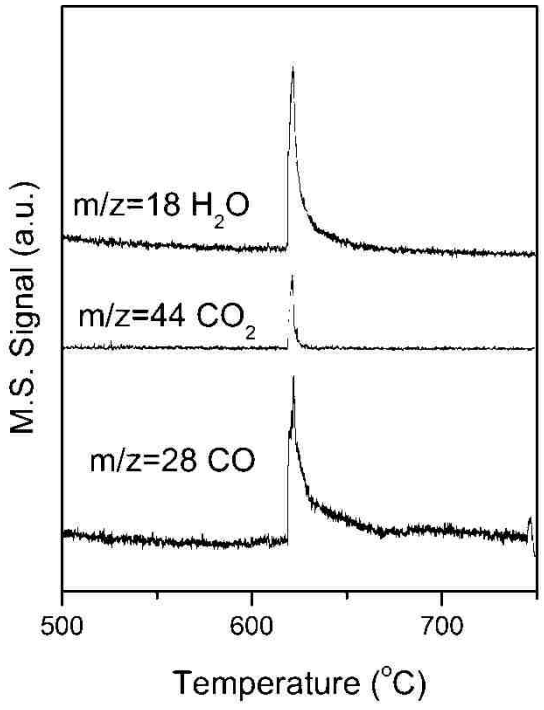

Figure 4- 19 CH_4-TPSR spectra over 2 % MoO_3/ZSM-5 (Si/Al=15)

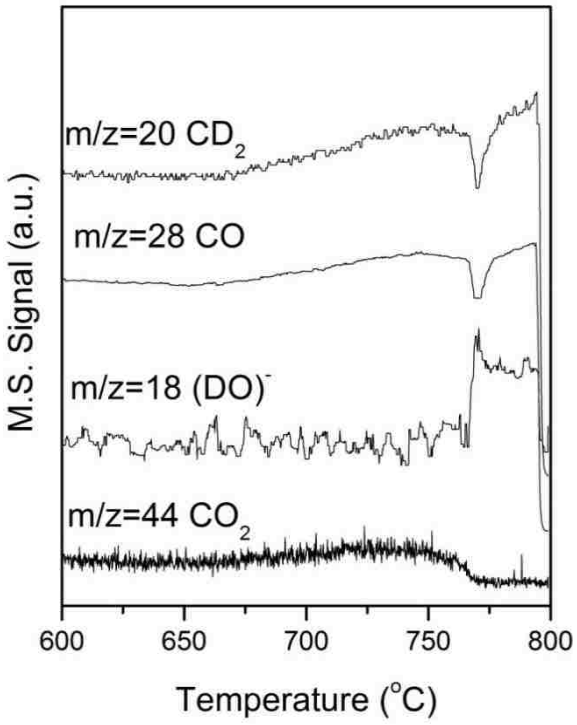

Figure 4- 20 CD_4-TPSR spectra over 2 % MoO_3/ZSM-5 (Si/Al=15)

The CH_4/CD_4-TPSR comparative spectra revealed a significant H-D isotopic effect for the methane DHA reaction. In the CH_4-TPSR spectra as shown in **Figure 4- 17**, the simultaneous consumption of CH_4 and evolution of C_6H_6 and H_2 occur at 625^{o}C in flowing 18% CH_4/Ar and is preceded by a sharp evolution of C_2H_4 and H_2 at 610^{o}C. The concomitant changes in CH_4, C_6H_6 and H_2 at 625 ^{o}C corresponding to the simultaneous formation of benzene and hydrogen from methane DHA. Furthermore, the slight delay in evolution of benzene relative to hydrogen desorption is expected because the recombination of hydrogen atoms occurs at a faster rate than the formation of C_6H_6 since the latter requires oligomerization of several C_xH_y intermediates. For the corresponding CD_4-TPSR spectra (**Figure 4- 18**), the simultaneous consumption of CD_4 and the evolution of D_2 and C_6D_6 occur at 769 ^{o}C. This dramatic isotope effect of ~150 ^{o}C in going from CH_4 to CD_4 is clearly evident that the rate-determining-step for methane

activation involves breaking its C-H bond. The absence of a lag in evolution between D_2 and C_6D_6 is apparently overcomed by the much higher temperature required to activate CD_4 than CH_4.

4.2.5. *In situ* Raman spectroscopy during catalyst regeneration with O_2

The time-resolved *in situ* Raman showed that the initial surface MoOx oxide species can be fully restored after regeneration treatment. Furthermore, the recovery of the isolated dioxo Mo oxide species on double Al-atom anchoring sites precedes that of isolated dioxo Mo oxide species on single Al-atom anchoring sites.

The *in situ* Raman spectra under regeneration conditions with gas-phase oxygen as a function of time for a 2 % MoO_3/ZSM-5(Si/Al=15) catalyst after reaction with methane are provided in **Figure 4- 21**.

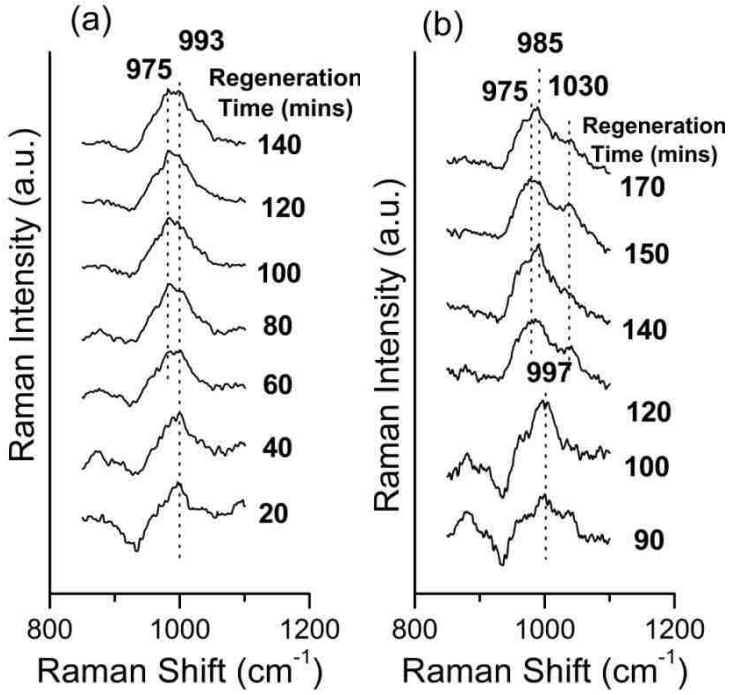

Figure 4- 21 Time-resolved *in situ* Raman spectra of regeneration of initial Mo oxide species of methane-reacted supported 2% MoO_3/ZSM-5 (Si/Al=15, a) and (Si/Al=25, b) catalysts in 5% oxygen/argon at 500 ^oC. Raman recorded at 442 nm laser excitation

After 20 mins of regeneration, a single Raman band is observed at 993 cm^{-1}, which corresponds to the evolution of isolated Mo oxide structures on double Al-atom anchoring sites of the zeolite framework from reduced Mo species. After 60 min, a second Raman band appears at 975 cm^{-1}, and its relative intensity increases with regeneration time in oxygen flow. This band corresponds to isolated dioxo $(O=)_2MoO_2$ structures on single Al-atom sites. The regenerated dioxo Mo oxide species first anchor on double Al-atom zeolite framework sites and then, with increasing time under

regeneration conditions, surface dioxo Mo oxide species also anchor on single Al-atom zeolite framework sites.

The time-resolved *in situ* Raman observed a retarded evolution of surface Mo oxide species for 2 % MoO_3/ZSM-5 (Si/Al=25) catalyst with a lower concentration of framework Al sites of zeolite as shown in **Figure 4- 21b**. Raman spectra prior to 90 min under regeneration conditions are not shown because they are dominated by fluorescence, which masks the bands from Mo oxide structures. The results in **Figure 4- 21b**; however, are sufficient to determine that initially, similar to ZSM-5 (Si/Al=15), regenerated Mo oxide structures preferentially anchor on double Al-atom zeolite framework sites. This is evidenced by a single Raman band at 993 cm^{-1} at 90 min of regeneration time. With increasing regeneration time, also similar to ZSM-5 (Si/Al=15), Mo oxide species migrate from double to single Al-atom zeolite framework anchoring sites, as evidenced by the appearance and growth of the Raman band at 975 cm^{-1} at 100 and 120 min. The recovery of mono-oxo Mo oxide species on external Al sites at 1030 cm^{-1} appears at 140 min. Importantly, however, a fourth Raman band at 984 cm^{-1} due to Mo oxide species anchored on Si sites on the external surface of the zeolite appears at 120 min and then increases in intensity with regeneration time. These Mo oxide structures and the corresponding band at 984 cm^{-1} are not observed for ZSM-5 (Si/Al=15) in **Figure 4- 21a**.

It is evident that the initial surface MoOx species can be regenerated after oxidation treatment. Regeneration time, however, should be controlled in less than 100 mins to prevent any dealumination of the ZSM-5 framework at high temperature.

4.2.6. Temperature Programmed Oxidation (TPO) of coke deposits on supported MoO_3/ZSM-5 catalysts from CH_4 DHA

Additional information about the nature and amount of the coke deposits on the supported MoO_3/ZSM-5 catalysts were chemically probed with TPO spectroscopy. Only CO and H_2O were observed as TPO reaction products and the ratio of CO/H_2O informs about the H content of the coke. The TPO spectra contained two major combustion peaks suggesting that there were two different types coke species formed on the supported MoO_3/ZSM-5 catalysts during the methane DHA.

For the lowest Mo loading, a more stable coke deposit that was hydrogen deficient was present. For intermediate and high Mo loading, a more reactive coke deposit that was hydrogen rich was also present. The different coke deposits may be related to the number of surface Brønsted acid sites that decreased with Mo loading on the ZSM-5 support. The detailed TPO spectra and their analysis are presented in **Figure 4- 22** and **Figure 4- 23**. The H/C ratios of coke species are summarized in **Table 4- 2**.

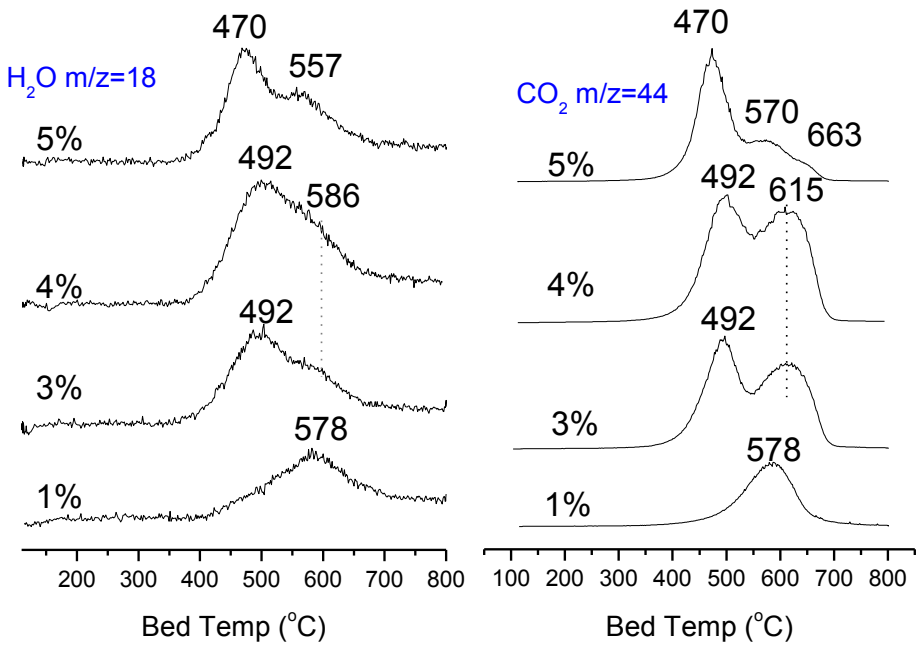

Figure 4- 22 TPO profiles of H_2O and CO_2 formed on coked 1-5% MoO_3/ZSM-5 catalysts in 18% CH_4/Ar at 800 ^oC

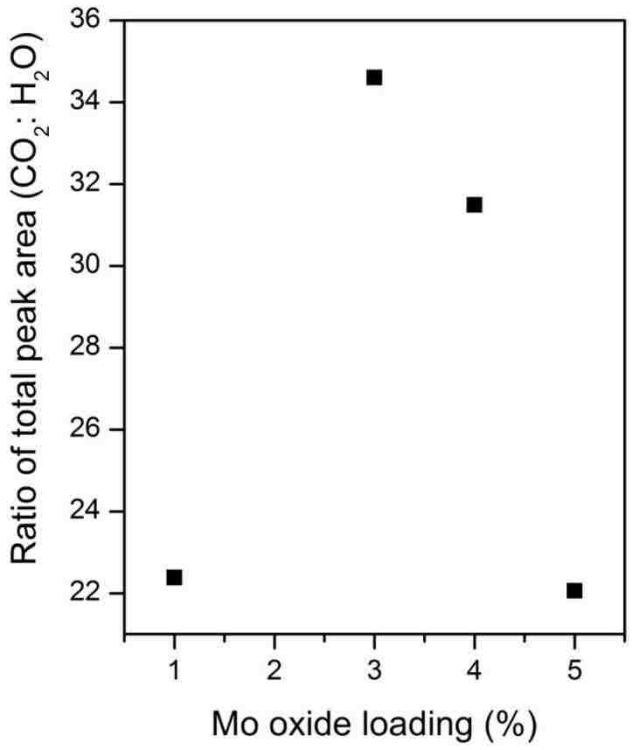

Figure 4- 23 The plot of ratio of total peak area (CO_2: H_2O) from TPO profiles against Mo oxide loading of the supported 1-5% MoO_3/ZSM-5 catalysts

Table 4- 2 Summary of peak temperature, integrated peak area and the peak area ratio (CO_2/H_2O) from TPO profiles on 1-5% MoO_3/ZSM-5

Mo oxide loading	Peak Temp(^{o}C)	Area(CO_2) (x 10^6)	Area(H_2O) (x 10^6)	Area ratio (H_2O/ CO_2)
1%	578	77.0	1.72	0.022
3%	492	100	1.94	0.019
	586	100	0.947	0.009
4%	492	121	2.54	0.021
	586	130	1.43	0.011
5%	470	97.7	1.71	0.017
	557	34.0	1.27	0.037
	630	12.0	0.298	0.025

The TPO profiles showed the evolution of CO_2 and H_2O when supported 1-5% MoO_3/ZSM-5 catalysts reacted with methane was exposed to 5% O_2/Ar with temperature increasing from 110 ^{o}C to 800 ^{o}C at a heating rate of 10 ^{o}C/min. The methane-reacted catalyst has molybdenum carbide/oxycarbide species and coke deposits. The combustion of coke species will generate CO_2 and H_2O, whereas the oxidation of molybdenum carbide species will also contribute to the evolution of CO_2 but not H_2O. **Figure 4- 22** showed the concomitant evolution of CO_2 and H_2O on 1-5% MoO_3/ZSM-5 catalysts which demonstrated that these peaks are mostly due to the combustion of coke deposits. The same rule was reported by other groups who studied coke by TPO experiments[18, 19].

The integrated peak area for CO_2 an H_2O and the peak area ratio (CO_2/H_2O) are listed in **Table 4- 2**. The ratio of total peak area of CO_2 against that of H_2O from all TPO profiles is plotted against the Mo oxide loading as shown in **Figure 4- 23**. The integrated peak area is proportional to the amount of CO_2 and H_2O which originated from the combustion, thus the peak area ratio CO_2 against H_2O reflects the C/H ratio of the coke species.

The amount of evolution peaks of CO_2 and H_2O in the TPO spectra is associated with the complexity of the composition of coke deposits. In **Figure 4- 22**, the TPO profile of 1% MoO_3/ZSM-5 has only one combustion peak for CO_2 and H_2O at 578 ^oC; and two distinguishable combustion peaks (495^oC and 615 ^oC) are present on 3 % and 4% MoO_3/ZSM-5; and three combustion peaks (470 ^oC, 557 ^oC and 630 ^oC) on 5% MoO_3/ZSM-5. The peak temperature values represent the stability of coke species. The first type of coke species, oxidized at 578 ^oC, is observed on 1% MoO_3/ZSM-5. The second type of coke species, with lower stability (oxidized below 500 ^oC), is found only on high Mo oxide loading catalysts (3-5% MoO_3/ZSM-5). The similar peak area ratio (CO_2/H_2O) of the first and the second coke species indicates that they are similar in hydrogen-content and degree of saturation. Their difference in stability could be associated with the same coke species associated with different locations. The first type of coke with the higher stability might be associated with Mo species within the pore channel of the zeolite as evident from *in situ* FTIR result on 1% MoO_3/ZSM-5 (see details in Chapter 2). The second type of coke with lower stability might be associated with Mo species on the external surface of zeolite since it was found that MoO_x species occupied external silanol groups at higher Mo oxide loading. It is reasonable to assume that the coke species confined within the micropores of zeolite is more difficult to be

oxidized than those on the external surface of the zeolite. The third type of coke, with the highest stability, has TPO peak temperature above 600 ^{o}C found only on high Mo oxide loading catalysts (3-5% MoO_3/ZSM-5). The high C/H ratio implies that they are hydrogen deficient. The high stability is likely due to the high thermodynamics of the unsaturated coke species in the oxidation reaction. It also implies that these coke species might be located within the zeolite pores approximating Brønsted acid sites since it was reported that coke species on Brønsted acid sites tend to have higher peak temperature in TPO[18].

As shown in **Table 4- 2**, the ratio of total peak area (CO_2/H_2O) evolved from the oxidization increases with increasing Mo oxide loading with the only exception found on 5% MoO_3/ZSM-5. This result corresponds to coke species with a higher C/H ratio and hydrogen-deficient which forms on formed on the catalysts with high Mo oxide loading. In another words, unsaturated carbonaceous deposits are favorable on catalysts with high Mo oxide loading. Exception is found only on 5% MoO_3/ZSM-5 since the total amount of coke deposited on 5% MoO_3/ZSM-5 is significantly smaller than samples with lower Mo oxide loadings as evident from the total peak areas of CO_2 and H_2O. Combined with the previous *operando* Raman-MS results on 5% MoO_3/ZSM-5, it is not hard to conclude that the reduction of surface MoO_x species and the methane DHA reaction occurs at 820 ^{o}C and 850 ^{o}C, respectively. The TPO profile is obtained on 5% MoO_3/ZSM-5 after reaction with methane at 800 ^{o}C, which is lower than the CH_4 activation temperature (850 ^{o}C) for 5% MoO_3/ZSM-5. Therefore, the coking is not severe at this temperature which explains the small amount of coke species found on 5 % MoO_3/ZSM-5.

From TPO experiments, at least three different types of coke species dependent on Mo oxide loading are identified on methane-reacted MoO_3/ZSM-5 catalysts.

The first type of carbon, oxidized below 500 ^oC, preferentially formed only on high Mo oxide loading (3-5%) catalysts during methane DHA. The absence of this type of carbon on 1% MoO_3/ZSM-5 suggested that it might be associated with either the MoO_xC_y/MoC_y species of large domain size which are only allowed at higher Mo oxide loading or Mo species at the external surface of the zeolite which were identified from *in situ* FTIR spectra of catalysts with high Mo oxide loading. The second assumption is reasonable since carbon at external surface is easier to be removed by combustion which is consistent with the low stability of this type of carbon in oxygen.

The second type of carbon oxidized at 578 ^oC forms on 1% MoO_3/ZSM-5 catalysts. The composition of the second type carbon is similar to the first type carbon due to their similar CO_2/H_2O area ratio as shown in **Figure 4- 23**, which implies similar composition of coke species; however the second type of carbon is more stable in oxygen as evident from the higher peak temperature. The higher stability might be because these coke species are formed inside the pore channels of the zeolite since Mo species are located at framework Al sites on 1% MoO_3/ZSM-5 as evident from the *in situ* Raman and IR results in Chapter 2.

The third type of carbon oxidized at about 615^oC forms on 3-4% MoO_3/ZSM-5 catalysts. The relative CO_2/H_2O area ratio of this type of carbon is approximately twice that of the first and second type of carbon. It suggested that the third type of carbon is hydrogen deficient and unsaturated, which explains the higher stability of this type of carbon.

4.3. Discussion

4.3.1. Mo oxide loading and Si/Al ratio-initial CH_4 DHA activity relationships

The temperature programmed CH_4-*operando* Raman-MS results revealed that the temperature for the initial evolution of benzene is not changing with catalysts with different MoOx species initial CH_4 DHA activity for benzene formation does not correlate with the initial surface MoOx structures as well as the Si/Al ratio of the ZSM-5 support as shown in **Figure 4- 10** and **Figure 4- 11**. The absence of a direct correlation between the initial surface MoOx structures and initial rates for benzene formation is most probably a consequence of the observation that the surface MoOx species undergo structural changes due to dealumination at the elevated reaction temperatures even prior to their activation to MoOxCy species (see figures from **Figure 4- 2** to **Figure 4- 9**).

4.3.2. Nature of activated Mo sites during the CH_4 DHA reaction

The *in situ* XANES/EXAFS measurements have shown that the activated catalytic active Mo sites of the supported MoO_3/ZSM-5 catalysts for methane DHA are present as poorly ordered MoOxCy clusters. The XANES edge energy position of the supported Mo sites during CH_4 DHA approximately matches that of bulk Mo_2C, implying that the activated Mo is predominantly about Mo^{2+}. The complementary EXAFS radial distribution possesses strong Mo-C bond peaks at 1.8 Å, a weak Mo=O bond peak at 1.0 Å, weak Mo-O bond peak at 1.5 Å, and weak Mo-Mo scattering from the second coordination sphere at ~2.2-2.6 Å. The small contribution from the Mo-Mo scattering implies that the

domain size MoOxCy species is very small since the scattering intensity of Mo-Mo in bulk Mo_2C is five times stronger than that of Mo-C coordination (see **Figure 4- 16**). It is estimated that the activated MoOxCy species has one neighboring Mo atom present in the second coordination during methane DHA which implies that the active sites are dispersed MoOxCy species. Similar results were found by Iglesia *et al.*[12] and dispersed MoOxCy species within zeolite channels were proposed. The present finding, consistently reveal that the activated supported Mo on ZSM-5 is present as dispersed MoOxCy species.[12] In subsequent work, Iglesia *et al.*[18] reported the active sites present as larger MoCy nanoclusters in an order of 6-10 Å. High Resolution Transmission Electron Microscopy (HR-TEM) images of much larger Mo_2C particles on the external zeolite surface of a spent MoO_3/ZSM-5 catalysts, ~50nm, have been reported in the literature[20]. These larger Mo_2C particles most probably arose from the presence of crystalline MoO_3 particles in the initial calcined catalysts since as shown in the present study crystalline MoO_3 is readily converted to crystalline Mo_2C under CH_4 DHA reaction conditions as shown in **Figure 4- 16**.

4.3.3. Reaction mechanism and rate-determining-step

The rate-determining-step for CH_4 DHA is the cleavage of the methane C-H bond as demonstrated by the dramatic kinetic isotopic effect when CH_4 was replaced by CD_4. The surface MoOx sites are activated by reduction with methane that initially yields CO and H_2O as the primary reaction products. The reduced Mo sites are then activated by formation of MoOxCy clusters on the ZSM-5 support that initiates the production of H_2 and C_2H_4. The formation of C_2H_4 is fleeting since it is rapidly reincorporated into a

hydrocarbon pool responsible for synthesis of C_6H_6. The formation rate of benzene lags that of H_2 and C_2H_4 reflecting these more rapid dimerization reaction steps than the slower oligomerization step responsible for C_6H_6 formation as shown in the *operando* Raman-MS spectra. The reaction steps are proposed as follows:

$n\ CH_4 + MoO_x \rightarrow MoO_xCy + CO + H_2O$ Activation of Mo site (1)

$CH_4 + MoO_xC_y \leftrightarrow CH_3\text{-}MoOC_yH + H_2O$ Activation of CH_4 , rds (2)

$CH_4 + CH_3\text{-}MoOC_yH \rightarrow (CH_3)_2\text{-}MoOC_yH + H_2$ (3)

$(CH_3)_2\text{-}MoOC_yH \rightarrow MoO_xC_y + C_2H_4 + H_2$ (4)

$C_2H_4 + ZSM\text{-}5 \rightarrow C_2H_4\text{-}ZSM\text{-}5$ (5)

$C_2H_4\text{-}ZSM\text{-}5 + H\text{-}ZSM\text{-}5 \leftrightarrow C_2H_5^+\text{-}ZSM\text{-}5$ (6)

$C_2H_4\text{-}ZSM\text{-}5 + C_2H_5^+\text{-}ZSM\text{-}5 \leftrightarrow C_4H_6\text{-}ZSM\text{-}5 + 3/2H_2$ (7)

$C_4H_6\text{-}ZSM\text{-}5 + C_2H_5^+\text{-}ZSM\text{-}5 \leftrightarrow C_6H_6\text{-}ZSM\text{-}5 + 5/2H_2$ (8)

$C_6H_6\text{-}ZSM\text{-}5 \leftrightarrow ZSM\text{-}5 + C_6H_6$ (9)

The above sequence of reaction steps with activation of methane being the rds results in the following reaction rate

$$rate = K_{ads} * k_{rds} (CH_4)^1 \quad (10)$$

Some researchers[21] claimed that hydrogen removal is the rds for methane DHA by supported MoO_3/ZSM-5 catalysts and employed a membrane reactor to facilitate H_2 removal to increase the reaction rate. There is no evidence that the H_2 removal as the rate determining step for CH_4 DHA. Based on the reaction equilibrium, the removal of H_2 shifts the equilibrium towards the right and C_6H_6 formation

4.3.4. Catalyst deactivation

The methane DHA reactions require high temperature to activate the C-H bond which poses a big challenge for the stability of catalyst. The CH_4-TPSR *operando* Raman-MS findings revealed that the methane DHA equilibrium is not enhanced by increasing reaction temperature (>700 ^oC) (See figures from **Figure 4- 2** to **Figure 4- 9**). According to thermodynamics, the conversion should be enhanced at elevated temperature. However, the formation of benzene is suppressed due to catalyst deactivation as evident from the CH_4-TPSR profiles. Several possible reasons could be responsible for the deactivation. First, from *operando* CH_4-Raman results, heavy coke species accumulate on the catalyst as the methane DHA proceeds, which will block the active sites and eventually leads to deactivation. The TPO results demonstrated that the amount of coke deposits on the catalyst is higher on high Mo oxide loading catalysts. Hydrogen-deficient coke with higher thermal stability is favored on higher Mo oxide loading catalysts (3-4 wt%). Combined with the *operando* Raman vibrations of the coke species formed in methane DHA, the hydrogen-deficient coke could consist of a mixture of heavy hydrocarbons such as polyaromatics, fused aromatic or pre-graphitic species. The current finding suggested that heavier coke species can be avoided by choosing low Mo oxide loading catalysts, which is consistent with the literature findings that the optimum catalyst is 2% MoO_3/ZSM-5 catalysts.[22]

4.3.5. Catalyst regeneration

The initial surface Mo oxide species after methane DHA reaction can be fully regenerated under oxygen treatment at elevated temperature. The time-resolved Raman

spectroscopic results demonstrate that surface Mo surface dioxo Mo oxide structures anchored on framework double Al-atom sites are regenerated first, followed by surface dioxo Mo oxide structures on framework single Al-atom sites, surface dioxo Mo oxide structures on external Si sites and mono-oxo Mo oxide structures on external Al sites. The regeneration ability of each surface Mo oxide structures falls into similar trend as their reactivity in the methane DHA reaction. In addition, these results also suggested that optimization of the regeneration time can avoid formation of the less active dioxo Mo oxide structures on external Si sites and, therefore, enhance catalytic performance.

4.4. Conclusions

The initial reactivity of supported MoO_3/ZSM-5 catalysts does not correlate to the surface MoOx species but increase with decreasing Si/Al ratio of ZSM-5 support during methane DHA reaction as evident from combined operando Raman-MS spectroscopy. No correlation between initial surface MoOx species with reactivity is probably due to the observed structural change of surface MoOx species during the reaction. The correlation between reactivity and Si/Al ratio of ZSM-5 support can be explained by the catalytic role of Brønsted acidity in the oligomerization step of methane to benzene conversion, which has been proved as a distinct catalytic feature of zeolite for cracking petroleum hydrocarbons.[23]

The fully oxidized MoOx species convert to reduced Mo species which are Raman inactive; therefore, the molecular structure of reduced Mo species were investigated *via in situ* EXAFS/XANES spectroscopy under reaction conditions. The active catalyst for the conversion of methane to benzene is a poorly ordered molybdenum oxycarbide (MoOxCy) cluster based on *in situ* EXAFS/XANES results.

The reduced molybdenum oxycarbide structure can be fully restored after regeneration in oxidizing environment at elevated temperature. The regeneration ability of different surface Mo oxide species is the same as their catalytic activity for methane DHA reaction. The regeneration at a constant temperature can successfully restore surface Mo species in the order of dioxo $(O=)_2MoO_2$ species on double Brønsted acid Al-Al sites >dioxo $(O=)_2MoO_2$ species on single Brønsted acid Al sites >>dioxo $(O=)_2MoO_2$ species on Si-Si sites ≈ mono-oxo $O=MoO_4$ species on external Al sites. In addition, these results also

suggested that optimization of the regeneration time can avoid formation of the less active dioxo Mo oxide structures on external Si sites.

Three different coke species related to the Mo oxide loading are identified from the TPO experiments. The first type of coke species, very unstable in oxygen, is associated with Mo species at the external surface of zeolite which are easier to be removed. The second type of coke species, more stable in oxygen but with similar hydrogen-concentration as the first type of coke, is associated with Mo species inside the zeolite channels which are more difficult to be removed. A third type of coke species, the most stable in oxygen and hydrogen-deficient, is present with a significant quantity on 3-4% MoO_3/ZSM-5 catalysts.

References

1. Weckhuysen, B. M.; Wang, D.; Rosynek, M. P.; Lunsford, J. H., *Journal of Catalysis* **1998,** *175* (2), 338-346.
2. Solymosi, F.; Cserényi, J.; Szöke, A.; Bánsági, T.; Oszkó, A., *Journal of Catalysis* **1997,** *165* (2), 150-161.
3. Solymosi, F.; Szöke, A.; Cserényi, J., *Catalysis Letters* **1996,** *39* (3-4), 157-161.
4. Solymosi, F.; Erdöhelyi, A.; Szöke, A., *Catalysis Letters* **1995,** *32* (1-2), 43-53.
5. Xu, Y.; Liu, S.; Guo, X.; Wang, L.; Xie, M., *Catalysis Letters* **1994,** *30* (1-4), 135-149.
6. Weckhuysen, B. M.; Wang, D.; Rosynek, M. P.; Lunsford, J. H., *Journal of Catalysis* **1998,** *175* (2), 347-351.
7. Aritani, H.; Tanaka, T.; Funabiki, T.; Yoshida, S.; Eda, K.; Sotani, N.; Kudo, M.; Hasegawa, S., *The Journal of Physical Chemistry* **1996,** *100* (50), 19495-19501.
8. Aritani, H.; Shinohara, S.; Koyama, S.-i.; Otsuki, K.; Kubo, T.; Nakahira, A., *Chemistry Letters* **2006,** *35* (4), 416-417.
9. Bedard, J.; Hong, D.-Y.; Bhan, A., *Physical Chemistry Chemical Physics* **2013,** *15* (29), 12173-12179.
10. Borry, R. W.; Kim, Y. H.; Huffsmith, A.; Reimer, J. A.; Iglesia, E., *The Journal of Physical Chemistry B* **1999,** *103* (28), 5787-5796.
11. Kim, Y.-H.; Borry Iii, R. W.; Iglesia, E., *Microporous and Mesoporous Materials* **2000,** *35–36* (0), 495-509.
12. Li, W.; Meitzner, G. D.; Borry Iii, R. W.; Iglesia, E., *Journal of Catalysis* **2000,** *191* (2), 373-383.
13. Xing, S.; Zhou, D.; Cao, L.; Li, X., *Chinese Journal of Catalysis* **2010,** *31* (4), 415-422.
14. Rutkowska-Zbik, D.; Grybos, R.; Tokarz-Sobieraj, R., *Structural Chemistry* **2012,** *23* (5), 1417-1424.
15. Li, C.; Stair, P. C., *Catalysis Today* **1997,** *33* (1–3), 353-360.
16. Takenaka, S.; Tanaka, T.; Funabiki, T.; Yoshida, S., *The Journal of Physical Chemistry B* **1998,** *102* (16), 2960-2969.
17. Gao, J.; Zheng, Y.; Fitzgerald, G. B.; de Joannis, J.; Tang, Y.; Wachs, I. E.; Podkolzin, S. G., *The Journal of Physical Chemistry C* **2014**.
18. Ding, W.; Li, S.; D Meitzner, G.; Iglesia, E., *The Journal of Physical Chemistry B* **2000,** *105* (2), 506-513.
19. Swaan, H. M.; Kroll, V. C. H.; Martin, G. A.; Mirodatos, C., *Catalysis Today* **1994,** *21* (2–3), 571-578.
20. Matus, E. V.; Ismagilov, I. Z.; Sukhova, O. B.; Zaikovskii, V. I.; Tsikoza, L. T.; Ismagilov, Z. R.; Moulijn, J. A., *Industrial & Engineering Chemistry Research* **2006,** *46* (12), 4063-4074.
21. Borry III, R. W.; C. Lu, E.; Kim, Y.-H.; Iglesia, E., Non-oxidative catalytic conversion of methane with continuous hydrogen removal. In *Studies in Surface Science and Catalysis*, A. Parmaliana, D. S. F. F. A. V. a. F. A., Ed. Elsevier: 1998; Vol. 119, pp 403-410.
22. Wang, D.; Lunsford, J.; Rosynek, M., *Topics in Catalysis* **1996,** *3* (3-4), 289-297.
23. Wang, W.; Jiang, Y.; Hunger, M., *Catalysis Today* **2006,** *113* (1–2), 102-114.

Chapter 5.

Molecular Structures of Supported MOx/ZSM-5 (M=V, Cr, Mo, W and Re) Catalysts

Abstract

The molecular structures and anchoring sites of dehydrated supported MOx (M=V, Cr, Mo, W and Re) species on ZSM-5 supports (Si/Al=15, 25, 40 and 140) were investigated with *in situ* UV-vis Raman, IR and XAS spectroscopy. The supported MOx/ZSM-5 catalysts were synthesized by incipient wetness impregnation of the appropriate precursors. Raman spectroscopy analysis demonstrated that the supported MOx species were completely dispersed on the ZSM-5 supports with the exception of the Si-rich ZSM-5 (Si/Al=140) that has a small amount of crystalline MOx nanoparticles (NPs) because of the limited number of available surface Brønsted acid Si-$(OH)^+$-Al sites. The results from UV-vis and XAS spectroscopy have shown that the dispersed surface MOx species on ZSM-5 were fully oxidized and present as isolated sites on the ZSM-5 supports. Raman, coupled with isotopic ^{18}O-^{16}O exchange studies, and XAS spectroscopy revealed that the isolated surface MOx species tend to primarily consist of MO_4 and MO_5 coordination: $O=VO_3$; $(O=)_2CrO_2$ and $O=CrO_4$; $(O=)_2MoO_2$, $(O=)_2Mo(OH)O_2$ and $O=MoO_4$; $(O=)_2WO_2$, $(O=)_2W(OH)O_2$ and $O=WO_4$; and $(O=)_3ReO$. Based on IR results, the surface MOx species primarily prefer to anchor at surface Brønsted acid Si-$(OH)^+$-Al in the zeolite pores, but also anchor at external extra-framework Al sites, Al_2O_3 NPs and Si-OH sites. This extensive and systematic investigation highlights for the first time how catalytic metal oxides interact with ZSM-5 materials.

Introduction

The molecular and electronic structures of highly dispersed group V-VII transition metal oxide supported on zeolites have received significant attention in recent years due to their industrial potential as catalysts for numerous chemical reactions[1-18]. For example, supported V_2O_5/ZSM-5 catalysts have been studied for selective catalytic reduction (SCR) of NO_x with ammonia[1], and oxidative dehydrogenation (ODH) of ethane to ethylene with CO_2[2]. Supported MoO_3/ZSM-5 catalysts have been investigated for non-oxidative dehydroaromatization (DHA) of methane[3], and partial oxidation of methane to formaldehyde[4]. Supported CrO_3/ZSM-5 catalysts have been examined for SCR of NO_x with hydrocarbons[5], propane dehydrogenation to propylene[6], ODH of ethane to ethylene with CO_2[7], photocatalytic partial oxidation of propane to acetone[8], toluene disproportionation[9], non-oxidative DHA of methane[10] and neutralization of volatile organic compounds (VOC) and chlorinated VOCs[11,12,13,14]. Supported WO_3/ZSM-5 catalysts have been studied for methane oxidation[15] and non-oxidative DHA of methane[16], and supported Re_2O_5/ZSM-5 catalysts have been found to be effective for conversion of ethane to benzene[17] and non-oxidative DHA of methane.[18]

The supported metal oxide phases on ZSM-5 are usually molecularly dispersed below monolayer surface coverage or the maximum dispersion limit. The supported surface metal oxide components provide redox/acid/basic sites while the ZSM-5 support contributes strong Brønsted acid sites and shape-selectivity not available for non-zeolitic supported metal oxide catalyst systems. Above monolayer coverage or maximum

dispersion limit, crystalline metal oxide nanoparticles (NPs) also form on the zeolite external surface and are generally undesirable because of their lower catalytic activity and tendency to block the micropores of ZSM-5.[19]

The nature of the supported MOx sites and their anchoring sites on ZSM-5 has received much attention in recent years and the literature findings are discussed in detail in Chapter 1 and are summarized in **Table 5- 1**.

Table 5- 1 Literature review of supported MOx/ZSM-5 catalysts (M=V, Cr, Mo, W and Re) indicating the proposed anchoring sites, molecular MOx structures and characterization techniques with the employed experimental conditions

MOx	Anchoring site	Nature of MOx Species	Characterization Techniques	References
VO_x	Brønsted acid site, external Si-OH	monomer $(O=)_2VO$, dimer $V_2O_4^+$	*in situ* ESR and IR, *ex situ* XPS, *in situ* Raman and XAS	61,73,74,75
CrO_x	Brønsted acid site	monomer $(O=)_3CrO$, $O=CrO_4$	*In situ* IR, *ex situ XPS* ,*in situ* IR and XAS	10,13,64,76
MoO_x	Brønsted acid site, external Si-OH, Al-OH	monomer $(O=)_2MoO_2$, dimer $Mo_2O_5^+$	UV-Vis, *in situ* IR, *ex situ* XPS, *in situ* Raman and XAS	65,66,67,68
WO_x	Brønsted acid sites	monomer $(O=)_2WO_2$	*ex situ* XPS, *in situ* XAS, *in situ* UV-Vis	15,16
ReO_x	Brønsted acid site, external Si-OH	monomer $(O=)_3ReO$, dimer$Re_2O_6^+$	*in situ* IR, *in situ* Raman and XAS, ex situ XAS	18,77

In spite of the extensive characterization studies on supported MOx/ZSM-5 catalysts, the details about the MOx anchoring sites, molecular and electronic structures are still not resolved. Although there is some agreement that the anchoring sites for the MOx species on the ZSM-5 supports are the surface Brønsted acid sites and Si-OH sites, there is no consensus about the nature of the MOx species. The lack of consensus is strongly related to the application of different characterization techniques under different conditions (ambient, *ex situ* and *in situ*). Many of the characterization measurements were taken

under ambient and *ex situ* conditions, with only a few *in situ* spectroscopic studies reported. The dynamic nature of catalysts under different environmental conditions is well established and that characterization under ambient conditions, in which the catalysts are hydrated, is not representative of the actual states of catalysts under relevant operational conditions (dehydrated and reaction conditions).[20,21]

The objective of this chapter is to determine the molecular details of the surface MOx (M=V, Cr, Mo, W and Re) species supported on ZSM-5 under oxidizing dehydrated conditions. The molecular details about the MOx anchoring sites, molecular and electronic structures on ZSM-5 supports (Si/Al=15-140) under dehydrated conditions were resolved by systematic application of *in situ* FT-IR, UV-vis, Raman and X-ray absorption spectroscopy (XAS).

5.1. Experimental methods

5.1.1. *In situ* IR spectroscopy

The *in situ* IR measurements were performed with a Thermo Scientific Nicolet 8700 Research FTIR spectrometer equipped with a liquid nitrogen cooled mercury-cadmium-telluride (MCT detector), a Harrick Praying Mantis accessory (model DRA-2), and a Harrick reaction chamber HT-100. Experimental details are described in Chapter 2, section 2.2.

5.1.2. *In situ* UV-vis Spectroscopy

The *in situ* UV-vis measurements were obtained with a Varian Cary 5E UV-Vis-NIR spectrophotometer employing the integration sphere diffuse reflectance attachment (Harrick Praying Mantis Attachment, DRA-2). Experimental details are provided in Chapter 2, section 2.3.

5.1.3. *In situ* Raman Spectroscopy

The *in situ* Raman spectra of the zeolite-supported metal oxide catalysts were obtained with a high resolution, dispersive Raman spectrometer system (Horiba-Jobin Yvon LabRam HR) equipped with three laser excitations (532, 442 and 325 nm), and more details are discussed in Chapter 2, section 2.4.

5.1.4. *In situ* X-ray absorption spectroscopy (XAS)

The X-ray absorption spectroscopy (XAS) of V K-edge, Cr K-edge, Mo K-edge, Re L_1-edge and W L_1-edge of supported MOx catalysts was performed in both transmission and fluorescence mode at the beam line X18A at the National Synchrotron Light Source (NSLS) at the Brookhaven National Laboratory, More details are provided in Chapter 2, section 2.5.1.

5.2. Results

5.2.1. *In situ* IR Spectroscopy

The parent HZSM-5 (Si/Al=15) has four characteristic surface hydroxyl IR absorptions: (1) Brønsted acid Al-$(OH)^+$-Si site in which alumina is coordinated as an AlO_4 unit (3610 cm^{-1}); (2) terminal Si-OH (3741 cm^{-1}); (3) extra-framework Al-OH with AlO_6 coordination (3660 cm^{-1}; Al-OH-I) and (4) extra-framework Al-OH-II of Al_2O_3 nanoclusters (3783 cm^{-1}; Al-OH II)[26,27]. The integrated IR bands of the four surface hydroxyls are compared against the MOx loading in order to determine the interaction of the MOx species with the different surface hydroxyl anchoring sites on the ZSM-5 support.

Supported V_2O_5/ZSM-5

The integrated *in situ* IR bands for the surface hydroxyls of dehydrated V_2O_5/ZSM-5 (Si/Al=15) catalysts as a function of vanadia loading are shown in **Figure 5- 1** and the corresponding IR spectra appear as **Figure 5- 2**.

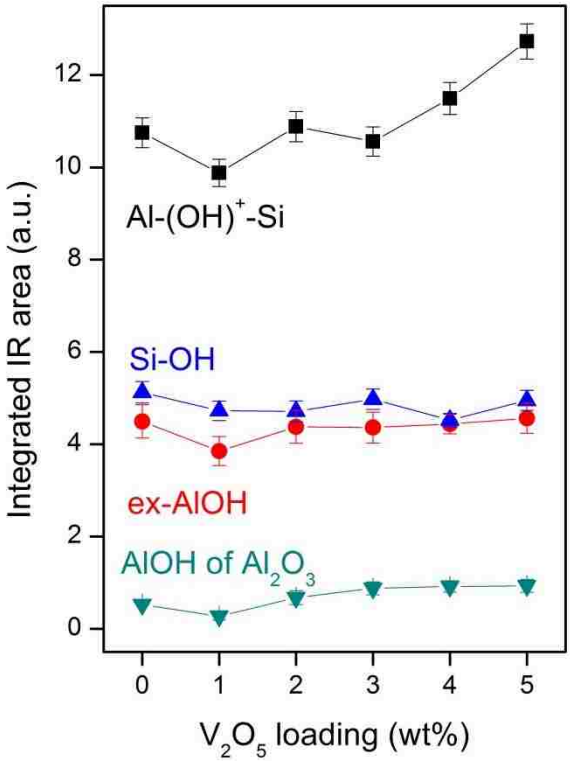

Figure 5- 1 Integrated IR bands of surface hydroxyls of dehydrated supported 0-5% V_2O_5/ZSM-5(Si/Al=15) catalysts

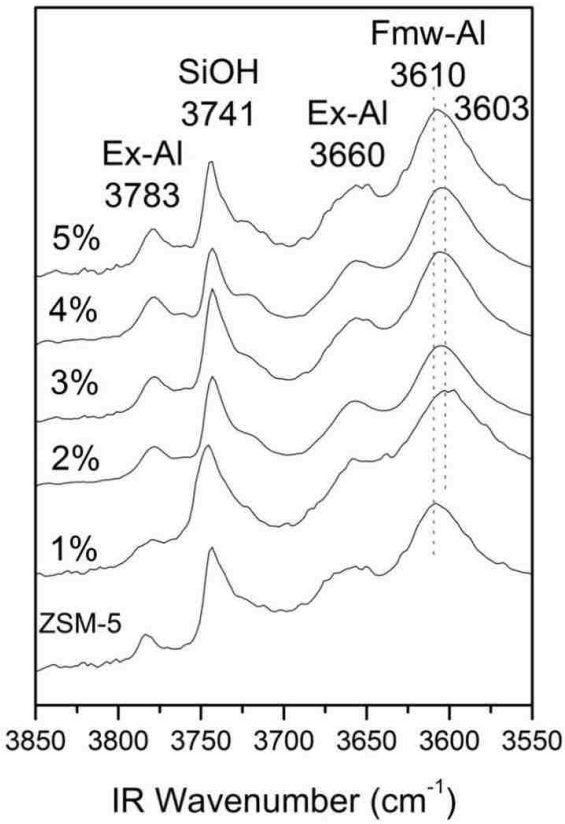

Figure 5- 2 *In situ* FTIR spectra of dehydrated supported 0-5% V_2O_5/ZSM-5(Si/Al=15) catalysts

The intensity of the Brønsted acid hydroxyl band at ~3610 cm^{-1} initially slightly decreases with1% V_2O_5 and then increases at higherV_2O_5 loading. The IR position of the Brønsted acid hydroxyl also shifts from 3610 to 3603 cm^{-1} with increasing vanadia loading (see **Figure 5- 2**), suggesting that new surface hydroxyls may be forming. This surface hydroxyl vibration coincides with surface V-OH hydroxyls at ~3600 cm^{-1} [28] or may be related to formation of V-$(OH)^+$-Al Brønsted acid sites[29,30] at higher vanadia loadings. The intensity of the silanol Si-OH band at 3741 cm^{-1} remains relatively constant indicating that the surface VOx species do not anchor on the external silanol hydroxyls. The intensity of the extra-framework Al-OH bands at 3660 and 3783 cm^{-1} slightly decrease for 1% V_2O_5 loading and then slightly increase with higher vanadia loading

suggesting some initial anchoring of surface VOx at these sites and that introduction of vanadia may also result in minor dealumination of framework Al. It appears that anchoring of surface VOx on ZSM-5 primarily takes place at surface Brønsted acid hydroxyl sites and some extra-framework Al-OH sites, and also leads to creation of new surface hydroxyls at ~3600 cm^{-1} at higher vanadia loadings.

Supported CrO_3/ZSM-5

The integrated *in situ* IR bands for the surface hydroxyls of the dehydrated CrOx/ZSM-5(Si/Al=15) catalysts as a function of chromia loading are presented in **Figure 5- 3** and the corresponding IR spectra appear as **Figure 5- 4**.

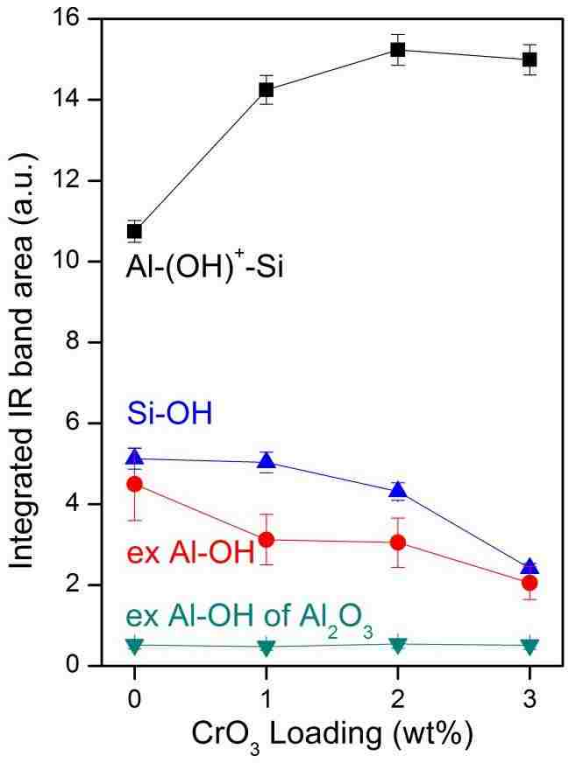

Figure 5- 3 Integrated IR bands of surface hydroxyls of dehydrated supported0-3% CrO_3/ZSM-5 (Si/Al=15) catalysts

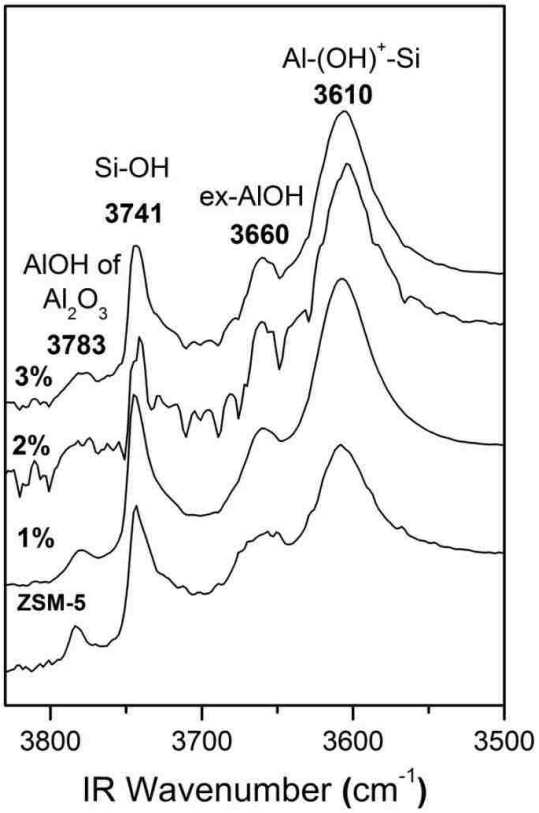

Figure 5- 4 *In situ* FTIR spectra of dehydrated supported 0-3% CrO_3/ZSM-5(Si/Al=15) catalysts

The intensity of the IR band at 3610 cm^{-1} of Brønsted acid hydroxyls markedly increases with introduction of surface chromium oxide species, which suggests that new surface Brønsted acid sites might be created by introduction of chromia to ZSM-5. Surface hydroxyls of Cr_2O_3 also vibrate at ~3606 cm^{-1} [31] that would overlap with hydroxyl vibrations of framework Al sites (Al-$(OH)^+$-Si). The IR bands of the external surface silanol Si-OH at 3741 cm^{-1} and the extra-framework Al-OH at 3660 cm^{-1} steadily decrease with increasing chromia loading reflecting anchoring of surface CrOx sites at these surface hydroxyls. The intensity of the IR band from the extra-framework Al-OH of Al_2O_3 NPs at 3783 cm^{-1} does not change with chromia loading indicating anchoring at this site or that dealumination is not taking place to a significant extent for the 1-3%

CrO_3/ZSM-5 catalysts. The observed trends suggest that surface CrOx preferably anchor at surface silanols and extra-framework Al-OH sites, and create new surface Brønsted acid hydroxyls. It is possible that surface CrOx species are also anchoring at the surface Brønsted acid sites, but are being overshadowed by the increasing surface hydroxyl IR band at ~3600 cm^{-1} with higher chromia loadings.

Supported MoO_3/ZSM-5

The integrated *in situ* IR bands of the dehydrated MoO_3/ZSM-5 (Si/Al=15) catalysts are shown in **Figure 5- 5** as a function of molybdena loading with the corresponding IR spectra appearing as **Figure 5- 6**.

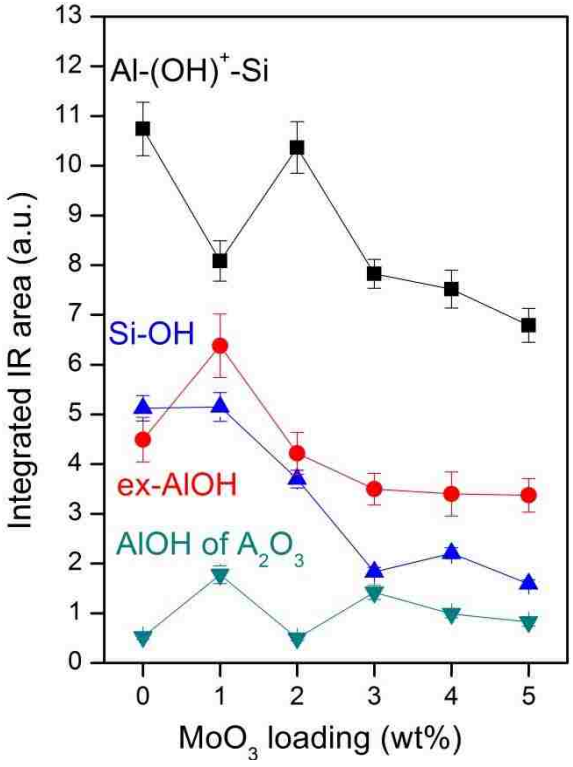

Figure 5- 5 Integrated IR bands of surface hydroxyls of dehydrated supported 0-5% MoO_3/ZSM-5 (Si/Al=15) catalysts

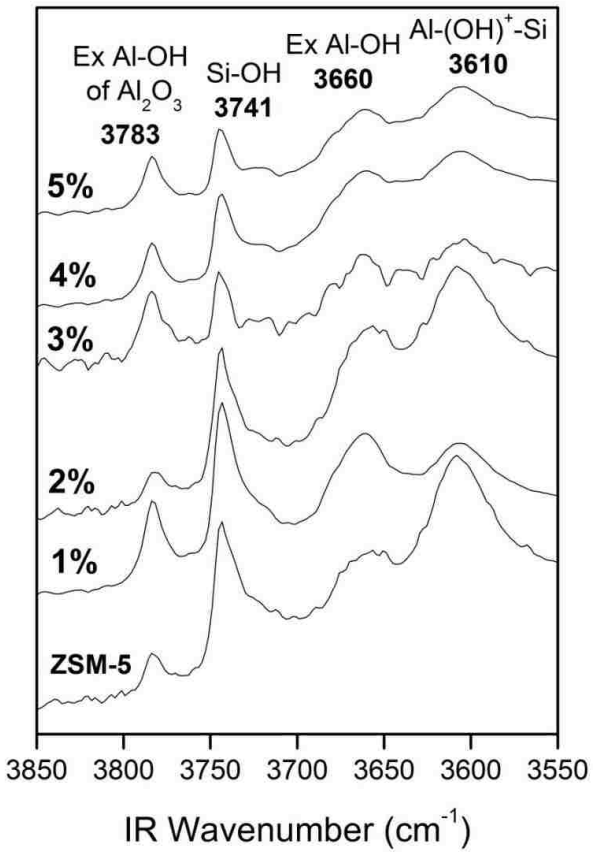

Figure 5- 6 *In situ* FTIR spectra of dehydrated supported 0-5% MoO_3/ZSM-5(Si/Al=15) catalysts

Introduction of just 1% MoO_3 has a significant effect on the ZSM-5 surface hydroxyls, the intensity of the IR bands corresponding to surface Brønsted acid hydroxyls at 3610 cm^{-1} markedly decrease, the bands associated with surface extra-framework Al-OH increase while the silanol Si-OH at 3741 cm^{-1} remained unchanged. These trends suggest that the initial surface MOx anchor at surface Brønsted acid hydroxyls and also cause dealumination. Increasing molybdena loading to 2% MoO_3/ZSM-5 restores the initial IR intensity for the Brønsted acid hydroxyls and decreases the intensity of all other surface hydroxyls. Further increasing the molybdena loading decreases the intensity of the IR bands for all surface hydroxyls except the extra-framework Al-OH associated with Al_2O_3 NPs that slightly increases. These surface hydroxyl trends with increasing molybdena

loading indicate that surface MOx species initially anchor at surface Brønsted acid hydroxyls inside the channels and subsequently also at external surface Si-OH and extra-framework Al-OH hydroxyls. Introduction of molybdena to ZSM-5 also causes dealumination and creates some new surface hydroxyls at ~3600 cm^{-1}.

Supported WO_3/ZSM-5

The integrated *in situ* IR bands of the dehydrated WOx/ZSM-5 (Si/Al=15) are presented in **Figure 5- 7** as a function of tungsta loading and the corresponding IR spectra are found as **Figure 5- 8**.

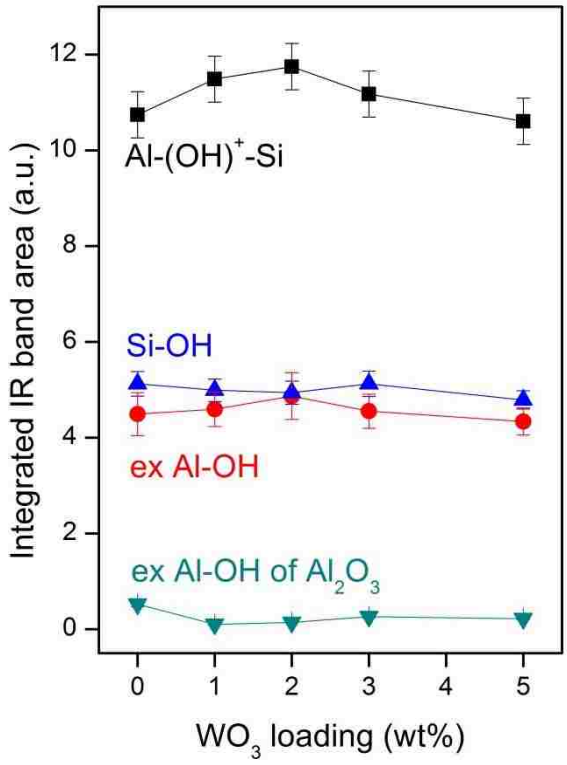

Figure 5- 7 Integrated IR bands of surface hydroxyls of dehydrated supported 0-5% WO_3/ZSM-5 (Si/Al=15) catalysts

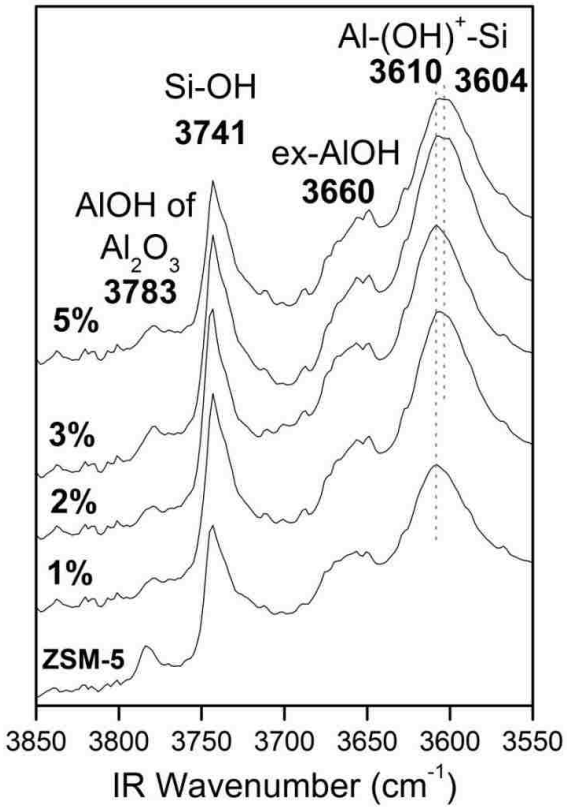

Figure 5- 8 *In situ* FTIR spectra of dehydrated supported 0-5% WO_3/ZSM-5(Si/Al=15) catalysts

The intensity of the IR band of the surface Brønsted acid hydroxyls initially slightly increases and then slightly decreases as well as shifting from 3610 to 3604 cm^{-1} with increasing tungsta loading. The band at 3604 cm^{-1} is too high to be the hydroxyl of tungsten trioxide, which vibrates at 3506 cm^{-1}.[32] The other surface hydroxyls are minimally perturbed. These trends indicate that surface WOx species primarily anchor at surface Brønsted acid hydroxyls on ZSM-5 and also create new surface hydroxyls corresponding to ~3600 cm^{-1} W-OH or W-$(OH)^+$-Si/Al.[33] The competition between titration and formation of surface hydroxyls vibrating at ~3600 cm^{-1} may be responsible for the lack of significant change in the intensity of this IR band.

Supported Re_2O_7/ZSM-5

The integrated *in situ* IR bands of the dehydrated ReOx/ZSM-5 (Si/Al=15) as a function of rhenia loading are depicted in **Figure 5- 9** with the corresponding IR spectra appearing as **Figure 5- 10**.

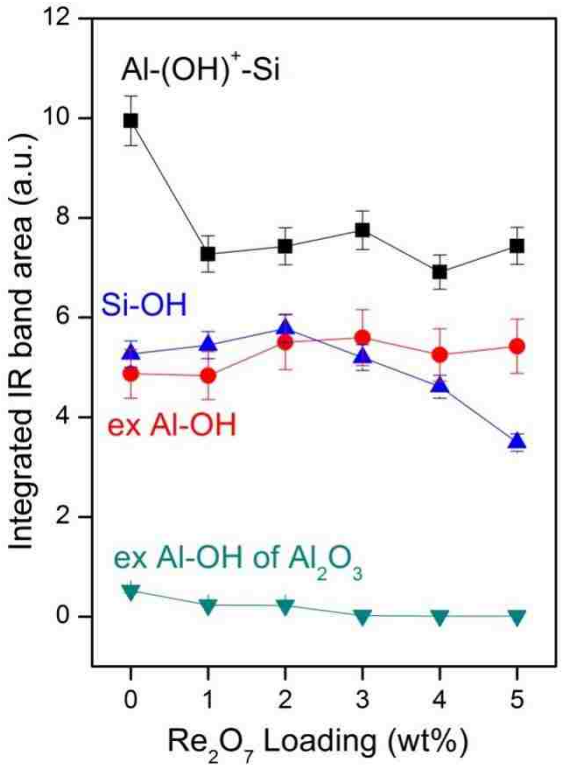

Figure 5- 9 Integrated IR bands of surface hydroxyls of dehydrated supported 0-5% Re_2O_7/ZSM-5 (Si/Al=15) catalysts

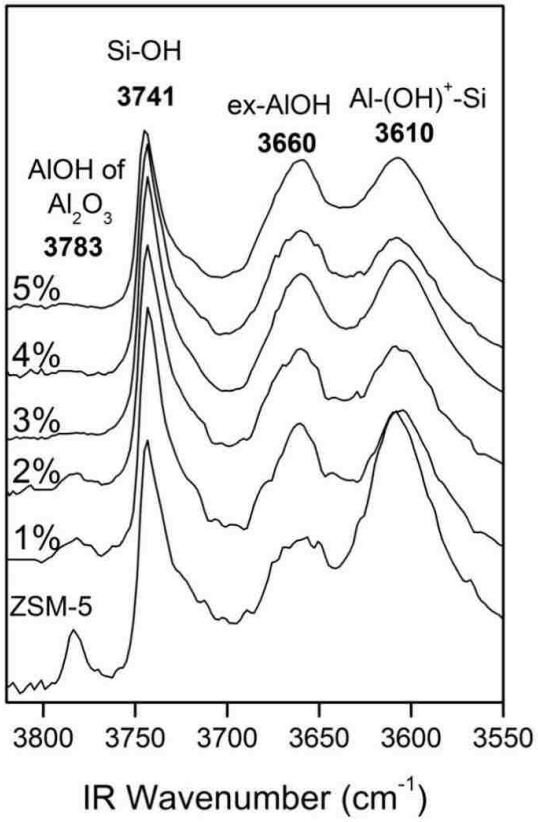

Figure 5- 10 *In situ* FTIR spectra of dehydrated supported 0-5% Re_2O_7/ZSM-5(Si/Al=15) catalysts

The intensity of the IR band associated with the surface Brønsted acid hydroxyl at 3610 cm^{-1} decreases markedly as 1% ReO_4 is introduced and remains unchanged at higher rhenia loadings. At higher rhenia loading, the intensity of the IR bands of the external silanol Si-OH at 3741 cm^{-1} decrease while that of the extra-framework Al-OH at 3660 cm^{-1} modestly increase. The IR band intensity of the surface Al-OH of Al_2O_3 NPs at 3783 cm^{-1} slightly increases with rhenia loading on ZSM-5. The slight increases in the surface Al-OH IR bands reflect dealumination taking place with introduction of rhenia into the ZSM-5 support. It appears that the surface Brønsted acid hydroxyls is the preferred anchoring site for surface ReOx on ZSM-5 and that external Si-OH hydroxyls become anchoring sites at higher rhenia loading.

5.2.2. *In situ* UV-vis Diffuse Reflectance Spectroscopy (DRS)

In situ UV-vis DRS spectroscopy provides local electronic structure of supported metal oxides by probing the optical energy gap (Eg) between the HOMO and LUMO electronic levels of semiconductor metal oxides.[34] Higher Eg values reflect isolated structures and lower Eg values indicate larger domain structures (dimers, oligomers, clusters and 3D structures). The relationships between UV-vis Eg values and reference semiconductor metal oxide compounds with known structures have been established in recent years that allow determining the domain size of supported metal oxide catalysts.[35,36,37] Fortunately, the ZSM-5 support is not a semiconductor and does not give rise to active UV-vis bands. Thus the UV-vis spectra only reflect the state of the supported MOx species on ZSM-5.

The *in situ* UV-vis Eg values for the dehydrated supported MOx/ZSM-5 catalysts are given in **Figure 5- 11** and compared with the Eg values of reference semiconductor compounds with known structures and supported MOx/AlOx/SiO_2 catalysts. The dehydrated UV-vis DRS spectra of supported MOx/ZSM-5 catalysts are provided in **Figure 5- 12** and **Figure 5- 13**. The Eg values for the dehydrated supported MOx/ZSM-5 catalysts are extremely high indicating the exclusive presence of isolated surface MOx sites on ZSM-5 with a high degree of symmetry in their molecular structures. The UV-vis Eg value for the supported VOx/ZSM-5 catalysts corresponds to the region in which monomeric VOx and dimeric V_2O_7 structures overlap making a structural conclusion based on UV-vis difficult. Nevertheless, there is no reason to suspect that VOx would behave different than the other surface MOx species on ZSM-5 as will be shown below from Raman and XAS.

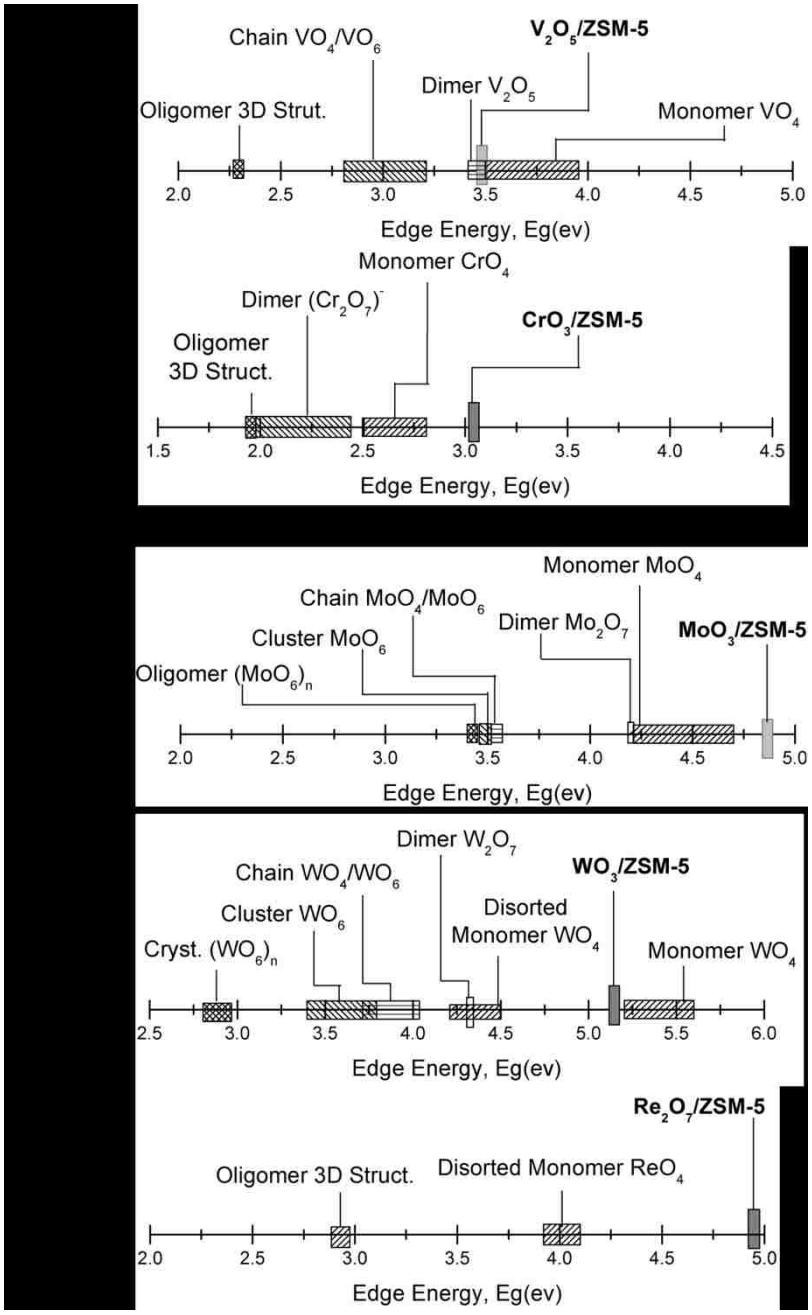

Figure 5- 11 UV-vis DRS edge energy, Eg, scale for reference metal oxide compounds with known structures and measured Eg values for dehydrated supported MOx/ZSM-5 catalysts, in which MOx is (A) VOx, dimer is V_2O_7 structure (B) CrOx, (C) MoOx, (D) WOx and (E) ReOx.

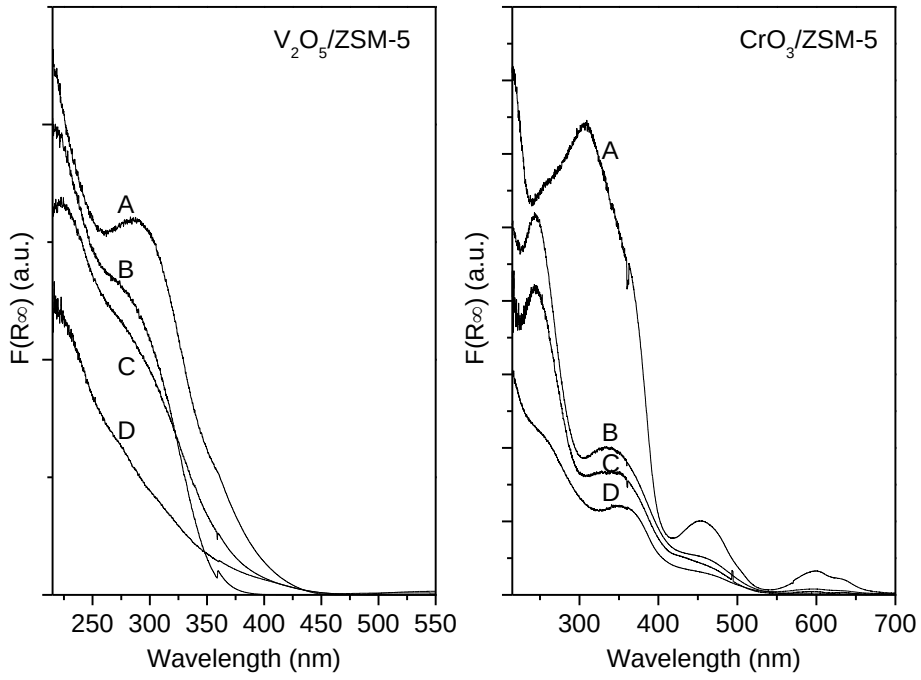

Figure 5- 12 *In situ* UV-vis DRS spectra of dehydrated MOx/ZSM-5, in which MOx= 2% V_2O_5 (left) and 2% CrO_3 (right) for (A) MOx/ZSM-5 (Si/Al=140), (B) MOx/ZSM-5 (Si/Al=40), (C) MOx/ZSM-5 (Si/Al=25), and (D) MOx/ZSM-5 (Si/Al=15) under oxidizing conditions at 400 ^oC.

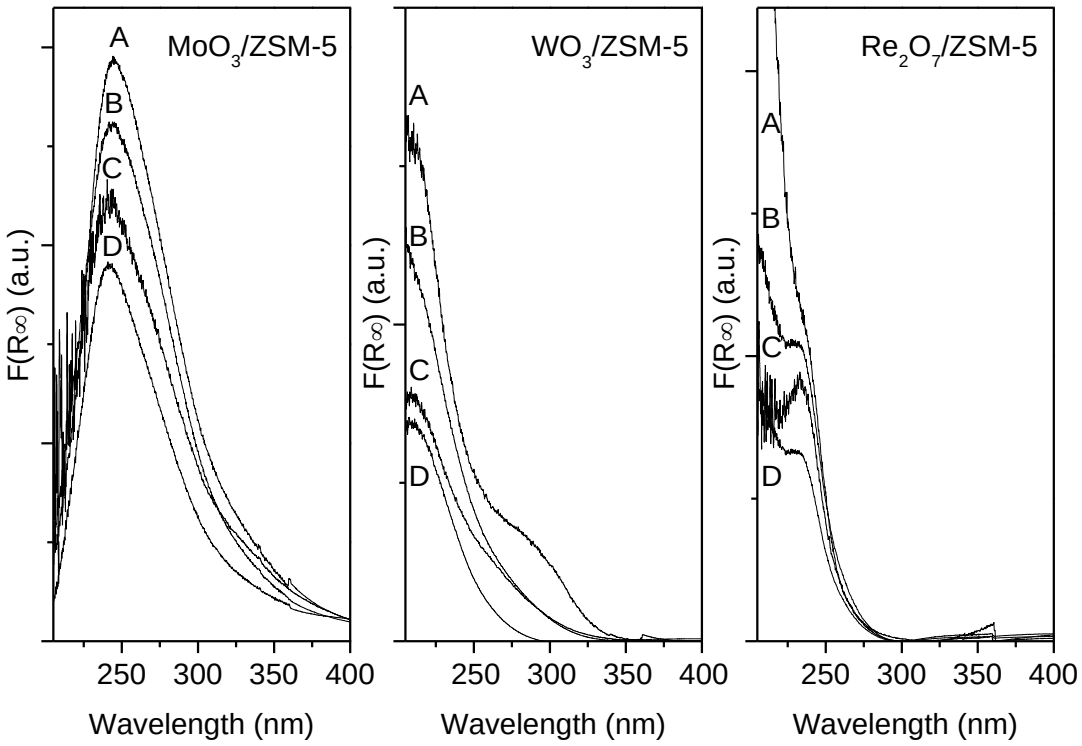

Figure 5- 13 *In situ* UV-vis DRS spectra of dehydrated supported MOx/ZSM-5, in which MOx = 2% MoO_3 (left), 3% WO_3 (center), and 3% Re_2O_7 (right) for (A) MOx/ZSM-5 (Si/Al=140), (B) MOx/ZSM-5 (Si/Al=40), (C) MOx/ZSM-5 (Si/Al=25), and (D) MOx/ZSM-5 (Si/Al=15) under oxidizing conditions at 400 ^{o}C. The small jump in the baseline at 360 nm is due to the window change of the light source and is an artifact in the spectra

Supported V_2O_5/ZSM-5 catalysts

The *in situ* UV-vis DRS spectra of the supported V_2O_5/ZSM-5 catalysts under dehydrated oxidizing conditions are shown in **Figure 5- 12** (left). A single ligand-to-metal charge transfer (LMCT) transition of the O (2p) to V (d) orbital is centered at 277-286 nm and is more evident at higher Si/Al ratios. The corresponding edge energy (Eg) values, which are presented in **Figure 5- 12**, are determined to be 3.5-3.6 eV and are consistent with isolated VO_4 sites that are present for bulk $Mg_3V_2O_8$ and Na_3VO_4 reference compounds[42] (3.5-3.9 eV) supported 5%V_2O_5/SiO_2[11] (3.5 eV), and supported 5% V_2O_5/5% Al_2O_3/SiO_2[46] (3.6 eV) catalysts. The UV-vis transitions for crystalline V_2O_5 NPs at 236,

334, and 481 nm (Eg = 2.3 eV) and polymeric VO_6 species at ~250 and 370 nm (Eg = 2.8 eV) are not detected and signify that the isolated surface VO_4 species are the dominant vanadia structures present on the ZSM-5 supports.[42,46]

Supported CrO_3/ZSM-5 catalysts

The *in situ* UV-vis DRS spectra of the dehydrated supported CrO_3/ZSM-5 catalysts under oxidative environments are provided in (right) and exhibit multiple LMCT transitions, with the corresponding Eg values given in **Figure 5- 11**. For the alumina-rich ZSM-5-supported CrOx catalysts (Si/Al=15 and 25), two LMCT transitions are present at 245 and ~345 nm and the corresponding Eg values are 4.0 and 3.1 eV, respectively. The spectral features for these supported CrOx/ZSM-5 catalysts match the UV-vis features for isolated surface CrOx species interacting with exposed alumina sites present in the dehydrated supported CrO_3/SiO_2-Al_2O_3 catalysts.[78,79,80] The supported CrO_3/ZSM-5 (Si/Al=40) catalyst, which possesses an intermediate concentration of lattice alumina, gives rise to LMCT transitions at 245 and 335 nm with a small new band at 450 nm. The former two bands are consistent with isolated surface CrOx species coordinated to exposed alumina sites and the small 450 nm band is indicative of isolated surface CrOx species interacting with exposed silica sites, with the latter representing the LMCT of the O (2p) to Cr (d) orbital of isolated surface CrOx species bound to silica (see **Figure 5-11**). The major UV-vis band at 335 nm yields a corresponding Eg value of 3.1 eV, which confirms that the CrO_3/ZSM-5 (Si/Al=40) catalyst primarily contains isolated surface CrOx species that are interacting with the exposed alumina sites. For the silica-rich supported CrO_3/ZSM-5 (Si/Al=140) catalyst, the LMCT transitions are centered at 305,

~350, and ~450 nm, and a new d-d transition is located at ~600 nm. The UV-vis transition at ~600 nm and its corresponding Eg value of 1.9 eV fall in the Eg range for polymeric chromia species, such as dimeric $O_3Cr—O—CrO_3$ comprised in $K_2Cr_2O_7$ and $CoCr_2O_7$ (Eg = 1.9 eV) and polymeric CrO_4 chains found in Cr_2O_3 (Eg = 1.8 eV). The ~600 nm band polymeric species are associated with Cr_2O_3 NPs since the NPs are also detectable in the corresponding Raman spectra (**Figure 5- 17**).[80] The LMCT band at ~450 nm and the corresponding Eg value of ~2.5 eV are consistent with that of isolated surface CrOx species present for the model supported CrO_3/SiO_2 catalyst (Eg=2.4 eV).[42] The silica-rich supported CrO_3/SiO_2 (Si/Al=140) catalyst, thus, contains isolated surface chromia species and crystalline Cr_2O_3 NPs. The formation of crystalline Cr_2O_3 NPs is due to the limited number of exposed alumina sites available for dispersion of the supported chromia phase on the ZSM-5 (Si/Al=140) support. Therefore, isolated surface CrOx species are the dominant species for supported CrOx/ZSM-5 catalysts for the alumina-rich ZSM-5 supports (Si/Al=15, 25 and 40), and crystalline Cr_2O_3 NPs are also present on silica-rich ZSM-5 supports (Si/Al=140).

Supported MoO_3/ZSM-5 catalysts

The *in situ* UV-vis DRS spectra of the dehydrated supported MoO_3/ZSM-5 catalysts under oxidative environments are shown in **Figure 5- 13** (left) and possess a single LMCT transition of the O (2p) to Mo (d) orbital centered at 242-245 nm for all Si/Al ratios of the ZSM-5 support. The absence of any d-d transitions at ~400 nm, characteristic to crystalline MoO_3 NPs, indicates that this phase is either not present or only present in trace amounts.[42] The corresponding Eg values for the molybdena species

at ~245 nm are approximately 4.6-4.9 eV and are listed in **Figure 5- 11**. These LMCT and Eg values are different than the model supported MoO_3/SiO_2 system that contains surface $O_2Mo(=O)_2$ species coordinated to SiO_2, which exhibits two LMCT transitions at ~237 and 274 nm corresponding to an Eg value of 4.1 eV.[42] Rather, the supported MoO_3/ZSM-5 catalysts are consistent with the supported $MoO_3/Al_2O_3/SiO_2$ catalyst system[46], which exhibits a single LMCT at 217 nm with a corresponding Eg of 4.9 eV and are assigned to isolated surface $O_2Mo(=O)_2$ species. The UV-vis spectra do not exhibit transitions for dimeric Mo_2O_7 dimer $MgMo_2O_7$ (Eg = 4.25 eV), 300 nm of linear chains of MoO_4/MoO_6 (Eg = 3.8 eV), 320 nm of clustered, distorted MoO_6 (Eg = 3.7 eV), nor ~330 nm of polymeric MoO_6 3D structure (Eg = 3.4 eV). Therefore, the predominant surface molybdena species present in supported MoOx/ZSM-5 catalysts consist of isolated surface MoOx species that are fully oxidized.

Supported WO_3/ZSM-5 catalysts

The *in situ* UV-vis DRS spectra of the dehydrated supported WO_3/ZSM-5 catalysts under oxidizing conditions exhibit a strong LMCT transition of the O (2p) to W (d) orbital at 215 nm for all Si/Al ratios as shown in **Figure 5- 13** (center). This single LMCT transition with a corresponding Eg of ~5.1 eV, listed in **Figure 5- 11**, is consistent with the spectral profile and Eg value found for isolated surface WOx species interacting with alumina sites in the bilayered supported 3% $WO_3/5\%Al_2O_3/SiO_2$ (Eg = 5.0 eV) catalyst.[46] The UV-vis spectra of the supported WOx/ZSM-5 catalysts with Si/Al=25 and 40 (**Figure 5- 13 B and C**) exhibit an additional broad shoulder at ~270 nm with corresponding Eg = 4.1 eV that is similar to the LMCT band at 265 nm of the model

supported WO_3/SiO_2 catalyst (Eg = 4.1 eV).[42] Therefore, the minor second LMCT transition likely arises from surface WOx species interacting with the silica sites of the ZSM-5 (Si/Al=25 and 40) supports. For the alumina-rich supported WO_3/ZSM-5 catalysts (Si/Al=15, 25, and 40), no transitions were detected at 262 and 320 nm assigned to linear chains of WO_4/WO_6 (Eg = 3.6 eV), 254 and 318 nm of clusters, distorted WO_6 (Eg = 3.4 eV) nor transitions at 267 and 328 nm of polymeric WO_6 3D structure (Eg = 2.8 eV).[46] Only for the silica-rich supported WO_3/ZSM-5 (Si/Al=140) catalyst, an apparent transition is detected at ~300 nm with a corresponding Eg of ~3.6 eV that is indicative of the polymeric WO_6 molecular structure such as crystalline WO_3 NPs.[42, 36] Thus, isolated surface WOx species are the predominant tungsten oxide species on the alumina-rich ZSM-5 supports (Si/Al ratios of 15, 25 and 40), and crystalline WO_3 NPs are also present on silica-rich ZSM-5 support (Si/Al=140).

Supported Re_2O_7/ZSM-5 catalysts

The *in situ* UV-Vis DRS spectra of the dehydrated supported Re_2O_7/ZSM-5 catalysts under oxidative conditions give rise to a single LMCT transition at 234 nm of the O (2p) to Re (d) orbital as shown in **Figure 5- 13** (right). The corresponding Eg values are 4.9-5.0 eV and are listed in in manuscript. The band maxima and Eg values are consistent with isolated, distorted ReOx molecular structures present in bulk NH_4ReO_4 (Eg =3.9-4.0 eV)[42], supported Re_2O_7/SiO_2[42], and $Re_2O_7/Al_2O_3/SiO_2$[46] (Eg = ~4.8 eV) catalysts.

5.2.3. *In situ* Raman Spectroscopy

The ZSM-5 zeolite of MFI-type, is a crystalline, microporous structure with a three-dimensional lattice comprising of corner-sharing TO_4 tetrahedral (T=Si, Al) and consisting of two sets of perpendicular, intersecting channels. When Al^{3+} substitutes for a Si^{4+} of a TO_4 tetrahedral, a proton or a cation is necessary to maintain charge neutrality.[38] The *in situ* Raman spectra of the dehydrated HZSM-5 supports are shown in **Figure 5- 14**.

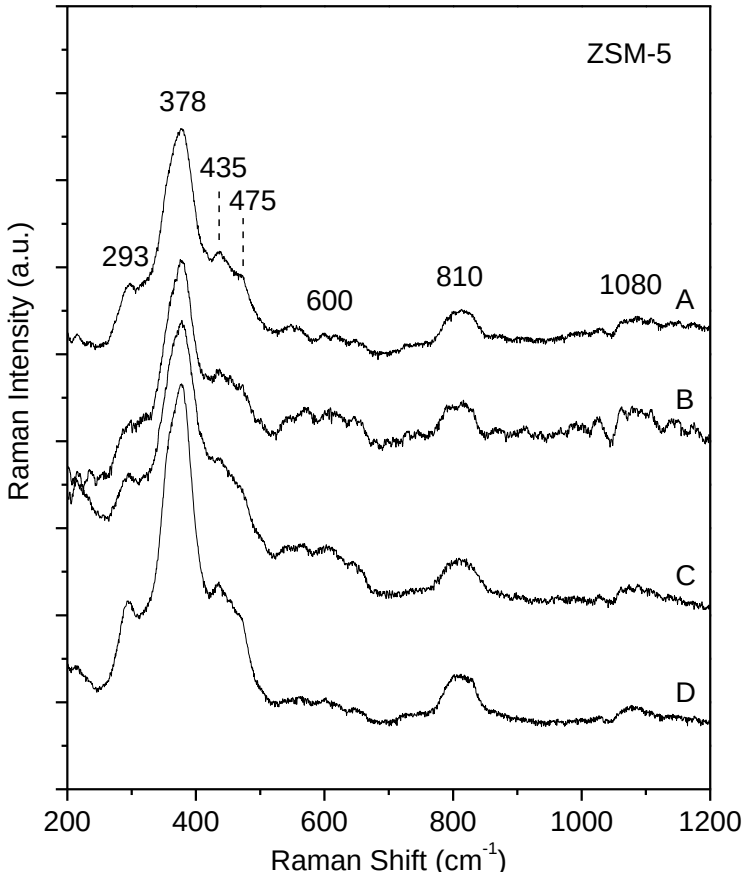

Figure 5- 14 *In situ* Raman spectra (Visible-532 nm) of dehydrated parent H-ZSM-5 containing (A) Si/Al=15, (B) Si/Al=25, (C) Si/Al=40, and (D) Si/Al=140 under oxidizing conditions at 450 ^{o}C.

The *in situ* Raman spectra of HZSM-5 support exhibit the bending mode of six-membered ring at 293 cm^{-1}, bending mode of five-membered ring at 378 cm^{-1}, the

bending mode of four-membered rings at 440-500 cm^{-1}, the symmetric stretching vibrations of T-O bonds in ZSM-5 at ~810-820 cm^{-1} and asymmetric stretching vibrations of T-O bonds in ZSM-5 at 1080-1250 cm^{-1}.[39,40,41] It is important to note that HZSM-5 does not possess Raman bands in the 900-1040 cm^{-1}region since this is in which MOx vibrations usually occur.[42] The *in situ* Raman bands of the dehydrated supported MOx/ZSM-5 catalysts are summarized in **Table 5- 2** and discussed in details below.

Table 5- 2 Positions of Raman bands (cm^{-1}) for dehydrated MOx/ZSM-5 catalysts under oxidizing conditions

Assignments	VO_x	CrO_x	MoO_x	WO_x	ReO_x
ν(M=O)	1038 (s)	1010 (m)	1027 (m)	1020 (w)	
ν_s(M(=O)$_2$)		978 (s)	970-990 (s)	972-990 (w)	
ν_{as}(M(=O)$_2$)		[a]	952 (m)	[a]	
ν_s(M(=O)$_3$)					1010 (s)
ν_{as}(M(=O)$_3$)					975 (m)
ν_s(M—O—Support)	900 (vw)	900 (w)	900 (w)	[a]	[a]

[a] Vibration too weak to be observed.

*Bending mode of O-M-O is obscured by the T-O bending modes of ZSM-5 support

Supported VO_x/ZSM-5

The *in situ* Raman spectra of the dehydrated supported V_2O_5/ZSM-5 catalysts under oxidizing conditions are presented in **Figure 5- 15** as a function of Si/Al ratio.

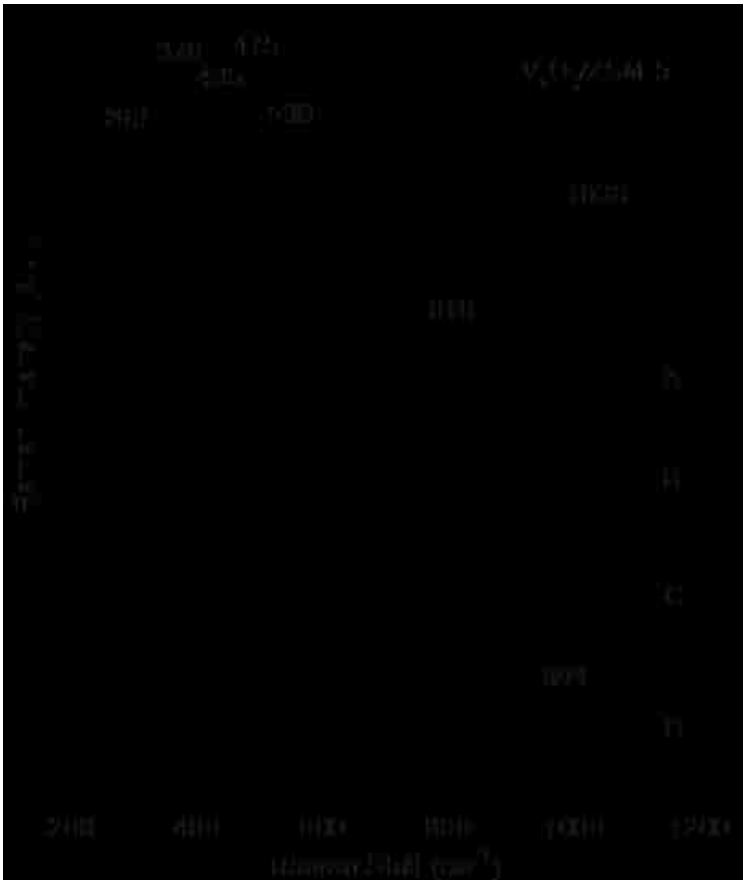

Figure 5- 15 *In situ* Raman spectra (442 nm) of dehydrated supported (A) 3% V_2O_5/ZSM-5 (Si/Al=15), (B) 3% V_2O_5/ZSM-5 (Si/Al=25), (C) 2% V_2O_5/ZSM-5 (Si/Al=40), (D) 2% V_2O_5/ZSM-5 (Si/Al=140) under oxidizing conditions at 450 ^{o}C

The absence of crystalline V_2O_5 NPs, characteristic sharp Raman band at 994 cm^{-1}, with the exception of a trace amount of crystalline V_2O_5 NPs for supported V_2O_5/ZSM-5 (Si/Al=140) having the lowest Al content, indicates that the supported vanadia phase is completely dispersed as surface species on the ZSM-5 support. The vanadia loading was decreased from 3% to 2% V_2O_5 for the two catalysts with the lowest content of alumina,

Si/Al=40 and 140, to minimize formation of V_2O_5 NPs since they formed on these ZSM-5 supports at higher vanadia loading. The Raman band at 1038 cm^{-1} is consistent with the mono-oxo $O=VO_3$ structure present in the model supported V_2O_5/SiO_2[42,43,44,45] (1038 cm^{-1}), bilayered supported $V_2O_5/AlOx/SiO_2$[46] (1035 cm^{-1}), $H_3SiMo_{11}VO_{40}$ Keggins[47] (1034 cm^{-1}) and DFT structural calculations of V_2O_5/SiO_2[48,49,50] (1038-1047 cm^{-1}). Time-resolved isotopic oxygen exchange with $H_2{}^{18}O$ (**Figure 5- 16**) further confirms the mono-oxo V=O nature of the surface VO_4 sites, that shifts from 1038 to 997 cm^{-1} for $V={}^{16}O$ to $V={}^{18}O$, respectively, as previously reported for mono-oxo V=O structures.[51] The corresponding bending O—V—O (δ) and V—O—support modes are expected to occur at ~340 cm^{-1} (δ) and ~900 cm^{-1}, respectively, but strong Raman bands of the ZSM-5 support in the same region make their detection difficult. The weak and broad band at ~530 cm^{-1} is tentatively assigned to the ν_s(V—O—V) vibration of a small amount of oligomeric surface VO_4 species.[51,52]

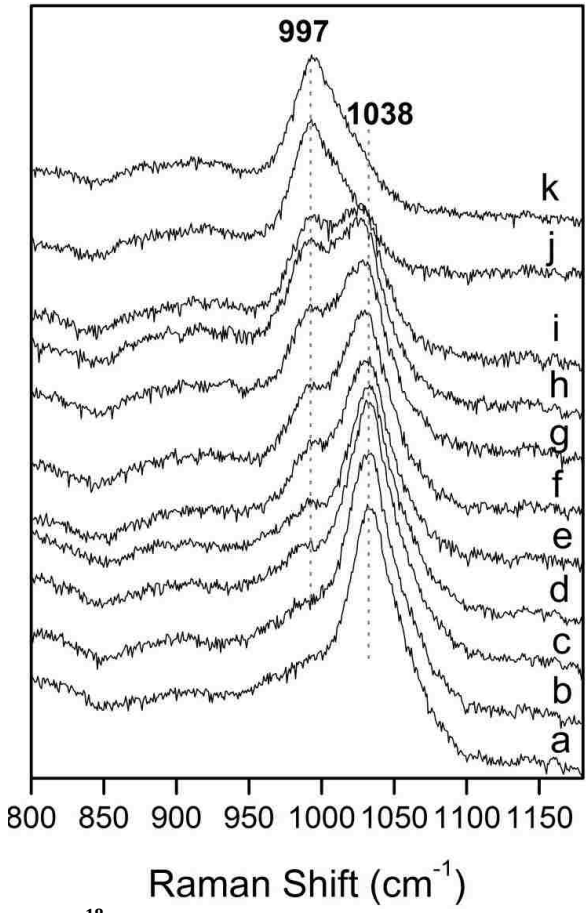

Figure 5- 16 Isotopic ^{18}O-exchange time-resolved *in situ* Raman spectra (442 nm) of dehydrated 3 % V_2O_5/ZSM-5 (Si/Al=15) catalyst upon exposure to $H_2{}^{18}O$ at 500 ^oC for (a) 0 min, (b) 5 min, (c) 10min, (d)15 min, (e) 20min, (f) 25min, (g)30min, (h) 35min, (i) 40min, (j) 50 min and (k) 60 min

Supported CrO_3/ZSM-5

The *in situ* Raman spectra of dehydrated supported 2% CrO_3/ZSM-5 catalysts under oxidizing conditions are shown in **Figure 5- 17** as a function of Si/Al ratio.

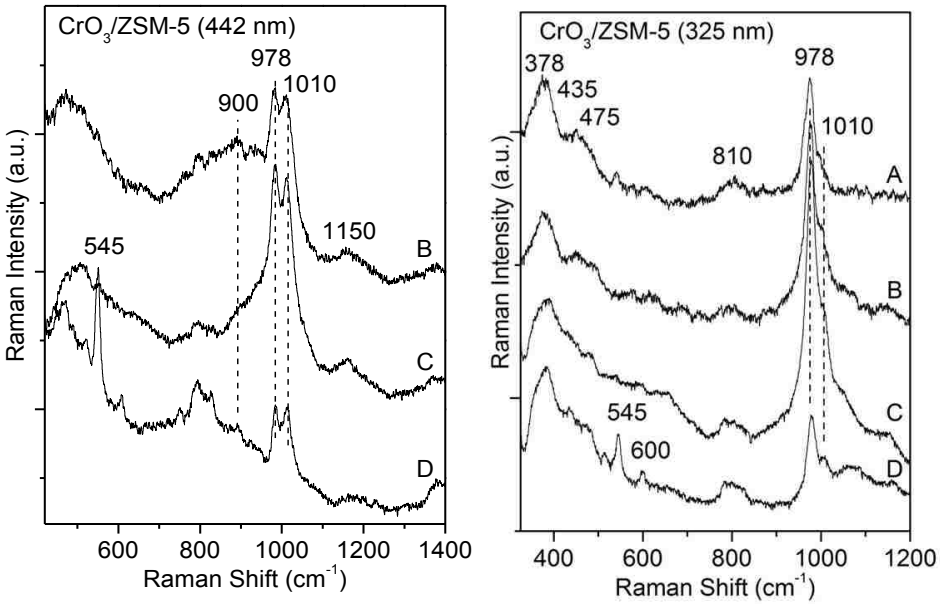

Figure 5- 17 *In situ* Raman spectra (442 nm, left; and 325 nm, right) of dehydrated supported (A) 2% CrO_3/ZSM-5 (Si/Al=15), (B) 2% CrO_3/ZSM-5 (Si/Al=25), (C) 2% CrO_3/ZSM-5 (Si/Al=40), and (D) 2% CrO_3/ZSM-5 (Si/Al=140) under oxidizing conditions at 500 ^oC.

A trace amount of crystalline Cr_2O_3 NPs with characteristic sharp Raman band at 545 cm^{-1} is present only on Si-rich CrO_3/ZSM-5 (Si/Al=140). In general, surface CrOx species are completely dispersed surface CrOx species on the ZSM-5 supports. The Raman spectrum of the ZSM-5 containing the highest amount of Al, Si/Al=15 ratio, could not be collected with 442 nm excitation because of sample fluorescence, but was successfully collected with 325 nm excitation and does not exhibit the vibrations of Cr_2O_3 NPs (see **Figure 5- 17**). The supported CrO_3/ZSM-5 catalysts have two strong vibrations at 978 and 1010 cm^{-1} which correspond to the dioxo $\nu_s((O=)_2CrO_2)$ and mono-oxo $\nu_s(O=CrO_4)$ stretching modes, respectively.[42,51] The corresponding weak

$\nu_{as}((O=)_2CrO_2)$ stretch is expected to appear at ~1010-1015 cm^{-1}, but is not readily evident against the strong mono-oxo $O=CrO_4$ vibration at this location. Excitation with 325 nm resonance enhances the dioxo $(O=)_2CrO_2$ species resulting in a strong and a weak band at 978 cm^{-1} and 1010 cm^{-1}, respectively. It is not clear if the weak band at 1010 cm^{-1} is related to the dioxo $\nu_{as}((O=)_2CrO_2)$ or mono-oxo $\nu_s(O=CrO_4)$ stretches, but the different dependence of the intensity of the major Raman bands at 978 and 1010 cm^{-1} with laser excitation confirms that the two bands arise from two distinct surface chromia structures on the ZSM-5 support.

Supported MoO_3/ZSM-5

The *in situ* Raman spectra of dehydrated supported 2% MoO_3/ZSM-5 catalysts under oxidizing conditions are given in **Figure 5- 18** as a function of Si/Al ratio.

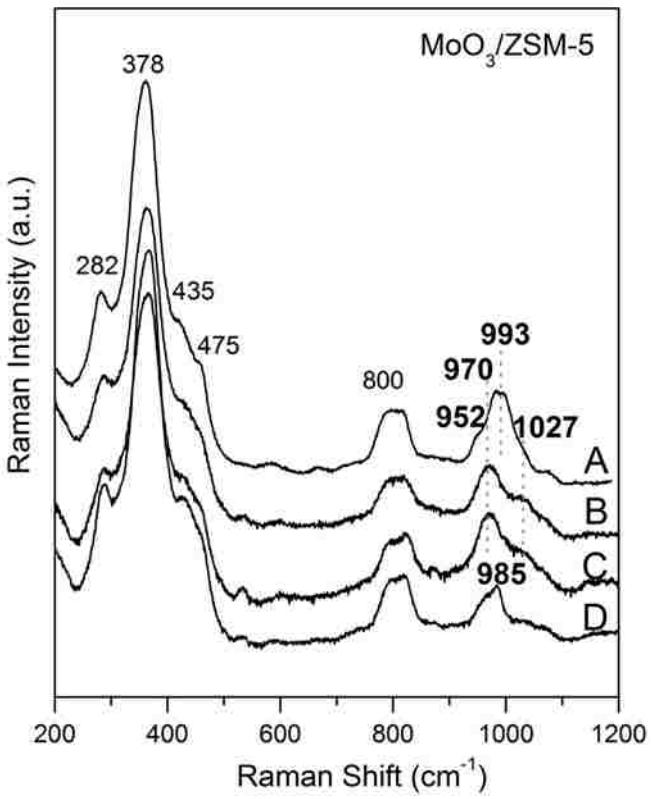

Figure 5- 18 *In situ* Raman spectra (442 nm) of dehydrated supported (A) 2% MoO_3/ZSM-5 (Si/Al=15), (B) 2% MoO_3/ZSM-5 (Si/Al=25), (C) 2% MoO_3/ZSM-5 (Si/Al=40), and (D) 2% MoO_3/ZSM-5 (Si/Al=140) under oxidizing conditions at 500 ^oC. All the catalysts were calcined at 500 ^oC.

Crystalline MoO_3 NPs has characteristic sharp vibration at 815 cm^{-1}. The absence of this band is evident of the presence of only dispersed surface MoOx species on the ZSM-5 support, but do form on the Si-rich ZSM-5 supports (Si/Al=40 and 140) at higher molybdena loadings. The nature of the surface MoOx species on ZSM-5 is sensitive to the Si/Al ratio. For the alumina-rich catalyst of Si/Al=15, the MoOx vibrations occur at

~960 (weak shoulder), 993 (strong) and ~1030 cm^{-1}(very weak, broad). For Si/Al=25 and 40, the MoOx vibrations appear at 970 (strong) and ~1027 (weak, broad) cm^{-1}. For the alumina-lean catalyst of Si/Al=140, the MoOx vibrations are present at ~960 (medium, broad), 985 (strong) and ~1027 (weak, broad) cm^{-1}. The changing intensities of the Raman bands at 970, 993, 985 and 1027 cm^{-1} with Si/Al ratio reflect the presence of four distinct surface MoOx species on the ZSM-5 support. Time-resolved *in situ* Raman spectroscopy during isotopic oxygen exchange with $H_2{}^{18}O$ provided additional structural details about the surface MoOx species (see **Figure 5- 19**).

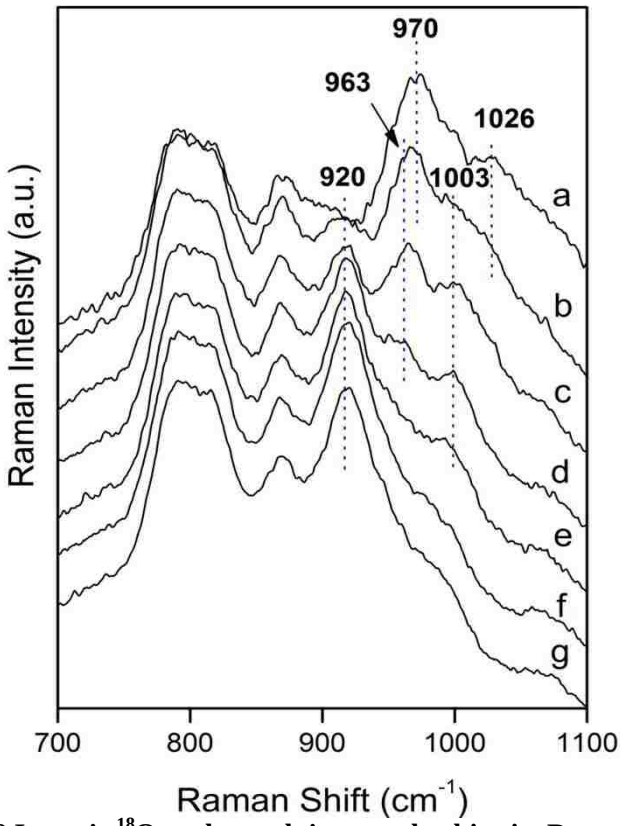

Figure 5- 19 Isotopic ^{18}O-exchanged time-resolved *in situ* Raman spectra of 2 % MoO_3/ZSM-5 (Si/Al=25) upon exposure to $H_2{}^{18}O$ at 400 ^oC for (a) 0 min, (b) 5min, (c) 10 min, (d) 15 min, (e) 20 min, (f) 55 min, (g) 115 min

For the MoOx/ZSM-5 (Si/Al=40) catalyst, the 970 cm^{-1} band shifts to 963 cm^{-1} and ultimately to 920 cm^{-1} and the broad band at 1027 cm^{-1} shifts to 1003 cm^{-1}. The shift

patterns of 970 cm^{-1} and 1026 cm^{-1} are in accordance with the assignment of dioxo $\nu_s((O=)_2MoO_2)$ and mono-oxo $\nu_s(O=MoO_4)$ species, respectively. The isotopic oxygen exchange pattern for the MoOx/ZSM-5 (Si/Al=15) catalyst is consistent with a dioxo species (see **Figure 5- 19**). The Raman band at 985 cm^{-1} for the alumina-lean MoOx/ZSM-5 (Si/Al=140) catalyst coincides with the vibration observed for dioxo $(O=)_2MoO_2$ species on amorphous SiO_2 and is assigned to dioxo $(O=)_2MoO_2$ species anchored at external Si-OH sites. Recent DFT calculations have provided additional details about the different surface MoOx species on the ZSM-5 support.[53] The 993 cm^{-1} band, only observed for the Al-rich Si/Al=15 support, is associated with dioxo $(O=)_2MoO_2$ species anchored at double Al-Al sites in the same silicate ring. The 970 cm^{-1} band, which is dominant for intermediate Al-containing Si/Al=25 and 40 supports, corresponds to dioxo$(O=)_2Mo(OH)O$ species anchored at single Al sites in the silicate ring. The 985 cm^{-1} band, which is dominant for low Al content ZSM-5 (Si/Al=140) is associated with dioxo $(O=)_2MoO_2$ species anchored at external double Si-Si sites. The broad band centered at ~1027 cm^{-1} is found to be related to mono-oxo $O=MoO_4$ species anchored at extra-framework Al_2O_3 NPs.[54] Thus, the multiple available anchoring sites in the ZSM-5 support are responsible for the presence of four distinct surface MoOx species.

Supported WO_3/ZSM-5

The *in situ* Raman spectra of dehydrated supported 3% WO_3/ZSM-5 catalysts under oxidizing conditions are presented in **Figure 5- 20** as a function of Si/Al ratio.

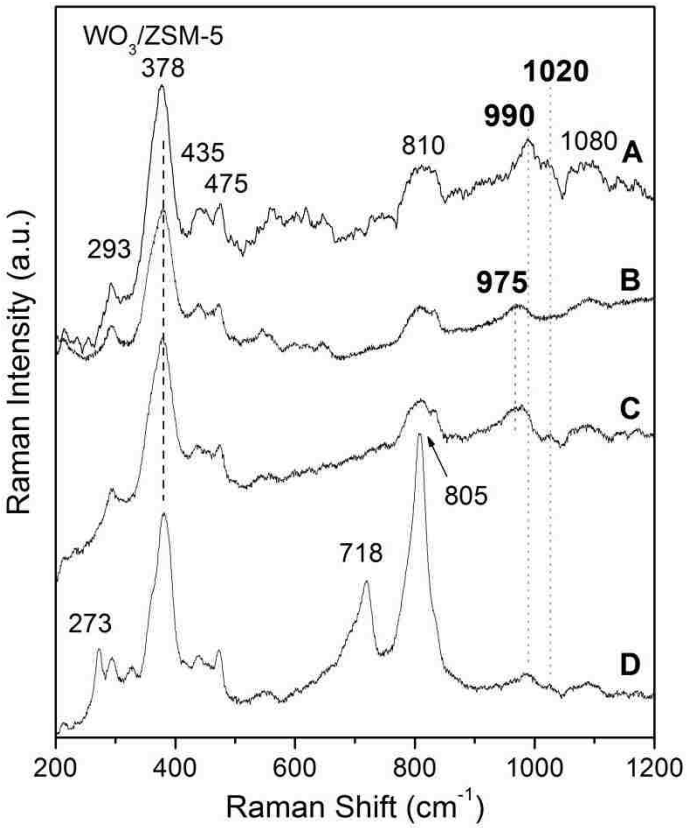

Figure 5- 20 *In situ* Raman spectra (532 nm) of dehydrated supported (A) 3% WO_3/ZSM-5 (Si/Al=15), (B) 3% WO_3/ZSM-5 (Si/Al=25), (C) 3% WO_3/ZSM-5 (Si/Al=40), and (D) 3% WO_3/ZSM-5 (Si/Al=140) under oxidizing conditions at room temperature following oxidative dehydration at 600 ^{o}C

A trace of crystalline WO_3 with characteristic strong Raman bands at 718 and 805 cm^{-1} is only present on the Al-lean WO_3/ZSM-5 (Si/Al=140) catalyst. In general, surface WOx species are completely dispersed on the Al-rich ZSM-5 supports (Si/Al=15, 25 and 40). The strong Raman bands from crystalline WO_3 NPs usually have enhanced light scattering of ~100x greater than that for dispersed surface WOx species. The sharp

Raman bands of WO_3 NPs represent only a small amount of WO_3 crystallites.[55] For the Al-rich ZSM-5 (Si/Al=15), the surface WOx Raman bands occur at 990 (strong) and 1020 (weak) cm^{-1}. At intermediate Al-containing ZSM-5 (Si/Al=25 and 40), the Raman bands occur at ~972 (strong) and 1020 (weak) cm^{-1}. For the Si-rich ZSM-5 (Si/Al=140), Raman bands at are present at 718/805 (strong), 972 (medium) and 1020 (weak) cm^{-1}. The surface WOx species give rise to Raman vibrations that are analogous to that found above for surface MoOx species on ZSM-5 and suggest the following: the 990 cm^{-1} band is related to dioxo $(O=)_2WO_2$ sites anchored at double Al-Al sites in the silicate ring, the 972 cm^{-1} band is associated with dioxo $(O=)_2W(OH)O$ anchored at single Al sites in the silicate rings, and the 1020 cm^{-1}band represents mono-oxo $O=WO_4$ species anchored at extra-framework Al_2O_3 NPs or silicate defect sites.

Supported Re_2O_7/ZSM-5

The *in situ* Raman spectra of the dehydrated supported 3% ReOx/ZSM-5 catalysts under oxidizing conditions are presented in **Figure 5- 21** as a function of Si/Al ratio.

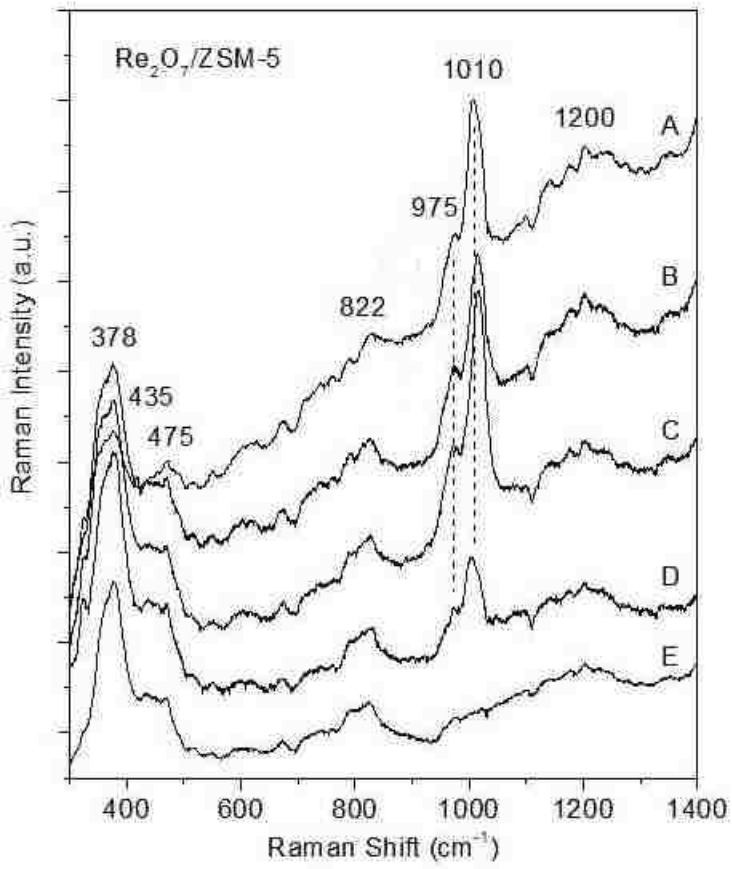

Figure 5- 21 *In situ* Raman spectra (325 nm) of dehydrated supported (A) 3% Re_2O_7/ZSM-5 (Si/Al=15), (B) 3% Re_2O_7/ZSM-5 (Si/Al=25), (C) 3% Re_2O_7/ZSM-5 (Si/Al=40), and (D) 3% Re_2O_7/ZSM-5 (Si/Al=140) under oxidizing conditions at 400 ^oC. The dehydrated ZSM-5 (Si/Al=140) support is provided in (E) for reference with 325 nm excitation energy.

Crystalline Re_2O_7 particles (major sharp Raman bands at 993, 854, 831, and 798 cm^{-1}) are not present on any of the supported ReOx/ZSM-5 because of the known volatility of such particles.[56] The surface ReOx species exhibit two vibrations at 1010 (strong) and 975 (weak) cm^{-1} independent of ZSM-5 Si/Al ratio suggesting that only one surface

ReOx species is present on the ZSM-5 support. The similar vibrations from trioxo $ReOx/SiO_2$ and pseudo-trioxo (dioxo) $ReOx/Al_2O_3$ complicate discrimination between these two anchoring sites.[42,46] The weaker Raman intensity from the surface ReOx species of the silica-rich ZSM-5 support (Si/Al= 140) indicates that ReOx volatilized from this catalyst during calcination and reflects the lower number of available alumina anchoring sites on this ZSM-5 support.

The Raman spectra of trioxo and pseudo trioxo (dioxo) surface ReOx species are quite similar and ^{18}O-^{16}O isotopic exchange experiments are required to distinguish between these two possibilities, but were not successful due to the volatility of ReOx species at prolonged heating and Raman fluorescence of ZSM-5 at low temperature.[51,57] Raman bands from bridging Re-O-Re bonds[46] at 456 (ν_s) and 186 (δ) cm^{-1} are absent suggesting isolated surface ReOx sites on the ZSM-5 support. Additional molecular structural details about the surface ReOx species are provided below from *in situ* XAS measurements.

5.2.4. *In situ* X-ray Absorption Spectroscopy (XAS)

X-ray absorption spectroscopy provides information about the metal oxide local coordination (MO_4 *vs.* MO_6), oxidation state and next nearest neighbors (M=O and M-O in the first coordination sphere and M-O-M in the second coordination sphere).[58,59] The information of local coordination and oxidation state is contained in the X-ray absorption near edge spectroscopy (XANES) portion and the nearest neighbor details are provided by the extended X-ray absorption fine structure (EXAFS) region. The XANES discriminates from different oxidation states because the edge energy shows significant edge shifts (binding energy shifts) with oxidation state. The XANES also discriminates

tetrahedral MO_4 from octahedral MO_6 coordination because the pre-edge transition is allowed and forbidden, respectively, due to the coordination symmetry selection rules.[58,59,60] The EXAFS portion contains information about the distances of atoms surrounding the cations (M=O, M-O-Si/Al and M-O-M). It is important to note that the XAS signals provide an average of all coordination and next nearest neighbors. Thus, in situations which more than one MOx structure on the ZSM-5 supports the XAS spectrum will be an average of the multiple sites. Nevertheless, XAS does provide important structural details about the MOx species present on the ZSM-5 support that aid in molecular structural determination.

The *in situ* XAS spectra of the dehydrated supported MOx/ZSM-5 catalysts and their corresponding reference compounds are presented in figures from **Figure 5- 22** and **Figure 5- 26**. The EXAFS results are summarized in **Table 5- 3**.

Table 5- 3 Summary of dehydrated surface MOx molecular structures on ZSM-5 supports from *in situ* XAS

Metal ions	Coordination	M=O bond	M-O-Al/Si bond	M-O-M bond
V	VO_4	Yes	Yes	No
Cr	$CrO_4/CrO_5/CrO_6$	Yes	Yes	No
Mo	$MoO_4/MoO_5/MoO_6$	Yes	Yes	No[a]
W	$WO_4/WO_5/WO_6$	Yes	Yes	No[a]
Re	ReO_4	Yes	Yes	No

a Exception only observed on WOx/ZSM-5 (Si/Al=140) when WO_3 NPs were present
NOTE: there was some M-O-M for Si/Al=140 for MoOx and WOx.

Supported V_2O_5/ZSM-5

The *in situ* XANES spectra reveal that dehydrated surface VOx species on ZSM-5 has a strong pre-edge intensity characteristic of VO_4 coordination as shown for sodium orthovanadate (Na_3VO_4) and magnesium pyrovanadate ($Mg_2V_2O_7$) reference compounds containing VO_4 coordination (see **Figure 5- 22**) and not that of the much weaker XANES

intensity of vanadium pentoxide V_2O_5 containing distorted square-*pyramidal* VO_5 structure.[61]

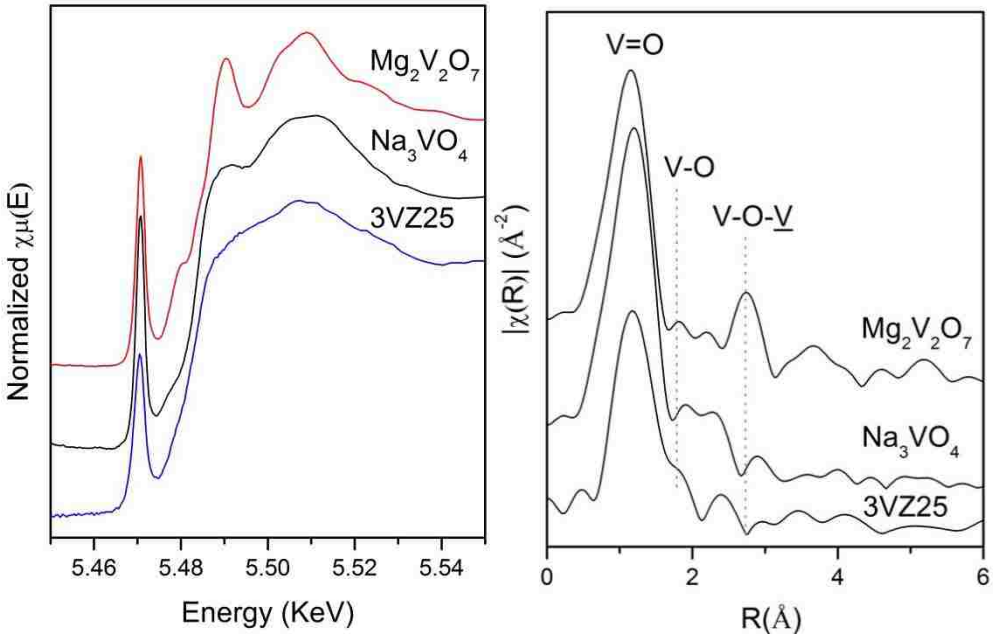

Figure 5- 22 Vanadium k-edge *in situ* XANES (left) and EXAFS (right) of supported 3% V_2O_5/ZSM-5 (Si/Al=25) (labeled as 3VZ25) under dehydrated condition (500 ^oC for 30 mins, and full XAS collection at 110 ^oC) and dimeric V_2Ox and monomeric VO_x reference compounds $Mg_2V_2O_7$ and Na_3VO_4, respectively.

The corresponding *in situ* EXAFS spectrum of supported VOx/ZSM-5 reveals the presence of V=O (~1Å) and V-O-Al/Si (~2Å) bonds in the first coordination sphere, but not a feature at ~3Å characteristic of V-O-V in the second coordination sphere. Although x-ray scattering is strongest from the terminal V=O bonds, the absence of the appearance of V-O-V bonds suggests that the dominant surface VOx sites are isolated on the ZSM-5 support. The *in situ* Raman spectra indicate that only one surface VOx structure is present for supported V_2O_5/ZSM-5 catalysts (see **Figure 5- 15**). Initial surface VOx species are monomeric and fully oxidized $O=VO_3$ species on ZSM-5 support.

Supported CrO_3/ZSM-5

The *in situ* XANES pre-edge intensity for dehydrated supported CrO_3/ZSM-5 is intermediate between that of the CrO_4 coordinated reference compounds ($(NH_4)_2CrO_4$ (isolated CrO_4 sites) and $(NH_4)_2Cr_2O_7$ (dimeric O_3Cr-O-CrO_3 sites)) and CrO_6 coordinated Cr_2O_3 (see **Figure 5- 23**).

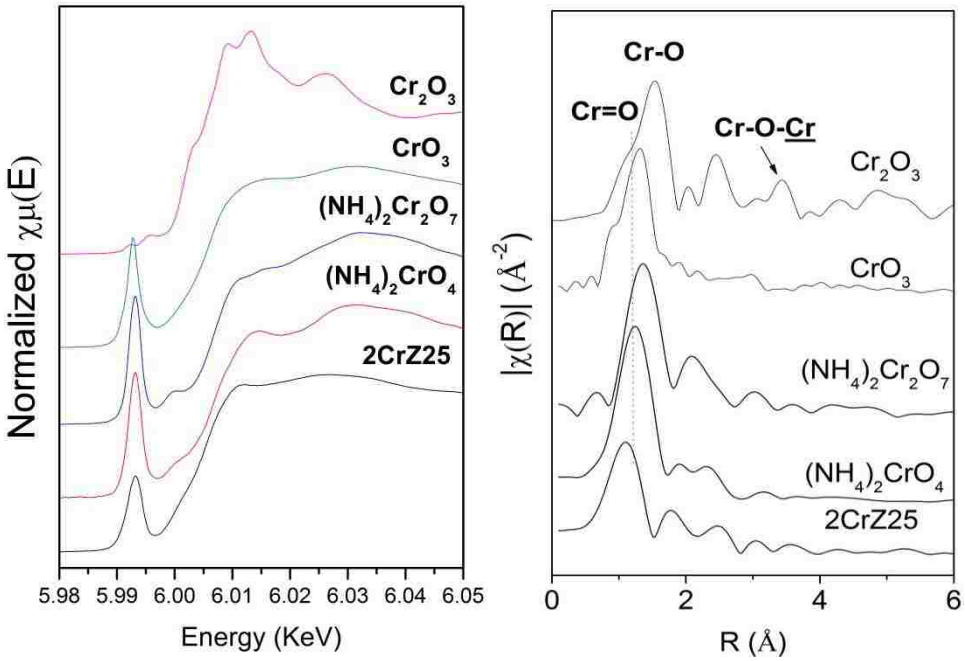

Figure 5- 23 Chromium k-edge *in situ* XANES (left) and EXAFS (right) of supported 2% CrO_3/ZSM-5 (Si/Al=25) (labeled as 2CrZ25) under dehydrated condition (500 ^oC for 30 mins, and full XAS collection at 110 ^oC in flowing He) and Cr_2O_3 (CrO_6 coordinated sites), CrO_3 (polymeric CrO_4 chain), $(NH_4)_2CrO_4$ (isolated CrO_4 sites) and $(NH_4)_2Cr_2O_7$ (dimeric O_3Cr-O-CrO_3 sites) isolated reference compounds.

The intermediate XANES pre-edge intensity indicates that the surface CrOx sites on ZSM-5 consist of a mixture of both CrO_4 and CrO_5/CrO_6 coordinated sites, which is consistent with the observation of multiple surface CrOx sites on ZSM-5 detected with *in situ* Raman spectroscopy (see **Figure 5- 17**). The corresponding *in situ* EXAFS spectra for the reference compounds contain the Cr=O (~1Å), Cr-O (~2Å) and Cr-O-Cr (~3Å)

bonds. The presence of Cr-O-Cr bonds in the second coordination sphere of Cr_2O_3 at ~3Å is pronounced but very weak for the dimeric $(NH_4)_2Cr_2O_7$ reference compound, which suggests a high degree of disorder in the structure of $(NH_4)_2Cr_2O_7$. Surprisingly, a high degree of disorder also persists for oligomeric CrO_3 since it also does not exhibit an EXAFS feature in the second coordination sphere. Thus, it is not possible to easily determine if oligomeric chromia sites are present on ZSM-5 just based on EXAFS analysis alone. The EXAFS spectra do indicate that surface CrOx on ZSM-5 contains short Cr=O (~1Å) and longer Cr-O-Al/Si (~2Å) bonds.

Supported MoO_3/ZSM-5

The *in situ* XANES pre-edge intensity for dehydrated supported MoO_3/ZSM-5 is intermediate between that of the MoO_4 coordinated reference compounds $Al_2(MoO_4)_3$ (isolated MoO_4 sites) and MoO_3 (oligomeric MoO_6 sites)) (see **Figure 5- 24**).

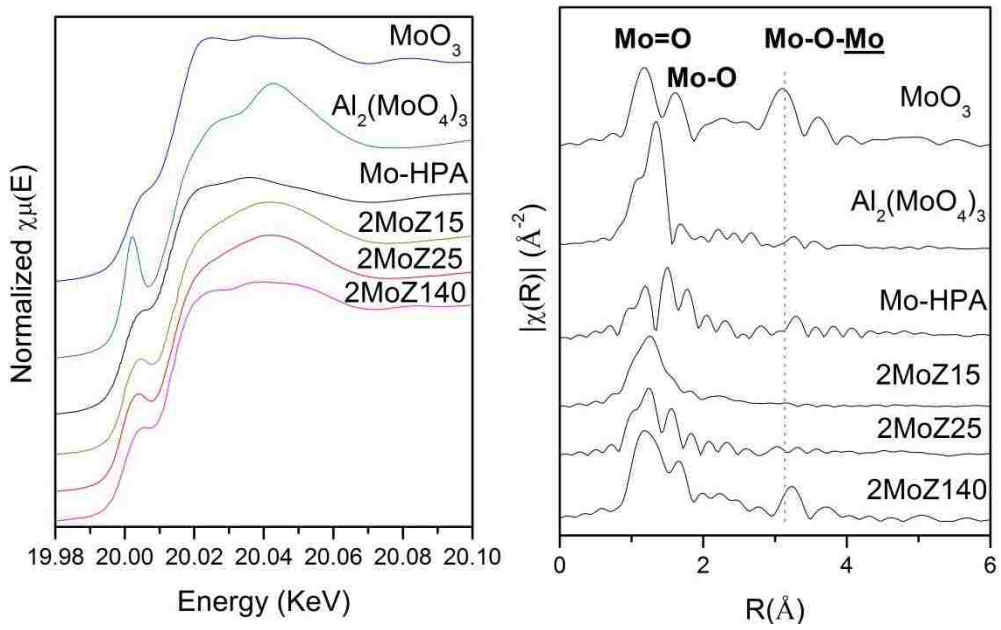

Figure 5- 24 Molybdenum k-edge *in situ* XANES (left) and EXAFS (right) of supported 2% MoO_3/ZSM-5 (Si/Al=15, 25, 140) (labeled as 2MoZ15, 2MoZ25 and 2MoZ140, respectively) under dehydrated condition (500 ^oC for 30 mins, and full XAS collection at 110 ^oC in flowing 10% O_2/He) and reference compounds phosphomolybdate acid (Mo-HPA, mono-oxo MoO_6 containing cluster), and $Al_2(MoO_4)_3$ (isolated tetrahedral MoO_4) and MoO_3 (oligomeric MoO_6 structure)

The intensity of the XANES pre-edge for supported MoOx/ZSM-5 also varies slightly with Si/Al ratio and is lowest for the highest Si/Al ratio. With the exception of the supported MoOx/ZSM-5 (Si/Al=140), the XANES pre-edge intensity for the other catalysts are stronger than for the mono-oxo MoO_6 containing cluster. The intermediate pre-edge intensity and its dependence on the Si/Al ratio indicates that the surface MoOx sites on ZSM-5 consist of a mixture of both MoO_4 and MoO_5/MoO_6 coordinated sites, which is consistent with the observation of multiple surface MoOx sites on ZSM-5 detected with *in situ* Raman spectroscopy (see **Figure 5- 18)**. The corresponding *in situ* EXAFS spectra for the reference compounds contain the short Mo=O (~1-1.5 Å), long Mo-O (~2 Å) and oligomeric Mo-O-Mo (~3Å) bonds. The presence of Mo-O-Mo bonds in the second coordination sphere of MoO_3 and dehydrated HPA at ~3Å is pronounced.

The isolated MoO_4 sites in $Al_2(MoO_4)_3$ do not exhibit the Mo-O-Mo bond at ~3Å. The details of the EXAFS spectra of the dehydrated supported MoOx/ ZSM-5 catalysts vary with Si/Al ratio reflecting the different surface MoOx sites present on ZSM-5. The strong features at ~1 and ~1.5Å are associated with Mo=O bonds, reflecting the presence of multiple sites, and the weaker feature at ~2Å is associated with Mo-O-Al/Si bonds. The 2MoZ140 catalyst has an EXAFS feature at ~3Å suggesting the presence of some oligomeric Mo-O-Mo sites on the Al-lean ZSM-5 support (Si/Al=140).

Supported WO_3/ZSM-5

The XANES pre-edge intensity for the WOx reference compounds strongly depends on the local coordination: isolated WO_4-containing $CeWO_4$ exhibits the strongest intensity; the mono-oxo WO_6-containing cluster indicates an intermediate intensity and the oligomeric WO_6-containing WO_3 with almost no pre-edge intensity. The intensity of the *in situ* XANES pre-edge for dehydrated supported WO_3/ZSM-5 is intermediate between that of the WO_4 coordinated reference compound $CeWoO_4$ (isolated WO_4 sites) and WO_3 (oligomeric WO_6 sites) (see **Figure 5- 25**).

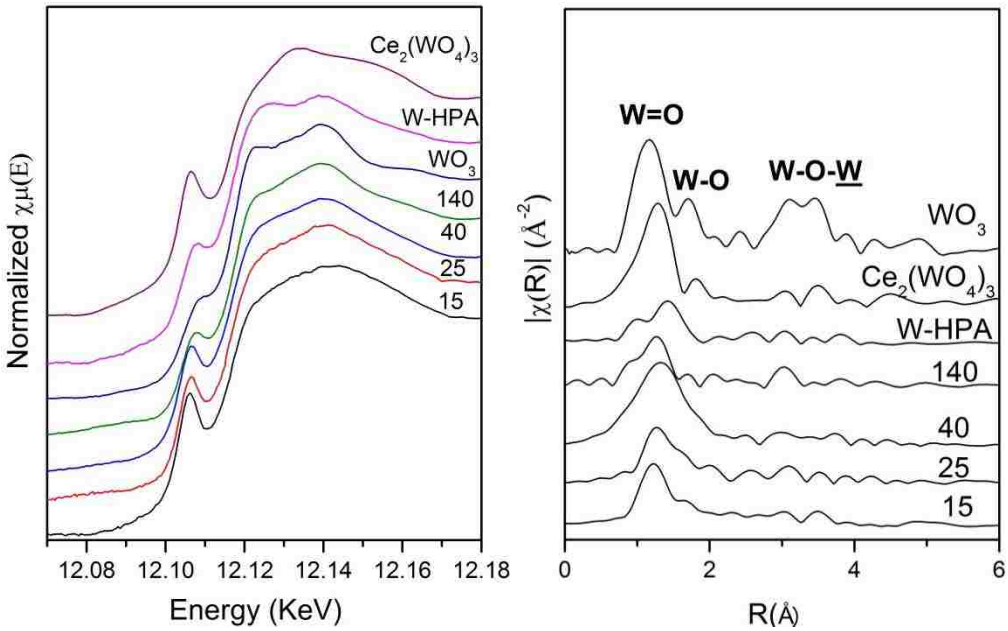

Figure 5- 25 Tungsten L_1-edge *in situ* XANES (left) and EXAFS (right) of supported 2% WO_3/ZSM-5 (Si/Al=15, 25, 40,140) (labeled as 15, 25 and 140, respectively) under dehydrated condition (500 ^oC for 30 mins, and full XAS collection at 110 ^oC in flowing he) and reference compounds phosphotungstate acid (W-HPA, mono-oxo WO_6 containing cluster), $Ce_2(WO_4)_3$ (isolated WO_4) and WO_3 (oligomeric WO_6 structure)

The intensity of the XANES pre-edge for supported WO_3/ZSM-5 also varies slightly with Si/Al ratio and is lowest for the highest Si/Al ratio. With the exception of the supported WO_3/ZSM-5 (Si/Al=140), the XANES pre-edge intensity for the other catalysts are

stronger than for the mono-oxo WO_6 containing cluster indicating that the surface WOx sites on ZSM-5 consist of a mixture of both WO_4 and WO_5/WO_6 coordinated sites, which is consistent with the observation of multiple surface WOx species on ZSM-5 detected with *in situ* Raman spectroscopy (see **Figure 5- 20**). The corresponding EXAFS spectra for the reference W compounds reflect the presence of short W=O (~1-1.5Å), long W-O (~2Å) and oligomeric W-O-W (~3Å) bonds. The features of the W-O-W bonds in the second coordination sphere of WO_3 and dehydrated PWA at ~3Å is not pronounced for the tungsten oxide compounds, which makes determination of dimeric or oligomeric tungstates somewhat difficult. The details of the *in situ* EXAFS spectra of the dehydrated supported WO_3/ZSM-5 catalysts vary with Si/Al ratio reflecting the different surface WOx sites present on ZSM-5. The strong features at ~1 and ~1.5Å are associated with W=O bonds, reflecting the presence of multiple sites, and the weaker feature at ~2Å is associated with Mo-O-Al/Si bonds. Only 2WZ140 catalyst has an EXAFS feature at ~3Å suggesting the presence of some oligomeric W-O-W sites on the Si-rich ZSM-5 support.

Supported Re_2O_7/ZSM-5

The *in situ* XANES pre-edge for dehydrated supported ReOx/ZSM-5 matches the intensity of the ReO_4 coordinated trioxo(triphenylsilyloxy) rhenium(VII) ($(O=)_3Re$-(O-Si-$(C_6H_5)_3$) reference compound and not the ReO_6 coordinated ReO_3 reference compound (see **Figure 5- 26**).

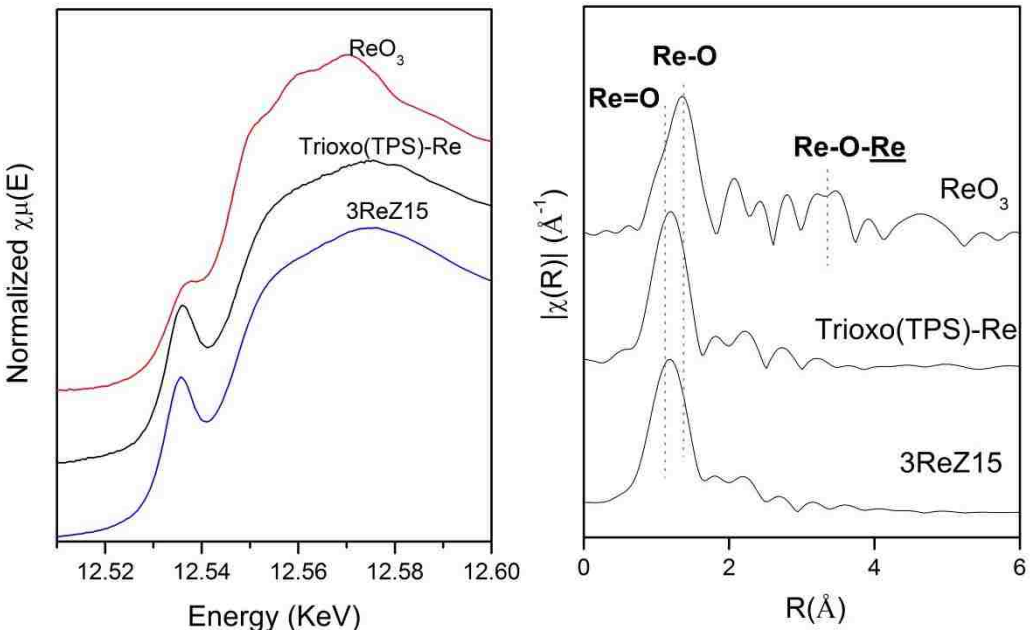

Figure 5- 26 Rhenium L_1-edge *in situ* XANES (left) and EXAFS (right) of supported 3% Re_2O_7/ZSM-5 (Si/Al=15) (500 ^oC for 30 mins, and full XAS collection at 110 ^oC in flowing He), and reference compounds ReO_3 (ReO_6 structure) and trioxo(triphenylsilyloxy)rhenium(VII) (Trioxo(TPS)-Re, isolated trioxo ReO_4 structure)

The similar strong XANES pre-edge intensity for both the supported ReOx/ZSM-5 and the trioxo $(O=)_3$Re-Si reference compound strongly supports the presence of trioxo surface $(O=)_3$ReO-Al/Si sites on ZSM-5. Pseudo-trioxo (dioxo) structures were also proposed on Al_2O_3 support[54], but it has a weaker XANES pre-edge intensity than trioxo(triphenylsilyloxy) rhenium (VII), therefore, pseudo-trioxo (dioxo) structure is not present on Re_2O_7/ZSM-5 catalysts. The corresponding *in situ* EXAFS spectra contain the Re=O bond (~1Å) and Re-O-Al/Si (~2Å). The absence of strong EXAFS Re-O-Re

features at ~3Å suggests that the trioxo surface ReO_4 sites are present as isolated sites on the ZSM-5 support. The *in situ* Raman spectra (see **Figure 5- 21**) indicate that only one surface ReOx structure is present for supported Re_2O_7/ZSM-5 catalysts.

To sum up, only the supported V_2O_5/ZSM-5 and Re_2O_7/ZSM-5 catalysts contain one surface metal oxide structure while multiple metal oxide structures are present for the other supported MOx/ZSM-5 (M = Cr, Mo and W) catalysts as discovered above from the *in situ* Raman spectra (see **Figure 5- 15**). The XAS spectra of supported VOx/ZSM-5 indicate that the surface VOx site possesses VO_4 coordination and is isolated on the ZSM-5 support as shown in **Figure 5- 22**. The XAS spectra of supported CrO_3/ZSM-5 reflect the presence of both CrO_4 and CrO_5/CrO_6 sites that are isolated on the ZSM-5 support (see **Figure 5- 23**). The XAS spectra of the supported MoO_3/ZSM-5 suggest the presence of both isolated MoO_4 and MoO_5/MoO_6 sites with their relative abundance varying with Si/Al ratio (see **Figure 5- 24**). The supported WOx/ZSM-5 catalysts exhibit the same trends as for supported MoO_3/ZSM-5 catalysts (see **Figure 5- 25**). The XAS spectra of supported Re_2O_7/SZSM-5 reflect the presence of an isolated surface ReO_4 site that is independent of Si/Al ratio (see **Figure 5- 26**).

In summary, the surface MOx sites on ZSM-5 are isolated and tend to favor surface MO_4 coordination; a small amount of surface MO_5/MO_6 coordinated sites are also found for the supported group 6 supported MOx/ZSM-5 (M=Cr, Mo and W) catalysts. The molecular structures of each supported MOx/ZSM-5 catalysts are provided in **Figure 5-27.**

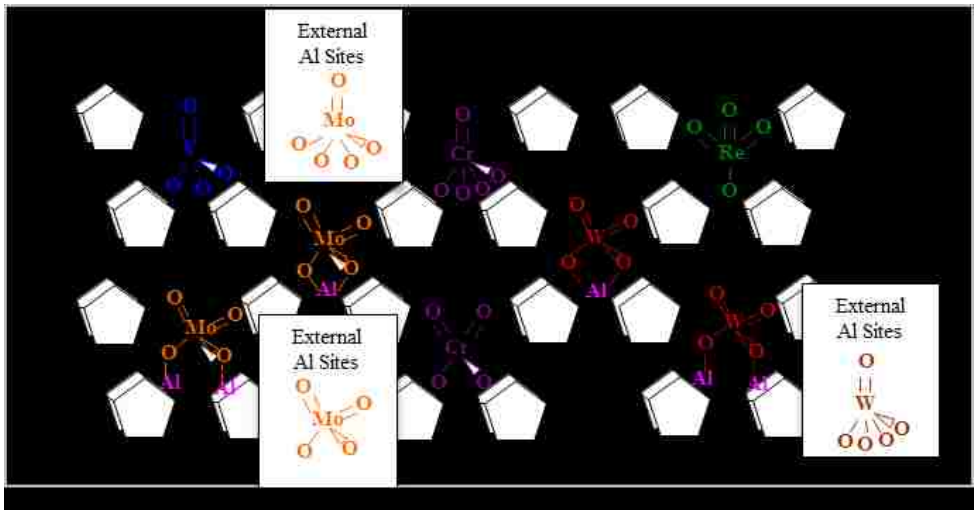

Figure 5- 27 Schematic of surface MOx species for A) V_2O_5/ZSM-5, B) CrO_3/ZSM-5, C) MoO_3/ZSM-5, D) WO_3/ZSM-5, and E) Re_2O_7/ZSM-5 catalysts. In all systems, the surface MOx species preferentially anchor on the framework AlOx sites inside the zeolite pores. Surface molybdena species in MoO_3/ZSM-5 catalysts consist of distorted dioxo species.

5.3. Discussion

5.3.1. Supported V_2O_5/ZSM-5

The surface vanadia species on ZSM-5 are fully oxidized as V^{+5} in oxidizing environments as indicated by the location of the *in situ* XANES pre-edge energy and absence of d-d transitions from the *in situ* UV-vis spectra (see **Figure 5- 22** and **Figure 5- 12**). The VO_4 coordination of the surface vanadia species on ZSM-5 is confirmed by the pronounced *in situ* XANES pre-edge feature (see **Figure 5- 22**). The dehydrated surface vanadia species on the ZSM-5 supports are primarily present as isolated, mono-oxo surface $O=V(—O)_3$ species. The mono-oxo structure is reflected by the position of the *in situ* Raman band at 1038 cm^{-1} that is characteristic of mono-oxo V=O bonds.[42] The absence of V—O—V features in the second coordination sphere of the *in situ* FT-EXAFS (see **Figure 5- 22**) confirms that the surface VO_4 species are predominantly isolated. The *in situ* UV-vis Eg value overlaps the values expected for isolated and dimeric vanadia species, which prevents determination of the VOx domain size (see **Figure 5- 12**). A minor amount of oligomeric $(VO_4)_n$ may also be present because of the *in situ* Raman band at ~530 cm^{-1} may reflect the ν_s(V-O-V) stretching mode (see **Figure 5- 15**).

The proposal that the surface VOx species on ZSM-5 supports are present as reduced VO^{+2} sites is not supported by the present *in situ* UV-vis and XANES findings, as well as other recent EXAFS studies[61], that confirm the surface VOx species are fully oxidized as V^{+5}. The high sensitivity of ESR and photoluminescence spectroscopy to traces of V^{+4} species probably accounts for previous detection of a trace amount of reduced surface

vanadia species under vacuum conditions.[43] Surface dioxo VO_2^+ monomers and dimeric $V_2O_4^{2+}$ structures were also proposed to be present for supported VOx/ZSM-5 catalysts (Si/Al~13.4) from both Raman measurements (band at 1065-1076 cm^{-1}) and DFT calculations.[61] The vibration of 1065-1076 cm^{-1} is too high for terminal V=O bonds since mono-oxo V=O structures vibrate in the 1015-1040 cm^{-1} range[42] and dioxo O=V=O bonds would give rise to ν_s and ν_{as} vibrations at even lower wavenumbers.[62] Raman bands at ~1070 cm^{-1} have been shown to originate from Si-O vibrations and are not associated with surface vanadia species.[39,40,41] The proposed dimeric surface $V_2O_4^{2+}$ species on ZSM-5 can't be a significant species as indicated by the unique presence of V=O bond in the FT-EXAFS.[61] Similarly, the FT-EXAFS spectra of supported V_2O_5/ZSM-5 catalysts prepared by solid-state thermal dispersion of crystalline V_2O_5 on H-ZSM-5 revealed the disappearance of neighboring V—O—V bonds as the crystalline V_2O_5 particles transformed into a dispersed state at elevated temperatures.[43] The current *in situ* FT-EXAFS spectra of supported V_2O_5/ZSM-5 prepared by incipient wetness impregnation consistently indicates the absence of V—O—V coordination. Thus, regardless of catalyst synthesis method (impregnation, sublimation, aqueous exchange or solid-state thermal dispersion), the dehydrated surface vanadia species on the ZSM-5 supports are primarily present as isolated, mono-oxo $O=VO_3$ species under oxidizing conditions.

Supported VOx species preferably anchor at surface Brønsted acid Al-$(OH)^+$-Si and extra-framework Al-OH sites of ZSM-5 at low vanadia loadings (see **Figure 5- 1**). The dispersion of vanadium oxide on ZSM-5 depends on the availability of these surface hydroxyl sites, especially Brønsted acid Al-$(OH)^+$-Si sites, since limiting their availability

results in formation of V_2O_5 NPs. Given that three anchoring sites are required for mono-oxo O=V(-O)$_3$ species, the anchoring mode to the ZSM-5 must involve both adjacent Al and Si sites. At high vanadia loadings, the supported VOx species also create new surface V-OH or V-(OH)$^+$-Al hydroxyl sites. Wichterlova *et al.*[63] claimed that surface VOx species anchor at surface Brønsted acid and external silanol sites, but the IR spectra were collected under ambient condition in which the VOx species and ZSM-5 support are hydrated and not representative of the catalyst at elevated temperature at which the surfaces are dehydrated. Lacheen *et al.*[61] observed a monotonic decrease in the surface Brønsted acid hydroxyls with increasing V/Al$_{framework}$ ratio as well as consumption of a small number of external silanols in their *in situ* IR spectra.

5.3.2. Supported CrO_3/ZSM-5

The dehydrated surface CrOx species on ZSM-5 are fully oxidized as $Cr^{+6}Ox$ species as indicated by the location of the *in situ* XANES pre-edge energy and high Eg values from the *in situ* UV-vis spectra (see **Figure 5- 23** and **Figure 5- 12**, respectively). The intermediate intensity of the XANES pre-edge feature indicates that both CrO_4 and CrO_5/CrO_6 coordinated structures are present for supported CrOx/ZSM-5 catalysts (see **Figure 5- 23**). The surface CrOx sites are isolated on ZSM-5 because of the high UV-vis Eg value (see **Figure 5- 11**) and absence of ν_s(Cr-O-Cr) vibrations from the Raman spectra (see **Figure 5- 17)**. The Raman spectra also reveal the presence of two distinct surface CrOx structures that have previously been assigned to surface dioxo $(O=)_2CrO_2$ (~978 cm^{-1}) and mono-oxo $O=CrO_4$ (~1010 cm^{-1}) species.[42] Crystalline Cr_2O_3 NPs are

only present on ZSM-5 (Si/Al=140), having the lowest number of surface Brønsted acid Al-$(OH)^+$-Si sites.[64]

Isolated dioxo and trioxo CrOx species, polychromate species and Cr_2O_3 NPs species were proposed present on supported CrO_3/ZSM-5 as reviewed in Chapter 1. The *in situ* EXAFS indicates the major presence of Cr=O bond in the first coordination shell and the presence of a small amount of Cr_2O_3 NPs with weak Cr-O-Cr bond at 0.25-0.42 nm at the second and third coordination shells. This analysis neglects the possible presence of multiple surface CrO_x species on the ZSM-5 support, which are known to be present on other oxide support materials such as SiO_2, Al_2O_3 and Al_2O_3/SiO_2.[42,46] Mimura and Yamashita *et al.*[23] performed *in situ* XAS measurements of supported CrOx/ZSM-5 (Si/Al=940) with a very high Si/Al ratio and observed Cr-O-Cr coordination indicating the presence of Cr_2O_3 NPs. The findings of Yamashita *et al.* are not self-consistent and in variance with the findings in the present measurements under dehydrated conditions.

The surface CrOx species preferentially anchor at the ZSM-5 extra-framework Al-OH sites at low loading and external Si-OH sites at high loading (see **Figure 5- 3** and **Figure 5- 4**). New surface Cr-OH or Cr-$(OH)^+$-Al hydroxyls are also created by deposition of chromia on ZSM-5 and complicate determination if surface Brønsted acid Al-$(OH)^+$-Si sites are also serving as anchoring sites for the surface CrOx species. The manner in which the dioxo and mono-oxo surface CrOx species anchor to the ZSM-5 support is still not clear. Slinkin *et al.*[64] reported that surface CrOx species anchor at surface Brønsted acid sites of ZSM-5, but these IR studies were performed under ambient conditions in which the catalyst surface is hydrated and not representative of the actual catalysts under dehydrated conditions as reported in the present investigation.

5.3.3. Supported MoO_3/ZSM-5

The dehydrated surface molybdena species on ZSM-5 are fully oxidized as $Mo^{+6}Ox$ species as indicated by the location of the *in situ* XANES pre-edge energy and absence of d-d transitions from the *in situ* UV-vis spectra (see **Figure 5- 24** and **Figure 5- 13**). The intermediate intensity of the XANES pre-edge feature indicates that both MoO_4 and MoO_5/MoO_6 coordinated structures are present for supported MoO_3/ZSM-5 catalysts (see **Figure 5- 23**). The surface MoOx sites are isolated on ZSM-5 because of the very high UV-vis Eg value (see **Figure 5- 11**) and absence of ν_s(Mo-O-Mo) vibrations in the Raman spectra (see **Figure 5- 18**). The Raman spectra reveal the presence of four distinct surface MoOx structures that with DFT calculations[53] have been assigned to isolated (*i*) dioxo$(O=)_2MoO_2$ species anchored at adjacent Brønsted alumina sites, (*ii*) dioxo$(O=)_2Mo(OH)O$ species anchored at single Brønsted alumina sites, (*iii*) dioxo$(O=)_2MoO_2$ species anchored at adjacent silica sites on the external surfaces and (*iv*) mono-oxo $O=MoO_4$ species anchored at external Al_2O_3 NPs.

The presence of oligomeric surface MoOx species on ZSM-5 supports such as dimeric Mo_2Ox structures have been proposed from *in situ* visible and UV Raman studies, respectively.[65,66] The *in situ* EXAFS study[65] claimed dimeric Mo_2O_5 species, but the absence of Mo-O-Mo distances in the reported EXAFS second coordination sphere do not support dimeric Mo_2O_5 structures. There has also been inconsistency in assignment of the *in situ* Raman bands for supported MoOx/ZSM-5 catalysts with the assignments made without supporting data. With visible Raman spectroscopy, vibrations were detected at 970 and 1045 cm^{-1} that were assigned to dimeric and isolated surface molybdena species, respectively.[65] With *in situ* UV Raman spectroscopy, bands were observed at 868 and

962 cm^{-1} that were assigned to the dimeric Mo-O-Mo stretch and isolated mono-oxo $O=MoO_4$ species, respectively.[66] The recent combined Raman and DFT studies of supported MoOx/ZSM-5 catalysts indicate that the vibration at ~962-970 cm^{-1} is actually from isolated surface dioxo $(O=)_2Mo(OH)O$ species anchored at single Brønsted alumina sites, the band at 1045 cm^{-1} corresponds to isolated surface mono-oxo $O=MoO_4$ species anchored at external Al_2O_3 NPs[24] and the band at 868 cm^{-1} is characteristic of Mo-O-Al/Si bonds.[42,46] The absence of dimeric and oligomeric MoOx sites on ZSM-5 and exclusive presence of the isolated surface MoOx sites on ZSM-5 is confirmed by the very high UV-vis Eg value of ~4.8 eV that only corresponds to isolated surface MoOx sites on ZSM-5 (see **Figure 5- 11**).[42,46,67]

The supported MoOx species preferably anchor at surface Brønsted acid sites at low molybdena loading, but also anchor at external surface Si-OH and extra-framework Al-OH sites at high molybdena loading (see **Figure 5- 5**). There is general consensus from multiple reported *in situ* IR studies[10,67,68] that both surface Al-$(OH)^+$-Si Brønsted acid and external Si-OH sites are the anchoring sites for surface MoOx species on H-ZSM-5. Xu *et al.*[67] reported that MoOx species preferably anchor at surface Brønsted acid sites over silanol hydroxyls for 6% MoO_3/ZSM-5 (Si/Al= 25) with *in situ* IR in which the dehydration was performed in vacuum. Lunsford and co-workers[10] observed with *in situ* IR spectroscopy that MoOx species migrated from external surface Si-OH sites and extra-framework Al-OH hydroxyls to framework Al-$(OH)^+$-Si sites at elevated calcination temperatures for a 2% MoO_3/ZSM-5 (Si/Al=25) catalyst prepared by impregnation. In contrast to the above observations, Iglesia *et al.*[65] assumed that surface Mo_2O_5 dimers anchor at two adjacent Al-$(OH)^+$-Al Brønsted acid sites, but it is based on titration of

Brønsted hydroxyls and no direct supporting information was provided. The probability of finding a high concentration of two adjacent Al framework Brønsted acid sites, however, is low according to Lowenstein's rule[69] and not enough of such paired sites are present for anchoring high loadings of MoOx on ZSM-5. Furthermore, dimeric $Mo_2O_5^+$ species are not supported by the present *in situ* UV-vis and EXAFS results as indicated above.

5.3.4. Supported WO_3/ZSM-5

The dehydrated surface tungsta species on ZSM-5 are fully oxidized as W^{+6}Ox species as indicated by the location of the *in situ* XANES pre-edge energy and absence of d-d transitions from the *in situ* UV-vis spectra (see **Figure 5- 25** and **Figure 5- 13**). The strong intensity of the XANES pre-edge feature indicates that WO_4 coordinated structures are the predominant structures for supported WOx/ZSM-5 (Si/Al=15, 25 and 40) catalysts (see **Figure 5- 25**). The weaker of the XANES pre-edge energy features for supported WOx/ZSM-5 (Si/Al=140) reflects the presence of significant surface WO_5/WO_6 coordinated sites in addition to surface WO_4 sites. The corresponding Raman spectra confirmed the presence of WO_6 coordinated WO_3 NPs for the silica-rich ZSM-5 (Si/Al=140) support that contains a limited number of alumina anchoring sites (see **Figure 5- 20**). The surface WOx sites are isolated on ZSM-5 due to their very high UV-vis Eg values (see **Figure 5- 11**) and unique presence of W=O with no contribution from a second coordination sphere in the EXAFS (see **Figure 5- 25**). In addition to the WO_3 NPs found for the silica rich WOx/ZSM-5 (Si/Al=140) catalyst, the Raman spectra reveal the presence of three distinct surface WOx structures that by analogy to supported

MoOx/ZSM-5 catalysts have been assigned to isolated (*i*) dioxo$(O=)_2WO_2$ species anchored at adjacent Brønsted alumina sites (~990 cm^{-1}), (*ii*) dioxo$(O=)_2W(OH)O$ species anchored at single Brønsted alumina sites (~975 cm^{-1}) and (*iii*) mono-oxo $O=WO_4$ species anchored at external Al_2O_3 NPs (~1020 cm^{-1}).

There is almost unanimous agreement among all researchers that the dehydrated surface WOx species on ZMS-5 are present as isolated species. Amin *et al.*[15] also concluded that surface WOx species on ZSM-5 are isolated from the high Eg value they measured with *in situ* UV-vis (LMCT ~ 215 nm). *In situ* EXAFS measurements indicated the absence of W-O-W bonds in the second coordination shell, which precludes the presence of dimeric and oligomeric WOx surface species. Although the dehydrated surface WOx species on ZSM-5 were proposed to possess dioxo $(O=)_2WO_2$ coordination, neither the XANES pre-edge feature and the number of terminal W=O bonds were reported.[16] Furthermore, the Raman spectra reveal that multiple surface WOx sites are present on ZSM-5 rather than one unique structure as proposed above.

The supported WO_x species on ZSM-5 anchor at external surface Al-OH of Al_2O_3 NPs and not on external Si-OH or extra-framework Al-OH sites. It is difficult to determine whether the framework Al site (Al-$(OH)^+$-Si) is also an anchoring site because of the creation of new surface W-OH or Brønsted acid W-$(OH)^+$-Al sites with increasing tungsta loading. By analogy with supported MoO_3/ZSM-5, the two dioxo surface WOx sites must be anchoring at surface Al-$(OH)^+$-Si Brønsted acid sites. Ding *et al.*[16] proposed that two neighboring surface Al-$(OH)^+$-Si Brønsted acid sites are necessary to anchor dimeric $W_2O_5^+$ species on ZSM-5 based on titration of the residual protons of ZSM-5, but the probability of finding a high concentration of two adjacent Al framework Brønsted

acid sites at high loadings of WOx on ZSM-5 is low according to Lowenstein's rule.[69] Furthermore, as mentioned above, the characterization studies demonstrate that surface WOx species are present as multiple isolated structures on ZSM-5.

5.3.5. Supported Re_2O_7/ZSM-5

The surface rhenia species on ZSM-5 are fully oxidized as Re^{+7} in oxidizing environments as indicated by the location of the *in situ* XANES pre-edge energy and absence of d-d transitions from the *in situ* UV-vis spectra (see **Figure 5- 26** and **Figure 5- 13**). The ReO_4 coordination of the surface rhenia species on ZSM-5 is confirmed by the pronounced *in situ* XANES pre-edge feature (see **Figure 5- 26**). The similar XANES pre-edge intensity for both the supported ReOx/ZSM-5 and the trioxo $(O=)_3$Re-Si reference compound corresponds to the presence of trioxo coordinated surface $(O=)_3$ReO-Al/Si sites on ZSM-5. The proposed pseudo-trioxo (dioxo) structures exhibit a weaker XANES pre-edge intensity than trioxo $(O=)_3$ReO species.[70] The dehydrated surface rhenia species on the ZSM-5 supports are exclusively present as isolated sites as reflected by the very high UV-vis Eg value of ~4.9 eV (see **Figure 5- 11**), and the presence of Re=O with no contribution from a second coordination sphere of the *in situ* EXAFS spectra (see **Figure 5- 26)**. Crystalline Re_2O_7 NPs, as well as surface dimeric or oligomeric rhenia species, are not present on ZSM-5 because of the volatility of Re_2O_7 and its oligomers. The volatility of the surface ReO_4 species is reflected in the reduced Raman intensity for silica-rich supported ReOx/ZSM-5 (Si/Al=140) in which a reduced number of surface Al-$(OH)^+$-Si Brønsted acid sites are available (see **Figure 5- 9**). The

Raman spectra also indicate that there is only one surface ReO_4 structure on the ZSM-5 support that is independent of the Si/Al ratio (see **Figure 5- 21**).

In agreement with the current findings, several research groups have proposed that the surface ReOx species on ZSM-5 are isolated and coordinated as trioxo $(O=)_3ReO$ species anchored to two oxygen sites associated with framework alumina (e.g. Si-O*-Al-O*-Si) from *in situ* Raman[71] and computational DFT calculations[72]. The *in situ* XANES/EXAFS studies[71] proposed that surface ReOx species on ZSM-5 are present as both monomeric ReO_4 species on one Al Brønsted acid site and dimeric $Re_2O_6^{2+}$ species on two adjacent Al Brønsted acid sites, but direct supporting molecular structural information was not provided and their *in situ* EXAFS spectra did not observe the expected Re-O-Re distance in the second coordination sphere. As already indicated above, the probability of finding a high concentration of two adjacent Al framework Brønsted acid sites at high loadings of ReOx on ZSM-5 is low according to Lowenstein's rule[69] and all rhenia oligomers are also volatile. All studies containing direct molecular structural data clearly indicate that the surface ReOx species are isolated on the ZSM-5 support and possess trioxo $(O=)_3ReO$ coordination.

The current findings demonstrate that supported ReOx species preferably anchor at surface Al-$(OH)^+$-Si Brønsted acid sites at low rhenia loading and also at external Si-OH sites at higher rhenia loading on the ZSM-5 support. The anchoring of surface ReOx species at surface Al-$(OH)^+$-Si Brønsted acid sites and external Si-OH sites are in agreement with the previous *in situ* IR study[71].

5.4. Conclusions

The anchoring sites, electronic and molecular structures of supported MOx species on ZSM-5 with varying Si/Al ratio from 15 to 140 under oxidizing conditions were determined with combined *in situ* FT-IR, UV-vis, Raman spectroscopy and X-ray absorption spectroscopy.

The appearance of crystalline metal oxide (V_2O_5, Cr_2O_3, MoO_3 and WO_3) nanoparticles for supported MOx/ZSM-5 catalysts with few framework alumina sites, Si/Al=140, indicates the important role of framework alumina (Al-$(OH)^+$-Si) sites in dispersing metal oxides on ZSM-5 supports. Although crystalline Re_2O_7 does not form on ZSM-5 (Si/Al=140) because of rhenia's volatility, the reduced number of alumina anchoring sites is manifested as a lower number of anchored surface ReOx sites. Although anchoring of MOx species at framework alumina (Al-$(OH)^+$-Si) sites is the preferred mechanism, the anchoring of surface of surface MOx species on ZSM-5, however, is more complex as shown by the titration of the different ZSM-5 surface hydroxyls upon deposition of surface MOx. The surface MOx species were found to anchor at both Brønsted acid sites inside the zeolite channel, external silica sites and traces of them also at external alumina sites. At low metal ion loadings, surface MOx species generally prefer to anchor at Brønsted acid sites. New Brønsted acid hydroxyls found on supported VOx, CrOx and WOx/ZSM-5 catalysts interfere with the analysis of framework Al sites of ZSM-5 support as their anchoring sites.

The surface MOx species on ZSM-5 are present as fully oxidized and almost exclusively present as isolated species under oxidizing conditions. The high Eg values of the supported MOx/ZSM-5 catalysts, the absence of M-O-M vibration in Raman spectra

and the absence of M-O-M coordination from EXAFS spectra consistently supported that the surface MOx species are monomeric and not dimeric species. The surface vanadia and rhenia species are only mono-oxo $O=VO_3$ and trioxo $(O=)_3ReO$ structure, respectively. Their Raman vibration positions were not perturbed by the Si/Al ratio. The surface chromia, molybdena and tungsta species are present as both dioxo $(O=)_2MO_2$ and mono-oxo $O=MO_4$ species. The Raman vibration positions of dioxo $(O=)_2MoO_2$ and $(O=)_2WO_2$ species slightly shifted with increasing Si/Al ratio. This is consistently observed on model MOx/SiO_2 and $MOx/Al_2O_3/SiO_2$ catalysts reported by Lee *et al.*[42,46] The Si/Al ratio affects the dispersion of surface MOx species. A high content of framework Al sites facilitates the dispersion of surface MOx species. The ZSM-5 (Si/Al=140) with the lowest Al content leads to the formation of crystalline nanoparticles in the case of supported V_2O_5/ZSM-5, CrO_3/ZSM-5 and WO_3/ZSM-5 catalysts.

The present study definitively provides a better understanding about the anchoring sites, oxidation states, oligomerization extent and molecular structures of the initial supported MOx species on ZSM-5 supports. These new insights about the structures of the surface MOx catalytic active sites in ZSM-5 supports are important for establishing molecular level mechanistic models for numerous catalytic reactions.

References

1. Wark, M.; Brückner, A.; Liese, T.; Grünert, W., *Journal of Catalysis* **1998,** *175* (1), 48-61.
2. Chang, Y. F.; Somorjai, G. A.; Heinemann, H., *Journal of Catalysis* **1995,** *154* (1), 24-32.
3. Wang, L.; Tao, L.; Xie, M.; Xu, G.; Huang, J.; Xu, Y., *Catalysis Letters* **1993,** *21* (1-2), 35-41.
4. de Lucas, A.; Valverde, J. L.; Rodriguez, L.; Sanchez, P.; Garcia, M. T., *Applied Catalysis A: General* **2000,** *203* (1), 81-90.
5. Traa, Y.; Burger, B.; Weitkamp, J., *Microporous and Mesoporous Materials* **1999,** *30* (1), 3-41.
6. Katranas, T. K.; Triantafyllidis, K. S.; Vlessidis, A. G.; Evmiridis, N. P., Dehydrogenation of propane over Ga and Cr modified, "fresh" and steamed, MFI-type zeolites. In *Studies in Surface Science and Catalysis*, Aldo Gamba, C. C. a. S. C., Ed. Elsevier: 2005; Vol. Volume 155, pp 347-354.
7. Mimura, N.; Takahara, I.; Inaba, M.; Okamoto, M.; Murata, K., *Catalysis Communications* **2002,** *3* (6), 257-262.
8. Yamashita, H.; Ohshiro, S.; Kida, K.; Yoshizawa, K.; Anpo, M., *Research on Chemical Intermediates* **2003,** *29* (7-9), 881-890.
9. Chaudhari, P. K.; Saini, P. K.; Chand, S. J. **Comparative performance of ion-exchanged ZSM-5 and Y-zeolite catalysts for toluene disproportionation reaction** *Journal of Science and Industrial Research* [Online], 2002, p. 810-816.
10. Weckhuysen, B. M.; Wang, D.; Rosynek, M. P.; Lunsford, J. H., *Journal of Catalysis* **1998,** *175* (2), 338-346.
11. Abdullah, A. Z.; Abu Bakar, M. Z.; Bhatia, S., *Industrial & Engineering Chemistry Research* **2003,** *42* (24), 6059-6067.
12. Abdullah, A. Z.; Bakar, M. Z. A.; Bhatia, S., *Catalysis Communications* **2003,** *4* (11), 555-560.
13. Rachapudi, R.; Chintawar, P. S.; Greene, H. L., *Journal of Catalysis* **1999,** *185* (1), 58-72.
14. Swanson, M. E.; Greene, H. L.; Qutubuddin, S., *Applied Catalysis B: Environmental* **2004,** *52* (2), 91-108.
15. Amin, N. A. S.; Pheng, S. E., *Catalysis Communications* **2006,** *7* (6), 403-407.
16. Ding, W.; Meitzner, G. D.; Marler, D. O.; Iglesia, E., *The Journal of Physical Chemistry B* **2001,** *105* (18), 3928-3936.
17. Solymosi, F.; Tolmacsov, P., *Catalysis Letters* **2004,** *93* (1-2), 7-11.
18. Lacheen, H. S.; Cordeiro, P. J.; Iglesia, E., *Chemistry – A European Journal* **2007,** *13* (11), 3048-3057.
19. Chen, L.; Lin, L.; Xu, Z.; Zhang, T.; Li, X., *Catalysis Letters* **1996,** *39* (3-4), 169-172.
20. Wachs, I. E.; Kim, T., *Metal Oxide Catalysis*. Wiley: New York, 2009.
21. Wachs, I. E.; Roberts, C. A., *Chemical Society Reviews* **2010,** *39* (12), 5002-5017.
22. Weber, R. S., *Journal of Catalysis* **1995,** *151* (2), 470-474.
23. Mimura, N.; Okamoto, M.; Yamashita, H.; Oyama, S. T.; Murata, K., *The Journal of Physical Chemistry B* **2006,** *110* (43), 21764-21770.
24. Tian, H.; Wachs, I. E.; Briand, L. E., *The Journal of Physical Chemistry B* **2005,** *109* (49), 23491-23499.
25. Mestl, G.; Srinivasan, T. K. K.; Knoezinger, H., *Langmuir* **1995,** *11* (10), 3795-3804.
26. Kiricsi, I.; Flego, C.; Pazzuconi, G.; Parker, W. O., Jr.; Millini, R.; Perego, C.; Bellussi, G., *The Journal of Physical Chemistry* **1994,** *98* (17), 4627-4634.
27. Glazneva, T. S.; Kotsarenko, N. S.; Paushtis, E. A., *kinetics and catalysis* **2008,** *49* (6), 859-867.
28. Schoiswohl, J.; Tzvetkov, G.; Pfuner, F.; Ramsey, M. G.; Surnev, S.; Netzer, F. P., *Physical Chemistry Chemical Physics* **2006,** *8* (13), 1614-1623.
29. Wachs, I. E., *Catalysis Today* **1996,** *27* (3–4), 437-455.
30. Turek, A. M.; Wachs, I. E.; DeCanio, E., *The Journal of Physical Chemistry* **1992,** *96* (12), 5000-5007.
31. Kuroda, Y.; Kittaka, S.; Takahara, S.; Yamaguchi, T.; Bellissent-Funel, M.-C., *The Journal of Physical Chemistry B* **1999,** *103* (50), 11064-11073.

32. Pfeifer, J.; Guifang, C.; Tekula-Buxbaum, P.; Kiss, B. A.; Farkas-Jahnke, M.; Vadasdi, K., *Journal of Solid State Chemistry* **1995,** *119* (1), 90-97.
33. Badlani, M.; Wachs, I., *Catalysis Letters* **2001,** *75* (3-4), 137-149.
34. Wachs, I. E.; Lee, E., *Silica and Silicates in Modern Catalysis*. 1st ed.; Transworld Research Network: 2010.
35. Gao, Z.-X.; Kim, H.-S.; Sun, Q.; Stair, P. C.; Sachtler, W. M. H., *The Journal of Physical Chemistry B* **2001,** *105* (26), 6186-6190.
36. Ross-Medgaarden, E. I.; Wachs, I. E., *The Journal of Physical Chemistry C* **2007,** *111* (41), 15089-15099.
37. Tian, H.; Roberts, C. A.; Wachs, I. E., *The Journal of Physical Chemistry C* **2010,** *114* (33), 14110-14120.
38. Anderson, J. R.; Foger, K.; Mole, T.; Rajadhyaksha, R. A.; Sanders, J. V., *Journal of Catalysis* **1979,** *58* (1), 114-130.
39. Yu, Y.; Xiong, G.; Li, C.; Xiao, F.-S., *Microporous and Mesoporous Materials* **2001,** *46* (1), 23-34.
40. Dutta, P. K.; Rao, K. M.; Park, J. Y., *The Journal of Physical Chemistry* **1991,** *95* (17), 6654-6656.
41. Dutta, P. K.; Puri, M., *The Journal of Physical Chemistry* **1987,** *91* (16), 4329-4333.
42. Lee, E. L.; Wachs, I. E., *Journal of Physical Chemistry C* **2007,** *111* (39), 14410-14425.
43. Zhang, S. G.; Higashimoto, S.; Yamashita, H.; Anpo, M., *The Journal of Physical Chemistry B* **1998,** *102* (29), 5590-5594.
44. Das, N.; Eckert, H.; Hu, H. C.; Wachs, I. E.; Walzer, J. F.; Feher, F. J., *Journal of Physical Chemistry* **1993,** *97* (31), 8240-8243.
45. Deo, G.; Wachs, I. E.; Haber, J., *Critical Reviews in Surface Chemistry* **1994,** *4* (3-4), 141-187.
46. Lee, E. L.; Wachs, I. E., *Journal of Physical Chemistry C* **2008,** *112* (51), 20418-20428.
47. Nakka, L.; Molinari, J. E.; Wachs, I. E., *Journal of the American Chemical Society* **2009,** *131* (42), 15544-15554.
48. Döbler, J.; Pritzsche, M.; Sauer, J., *Journal of the American Chemical Society* **2005,** *127* (31), 10861-10868.
49. Magg, N.; Immaraporn, B.; Giorgi, J. B.; Schroeder, T.; Bäumer, M.; Döbler, J.; Wu, Z.; Kondratenko, E.; Cherian, M.; Baerns, M.; Stair, P. C.; Sauer, J.; Freund, H.-J., *Journal of Catalysis* **2004,** *226* (1), 88-100.
50. Avdeev, V.; Zhidomirov, G., *Research on Chemical Intermediates* **2004,** *30* (1), 41-64.
51. Lee, E. L.; Wachs, I. E., *Journal of Physical Chemistry C* **2008,** *112* (16), 6487-6498.
52. Tian, H. J.; Ross, E. I.; Wachs, I. E., *Journal of Physical Chemistry B* **2006,** *110* (19), 9593-9600.
53. Gao, J.; Zheng, Y.; Fitzgerald, G. B.; de Joannis, J.; Tang, Y.; Wachs, I. E.; Podkolzin, S. G., *The Journal of Physical Chemistry C* **2014**.
54. Handzlik, J.; Sautet, P., *The Journal of Physical Chemistry C* **2008,** *112* (37), 14456-14463.
55. Chan, S. S.; Wachs, I. E.; Murrell, L. L.; Wang, L.; Hall, W. K., *The Journal of Physical Chemistry* **1984,** *88* (24), 5831-5835.
56. Vuurman, M. A.; Wachs, I. E., *Journal of Molecular Catalysis* **1992,** *77* (1), 29-39.
57. Handzlik, J.; Kuzminska, J.; Lwin, S.; Keturakis, C.; Sautet, P.; Wachs, I. E. Nature of Rhenium Oxide Species in Aluminum Oxide Supported Perrhenate Catalysts: Trioxo, Dioxo or Monooxo Functionality in preparation.
58. Gao, X. T.; Bare, S. R.; Fierro, J. L. G.; Wachs, I. E., *Journal of Physical Chemistry B* **1999,** *103* (4), 618-629.
59. Bare, S. R., *Langmuir* **1998,** *14* (6), 1500-1504.
60. Horsley, J. A.; Wachs, I. E.; Brown, J. M.; Via, G. H.; Hardcastle, F. D., *The Journal of Physical Chemistry* **1987,** *91* (15), 4014-4020.
61. Lacheen, H. S.; Iglesia, E., *The Journal of Physical Chemistry B* **2006,** *110* (11), 5462-5472.
62. Nakamoto, K., *Infrared and Raman Spectra of Inorganic and Coordination Compounds*. Wiley: New York, 1986.
63. Petras, M.; Wichterlova, B., *The Journal of Physical Chemistry* **1992,** *96* (4), 1805-1809.
64. Slinkin, A. A.; Kucherov, A. V.; Gorjachenko, S. S.; Aleshin, E. G.; Slovetskaja, K. I., *Zeolites* **1990,** *10* (2), 111-116.
65. Li, W.; Meitzner, G. D.; Borry Iii, R. W.; Iglesia, E., *Journal of Catalysis* **2000,** *191* (2), 373-383.

66. Rzhevskii, A. M.; Choi, P.; Ribeiro, F. H.; Gulotty, R. J.; Olken, M. M., *Catalysis Letters* **2001,** *73* (2-4), 187-191.
67. Liu, W.; Xu, Y., *Journal of Catalysis* **1999,** *185* (2), 386-392.
68. Wang, D.; Lunsford, J. H.; Rosynek, M. P., *Journal of Catalysis* **1997,** *169* (1), 347-358.
69. Bell, R. G.; Jackson, R. A.; Catlow, C. R. A., *Zeolites* **1992,** *12* (7), 870-871.
70. Vicente, B. C.; Nelson, R. C.; Moses, A. W.; Chattopadhyay, S.; Scott, S. L., *The Journal of Physical Chemistry C* **2011,** *115* (18), 9012-9024.
71. Lacheen, H. S.; Cordeiro, P. J.; Iglesia, E., *Journal of the American Chemical Society* **2006,** *128* (47), 15082-15083.
72. Rice, M. J.; Chakraborty, A. K.; Bell, A. T., *Journal of Catalysis* **1999,** *186* (1), 222-227.
73. Weckhuysen, B. M.; Wang, D.; Rosynek, M. P.; Lunsford, J. H., *Journal of Catalysis* **1998,** *175* (2), 347-351.
74. Kucherov, A. V.; Slinkin, A. A., *Zeolites* **1987,** *7* (1), 38-42.
75. Kucherov, A. V.; Slinkin, A. A., *Journal of Molecular Catalysis* **1994,** *90* (3), 323-354.
76. Ayari, F.; Mhamdi, M.; Debecker, D. P.; Gaigneaux, E. M.; Alvarez-Rodriguez, J.; Guerrero-Ruiz, A.; Delahay, G.; Ghorbel, A., *Journal of Molecular Catalysis A: Chemical* **2011,** *339* (1–2), 8-16.
77. Tada, M.; Bal, R.; Sasaki, T.; Uemura, Y.; Inada, Y.; Tanaka, S.; Nomura, M.; Iwasawa, Y., *The Journal of Physical Chemistry C* **2007,** *111* (27), 10095-10104.
78. Weckhuysen, B. M.; Wang, D.; Rosynek, M. P.; Lunsford, J. H., *Angewandte Chemie International Edition in English* **1997,** *36* (21), 2374-2376.
79. Weckhuysen, B. M.; Verberckmoes, A. A.; Baets, A. R. D.; Schoonheydt, R. A., *Journal of Catalysis* **1997,** *166* (2), 160-171.
80. Weckhuysen, B. M.; Wachs, I. E.; Schoonheydt, R. A., *Chemical Reviews* **1996,** *96* (8), 3327-3349.

Chapter 6.

Catalytic reactivity of supported MOx/ZSM-5 (M=V, Cr, Mo, W and Re) catalysts during methane DHA

Abstract

The reactivity of the supported MOx/ZSM-5 catalysts for methane dehydroaromatization was investigated with the aid of temperature-programmed *operando* Raman-MS spectroscopy. The surface metal oxide structures were successfully identified in Chapter 5, and the catalytic role of each surface metal oxide structure present on MOx/ZSM-5 during methane DHA is studied in this chapter. Supported CrO_3/ZSM-5 and V_2O_5/ZSM-5 catalysts are no selective to benzene and form only carbon monoxide and hydrogen. Only supported Re_2O_7/ZSM-5, MoO_3/ZSM-5 and WO_3/ZSM-5 catalysts are selective and active catalysts for dehydroaromatization of methane to benzene. The temperature for initial benzene formation decreases in the order of WO_3/ZSM-5 (780-820^oC) > MoO_3/ZSM-5 (750~791 ^oC) >Re_2O_7/ZSM-5 (630-390 ^oC). The reactivity of the supported MOx/ZSM-5 (M=Mo, Re and W) catalyst is related to the reducibility of surface MOx (M=Mo, Re and W) species on the ZSM-5 support. The reducibility of surface metal oxide species decreases in an order of WOx (780-812 ^oC) >MoOx (748-788 ^oC) > ReOx (500-510 ^oC). The reactivity is also related to the content of Brønsted acid sites of ZSM-5 support. The reactivity decreases on catalysts with low contents of Brønsted acid sites which play a crucial role in oligomerization of C_2H_x intermediates to C_6H_6. The present study provides insights about the anchoring sites and molecular structures of the initial supported MOx species on ZSM-5 supports, and the nature of catalytic active phase of the catalysts during methane DHA.

Introduction

The reactivity of supported MOx/ZSM-5 (M=V, Cr, Mo, W and Re) catalysts for methane dehydroaromatization (DHA) have received much attention in the past. Lunsford *et al*.[1] investigated supported MOx/ZSM-5 (M=V, Cr, Mo and W) catalysts and their reactivity decreased in the order of Mo > W > Cr > V. Iglesia *et al*.[2] studied the reactivity of supported Mo, W and Re oxides on ZSM-5 catalysts and found that the benzene formation rate decreases in the order of Re > Mo > W>>V. In spite of the superior catalytic activity of supported Re_2O_7/ZSM-5 catalysts, the volatile nature of Re oxide makes it an impractical catalyst.[2] The supported MoO_3/ZSM-5 system represents the most promising catalysts due to its near equilibrium conversion.[1,3]

In spite of extensive characterization studies reported in the literature about the supported MOx/ZSM-5 catalysts, a general consensus has not been reached on the nature of the catalytic active sites present for the supported MOx/ZSM-5 catalysts. Most characterization measurements were performed under ambient or *ex situ* conditions and only a few under *in situ* conditions (please see Chapter 1 for a more extensive review). Characterization of catalysts under ambient or *ex situ* conditions does not represent the molecular structures under *in situ* and reaction conditions. Thus, it is important to elucidate the actual catalytic active sites for methane DHA by supported MOx/ZSM-5 catalysts with *in situ* or *operando* characterization techniques. Furthermore, most of the characterization studies focused on the structure of catalytic active sites of the supported MOx/ZSM-5 catalysts before and after methane DHA, and ignored the dynamic

transformation from the initial surface metal oxide species to the catalytic active sites during the methane DHA reaction. It is equally important to understand the activation of the catalyst and the catalytic role of initial surface metal oxide species since such information can provide new insights into designing more effective catalysts.

The focus of this chapter is to investigate the reactivity of supported MO_x/ZSM-5 for the methane DHA reaction *via operando* Raman-MS spectroscopy. This powerful modern approach to catalysis research allows monitoring the dynamic structural changes of the initial surface MOx species during methane DHA and simultaneously providing analysis of the gas phase composition *via* online mass spectrometer. This is the first *operando* spectroscopy study for methane DHA by supported MOx/ZSM-5 catalysts reported in the literature.

6.1. Experimental methods

6.1.1. CH_4 *operando* Raman-MS Spectroscopy

The *operando* Raman-MS spectroscopy and experimental procedures were described in Chapter 2, section 2.4.2.

6.2. Results

6.2.1. CH_4 *operando* Raman-MS spectroscopy

The reactivity of the supported MOx/ZSM-5 catalysts for methane conversion to benzene was investigated with temperature-programmed *operando* Raman-MS spectroscopy. The *operando* Raman spectroscopy provides information about the ease of reduction or activation of surface MOx species on ZSM-5 and the online MS provides initial temperatures for benzene formation.

The Raman spectrum of the ZSM-5 (Si/Al=15) support is presented in the supplementary information section as **Figure 6- 1**.

Figure 6- 1 *In situ* Raman spectra (Visible-532 nm) of dehydrated parent H-ZSM-5 containing (A) Si/Al=15, (B) Si/Al=25, (C) Si/Al=40, and (D) Si/Al=140 under oxidizing conditions at 450 ^{o}C.

The ZSM-5 (Si/Al=15) support exhibits the bending mode of six-membered rings at 293 cm^{-1}, the bending mode of five-membered rings at 378 cm^{-1}, the bending mode of four-membered rings 440-500 cm^{-1}, symmetric stretching vibrations of T-O bonds in ZSM-5 at ~810-820 cm^{-1} and asymmetric stretching vibrations of T-O bonds in ZSM-5 at 1080-1250 cm^{-1}.[4,5,6] The absence of any Raman bands in the range of 900-1050 cm^{-1} from the ZSM-5 support indicates that Raman bands in this region when surface metal oxide species are present must arise from the supported surface metal oxide phase.

Supported V_2O_5/ZSM-5

The *operando* Raman-MS CH_4-TPSR spectra for the supported 3% V_2O_5/ZSM-5(Si/Al=15) catalyst are presented in **Figure 6- 2**.

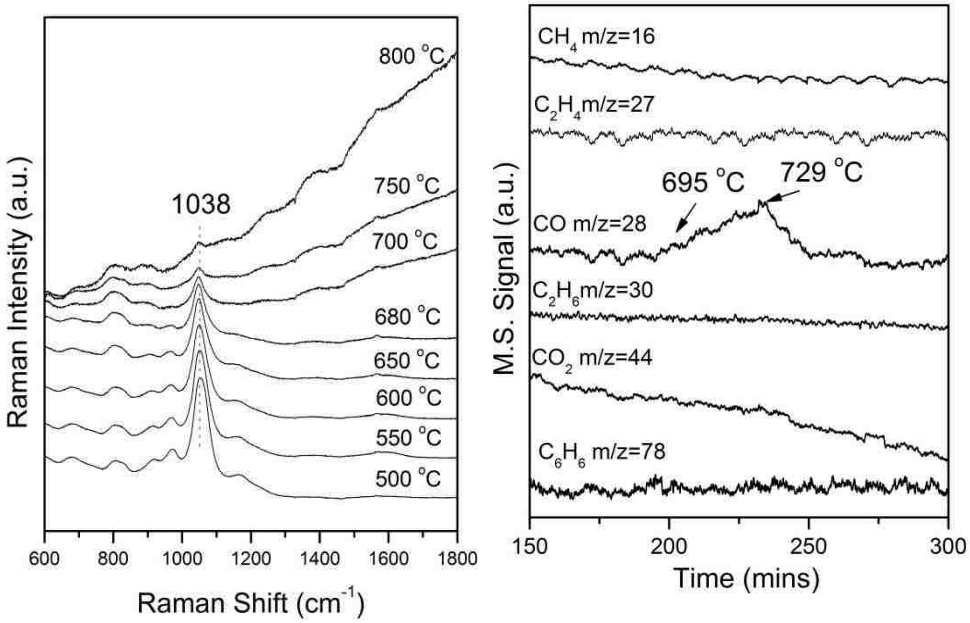

Figure 6- 2 *Operando* Raman-MS (442nm) spectra for 3% V_2O_5/ZSM-5 (Si/Al=15) during CH_4-TPSR

The supported V_2O_5/ZSM-5 catalyst is not active for benzene formation and only yields CO as the primary carbon reaction product at ~700^{o}C. The conversion of methane must

be small since no significant decrease in the methane signal is observed. The corresponding Raman spectra also do not exhibit the characteristic bands of surface coke at 1300-1600 cm^{-1}. The Raman band of the isolated surface mono-oxo $O=VO_3$ species at 1038 cm^{-1} is fairly stable in the methane stream up to ~650^oC and gradually decreases above 650 ^oC, which reflects its slow reduction by methane. The *operando* Raman-MS CH_4-TPSR spectroscopy experiment reveals that the initial surface $O=VO_3$ species becomes reduced in the methane environment above 650^oC and forms CO as the only carbon reaction product. The supported V_2O_5/ZSM-5 catalysts are not active for methane dehydroaromatization to benzene and instead pyrolyze methane to CO and H_2O.

Supported CrO_3/ZSM-5

The *operando* Raman-MS CH_4-TPSR spectra for the supported 1% CrO_3/ZSM-5(Si/Al=15) catalyst is given in **Figure 6- 3**.

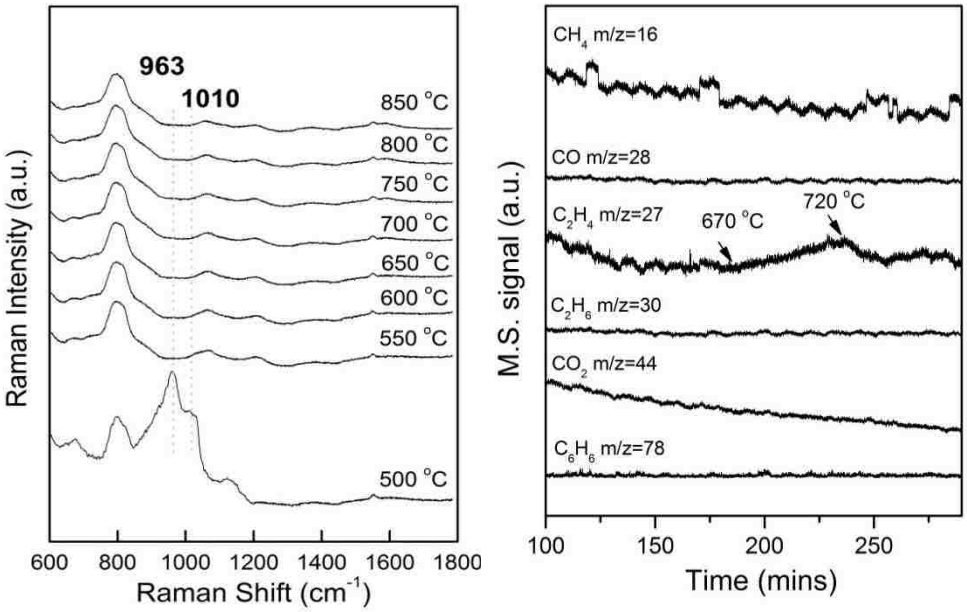

Figure 6- 3 *Operando* Raman-MS (442nm) spectra for 1% CrO_3/ZSM-5 (Si/Al=15) during CH_4-TPSR

The supported CrO_3/ZSM-5 catalyst is also not active for benzene formation and only yields CO as the primary carbon reaction product above 670^oC. The conversion of methane must be small since no significant decrease in the methane MS signal is observed. The corresponding Raman spectra also do not exhibit the characteristic bands of surface coke at 1300-1600 cm^{-1}. The Raman bands at 978 and 1010 cm^{-1} have been assigned to surface dioxo $(O=)_2CrO_2$ and mono-oxo $O=CrO_4$ species, respectively.[7,8] The surface CrOx species are not stable in nonoxidative environments since their Raman bands immediately disappear even when switching from molecular O_2 to an inert gas such as argon. Consequently, the Raman bands of the surface CrOx species are not detectable during the CH_4-TPSR experiment. The supported CrO_3/ZSM-5 catalyst is not active for methane dehydroaromatization to benzene and instead pyrolyzes methane to CO and H_2O.

Supported MoO_3/ZSM-5

The *operando* Raman-MS CH_4-TPSR spectra for the supported 2% MoO_3/ZSM-5 (Si/Al=15) catalyst is shown in **Figure 6- 4**.

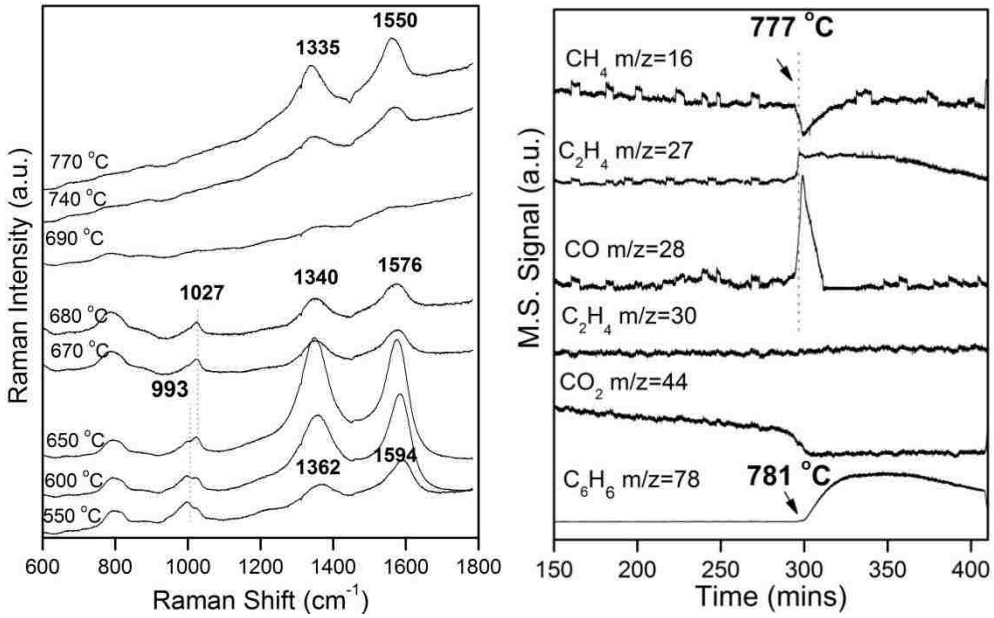

Figure 6- 4 *Operando* Raman-MS (442 nm) spectra of 2% MoO_3/ZSM-5 (Si/Al=15) during CH_4-TPSR

Unlike the supported V_2O_5/ZSM-5 and CrO_3/ZSM-5 catalysts, the supported 2% MoO_3/ZSM-5 catalyst is active for methane DHA to benzene. Production of CO spikes in the 770-785^oC range indicating reduction of the surface MoOx species and coincides with a dip in the CH_4 signal as well as the appearance of C_2H_4 and benzene reaction products. The corresponding Raman spectra contain the characteristic bands of polyaromatic coke in the 1300-1600 cm^{-1} range. The Raman band at 1580 cm^{-1} is the E_{2g} carbon-carbon in-plane stretching vibration[9,10] and the band at 1360 cm^{-1} is associated with the defects or edges present in the structural units of the pre-graphite species, and has been designated

the D-band.[11] The Raman spectrum in **Figure 6- 4** at 550°C is dominated by a band at 993 cm^{-1} from isolated surface dioxo $(O=)_2MoO_2$ species coordinated to two adjacent Al-Al sites and a weaker shoulder band at 1027 cm^{-1} from surface isolated surface mono-oxo $O=MoO_4$ species located at extra-framework Al sites. As the reaction temperature is increased, the band for the surface dioxo $(O=)_2MoO_2$ species decreases and the band for mono-oxo $O=MoO_4$ species does not change in intensity during temperature-programmed CH_4 reaction. Therefore, the surface dioxo $(O=)_2MoO_2$ species is more reactive than mono-oxo $O=MoO_4$ species during the reduction by methane.

Supported WO_3/ZSM-5

The *operando* Raman-MS spectra for the supported 1% WO_3/ZSM-5(Si/Al=15) catalyst are shown in **Figure 6- 5**.

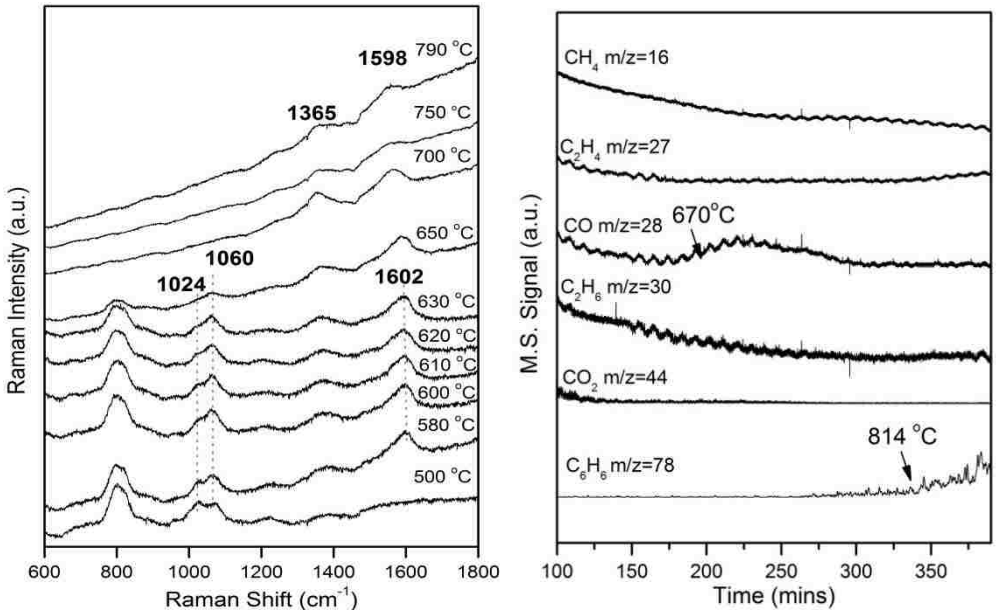

Figure 6- 5 *Operando* Raman-MS (442nm) spectra of 1% WO_3/ZSM-5 (Si/Al=15) during CH_4-TPSR

The supported WO_3/ZSM-5 catalyst possesses a low activity for methane DHA to benzene above 776 ^oC. The consumption of CH_4 and evolution of CO are modest over the temperature range 670-770^oC, without any spikes in reactivity, with formation of CO reflecting partial reduction of the surface WOx species. Interestingly, the formation of benzene initiates only after CO production ceases at 760^oC. Small amounts of coke are also present on the catalyst as reflected in their characteristic Raman bands in the 1300-1600 cm^{-1} region. The intensity of the band at 1365 cm^{-1} is significantly weaker than that of the band at 1598 cm^{-1} suggesting that the coke is composed of pre-graphitic species with a small concentration of defects or edges.[11] The corresponding Raman spectra possess bands at 1024 and 1060 cm^{-1} from isolated surface mono-oxo $O=WO_4$ species and $Al_2(WO_4)_3$ nanoparticles, respectively[12]. The $Al_2(WO_4)_3$ nanoparticles are not present in the initial catalyst and most likely are formed by reaction between the surface WOx and alumina during dealumination of the catalysts at high temperatures during the CH_4 DHA reaction. The intensity of the Raman band from the surface mono-oxo $O=WO_4$ species gradually diminishes with temperature because of its transformation to $Al_2(WO_4)_3$ and its reduction by methane. Above 700^oC, sample fluorescence masks the Raman bands for the surface mono-oxo $O=WO_4$ species, $Al_2(WO_4)_3$ nanoparticles and ZSM-5 support.

Supported Re_2O_7/ZSM-5

The *operando* Raman-MS spectra of supported Re_2O_7/ZSM-5 are given in **Figure 6- 6**.

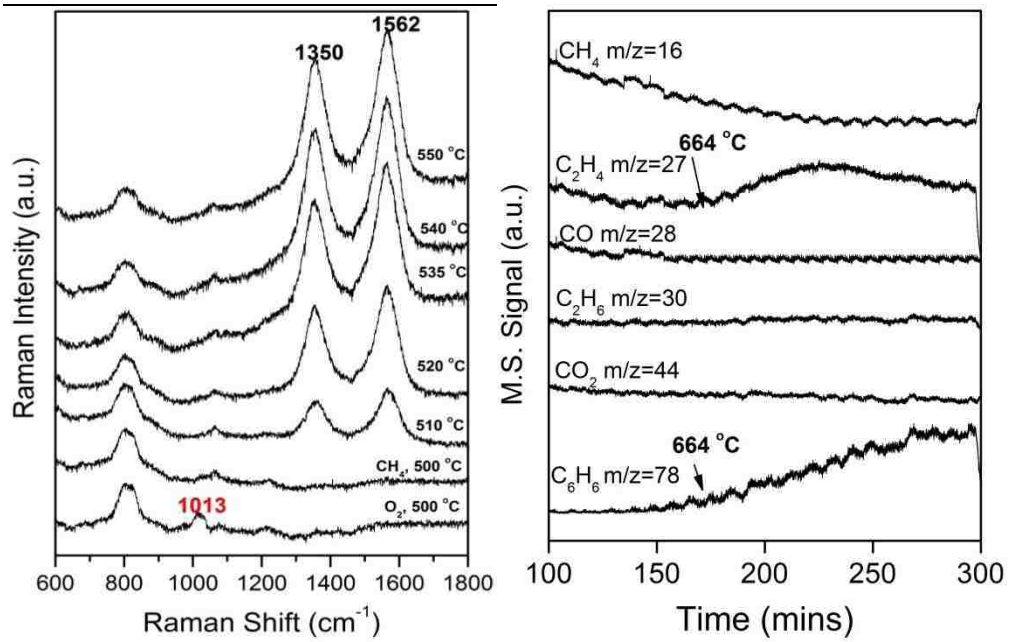

Figure 6- 6 *Operando* Raman-MS (442 nm) spectra of 1% Re_2O_7/ZSM-5 (Si/Al=15) during CH_4-TPSR

The supported Re_2O_7/ZSM-5 catalyst is also active for CH_4 DHA to benzene as well as C_2H_4 above 664^{o}C. The Raman bands at 1350 and 1562 cm^{-1}, characteristic of D and G-band of pre-graphitic species, grow with reaction temperature and also indicate the formation of aromatic intermediates. The corresponding Raman band at 1013 cm^{-1} arises from the isolated surface trioxo $(O=)_3ReO$ species and quickly disappears in flowing methane between 500-550 ^{o}C due to its partial reduction at relatively milder temperatures. The Raman spectra above 550 ^{o}C were obscured by sample fluorescence and are not shown for brevity.

Influence of specific metal oxide and Si/Al ratio of ZSM-5 support

The performance of the supported MOx/ZSM-5 catalysts (M=Re, Mo and W) were examined for the reduction temperature of the surface MOx species and the initial benzene formation temperatures, and are summarized as a function of Si/Al ratio in .

Table 6- 1 Reactivity of supported MOx/ZSM-5 (M=Re, Mo and W) for methane DHA to benzene during *operando* Raman-MS CH_4-TPSR spectroscopy

Si/Al ratio	ReOx		MoOx		WOx	
	$T_{red}(^oC)$[a]	$T_{C6H6}(^oC)$[b]	$T_{red}(^oC)$[a]	$T_{C6H6}(^oC)$[b]	$T_{red}(^oC)$[a]	$T_{C6H6}(^oC)$[b]
15	~500	664	740	781	745[c]	780
25	~510[c]	630	740	750	760[c]	804
40	~510[c]	660	760	778	812	820
140	~510[c]	690	788[c]	791	n/a[d]	n/a[d]

[a] Temperature at which surface MOx species were completely reduced
[b] Temperature for initial benzene formation determined from *operando* Raman-MS CH_4-TPSR spectroscopy
[c] The Raman signal of the surface MOx species was masked by sample fluorescence that prevented monitoring at higher temperatures, so the complete reduction temperature of surface WOx is estimated by the formation of CO in MS spectra
[d] The supported 3% WO_3/ZSM-5 (Si/Al=140) is not active for benzene and no CO is observed in methane flow from 500 to 900 ^oC

Although the reduction temperature trend of the supported MOx/ZSM-5 catalysts is WOx > MoOx > ReOx, there is minimal influence of the Si/Al ratio of the ZSM-5 support on the reduction temperature of each surface MOx species. The temperatures for initial benzene formation follow the same trend with WOx > MoOx > ReOx and modestly increase with Si/Al ratio, which implies that the number of surface Brønsted acid sites is an important factor in benzene formation. Furthermore, the activation of the

surface MOx sites on ZSM-5 for benzene formation initially requires reduction of the surface MOx sites. The most important parameters in controlling the performance of the supported MOx/ZSM-5 catalysts for benzene formation during methane DHA are the nature of the element of the catalytic active site (Re, Mo or W) and the number of surface Brønsted acid sites (Si/Al ratio of ZSM-5 support).

6.3. Discussion

6.3.1. Nature of Supported MOx species during methane DHA

The *operando* Raman-MS CH_4-TPSR results demonstrated that surface MOx species change structure during methane DHA at elevated temperatures. The initial surface VOx and CrOx species are reduced but no carbide is formed since the color of spent catalyst remains light and white. Initial surface dioxo MoO_4 species were converted to mono-oxo MoO_5 species at elevated temperatures during methane DHA and eventually converted to poorly ordered MoOxCy nanoparticles at 700 ^{o}C. The structure of surface MoOx species are dynamically altered which makes the reactivity-structure correlation impossible as evident from the *operando* Raman-MS results. Surface WOx species are gradually reduced to possible tungsten oxycarbide or carbide species as identified in the literature[13]; in the meanwhile, the formation of $Al_2(WO_4)_3$ species with a characteristic Raman band at 1064 cm^{-1} is observed at elevated temperatures during methane DHA. The WO_3/ZSM-5 (Si/Al=140) catalyst with crystalline WO_3 species is not reactive towards methane DHA, which suggests that only dispersed W species are capable of catalytic conversion of methane to benzene. The initial ReOx species are quickly reduced to Raman-inactive

species at low reaction temperatures. The reduced Re species is likely to be metallic Re species as reported by an *in situ* XAS study[14].

6.3.2. Nature of activated catalytic active sites during methane DHA

Supported V_2O_5/ZSM-5 catalyst

The supported V_2O_5/ZSM-5 is not active for methane DHA. The initial surface VOx species are gradually reduced in temperature-programmed methane DHA reaction, but this catalyst is not active for the conversion of methane to benzene and forms CO and H_2 only. The surface vanadia redox center ($V^{5+} \rightarrow V^{4+/3+}$) are not able to activate methane molecule to form any higher hydrocarbon. The reactivity of the current study is consistent with the report.[1] No *in situ* study has been reported for the catalytic active sites of V_2O_5/ZSM-5 for methane DHA probably due to its poor catalytic performance for this reaction. Only *ex situ* XPS studies[15] were reported and surface reduced V^{3+}Ox species were proposed as the active sites for methane DHA. The low reactivity of supported V_2O_5/ZSM-5 is probably due to the failure to form metal carbide or metal species during the catalyst activation step, which were reported as the catalytic active sites for supported Mo, W and Re oxides on ZSM-5, respectively.

Supported CrO_3/ZSM-5 catalyst

The supported CrO_3/ZSM-5 is not active for methane DHA. The initial surface Cr^{6+}Ox species is not stable and reduced to Cr^{3+} oxide species during methane DHA reaction; however, the chromia redox center ($Cr^{6+} \rightarrow Cr^{3+}$) is not able to activate the methane to form any higher hydrocarbon. The reactivity result on supported CrO_3/ZSM-5 is

consistent with results in the literature[15]. No *in situ* XAS study has investigated the catalytic active sites of supported CrO_3/ZSM-5 for methane DHA probably due to its poor catalytic performance. Only an *ex situ* XPS study[15] reported that Cr^{3+} oxide species is present after methane DHA treatment. Similar to the supported V_2O_5/ZSM-5 catalyst, the low reactivity of supported CrO_3/ZSM-5 can be attributed to the failure to form metal carbide or metal species which were the catalytic active sites for supported Mo, W and Re oxide on ZSM-5, respectively.

Supported MoO_3/ZSM-5 catalyst

The *operando* Raman-MS spectra observed that initial surface MoOx species are not responsible for the activity of methane DHA. The *in situ* XANES/EXAFS measurements have shown that the activated catalytic active Mo sites of the supported MoO_3/ZSM-5 catalysts for methane DHA are present as poorly ordered MoOxCy nanoparticles. It is estimated that the activated MoOxCy species has three neighboring Mo atom present in the second coordination during methane DHA which implies that the active sites are Mo_4OxCy nanoparticles. Similar results were found by Iglesia *et al*.[16] and poorly ordered MoOxCy species within zeolite channel were proposed. The present findings, consistently reveal that the activated supported Mo on ZSM-5 is present as dispersed MoOxCy species.[16] In subsequent work, Iglesia *et al.*[17] reported the active sites present as larger MoCy nanoclusters in an order of 6-10 Å. High Resolution Transmission Electron Microscopy (HR-TEM) images of much larger Mo_2C particles on the external zeolite surface of a spent MoO_3/ZSM-5 catalysts, ~50nm, have been reported in the literature[18]. These larger Mo_2C particles most probably arose from the presence of crystalline MoO_3

particles in the initial calcined catalysts since as shown in the present study crystalline MoO_3 is readily converted to crystalline Mo_2C under CH_4 DHA reaction conditions as demonstrated in Chapter 4.

Supported WO_3/ZSM-5 catalyst

The *operando* CH_4 Raman-MS spectra observed that the surface WOx species are resistant to reduction and a very low yield to benzene. The initial surface WOx species are not the catalytic active sites. The proposed catalytic active site of supported WO_3/ZSM-5 during methane DHA was tungsten carbide (WC_y) nanoclusters in an order of 5.5-5.7 Å located inside the zeolite channel[13]. The relatively large domain size of the proposed tungsten carbide could be a result of the presence of crystalline WO_3 introduced by sublimation of WO_3 and HZSM-5 from the solid-state reaction synthesis procedure. Furthermore, the proposed structure is not measured at the initiation of benzene; therefore, it cannot exclude the possibility of tungsten oxycarbide species as the active phase similar to the MoO_3/ZSM-5 catalyst system. It is reasonable to believe that tungsten oxycarbide is present at the initiation of benzene since surface WOx species are more difficult to be reduced than surface MoOx species as revealed in **Figure 6- 5**. Finally, they also failed to report the formation of $Al_2(WO_4)_3$ species as observed in current findings[13].

Supported Re_2O_7/ZSM-5 catalyst

The *operando* CH_4 Raman-MS spectra observed the surface ReOx species lead to a lower activation temperature of methane and formation temperature of benzene. The fully initial

oxidized trioxo $(O=)_3ReO$ species is not the catalytic active site, and the catalytic active Re phase is Raman inactive. It was proposed that the catalytic active site of supported Re_2O_7/ZSM-5 during methane DHA as metallic Re nanocluster in an order of 8.2 Å at external zeolite surfaces.[14,19] The formation of metallic Re nanocluster can be achieved at a lower temperature of 667 ^oC than MoO_3/ZSM-5 and WO_3/ZSM-5 catalysts[14,19]. The reported *in situ* EXAFS/XANES spectroscopy[14] observed the reduction of isolated $(O=)_3ReO$ species to metallic Re nanoclusters with the absence of any Re-O or Re-C coordination. The reactivity of supported Re_2O_7/ZSM-5 catalyst decreases with increasing domain size of metallic Re nanocluster for propane dehydroaromatization[14,19].

6.3.3. Dependence of reactivity and selectivity on specific metal

The supported V_2O_5/ZSM-5 and CrO_3/ZSM-5 catalysts are not active for methane DHA and forms pyrolysis products such as CO and H_2O only. Supported MoO_3/ZSM-5, WO_3/ZSM-5 and Re_2O_7/ZSM-5 catalysts are catalytically active and selective towards the conversion of methane to benzene. The reactivity of these catalysts decreases in an order of Re > Mo > W >> V≈ Cr. The reactivity trend of supported MOx/ZSM-5 (M=V, Cr, Mo, Re and W) catalysts for CH_4 DHA obtained from the current *operando* Raman-MS study is consistent with the trend of reactivity reported by Lunsford *et al.*[1] and Iglesia *et al.*[2,13,19] The low reactivity of supported V_2O_5/ZSM-5 and CrO_3/ZSM-5 might be due to the failure to form metal carbide of metallic species by reacting with methane, which are observed as the catalytic active sites for supported MoO_3/ZSM-5,[2] WO_3/ZSM-5[19] and Re_2O_7/ZSM-5[13] catalysts. Despite the high reactivity of the supported Re_2O_7/ZSM-5 catalyst, the ReOx phase is volatile[13] and its high cost makes it an impractical catalyst.

Supported WO_3/ZSM-5 catalysts are selective for benzene formation but the conversion temperature is extremely high and causes severe coke deposition and destruction of the zeolite framework. Supported MoO_3/ZSM-5 catalysts appear to be the best catalyst for methane DHA because of their high selectivity towards benzene and near equilibrium conversion. However, the catalyst also suffers from coke deactivation.

The ease of reduction of surface MOx species follows the same order as the initial temperature for benzene formation. The reduction temperature for surface MOx species decreases in the order of WO_3/ZSM-5 (780-820^oC) > MoO_3/ZSM-5 (781~791 ^oC) >Re_2O_7/ZSM-5 (630-390 ^oC). The reduction of MOx species does not immediately lead to the formation benzene implies the necessity of formation of a reduced phase. These observations suggest that the fully oxidized MOx species are transformed to reduced phases which are the active catalyst for benzene formation. In Chapter 3, poorly ordered molybdenum oxycarbide (MoO_xC_y) was identified as the active phase. In recent *in situ* EXAFS/XANES studies, tungsten carbide (WC_y) small clusters[13] and metallic Re small clusters[14] are proposed as the active phases for supported WO_3/ZSM-5 and Re_2O_7/ZSM-5 catalyst, respectively.

6.3.4. Nature of coke deposits on different catalysts

Combined with the *operando* Raman vibrations of the coke species, the hydrogen-deficient coke species with defects or edges are identified on supported MOx/ZSM-5(M=Mo, W and Re) catalysts. No coke species is observed on nonreactive V_2O_5/ZSM-5 and CrO_3/ZSM-5 catalysts suggested dehydrogenation is not occurring on these catalysts, and only pyrolysis products such as carbon monoxide and water were formed. The

Raman vibrations in the range of 1300-1400 cm^{-1} and 1500-1600 cm^{-1} are characteristic of D band and G band of polyaromatic species, respectively. The polyaromatic species generally have ring vibrations near or below 1600 cm^{-1}.[9, 10] In general, the broad Raman bands of the coke species suggested that they consist of a mixture of heavy hydrocarbons such as polyaromatics and pre-graphitic species.

The formation temperature of coke species is related to the specific metal species. For supported MoO_3/ZSM-5, the Raman bands of coke species at 1362 and 1594 cm^{-1} grew in intensity but diminished at 670-690 ^oC, and reappeared at 740 ^oC and shifted to lower wavenumber at 1335 and 1550 cm^{-1} with increasing reaction temperature. These observations suggested chemical changes in the coke species. The Raman band at 1594 cm^{-1} is indicative of conjugated olefinic species which were dehydrogenated. The disappearance of these species at 670-690 ^oC suggested that they reacted as intermediate species for methane DHA. Reappearance of Raman bands at 1335 and 1550 cm^{-1} are characteristic of polyaromatic species which were produced during aromatization steps. For supported WO_3/ZSM-5, the Raman bands of coke species at 1374 and 1602 cm^{-1} formed at 580-630 ^oC and shifted to lower wavenumbers to 1365 and 1598 cm^{-1}, which suggested the conjugated olefinic species experience further dehydrogenation and formed aromatic species at high reaction temperature. The relatively low intensity of the coke species suggested small amount of coke formed on WO_3/ZSM-5 catalysts. The low yield of benzene and the small amount of coke deposits consistently suggested that supported WO_3/ZSM-5 catalyst is not very reactive for methane activation. For supported Re_2O_7/ZSM-5, the Raman bands at 1350 and 1562 cm^{-1} were observed at very low temperature and grew in intensity with no shift at higher temperatures which implied that

the same type of coke species accumulated on the catalysts. The accumulation of heavy cokes and the benzene initiation on Re_2O_7/ZSM-5 catalysts occurred at lower temperatures than MoO_3/ZSM-5 and WO_3/ZSM-5. This implies that the dehydroaromatization of methane on Re_2O_7/ZSM-5 has lower activation energy than those on supported MoO_3/ZSM-5 and WO_3/ZSM-5 catalysts. The lower activation energy of Re_2O_7/ZSM-5 catalyst implies that metallic Re species is more reactive active phase than metal carbide/oxycarbide (metal refers to Mo and W).

6.4. Conclusions

The reactivity of supported MOx/ZSM-5 during methane dehydroaromatization (DHA) reaction was investigated *via operando* Raman-MS spectroscopy. The supported V_2O_5/ZSM-5 and CrO_3/ZSM-5 catalysts are not selective to benzene and only pyrolysis products such as carbon monoxide and water are formed. The poor catalytic activity might be associated to their failure to form metal carbide or metallic species which are identified as catalytic active sites for MOx/ZSM-5(M=Mo, W and Re) catalyst systems. Only supported Re_2O_7/ZSM-5, MoO_3/ZSM-5 and WO_3/ZSM-5 catalysts are selective and active catalysts for dehydroaromatization of methane to benzene. The temperature for initial benzene formation decreases in the order of WO_3/ZSM-5 (780-820^oC) > MoO_3/ZSM-5 (750~791 ^oC) > Re_2O_7/ZSM-5 (630-390 ^oC). The reactivity of the supported MOx/ZSM-5 (M=Mo, Re and W) catalyst correlates to the reducibility of surface MOx (M=Mo, Re and W) species on the ZSM-5 support which decreases in an order of WOx (780-812 ^oC) >MoOx (748-788 ^oC) > ReOx (500-510 ^oC). Active sites were identified as metallic Re nanoclusters for Re_2O_7/ZSM-5, dispersed metal carbide carbide/oxycarbide for MoO_3/ZSM-5 and WO_3/ZSM-5, respectively. The metallic Re is more reactive than metal carbide/oxycarbide; however, the volatile nature of Re oxide makes it impractical as commercial catalyst. Benzene formation on the supported WO_3/ZSM-5 catalysts requires extremely high temperature which will cause destruction of zeolite framework. Supported MoO_3/ZSM-5 remains the most promising catalyst for methane DHA; however, it also suffers from coke deactivation. The reactivity is also related to the content of Brønsted acid site of ZSM-5 support. The reactivity decreases on

catalysts with low content of Brønsted acid site which plays a crucial role in oligomerization of C_2H_x intermediates to C_6H_6. Coke formation follows the same trend as the reactivity of supported metal oxide catalysts (Re > Mo > W). Two different types of coke species are identified. Conjugated olefinic species (Raman vibration close to 1600 cm^{-1}) formed in the temperature range of 500-630 ^oC on MoO_3/ZSM-5 could be important intermediates for the production of benzene. Polyaromatic species with defects or edge (Raman vibration below 1600 cm^{-1}) are responsible for blocking the active sites which eventually deactivates catalyst.

References

1. Weckhuysen, B. M.; Wang, D.; Rosynek, M. P.; Lunsford, J. H., *Journal of Catalysis* **1998,** *175* (2), 338-346.
2. Lacheen, H. S.; Iglesia, E., *Physical Chemistry Chemical Physics* **2005,** *7* (3), 538-547.
3. Wang, D.; Lunsford, J.; Rosynek, M., *Topics in Catalysis* **1996,** *3* (3-4), 289-297; Chen, L. Y.; Lin, L. W.; Xu, Z. S.; Li, X. S.; Zhang, T., *Journal of Catalysis* **1995,** *157* (1), 190-200.
4. Yu, Y.; Xiong, G.; Li, C.; Xiao, F.-S., *Microporous and Mesoporous Materials* **2001,** *46* (1), 23-34.
5. Dutta, P. K.; Rao, K. M.; Park, J. Y., *The Journal of Physical Chemistry* **1991,** *95* (17), 6654-6656.
6. Dutta, P. K.; Puri, M., *The Journal of Physical Chemistry* **1987,** *91* (16), 4329-4333.
7. Lee, E. L.; Wachs, I. E., *Journal of Physical Chemistry C* **2008,** *112* (51), 20418-20428.
8. Lee, E. L.; Wachs, I. E., *Journal of Physical Chemistry C* **2007,** *111* (39), 14410-14425.
9. Li, C.; Stair, P. C., *Catalysis Today* **1997,** *33* (1–3), 353-360.
10. Kwizera, P.; Dresselhaus, M. S.; Dresselhaus, G., *Carbon* **1983,** *21* (2), 121-129.
11. Nakamizo, M., *Carbon* **1991,** *29* (6), 757-761.
12. Ross-Medgaarden, E. I.; Wachs, I. E., *The Journal of Physical Chemistry C* **2007,** *111* (41), 15089-15099.
13. Ding, W.; Meitzner, G. D.; Marler, D. O.; Iglesia, E., *The Journal of Physical Chemistry B* **2001,** *105* (18), 3928-3936.
14. Lacheen, H. S.; Cordeiro, P. J.; Iglesia, E., *Chemistry – A European Journal* **2007,** *13* (11), 3048-3057.
15. Weckhuysen, B. M.; Wang, D.; Rosynek, M. P.; Lunsford, J. H., *Journal of Catalysis* **1998,** *175* (2), 347-351.
16. Li, W.; Meitzner, G. D.; Borry Iii, R. W.; Iglesia, E., *Journal of Catalysis* **2000,** *191* (2), 373-383.
17. Ding, W.; Li, S.; D Meitzner, G.; Iglesia, E., *The Journal of Physical Chemistry B* **2000,** *105* (2), 506-513.
18. Matus, E. V.; Ismagilov, I. Z.; Sukhova, O. B.; Zaikovskii, V. I.; Tsikoza, L. T.; Ismagilov, Z. R.; Moulijn, J. A., *Industrial & Engineering Chemistry Research* **2006,** *46* (12), 4063-4074.
19. Lacheen, H. S.; Cordeiro, P. J.; Iglesia, E., *Journal of the American Chemical Society* **2006,** *128* (47), 15082-15083.

VITA

Yadan Tang

ROOM 117, 7 ASA DR SINCLAIR LAB CELL: (484) 707-0454
BETHLEHEM, PA 18015 EMAIL: tangyadcn@gmail.com

Profile

- **PhD candidate** in **Chemistry** at **Lehigh University**
- Expertise in development, characterization and evaluation of exhaust treatment catalysts and methane to benzene conversion catalysts
- 3-year of experience in design of experimental protocols to identify catalytic active sites, structure/activity correlations and reaction mechanisms
- Hands-on experiences in various modern *in situ/operando* spectroscopies techniques (Raman with online GC-MS, UV-Vis, FTIR, TPSR with online mass spectrometry, X-ray absorption spectroscopy).
- On-site experiences at Brookhaven National Laboratory for catalyst characterization.
- Skilled in organic synthesis and analysis for air- and moisture-sensitive materials.
- Publications and multiple awards for presentations.
- English and Chinese Proficiency

Education

- **Ph.D.** Lehigh University, ***USA*** GPA 3.56/4
  Chemistry, May 2014
  Dissertation: *Operando* Molecular Spectroscopic Investigation of Methane Aromatization by Zeolite-supported Transition Metal Oxide Catalysts
- **M.S.** Lehigh University, ***USA*** GPA 3.48/4
  Chemistry, May 2010
  Dissertation: Synthesis of amine-bridged mesoporous organosilica for CO_2 capture
- **B.S.** East China University of Sci. and Tech., ***China*** GPA 3.60/4 Mater. Sci., June 2006

Research Experiences

Research Associate, Lehigh University August 2010-till present

Project 1: Operando spectroscopic investigations on zeolite-supported metal oxides for methane dehydroaromatization

- Synthesized zeolite-supported metal oxide catalysts via incipient wetness impregnation
- Identified the active sites of supported metal oxide species *via in situ* Raman, UV-Vis, FT-IR, and Temperature programmed surface reactions (TPSR with mass spectrometry).
- Established structure/activity correlation *via in situ* Raman/GC-MS and XANES/EXAFS
- Provided molecular and mechanistic understanding of the zeolite-supported catalysts to guide and optimize catalyst design for more efficient process

Project 2: Revisited the classic volcano curve by studying the kinetics of formic acid decomposition on bulk metal catalysts

- Tested trace amount of impurities on the topmost atomic layer of bulk metals via high resolution low energy ion scattering (HR-LEIS)
- Investigated catalytic reactivity of different metals (Fe, Cu, Co, Ni, Ag, Au, Pt, Pd and Rh) by TPSR and *in situ* FTIR using formate decomposition as a chemical probe
- Derived the key kinetics of the reactivity of metal catalysts to show that classic volcano plot based on *bulk* rather than *surface* parameters is problematic for surface chemistry

Research Assistant and Intern, Lehigh University & Air Product and Chemicals, Inc., *PA* 2008-2010

Project: Developed and synthesized a solid amine sorbent for selective CO_2 capture

- Synthesized, purified and characterized air- and moisture-sensitive organosilanes
- Prepared family of amine-bridged solid porous sorbents to avoid the use of corrosive liquid amines for selective CO_2 capture
- Investigated the porosity and morphology of the sorbent using nitrogen sorption (BET isotherm), SEM and small angle X-ray diffraction techniques
- Served as on-site project leader and responsible for project planning, updates and oral presentations

Course Projects

- **ChE 413** Heterogeneous catalysis----Mechanistic study on supported *Fe/ZSM-5 catalysts for Selective Catalytic Reduction (SCR) of NO with* NH_3

- **ChE 367** Environmental catalysis----Economic study and technology review of Lithium ion battery for vehicles
- **ChE 497** Advanced heterogeneous catalysis—Operando studies on zeolite catalysts

Honors and Awards

- Catalysis Society of Metropolitan NY Annual Student Poster Contest -2nd place award 2014
- Catalysis Club of Philadelphia Annual Student Poster Contest – 2nd place award 2013
- Kokes award winner for 23rd North American Catalysis Society Meeting 2013
- Invited student speaker as poster contest winner Catalysis Club of Philadelphia 2012
- Catalysis Club of Philadelphia Annual Student Poster Contest – 2nd place award 2011
- Top 10 graduate with B.S. degree, East China University of Sci. & Tech. 2006
- Scholarship for Academic Excellence, East China University of Sci. & Tech. 2004,2005

Publications

- Structure of Mo_2C_x and Mo_4C_xMolybdenum Carbide Nanoparticles and Their Anchoring Sites on ZSM-5 Zeolites". J. Gao, Y Zheng, G.B. Fitzgerald, J. Joannis; **Y. Tang**, I.E. Wachs, S. G. Podkolzin, *J. Phys. Chem. C* **2014**, *118,*4670.

- Identification of Molybdenum Oxide Structures and their Anchoring Sites on ZSM-5 for Catalytic Conversion of Natural Gas to Liquids, Jie Gao; Jih-Mirn Jehng; **Yadan Tang**; Israel E. Wachs, and Simon G. Podkolzin; *Science*, Submitted,**2014**

- CO_2Sorption Properties of Organosilicas with Bridging Amine Functionalities Inside the Framework, **Y. Tang**, K. Landskron, *J. Phys. Chem. C* **2010**,*114*, 2494.

- Nature of Catalytic Active Sites of Supported Transition Metal Oxides MOx/ZSM-5: Anchoring Sites, Molecular Structures and Reactivity, **Y. Tang**, E. Lee, I.E. Wachs, *manuscript in preparation*

- Aqueous Synthesis of Co-Precipitated WO_3-TiO_2 Catalysts under Controlled pH, Yuanyuan He, **Yadan Tang**, Qingcai Liu, Israel E. Wachs, *manuscript in preparation.*

- Comparison of Co-Precipitation and Impregnation Syntheses of Supported V_2O_5-WO_3/TiO_2 Catalysts for SCR of NO with NH_3, Yuanyuan He, Israel E. Wachs, Qingcai Liu, Mike E. Ford, and **Yadan Tang**, *manuscript in preparation.*

- Revisiting Formic Acid Decomposition on Bulk Metal Catalysts, **Yadan Tang**, Charles A. Roberts, Ryan Perkins and Israel E. Wachs, *to be submitted*

- A Decade of *Operando* Molecular Spectroscopy, I. E. Wachs, C. J. Keturakis, S. Lwin, **Y. Tang**, M. Zhu, A. Chakrabarti, M. Ford, D. Gregory, Z. Yang, and R. Hu, *to be submitted.*

Professional Affiliations

- American Chemistry Society, member *2009-present*
- Catalysis Society of Metropolitan New York, *2011-present*
- Catalysis Club of Philadelphia, *2011-present*